UNIVERSITY OF CRETE
FACULTY OF SCIENCES
DEPARTMENT OF BIOLGY

Doctoral thesis of

ERALDA SALATAJ

CHROMATIN ORGANIZATION AT THE NUCLEAR PERIPHERY

Subnuclear localization and expression of microRNA genes in cells of the murine adaptive immune system

HERAKLEION, 2019

ΠΑΝΕΠΙΣΤΗΜΙΟ ΚΡΗΤΗΣ
ΣΧΟΛΗ ΘΕΤΙΚΩΝ ΕΠΙΣΤΗΜΩΝ
ΤΜΗΜΑ ΒΙΟΛΟΓΙΑΣ

Διδακτορική Διατριβή της

ΕΡΑΛΝΤΑ ΣΑΛΑΤΑΙ

ΟΡΓΑΝΩΣΗ ΤΗΣ ΧΡΩΜΑΤΙΝΗΣ ΣΤΗΝ ΠΕΡΙΦΕΡΕΙΑ ΤΟΥ ΚΥΤΤΑΡΙΚΟΥ ΠΥΡΗΝΑ

Υποπυρηνική τοποθέτηση και έκφραση των microRNA γενετικών τόπων στο επίκτητο ανοσοποιητικό σύστημα του ποντικού

ΗΡΑΚΛΕΙΟ, 2019

Dedikuar dy njerezve me te vecante te botes time

Gjysherve te mi....

University of Crete
Department of Biology

FORTH
Institute of Molecular Biology and Biotechnology

Subnuclear localization and expression of microRNA genes in cells of the murine adaptive immune system

Supervisor
Assistant Professor Charalampos (G) Spilianakis

This study has been conducted at the Institute of Molecular Biology and Biotechnology, Foundation of Research and Technology (IMBB-FORTH), under the supervision of Dr. Prof. Charalampos G. Spilianakis, Laboratory of Gene Regulation in the Immune system.

This research has been co-financed by the European Union (European Social Fund - ESF) and Greek national funds through the Operational Program “Education and Lifelong Learning” of the National Strategic Reference Framework (NSRF). THALIS Research Funding program ‘miREG’ -microRNAs and Transcription Factor Networks in the Regulation of Cell differentiation, Aging and Tumorigenesis. Excellence Grant (THALIS)

Scientific Advisory Committee

Spilianakis G. Charalampos

Associate Professor, Department of Biology, University of Crete

Garinis Georgios

Professor, Department of Biology, University of Crete

Kalantidis Kriton

Associate Professor, Department of Biology, University of Crete

Scientific Examination Committee

Garinis Georgios

Professor, Department of Biology, University of Crete

Delidakis Christos

Professor, Department of Biology, University of Crete

Kalantidis Kriton

Associate Professor, Department of Biology, University of Crete

Nikolaou Christoforos

Assistant Professor, Department of Biology, University of Crete

Spilianakis Charalampos

Associate Professor, Department of Biology, University of Crete

Stroumpoulis Ioannis

Research Professor, IMBB-FORTH, Crete

Talianidis Iannis

Researcher A, BSRC Alexander Fleming, Athens

Abbreviations

Ac: Acetylation

AGO: Argonaute

ChIP: Chromatin Immunoprecipitation

CTCF: CCCTC-binding protein

CD: Chromosomal domain

cKO: Conditional knock out

CT: Chromosome territory

DAPI: 4',6-diamidino-2-phenylindole

DamID: DNA adenine methyltransferase identification

DGCR8: DiGeorge syndrome critical region gene 8

EDTA: Ethylenediamine tetraacetic acid

EGTA: Ethylene glycol tetraacetic acid

ER: Endoplasmic Reticulum

EXP5: Exportin 5

FACS: Fluorescence-Activated Cell Sorting

FBS: Fetal Bovine Serum

FISH: Fluorescence *in situ* Hybridization

H3K9: Histone H3 lysine 9

HEPES: 4-(2-hydroxyethyl)piperazine-1-ethanesulfonic acid

***HXK1*:** Hexokinase isoenzyme 1

HP1: Heterochromatin Protein 1

IP: Immunoprecipitation

LAD: Lamin Associated Domain

LAP: Lamin Associated Protein

LBR: Lamin B Receptor

LCR: Locus Control Region

LINE: Long Interspersed Elements

LTR: Long Terminal Repeat

me3: Trimethylation

miRISC: microRNA-induced silencing complex.

NAD: Nucleolus Associated Domain

NL: Nuclear Lamina

NPC: Nuclear Pore Complex

PBS: Phosphate buffered saline

PCR: Polymerase chain reaction

PcG: Polycomb group proteins

PE: Phycoerythrin

PML: Promyelocytic leukemia

Pol II: RNA polymerase II

SATB1: Specific AT-rich binding protein 1

TAD: Topologically Associated Domain

TCR: T cell receptor

TE: Transposable elements

TEM: Transmission electron microscopy

TLR: Toll like receptor

TNFα: Tumor necrosis factor α

TRBP: TAR RNA-binding protein

TSS: Transcription start site

SINE: Short Interspersed Elements

Contents

ABSTRACT

The last few years it has become increasingly clear that higher order chromatin organization controls the regulation of genome activity and serves as an additional epigenetic mechanism that modulates cellular functions and gene expression programs in diverse biological processes. Spatial positioning of different gene loci can be directly linked to gene expression while deregulation of the nuclear architecture can be linked to severe diseases. Control of gene expression is of vital importance for all organisms. Allelic interactions and gene repositioning with functional importance are common during the regulation of immune responses. Nowadays more and more studies support the correlation between chromatin organization and gene regulation. Except from the histone modifications and transcription factors non coding RNAs can also control gene expression.

MicroRNAs constitute an abundant class of endogenous and highly conserved small non-coding RNAs molecules (ncRNAs) that play an important role in modulating gene expression at the transcriptional and post-transcriptional level. microRNAs have been implicated in quite diverse biological processes including stem cell self-renewal, differentiation, proliferation, apoptosis and the regulation of immune responses in both innate and adaptive immune system. Although there is cumulative information regarding the steady state mature microRNA levels and their respective targets, little is known about the effect of the three-dimensional chromatin architecture on the transcriptional regulation of microRNA gene loci.

In this study we sought to investigate the impact of nuclear architecture as an epigenetic mechanism regulating the expression and the subnuclear localization of eight microRNA genes upon transcriptional activation in $CD4^+$ T cells during development and differentiation, in discrete T cell lineages. More specifically, we investigated the role of subnuclear localization of microRNA gene loci as a potential mechanism affecting non-coding genome expression. Apart from highlighting the impact of the nuclear periphery in microRNA gene expression, this study introduces other factors that may modulate the subnuclear positioning or the expression.

Our results show that eight microRNA gene loci (*miR-181a1b1*, *miR-181a2b2*, *miR-181c*, *miR-142*, *miR-146a*, *miR-17-92*, *miR-155* and *miR-let7e*) are mainly monoallelically expressed and localized in the cell

nuclear periphery irrespective of the gene's transcriptional status or the cell's differentiation state. Moreover, our results show that the microRNA Microprocessor complex [comprised by DROSHA and DiGeorge syndrome critical region gene 8 (DGCR8) proteins also localizes in the nuclear periphery of T cells, indicating a functional role in the transcriptional regulation of microRNA genes.

We also found that microRNA gene loci were significantly enriched, compared to coding genes, for nuclear pore proteins (NUP) (such as NUP153 and NUP93) implying that nuclear pore proteins may be implicated in tethering microRNA gene loci to the nuclear periphery. The genome organizer protein SATB1 can affect the expression and the localization of microRNA genes in thymocytes but also in $CD4^+$ cells, showing its important role as the main chromatin organizer in T cells. Fianlly, the expression profile and perinuclear localization of microRNA genes are developmentally conserved while their localization outside constitutive lamin associated domains (cLAD) is cross-species conserved in *H. sapiens, M. musculus, D. melanogaster* and *C. elegans*.

In conclusion all the above data unveil a link between the 3D architecture of chromatin in T cells and its impact on the subnuclear localization and expression of microRNA gene loci. Our results pinpoint the impact of nuclear periphery in microRNA gene expression, shed light on chromatin organization at the nuclear periphery and allow for a better understanding of the T cell genome organization.

INTRODUCTION

1.1 Immune system

The immune system can create several strategies in order to combat infectious threats and maintain cellular homeostasis and physiology. The immune system activates a plethora of mechanisms in order to eliminate any kind of pathological microbes, toxic or allergenic proteins. The structure of the immune system in mammalian is quite complicated, since it consists of several organs such as bone marrow, spleen, thymus, Peyer's patches, tonsils, peripheral lymph nodes and specific cell types such as lymphocytes and macrophages (**Figure 1**).

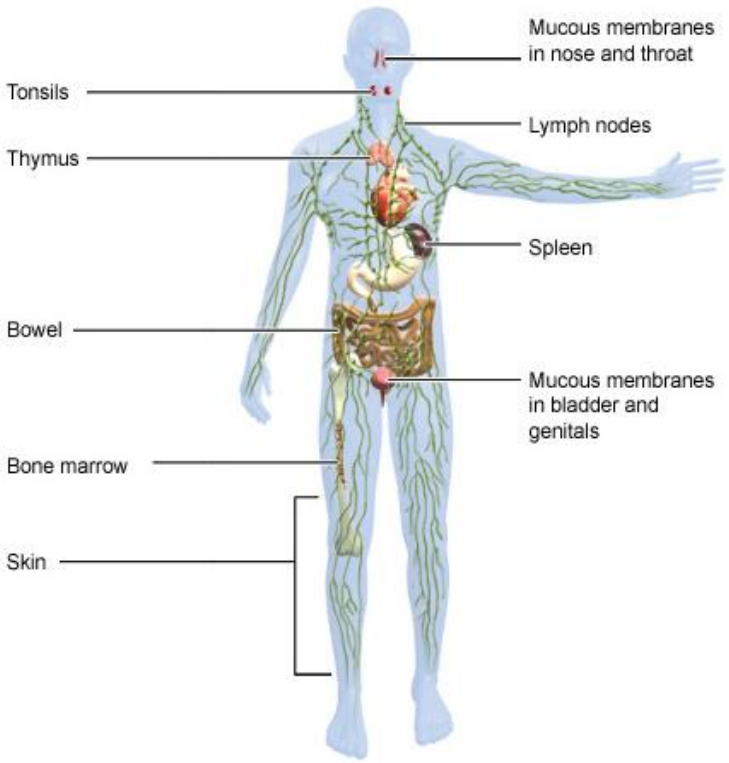

Figure 1. Primary and secondary organs of the human Immune system. Bone marrow and the thymus are considered as primary organs while the secondary lymphoid organs include the lymph nodes, the spleen, and the tonsils.

The immune system relies on two basic pillars: the innate and the adaptive immune response. Innate immunity (also termed native or natural immunity) mediates the initial phase of protection against infections, while adaptive immunity (also named specific or acquired immunity) develops more slowly and mediates the late stage in the specific defense against microbes. The adaptive and innate immune systems are equipped with sophisticated and integrated functions so that they can manage the proper function of the immune system.

Innate immunity: Phylogenetically, it is the oldest type of immunity and can be found in all multicellular organisms. It refers to all those protective factors that exist from the moment of birth and remain throughout one's life. The innate defense consists of several elements: a) Physical barriers, such as skin and mucous membranes in the body openings, which form external barriers, b) Soluble factors such as lysozyme, complement, acute phase proteins (inflammatory, response), humoral mediators, prostaglandins, peroxidases, nitric acid, leukotrienes, platelet activating factor, histamine and serotonin.

c) Phagocytes (monocytes, macrophages, neutrophils), natural killer cells (natural killers, NK), platelets, mast cells (tissue mast cells) (**Figure 2**).

Adaptive immunity: The adaptive immunity is an antigen-specific defense mechanism which leads to specific immunity, characterized by specificity and memory. There are two types of adaptive immunity, humoral and cellular, mediated by different molecules and cells which provide protection against extracellular or intracellular microorganisms, respectively. Humoral immunity is mediated by proteins called antibodies which are produced by B-lymphocytes. The defense against intracellular microorganisms that live and multiply within infected cells is named cellular immunity because it is mediated by T cells. The adaptive immune system has specific characteristics that separate it from other body systems such as specificity, memory and the distinguish between the body's own cells, recognized as "self," and foreign cells, or "non-self" (**Figure 2**).

1.2 Cells of the immune system

The innate immune system is composed of monocytes, eosinophils, basophils and neutrophils, while the adaptive immune system is composed of B-cells and T cells (cytotoxic T cells and helper T cells) **(Figure 2**). Macrophages and dendritic cells are the only cells of the immune system that can be part of both innate and adaptive immunity. All cells of the immune system derive from multipotent bone marrow progenitor cells known as hematopoietic stem cells. The pluripotent hematopoietic stem cell can generate two more specialized types of stem cells, a common lymphoid progenitor (CLP) that produces T and B lymphocytes responsible for adaptive immunity and a common myeloid progenitor (CMP) that produces macrophages, dendritic cells and mast cells. The major types of immune system cells are:

a) lymphocytes (T-cells, B-cells and large granular cells)

b) phagocytes (monocytes, macrophages and polymorphonuclear granulocytes)

c) Secondary cells (mast cells, platelets and endothelial cells).

Lymphocytes are considered as the basal cells of the specific immune response and consist 20-30% of blood cells. There are two major groups of lymphocytes:

A) B-cells, which when activated differentiate into plasma cells that secrete immunoglobulins or antibodies

B) T cells, which when activated can differentiate into cytotoxic T cells or helper T cells. Cytotoxic T cells, can kill other cells infected with viruses, whereas T helper cells activate other cells such as B cells and macrophages.

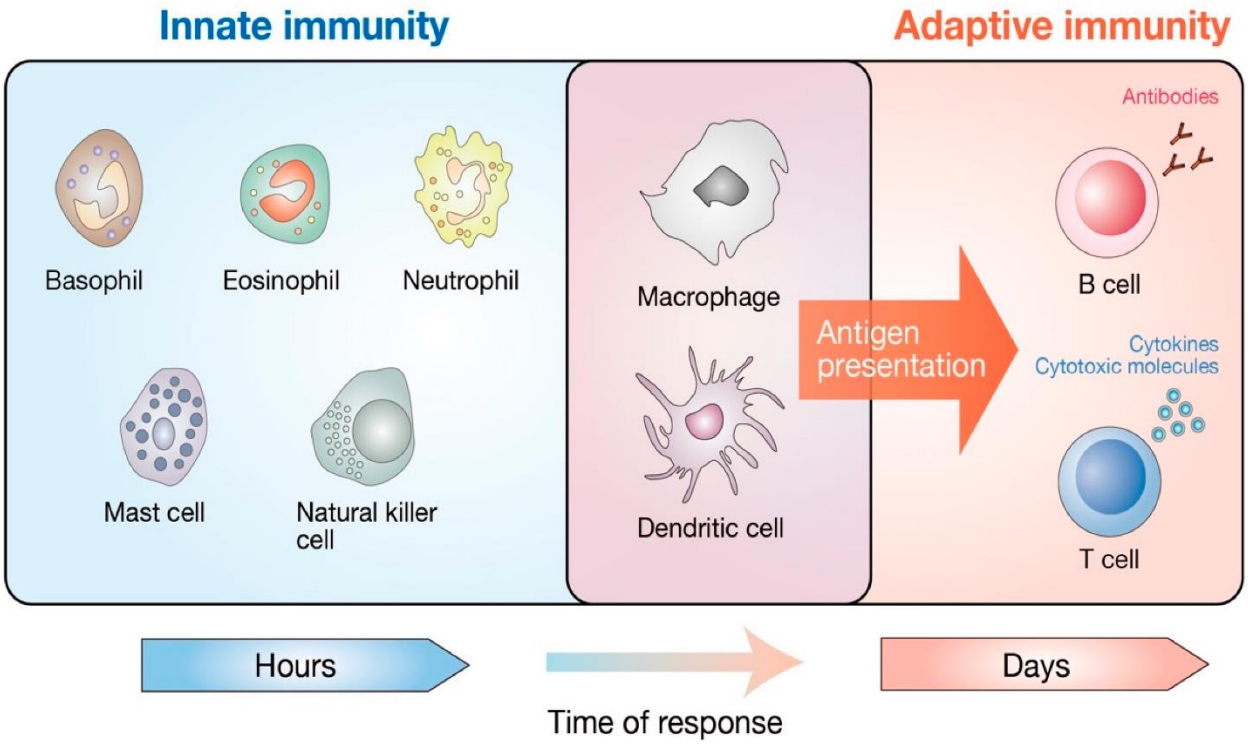

Figure 2. Cells of the mammalian immune system. Innate immunity is mediated through the basophils, eosinophils, neutrophils, mast cells, natural killer cells, macrophages, and dendritic cells by providing protection against bacteria, viruses, and cancer. The adaptive immune system is based on specificity and is mediated through B- and T- cells. The activation of adaptive immune system is mediated through the antigen presenting cells (APC) to antigen specific T and B cells. APCs include Macrophages and dendritic cells (DC) which are considered mediators on bridging the innate and adaptive immune responses (Yamauchi and Moroishi 2019).

1.3 T cell development and differentiation

Until now, two models of hematopoiesis have been described **(Figure 3**). The first model, which is also called the classical model, is based on the precise separation of the lymphoid and myeloerythroid lineages. Common myeloid progenitors (CMP) can produce myeloid or erythroid cells while common lymphoid progenitor cells (CLP) can generate only lymphoid cells. According to the classical model thymus is exclusively related to CLP cells and the generation of T, B and NK lineages. Instead, the revised model suggests that the thymus is composed of myeloid and lymphoid cells, which have the potential to differentiate to myeloid, T and other cell lineages (Lu et al. 2002). This revised model is based on the evidence that lymphoid primed multipotent progenitors (LMPP) can be detected in adult mice, suggesting a CMP/CLP-independent pathway to generate the lymphoid lineage in adult hematopoiesis (Adolfsson et al. 2005). Moreover LMPP cells express important lymphoid-associated genes e.g. recombination activating gene 2 (RAG2) and (DNA Nucleotidylexotrasnferase (DNTT), which are expressed prior to T and B cell lineage differentiation, indicating the existence of alternative pathways for lymphoid lineage commitment (Mansson et al. 2007).

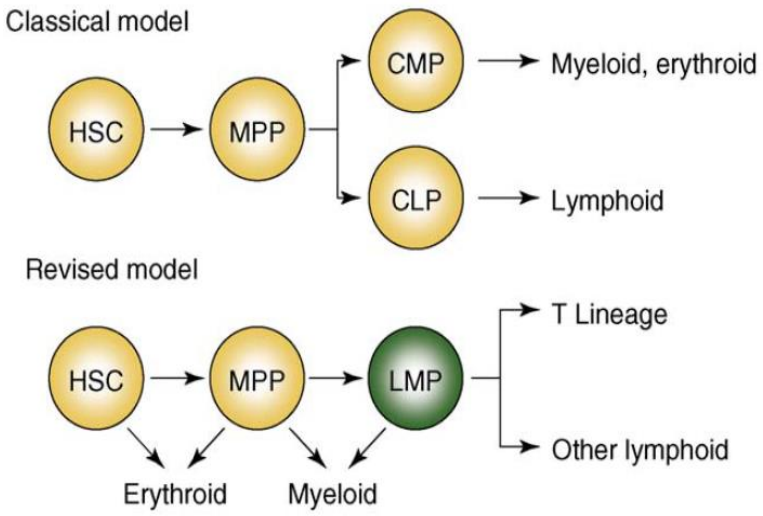

Figure 3. Two distinct models supporting the theory of hematopoiesis (Chi et al. 2009).

Hematopoietic progenitors (myeloid or lymphoid) leave the bone marrow and migrate to the thymus as early as embryonic day 11.5 (E11.5) in mice and the eighth week of gestation in humans (Takahama 2006). The microenvironment of the thymus is responsible for the restriction of multipotent lineages strictly to a T cell specific lineage. HSCs in adult bone marrow can be divided into two subtypes, long-term HSCs (identified as $lin^{-}ckit^{+}Sca1^{+}CD150^{+}CD48^{-}CD34^{-}Flt3^{-}$) and short-term HSCs (identified as $lin^{-}ckit^{+}Sca1^{+}CD150^{+}CD48^{-}CD34^{+}Flt3^{-}$) (Koch and Radtke 2011). The lineage commitment of HSCs to a specific T cell progenitor is a procedure which includes different stages of development and implicates strict limitations on the potential to intermingle with differentiation to other cell lineages. Despite the fact that all progenitors are generated in the bone marrow, the thymus is the primary organ being

responsible for the self-MHC-restricted and self-tolerant T cell repertoire (Rodewald 2008). The entrance of T-lymphoid progenitor cells is mediated via large vessels at the boundary between the cortex and medulla. During their migration through the cortex, the progenitor T cells first follow the T cell lineage. The next step includes the rearrangement and the expression of the T cell receptor (TCR) (α- and β-). After the TCR rearrangement, T cells undergo positive selection and acquire the ability to recognize self MHC. Right after the migration at the medullary regions, a second selection takes place where positively selected thymocytes are being negatively selected to eliminate any self-reactive thymocytes. Cells that survived both selections may at this point exit the thymus. The strictly organized trafficking of T cells in the well compartmentalized thymus requires the collaboration of different thymic stromal components, including epithelial cells (cortical and medullary epithelial cells), fibroblasts, endothelial cells, dendritic cells and macrophages emphasizing the fact that optimal development of T cells requires all these well synchronized cross talks between several thymic components (Manley et al. 2011).

1.3.1 Migration and selection

The migration of T cells through the thymus initially includes three basic stages: the double negative stage, the double positive stage and the single positive stage. The earliest T cell progenitors (ETPs) in the thymus are termed double negative (DN) due to the expression of CD25, CD44, CD117 and lack of expression for CD4 and CD8 cell surface markers. The double negative stage consists of four subtypes DN1, DN2, DN3 and DN4 (**Figure 4**). DN1 thymocytes ($CD24^{-/lo}CD27^{hi}$) compose only 0.01% of the total thymic cell pool and express high levels of CD117 (Allman et al. 2003).

Initially the DN1 cells receive stimulatory signals from the cortical thymic epithelial cells (cTEC) and fibroblasts, then migrate into the cortex and differentiate into DN2 cells ($D24^{+}CD25^{+}CD27^{int/hi}$ $CD44^{+}CD117^{+}$) (Petrie and Zuniga-Pflucker 2007). In order to express functional TCR chains, the rearrangement of TCRγ, TCRβ and TCRδ gene loci takes place at the DN2 stage of thymocyte development and it gets completed at the DN3 stage. Within the subcapsular zone, only DN3 thymocytes ($CD24^{+}CD25^{+}CD44^{lo}CD117^{lo}$) that express the TCRβ chain can differentiate into DN4 thymocytes ($CD117^{-/lo}CD44^{-/lo}CD25^{-/lo}$ $CD24^{hi}CD27^{hi}$). The successful expression of a functional TCR is considered as the last step of the T cell development. TCR expression leads to differentiation of DN4 cells to double positive cells (DP) ($\alpha\beta^{-}TCR^{+}CD4^{+}CD8^{+}$). At this point the TCRα chain is replaced with a newly rearranged TCRα chain, which can produce a complete αβ TCR. DP cells interact with cortical epithelial cells that

express a broad range of MHC class I and class II molecules, and then begin to migrate back towards the medulla. The DP cells will generate single positive (SP) cells, either $CD4^+$ ($CD4^+CD8^-$) or $CD8^+$ ($CD4^-CD8^+$) cells. A second selection (known as negative selection) takes place at the medulla where thymocytes with high affinity TCRs for self-antigens are being eliminated in order to avoid the generation of autoreactive T cells. TCR levels change from cortical DP cells to medullary SP cells. High intensity signals lead to apoptosis (clonal deletion) while low intensity signals enhance survival and differentiation (positive selection)

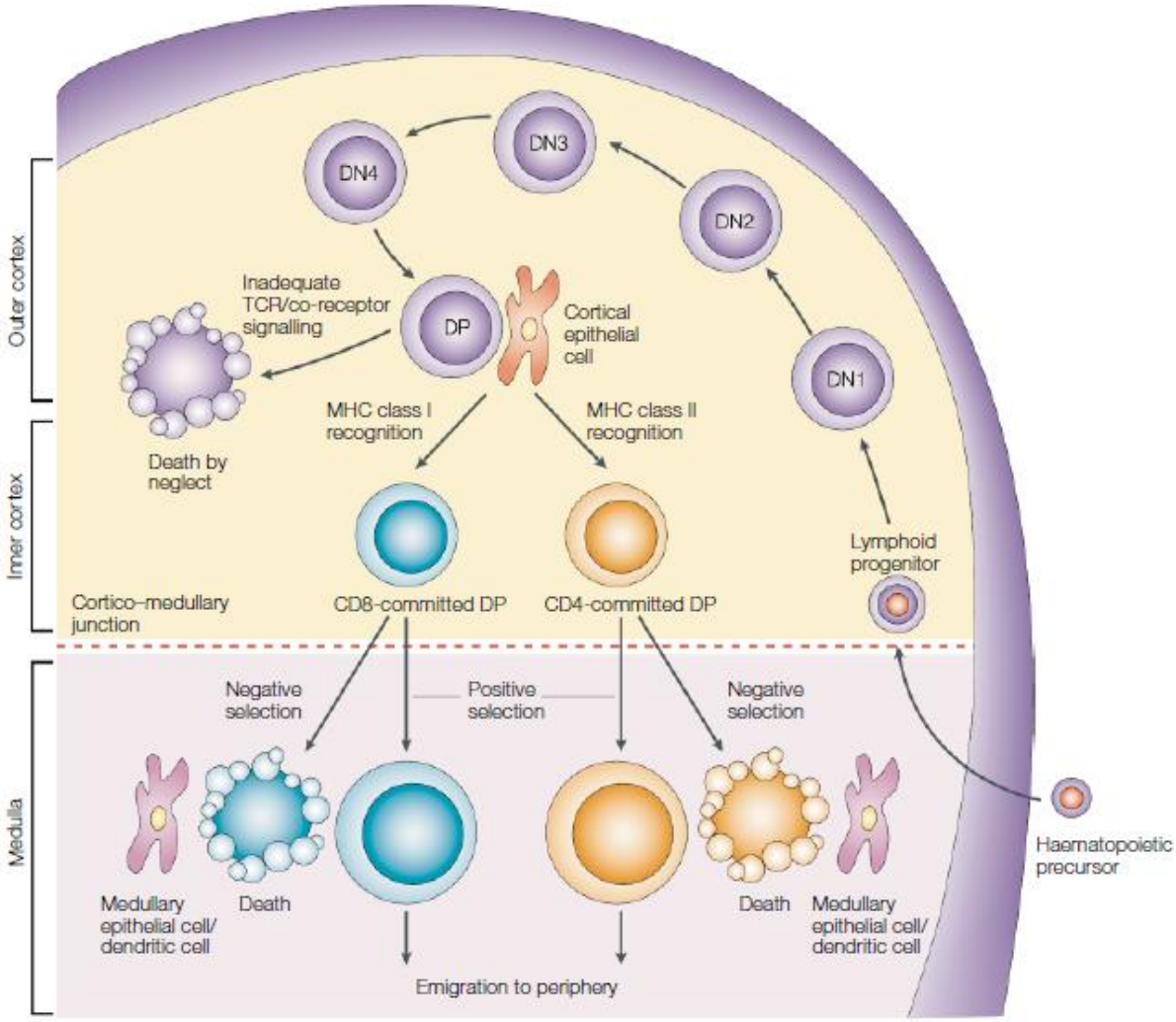

Figure 4. Overall depiction of T-cell development in the thymus (Germain 2002).

(Hogquist and Jameson 2014). The migration of single positive cells, $CD4^+$ or $CD8^+$ begins with their export from the medulla to the secondary peripheral lymphoid organs such as the spleen and the lymph nodes. At this point, single positive cells express surface markers such as $CD62L^{hi}$ and $CD45RB^{hi}CD44^{lo}$ and are characterized as naïve due to the lack of prior encounter with antigen.

Single positive cells are also called as quiescent (resting) cells because they do not divide or are implicated in any other immune response (effector cells). During T cell development and maturation there are several checkpoints that control these processes at the transcriptional level. The Notch signaling pathway and transcription factor GATA3 play a crucial role in generating ETP. Studies where either Notch signaling (Sambandam et al. 2005) or GATA3 (Hosoya et al. 2009) were repressed showed damage of ETP and a defect on developing DN1 cells. RUNT-related transcription factor (RUNX), can control the expression of CD4 and CD8 genes. These factors can bind to the intronic transcriptional silencer of the CD4 gene (Taniuchi et al. 2002) and to the enhancer of CD8 locus (Sato et al. 2005). Another transcription factor that plays a central role in T cell development is the *Zbtb7b* gene which encodes the Th-inducing POZ Kruppel factor (ThPOK). The RUNX complex was shown to interact with *Zbtb7b* at two different regions, at the distal regulatory element (DRE) (Setoguchi et al. 2008) and at the proximal regulatory element (PRE) (He et al. 2008). DRE and PRE are both *cis*-acting regulatory elements in the *Zbtb7b*locus. DRE is a 500 base pair region which is located upstream of exon 1a and possesses a transcriptional silencer activity. PRE is located downstream of exon 1b shows transcriptional enhancer activity. Furthermore, it has been reported that Myc-associated zing finger-related factor (MAZR) repress CD8 expression (Bilic et al. 2006) while Myb promotes $CD4^+$ lineage development (Maurice et al. 2007). Two more transcription factors, GATA3 (Wang et al. 2008) and TOX (thymocyte selection-associated high-mobility group box transcription factor) (Aliahmad and Kaye 2008) were also implicated on the transcriptional control of T cell development by promoting ThPOK expression.

1.3.2 $CD4^+$ T cell lineage plasticity and differentiation

Immature $CD4^+$ T cells have the ability to differentiate into effector subtypes of T helper cells when the TCR encounters its cognate antigen, which is bound to MHC class II molecules in antigen presenting cells. Firstly, two effector CD4 cell sybtypes T_H1 and T_H2 were identified by Mosmann and Cofmann (Mosmann and Coffman 1989). Naive $CD4^+$ T cells can differentiate into T_H1 cells in the presence of IL-12 and IFNγ cytokines with the activation of the master regulator transcription factor T-bet via STAT4 signaling. T_H2 cell differentiation includes the expression of IL-4, IL-5, IL-6, IL-9, IL-10, IL-13, IL-25 and IL-33, which promote the activation of STAT6 and GATA3.

Since the 1980s the range of T cell subtypes has broadened and other subtypes are characterized including T_H17 (Korn et al. 2009), T_H9 (Schmitt et al. 2014), T_H22 (Trifari et al. 2009), follicular helper (Tfh) (Crotty

2011), thymically derived and peripherally induced regulatory T cells (tT_{Reg} and pT_{Reg}) (Elkord 2014) (**Figure 5**). Pro-inflammatory cytokines IL-6 and IL-23 in combination with the immunosuppressive cytokine TGF-b drive the differentiation of naïve $CD4^+$ T cells towards T_H17 cells by activating STAT3 and RORγ (Korn et al. 2009). TNFα in collaboration with the pro-inflammatory cytokine IL-6, promote the activation of Aryl Hydrocarbon receptor (AHR), and lead to differentiation of T_H22 cells (Trifari et al. 2009). IRF4 and PU-1 induce the differentiation towards T_H9 cells. These genes can be activated by the combination of the immunosuppressive cytokines TGF-b and IL-4 (Schmitt et al. 2014). Activation of Bcl-6 is mediated by the cytokines IL-6 and IL-2, which induce the differentiation of naive $CD4^+$ T cells into TfH. $Foxp3^+$ regulatory T (Treg) cells maintain immune homeostasis by limiting different types of inflammatory responses. The cytokines IL-10, IL-35 and TGF-β promote the induction of T_{regs} cells which are controlled by the transcription factor Foxp3. Two more subsets of T_{regs} exist in immune system including Tr1 regulatory cells (IL-10-producing CD4 T cells) (Zeng et al. 2015) and T_H3 (TGFβ-producing CD4 T cells) (Weiner 2001).

It has been reported that apart from the differentiation of CD4 cells into helper subsets, TH cells also show a heterogeneity and plasticity of trans-differentiation within the T helper state (Shi et al. 2008; Bending et al. 2009; Komatsu et al. 2009; Lee et al. 2009; Wei et al. 2009; Hegazy et al. 2010; Upadhyaya et al. 2011; Gallo et al. 2012; Miyao et al. 2012). At early stages of TH differentiation, each subset can be easily reprogrammed into different lineages on receiving the appropriate stimulus (O'Shea and Paul 2010). However, this is not the case for Th17 where at later stages they are more plastic than T_H1 and T_H2 cells, suggesting that T_H17 cells may represent cells that are not terminally differentiated (Zhu and Paul 2010). Understanding the mechanisms of reprogramming through one TH cell subtype to another would have enormous implications for immune intervention. Research in the de-differentiation (reprogamming of TH cells back to naïve stage) and re-differentiation of T cells would be promising in the future to possibly treat severe autoimmunity diseases and cancer.

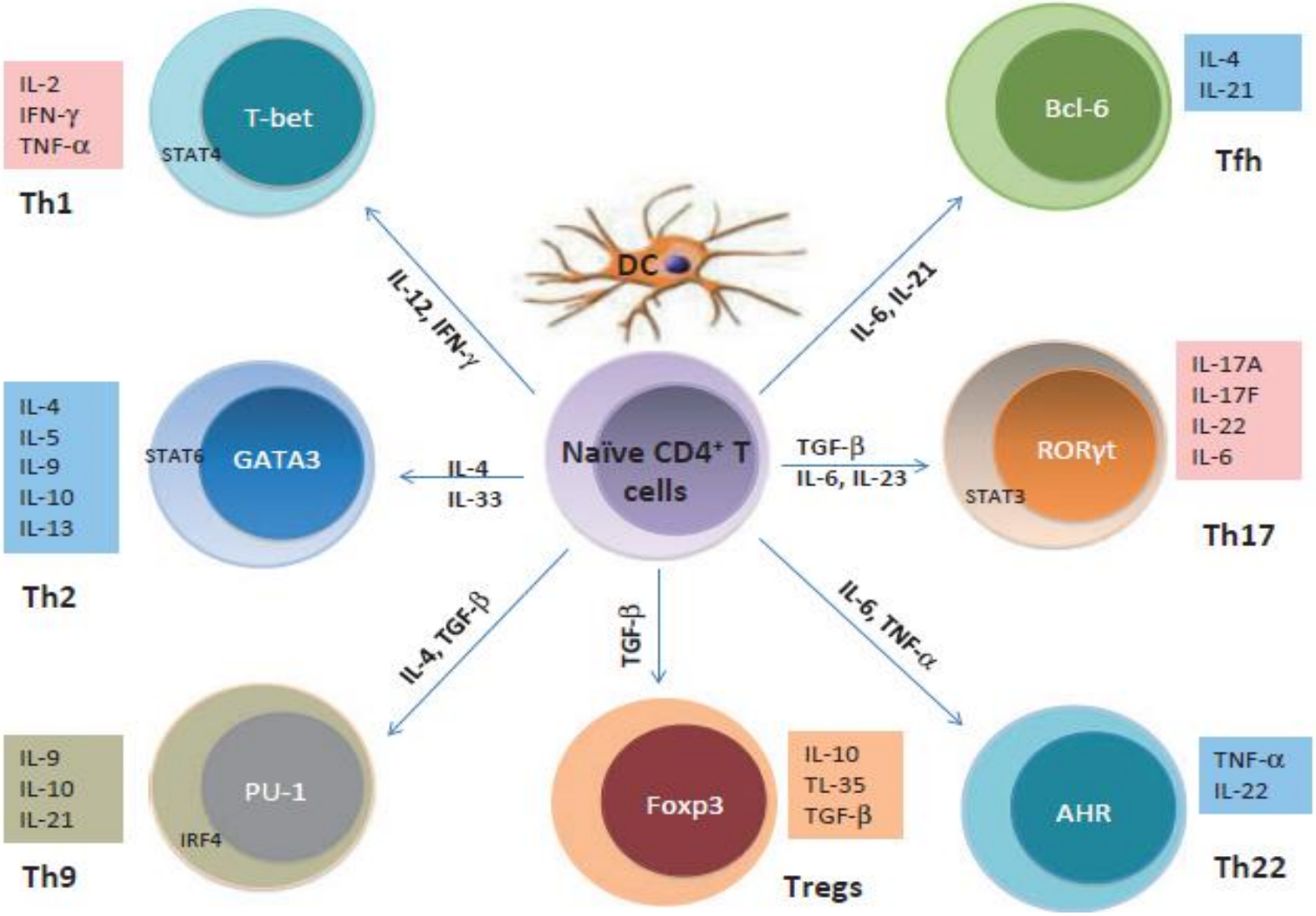

Figure 5. Schematic overview of T cell differentiation. ((Liu et al. 2013)

1.4 The non-coding genome

The genomes of large multicellular eukaryotes are mostly comprised of non-protein coding DNA. According to the results of the Human Genome Project (1990-2003), the catalog of human protein-coding genes listed a total of ≈24,500 putative protein-coding genes. This number is not correct and it continues to fall. Today, at least 19,950 and 22,018 protein-coding genes have been verified in human and mouse respectively, which consist 1-2% of the whole genome. The rest of the genome, the non-coding genome, named in the past as "dark matter" or "junk DNA" is suggested that may regulate and fine tune the expression of coding genes. In 2012, data from the Encyclopedia of DNA Elements (ENCODE) project proposed that around 80% of the non-coding genome has a function. However it has been proved experimentally that around 10-20% of the non-coding genome has a functional role on the coding genome (Consortium 2012).

At steady state, the mammalian cell RNA is composed of ribosomal RNA (rRNA) and transfer RNA (tRNA). Except from these basic RNA molecules, several other RNAs have been characterized such as long non coding RNA (lncRNAs) and small non coding RNAs. Small non coding RNAs are defined by their length (20–30 nucleotides), their association with Argonaute family proteins (AGO family proteins) and they are classified into three classes in animals: microRNA (microRNA), siRNA and PIWI-interacting RNA. Main classes of multiple types of non-coding RNAs that have been discovered at present are shown in **Figure 6**. In brief, they include the following groups:

a) Long non-coding RNAs (lncRNA's) >200nt are autonomously transcribed RNAs that do not encode for a protein, are often capped and polyadenylated and can be nuclear, cytoplasmic or both (Yao et al. 2019).

b) Micro RNAs (microRNAs) ~ 20-22nt, that in complex with AGO protein use seed sequences near their 5' end to base pair with a target mRNA to induce translational repression or mRNA decay (Bartel 2018).

c) The small nuclear RNAs (snoRNA's) which have a size of ~70nt are essential for pre-rRNA processing or modification by serving as a guide RNA to direct a bound enzyme to either 20-O-methylate or pseudouridylate a complementary sequence in rRNA (Maden and Hughes 1997).

d) PIWI-associated RNA (piRNA's), ~27nt RNA that directs the modification of chromatin to repress transcription (Seto et al. 2007).

e) Small interfering RNA (siRNA's) ~22nt, product of DICER as a cleavage of dsRNA, which by interacting with AGO protein can induce cleavage of a perfectly-complementary target RNA (Hamilton and Baulcombe 1999; Elbashir et al. 2001).

f) Transcriptional enhancer element RNA (eRNA), ~200–500 nt, which binds Mediator in order to enhance transcription and can act as scaffolds, by regulating the 3D architecture of chromosomes at the proximity of their transcription starting site (TSS) (Lai et al. 2013).

g) circular RNA which due to the lack of 5' and 3' ends are quite stable and can regulate microRNAs in mammalian cells (Wilusz and Sharp 2013).

All the aforementioned regulatory RNA molecules play a crucial role in essential biological processes, including chromatin/nuclear organization (snRNA, snoRNA and lncRNA), mRNA splicing (snRNA), ribosome biogenesis (rRNA), translation (tRNA) and regulation of mRNA levels (siRNA and niRNAs). These RNA regulatory elements are considered to be an additional layer of the circuitry controlling gene expression in the nucleus, by modulating transcription or via post-transcriptional mechanisms. As the vast majority of the mammalian genomes can be transcribed and the growing evidence that the non-coding genome have a functional role on controlling the protein-coding genes, then maybe the term "junk DNA" should be reconsidered as functional RNA that can serve as a regulator/controller of the coding genome.

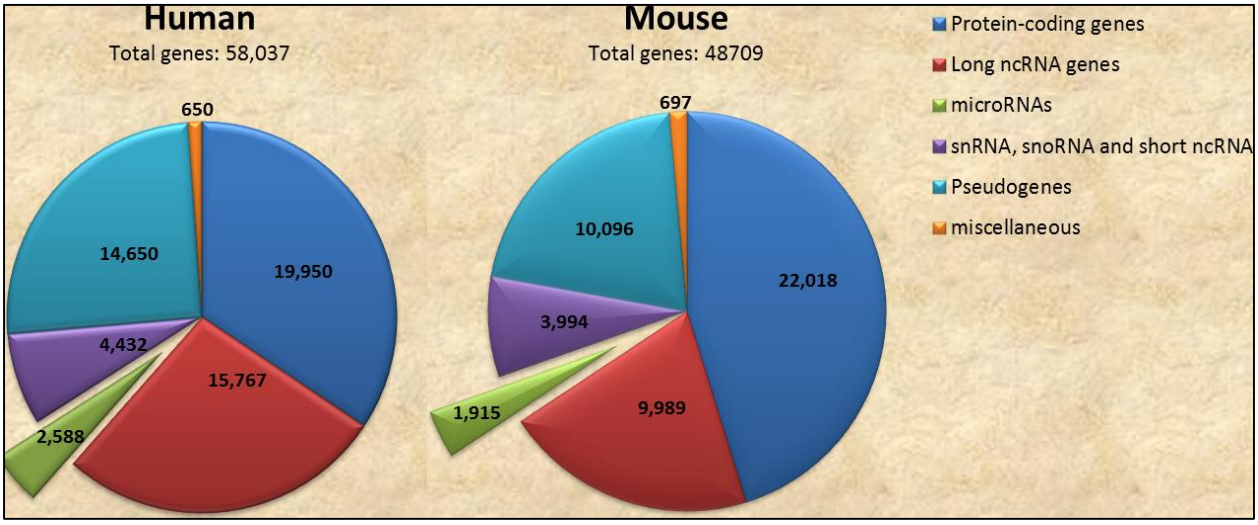

Figure 6. Pie charts showing the genome-wide distribution of protein- and non-coding genes in the human and mouse genomes. Numbers shown are calculated from the GENCODE version M11 (March 2016 freeze, GRCm38 and GRCh38 - Ensembl 86; http:// www.gencodegenes.org)

1.5 microRNAs

MicroRNAs are small (20-25 nucleotides in length) endogenously expressed RNAs that regulate gene expression, found to be evolutionarily conserved between animals and plants (Fabian et al. 2010). microRNA genes constitute one of the most abundant gene families, and are widely distributed in animals, plants, protists and viruses (Griffiths-Jones et al. 2008). *Lin-4* was the first small RNA that was discovered in 1993 by genetic screens in nematode worms (Lee et al. 1993). Since then, the number of microRNA genes that are being annotated to microRNA database (http://www.mirbase.org/) has expanded. The latest release of the miRBase has catalogued 466 microRNA genes from *D. melanogaster*, 434 microRNA genes from *C. elegans*, 1915 microRNA genes from *M. musculus,* 427 microRNA genes from *A. Thaliana* and 2588 microRNA genes from *H. sapiens.* microRNAs have also been reported in sponge and sea anemone (Grimson et al. 2008). The functional importance of many of these microRNA annotations still remains to be determined (Chiang et al. 2010; Kozomara and Griffiths-Jones 2014). MicroRNAs are implicated in the regulation of several developmental and physiological processes in plants, fungi, worms and animals. More than 60% of human protein-coding genes contain at least one conserved microRNA-binding site, which indicates that probably most of the protein-coding genes may be under the control of microRNAs (Friedman et al. 2009). Thus, it is not surprising that the biogenesis and function of microRNAs themselves are tightly regulated, and their dysregulation is often associated with human diseases, including developmental diseases, neuronal diseases and cancer (Lang and Shi 2012; Lujambio and Lowe 2012). Intracellularly, microRNA can regulate transcription factors that are related with extracellular signaling proteins, epigenetic factors, chromatin remodelers, methylation factors, splicing factors and transcription factors (Bartel 2009). More specifically, they can mediate the stem cell differentiation (Gangaraju and Lin 2009), haematopoiesis (Chen et al. 2004), cardiac and skeletal muscle development (Cordes and Srivastava 2009), neurogenesis (Shen and Temple 2009), insulin secretion & cholesterol metabolism (Rottiers and Naar 2012), immune response & autoimmune diseases (Ceribelli et al. 2012; Chen et al. 2013) and cancer (Lu et al. 2005; Volinia et al. 2006; Xu and Li 2007; Lujambio and Lowe 2012). Recently, microRNAs field has developed more applications. Differences in mRNA expression profiles between physiological and pathological conditions, have led to the use of several microRNAs as prognostic biomarkers of many diseases (Llaurado et al. 2014; Georgi et al. 2015; Xia et al. 2015) .

1.5.1 Evolution of microRNAs

Although the functional roles of microRNA genes on transcriptional and post-transcriptional level are molecularly well understood, there are still open questions regarding the molecular evolution of these small genes. In order to study the evolution of microRNA genes, global synteny map and phylogenetic analysis in more than 80 species have shown that microRNAs are mainly derived from transposable elements (TEs). The number of microRNAs increases as their morphological complexity increases. Rodents and primates seem to have the highest percentage of microRNAs. The initial reports about the origin of microRNA was published in 2005 and it demonstrated that microRNAs have originated from TE and formed through rounds of segmental duplication (Smalheiser and Torvik 2005). MicroRNAs are localized at the intersection of related convergent TEs (Borchert et al. 2006). A large proportion of the mammalian microRNA genes have paralogues (for example, the let-7e microRNA gene family has 12 loci in humans) which may probably the result of gene duplications (Hertel et al. 2012).

So far three basic models of evolution of plant and animal microRNAs have been described (Niwa and Slack 2007; Axtell et al. 2011; Berezikov 2011; Nozawa et al. 2012). The first model supports the idea of intragenomic duplications-derived microRNA genes. This model is quite common in plants (Allen et al. 2004). The second model describes that the inverted repeats and hairpins might also have emerged from initially long transcripts with unstructured sequences. This appears to be the dominant mode of microRNA emergence in animals (Bartel and Chen 2004). The third model suggests evolution of microRNA genes from long RNA degradation products (Axtell et al. 2011). In 2012, data from next generation sequencing in combination with computational *in silico* meta-analysis showed that about 15% of the annotated microRNA (genomes from human, mouse, chicken, fungi, worms and plants) had significant sequence homology to defined TEs (Cai et al. 2012; Shao et al. 2012; Tempel et al. 2012; Wen et al. 2012). As reviewed by Roberts in 2014, elements such as Long Terminal Repeat (LTR) retrotransposons, non-LTR retrotransposons, Long Interspersed Elements (LINEs), Short Interspersed Elements (SINEs), satellite and noncoding RNA sequences, such as snoRNAs and tRNAs, might also have contributed in the generation of microRNA genes (Roberts et al. 2014). An additional potent mechanism that has been reported regarding the evolution of human microRNA genes (hsa-mir-548 locus contains seven microRNA genes), includes their origin from Made1 transposable elements (Piriyapongsa and Jordan 2007). The RNA of Made1 transposable elements forms a stable hairpin loop structure that is processed into mature RNA by the RNAi machinery, suggesting an evolutionary link between transposable elements, siRNA and microRNA

(Piriyapongsa and Jordan 2007) (Liang et al. 2012). Other mechanisms that describe the *de novo* generation of microRNA genes are the duplication of existing microRNA genes or the unstructured transcripts that originate from introns and present microRNA-like hairpins. Non-coding RNA structures such as tRNA and small nucleolar RNA (snoRNA), can lead to novel microRNAs through the microRNA-like hairpin structures. Furthermore, it has been shown that antisense transcription of microRNAs can also generate novel mature microRNAs (Berezikov 2011; Scott and Ono 2011). Finally, the ancient origin of the microRNA genes, the high rate of conservation and their capacity of controlling transcription suggest that microRNAs may be critical in the evolution of the organismal complexity.

1.5.2 Genomic locations and gene structure of micro*R*NAs

According to their genomic structure and location microRNA gene loci can be characterized either intragenic or intergenic. More than 50% of microRNA genes are located within protein coding genes (Rodriguez et al. 2004; Ozsolak et al. 2008; Saini et al. 2008; Monteys et al. 2010; He et al. 2012). Intragenic microRNAs are located within introns or exons of other genes (host genes) in a sense or antisense strand orientation, in either coding or non-coding genes and are regulated by promoters of the hosting genes (Rodriguez et al. 2004). Intergenic microRNA genes are located between other genes, they have their own distinct promoters and they can be transcribed as single or as polycistronic units (Kim and Kim 2007). Micro RNAs can be either intronic or exonic according to their genomic localization (**Figure 7**). MicroRNA genes can be located in non-coding transcripts, such as miR-15a-16-1, which is located in the intron of a well-defined non-coding RNA gene, *DLEU2* (Tam 2001; Calin et al. 2002). Micro RNA genes can be exonic in non-coding transcripts, such as miR-155 which is located within the *BIC* gene that encodes a *non-coding RNA* (Calin et al. 2002). Intronic microRNAs can be located either in protein-coding genes such as miR- 25-93-106b cluster (which is located within the intron of DNA replication licensing factor MCM7). Exonic microRNA genes are located in protein-coding transcripts (e.g. miR-985 hairpin is found within the last exon of calcium voltage gated channel auxiliary subunit gamma 8 (CACNG8) mRNA (Kim et al. 2009). Although the sense orientated microRNA genes are regulated by the promoters of hosting genes, it has been reported that in *C. elegans* ~50% of the same-strand intronic microRNAs contain long regions of extensive conservation exactly upstream of the pre-microRNAs. These regions, which seem to be highly conserved between nematodes, show promoter properties and produce specific expression patterns that are different from the host gene expression patterns (Isik et al. 2010). Recently, another category of

microRNA genes was discovered, the divergent pri-micro RNA. These microRNAs were found in human and mouse and originate from divergent transcription in promoters of active genes or partially overlapping with annotated long non-coding RNAs (Georgakilas et al. 2014).

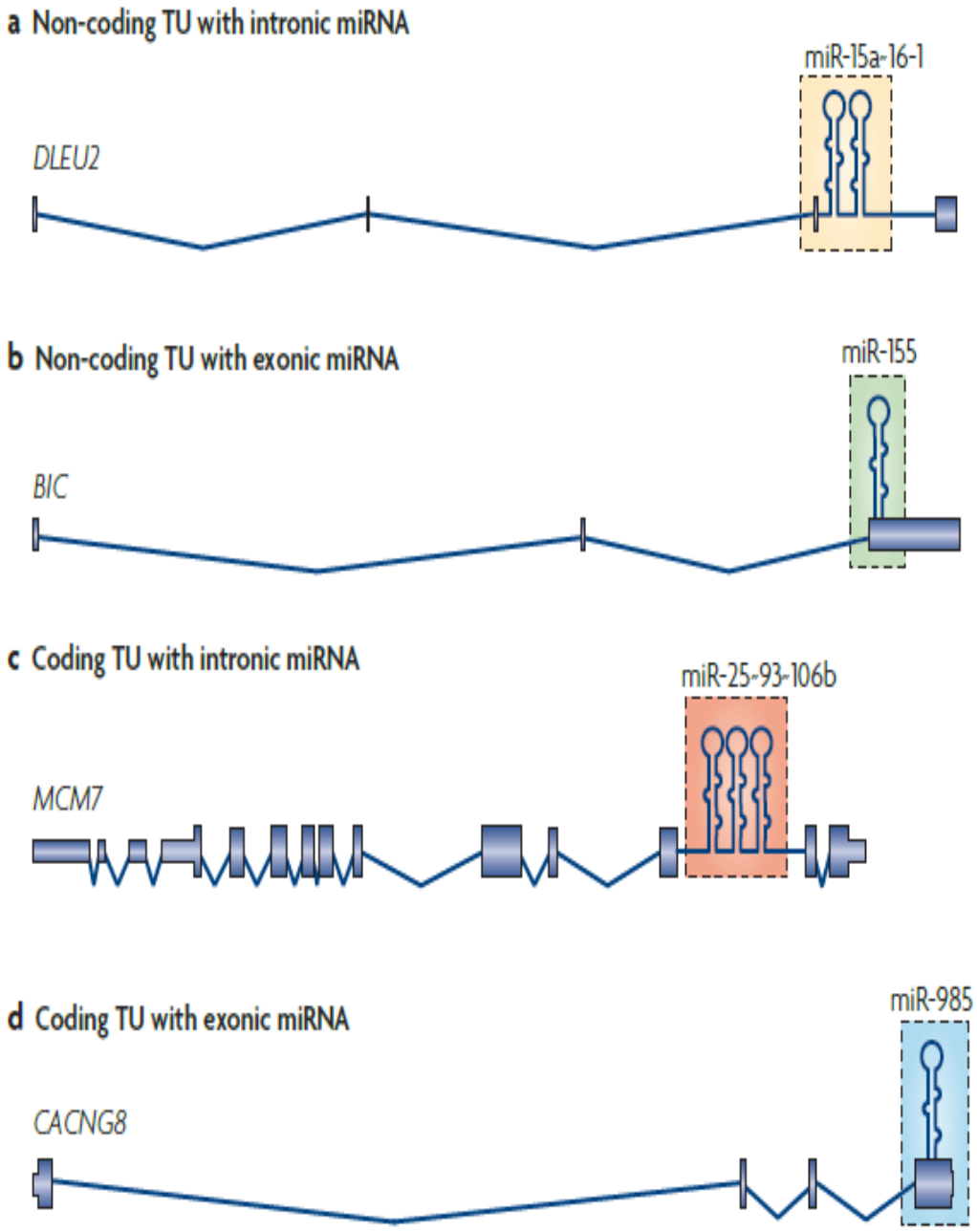

Figure 7. Schematic depiction of *MIR* genes genomic locations depicting (a)a non-coding transcription unit with intronic microRNA, (b) a non-coding transcription unit with exonic microRNA, (c) a coding transcription unitwith intronic microRNA and (d) a coding transcription unit with exonic microRNA (Kim et al. 2009).

1.5.3 microRNA biogenesis

The canonical biogenesis of microRNAs (microRNAs) includes a three-step processing pathway to yield approximately 20-22 nucleotide small RNAs that regulate gene expression at the post-transcriptional level. Initially, microRNA genes are transcribed into primary microRNAs (pri-microRNAs) by RNA polymerase II (Pol II) (Cai et al. 2004; Lee et al. 2004a). These primary transcripts usually are more than 1kb long and they contain a stem loop (**Figure 8**) where the mature microRNA is located. pri-microRNA consists of a stem of 33–35bp, a terminal loop and single-stranded RNA segments at both the 5' and 3' sides. Majority of microRNA genes are transcribed by RNA pol II, although it has been reported that RNA Pol III transcribes several human and viral microRNAs (Pfeffer et al. 2005; Borchert et al. 2006).

DROSHA cleavage: The maturation of microRNAs is initiated upon cleavage at the stem of the hairpin domain by the ribonuclease III DROSHA (RNase III). DROSHA interacts with an RNA binding protein (RBP) termed Di George syndrome critical region gene 8 (DGCR8) (named PASHA in *D. melanogaster* and *C. elegans*) in order to form the Microprocessor complex (Yeom et al. 2006). The Microprocessor complex through the DGCR8, recognizes the single-stranded RNA tails, the stem of ~35 bp in length and the terminal loop of the primary microRNA (pri-microRNA). DROSHA cleaves the hairpin at approximately 11bp away from the 'basal' junction between single-stranded RNA and dsRNA, and approximately 22 bp away from the 'apical' junction linked to the terminal loop (Zeng et al. 2005; Han et al. 2006; Quick-Cleveland et al. 2014). The human DROSHA protein contains two DGCR8-binding sites, one on each RNase III domain (RIIID), which mediate the assembly of the Microprocessor complex. The stem loop contains 33 bp (11bp lower bp and 22 upper bp) (Kwon et al. 2016). DGCR8 interacts with the stem and the apical elements of primary transcript to ensure fidelity of processing and interacts with DROSHA to process the cleavage. Except from acting as a "scissor", it has been demonstrated that DROSHA can also recognize and measure the basal segments of the stem loop (11bp in both sides of the stem loop) (Nguyen et al. 2015). Pri-microRNAs are processed into hairpin structures ~65-70nt long, known as precursor microRNAs (pre-microRNAs) (Lee and Kim 2007). It has been reported that the canonical biogenesis of intronic microRNAs can be a co-transcriptional process before splicing (Morlando et al. 2008). Initially, the spliceosome gathers the introns in order to be spliced while DROSHA cleaves the microRNA hairpin as it is shown in **Figure 6**. Finally, the pre-mRNA transcripts lead to production of mature mRNA for protein synthesis, while the pre-microRNA undergoes the microRNA pathway.

Nuclear export: The transport of pre-microRNAs from the nucleus to the cytoplasm is mediated by Exportin 5 (EXP5) (Bohnsack et al. 2004; Lund et al. 2004). EXP5 is a RanGTP-dependent dsRNA-binding protein, a member of nuclear transport receptor family and can recognize the ~2-3nt overhang before the stem loop (Yi et al. 2003; Bohnsack et al. 2004). Initially, EXP5 was recognized as an export factor for tRNAs. EXP5 interacts with Ran-GTP in the nucleus and releases the cargo after the hydrolysis of GTP in the cytoplasm (Okada et al. 2009).

DICER cleavage: After being transferred to the cytoplasm the pre-microRNA is being cleaved near the terminal loop for a second time by another RNase III enzyme named DICER (Ketting et al. 2001; Knight and Bass 2001). DICER binds to pre-microRNA with a preference for a two-nucleotide-long 3′ overhang that was initially generated by DROSHA (Zhang et al. 2004). DICER collaborates with two other proteins, the TAR RNA-binding protein (TRBP) and Protein Activator of the interferon-induced protein kinase (PACT) (Tsutsumi et al. 2011). After the DICER cleavage the 20-22bp dsRNA is released in the cytoplasm (Hutvagner et al. 2001; Lee et al. 2004b).

miRISC complex: after the DICER cleavage, when the loop is removed, the dsRNA is then loaded to the Argonaute (AGO) complex in order to form the microRNA-induced silencing complex (miRISC) (Hammond et al. 2001). Accumulation of RISC complex induces two steps: the loading of the dsRNA and the unwinding of the duplex (Kawamata and Tomari 2010). In flies, microRNA duplexes are loaded into AGO1 and AGO2, while in humans the microRNA duplexes are loaded into AGO1, AGO2, AGO3 and AGO4 (Forstemann et al. 2007; Su et al. 2009). The strand that remains with the AGO protein is the mature strand (usually the strand with the unstable terminus at the 5') and it is named the *guide strand* or the mature microRNA. Thermodynamic studies have demonstrated that the strand which is chosen to load into the miRISC is the strand with unstable base pairs at the 5' end (Khvorova et al. 2003; Schwarz et al. 2003). Furthermore it has been reported that one additional selection criteria of the Ago proteins is the first nucleotide, as AGO select as guide strands with a U at nucleotide position 1 (Kawamata et al. 2009; Okamura et al. 2009). The other strand which is called *the passenger strand* or the microRNA* is being degraded. Strand selection is not completely strict, as it has been shown that both strands can be selected with different frequency. This phenomenon it is called "arm switching" and it has been reported in several tissues (Chiang et al. 2010; Chak and Okamura 2014). One example is the miR-142, where miR-142-5p is a dominant isoform in ovaries, testes and the brain, whereas miR-142-3p is found more frequently in embryonic and newborn tissue samples (Wu et al. 2009; Ha and Kim 2014).

Non canonical biogenesis of microRNA: Apart from the canonical biogenesis pathway microRNA molecules can be generated from alternative non-canonical pathways (Cheloufi et al. 2010; Miyoshi et al. 2010; Havens et al. 2012; Xie and Steitz 2014). High-throughput sequencing experiments in thymocytes and ES cells in DROSHA, DGCR8 and DICER deficient mice have shown that microRNA can be produced in a Microprocessor or DICER- independent process (Chong et al. 2010) (Babiarz et al. 2008). The most well studied pathway is the spliceosome-dependent mechanism. Small intronic RNAs, characterized as mirtrons do not require cleavage by DROSHA. Splicing of these RNAs can generate the mature mRNA or branched pre-mirtrons. After splicing of host mRNAs, the lariat is debranched and refolds into a short stem–loop structure that resembles a pre-microRNA. Trimming of the debranched pre-mirtrons can avoid the DROSHA processing by leading directly to DICER in order to be further processed (Berezikov et al. 2007; Okamura et al. 2007; Ruby et al. 2007; Flynt et al. 2010). Microprocessor-mediated processing is also bypassed in cases where small RNAs can generate from different non-coding RNAs and their biogenesis is DICER-dependent. It has been reported that small nucleolar RNAs (snoRNAs) (Ender et al. 2008), tRNA-like precursors (Babiarz et al. 2008) and small nuclear RNA-like viral RNAs (Cazalla et al. 2011) can generate microRNA genes. Surprisingly, although most non-canonical biogenesis mechanisms are DICER dependent, biogenesis of miR-451 does not require DICER processing (Cifuentes et al. 2010; Yang et al. 2010). DROSHA processing of miR-451 produces a small hairpin with a short stem of 18bp, which is too short to be cleaved by DICER. miR-451 is directly loaded onto AGO-2 where it is sliced in the middle of its 3′ strand, (AGO-cleaved pre-mir-451 (ac-pre-mir-451)). The 3′ end of ac-pre-mir-451 is trimmed by Poly(A)-specific ribonuclease (PARN) and produces the mature *miR-451*, which is ~23 nucleotides in length (Cifuentes et al. 2010; Yoda et al. 2013; Ohno et al. 2016). Furthermore, it has been demonstrated that in vertebrates most of the members of the let-7 family carry a shorter (1-nucleotide long) 3′ overhang. These pre-microRNAs are extended by 1 nucleotide through monouridylation mediated by terminal uridylyl transferases (including TUT2, TUT4 and TUT7) (Ha and Kim 2014) .

1.5.4 Non canonical functions of Microprocessor and DICER

DROSHA and DICER proteins are the most well studied members of the RNAse III family. It has been shown that except from their central role in the biogenesis of microRNAs these two proteins have also non-canonical functions (Burger and Gullerova 2015; Kim et al. 2016; Cirera-Salinas et al. 2017; Kim et al. 2017; Rolando and Taylor 2017; Pong and Gullerova 2018). Genetic evidence from recent development of

mutant mouse models for DROSHA and DICER has increased the discovery of microRNA-independent functions for both proteins.

As mentioned previously DROSHA recognizes the stem loop structure of the pri-microRNAs. The first microRNA-independent role of DROSHA characterized is the recognition and the cleavage of mRNA stem loop structure. DROSHA recognizes and cleaves the stem-loop structures within the 3' UTR of DGCR8 and Neurogenin2 (Ngn2) (Knuckles et al. 2012) (Han et al. 2009). In addition, genetic ablation of *Drosha* gene causes a defective myelopoieisis. It has been reported that DROSHA deficiency at the DP thymocyte stage results in T lymphopenia, T cell activation, spontaneous inflammatory disease and premature mortality of the mice (Chong et al. 2008). Moreover, DROSHA deficiency represses the development of DCs at an early stage, by repressing the expression of two mRNAs encoding inhibitors of myelopoiesis in early hematopoietic progenitors (Johanson et al. 2015). Recently DROSHA has been characterized as an interferon-independent antiviral factor, as it was shown that deficiency of DROSHA leads to increased RNA virus replication (Shapiro et al. 2014). Furthermore, DORSHA/DGCR8 complex regulates HIV-1 transcription through an RNAi-independent process. The Microprocessor lead to repression of transcription by recruiting factors such as helicase senataxin (Setx) and 5'-3' Exoribonuclease 2 (Xrn2) and the exosome complex exonuclease (Rrp6), in order to repress transcription (Wagschal et al. 2012; Harwig et al. 2016).

DICER has also been reported of having microRNA-independent functions by cleaving other dsRNA structures. DICER process the biogenesis of endogenous small interfering RNAs by cleaving the double stranded siRNA (Fire et al. 1998). One additional function of DICER is the processing of repeat-element-derived transcripts, such as from short interspersed elements (SINEs). Inactivation of *Dicer-1* gene causes the accumulation of SINE, phenomenon that is not recapitulated when other proteins of the processing machinery are inactivated indicating that the effect of DICER is independent of microRNA pathway (Kaneko et al. 2011). In *C. elegans* DICER shows a DNAse activity. The caspase CED-3 cleaves the first of the two RNase III domains of Dicer, leaving a truncated catalytically active protein which can bind to and nick one strand of dsDNA (Widlak et al. 2005; Nakagawa et al. 2010; Okamura and Lai 2010). Lastly, the production of small RNAs from DNA damage, the DNA-damage RNAs (DDRNAs) which are products of a specific enzymatic cleavage and possess biological activity, require both DROSHA and DICER (Tang and Ren 2012; Wei et al. 2012; d'Adda di Fagagna 2014). Apart from the RNAse III proteins DROSHA and DICER, it has been shown that DGCR8 may also have microRNA-independent functions. DGCR8 binds mature snoRNA molecules and control the stability of C/D and H/ACA box snoRNAs in a Drosha-independent

manner (Macias et al. 2012; Roth et al. 2013). In addition, it was reported that DGCR8 (which forms a complex with the exosome) can act as an adaptor to recruit the exosome to mature snoRNAs and human telomerase RNA for degradation (Macias et al. 2015). Recently, it was also reported that in human mesenchymal stem cells (hMSCs), DGCR8 shows microRNA-independent functions by stabilizing heterochromatin through direct interaction with nuclear lamina components LaminB1 and HP1γ (Deng et al. 2019).

All the aforementioned microRNA-independent functions of Microprocessor and DICER highlight the important roles of these proteins in RNA biology and chromatin organization by showing their involvement in various RNA metabolic pathways and in the processing of biologically important non-coding and protein-coding RNAs.

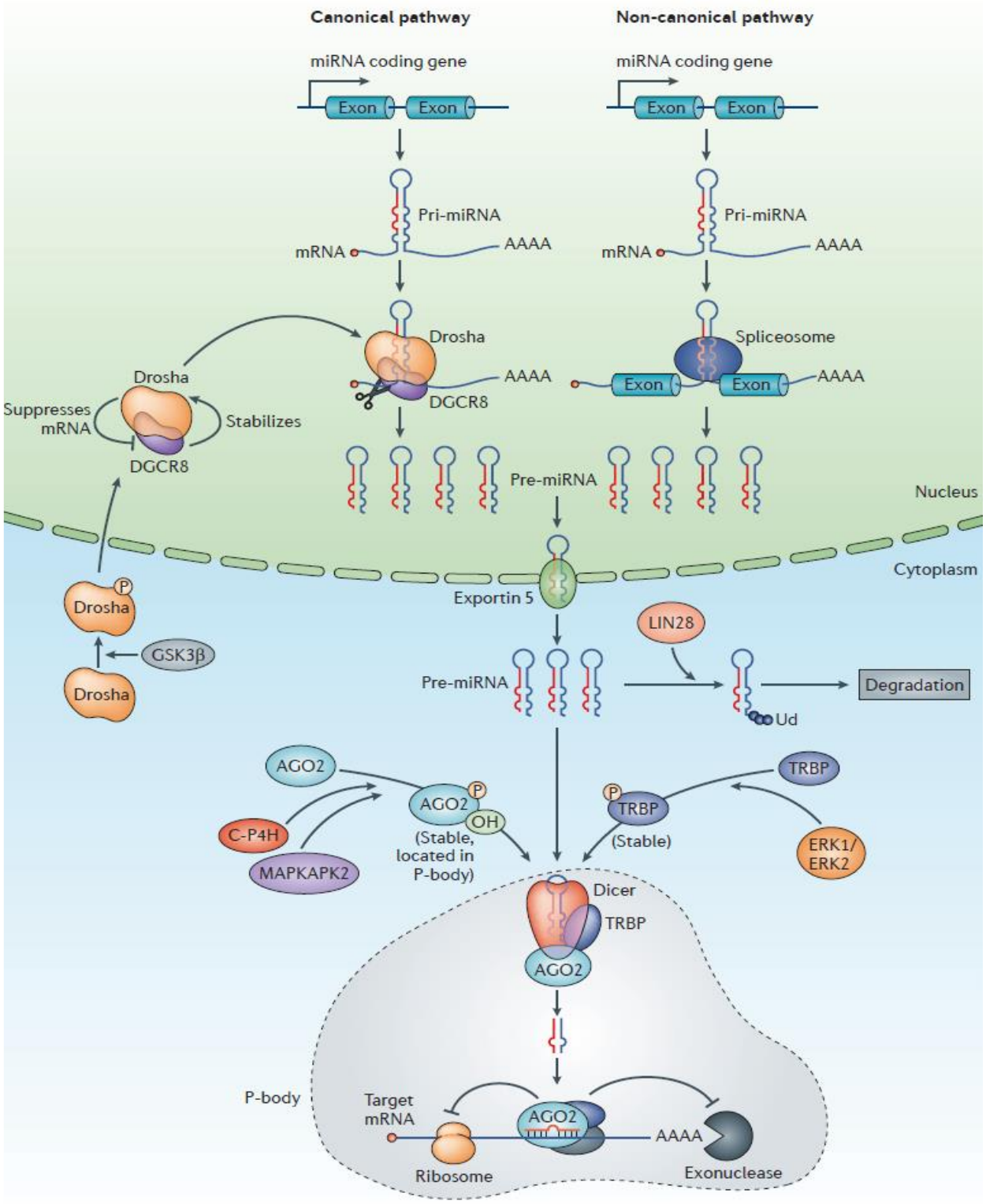

Figure 8. Representation of canonical and non-canonical biogenesis pathways of small microRNA genes (Li and Rana 2014).

1.5.5 microRNA-mediated gene silencing

The single stranded RNA once is loaded onto AGO proteins and forms the miRISC complex, then it can mediate either translation, repression or the degradation of its mRNA targets (O'Brien et al. 2018). Only the mature microRNA that bound to AGO protein can form the core of the miRISC complex. The AGO protein recruits other protein complexes which are capable of inhibiting translation and deadenylate the targeted mRNA by leading to mRNA decapping and degradation. microRNAs bind their target mRNAs by base-pairing partially with complementary sequences in the 3'-UTR. These sequences are highly conserved, which indicates that microRNAs might have co-evolved with their targets (Penso-Dolfin et al. 2018). Nucleotides in positions 2–8 from the 5'-end of a microRNA (termed the seed sequence) play a crucial role for target recognition. The ribonucleoprotein complex miRISC, consist of a microRNA loaded into an AGO protein, a glycine tryptophan repeat-containing protein (182 kDa, also named GW182), a Poly(A)-binding protein (PABP) protein and complexes of poly(A)-nuclease (PAN2-PAN3) and C-C chemokine receptor type 4/negative regulator of transcription subunit 1 (CCR4-NOT) proteins (Pratt and MacRae 2009). Although the exact mechanisms of how miRISC complex act has not been determined in detail yet, it has been reported that miRISC can inhibit protein translation (Humphreys et al. 2005; Pillai et al. 2005; Petersen et al. 2006) and facilitate mRNA decay (Wu et al. 2006) as indicated in **Figure 9**.

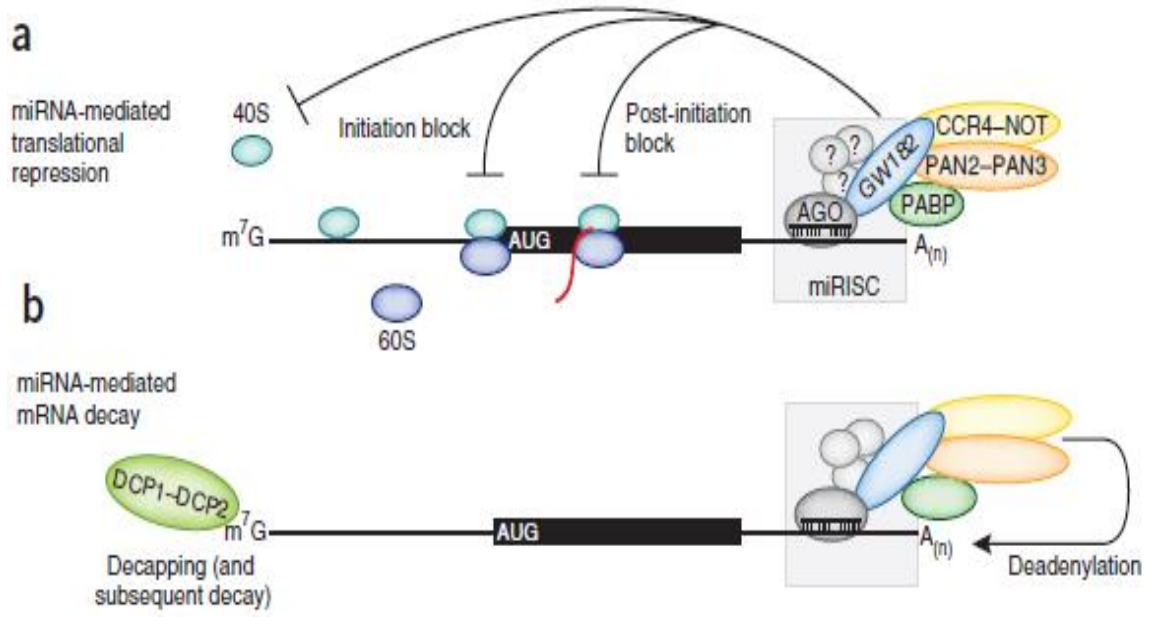

Figure 9. a) miRISC mediates translation repression through initiation block of 40S and 60S subunits. b) microRNA-mediated destabilization of target mRNAs. (Fabian and Sonenberg 2012) (Li and Rana 2014).

1.5.6 Transcriptional regulation of microRNAs

Although thousands of microRNAs have been discovered in almost all species, there is no evidence of how these small non-coding RNAs are being transcriptionally regulated. Despite the fact that three different RNA polymerases have been identified in mammals (RNA polymerase I transcribes the large ribosomal RNA, RNA polymerase II transcribes the mRNA-coding genes while RNA polymerase III transcribes ncRNA genes), most of the microRNAs (intergenic and polycistronic) are being transcribed from RNA Polymerase II (Pol II) (Lee et al. 2004a). Only a small part of microRNA genes are being transcribed by RNA Pol III (Borchert et al. 2006). More specifically, it has been shown that the largest primate-specific microRNA cluster in the human chromosome 19 (C19MC) is being transcribed by RNA Pol III (Pfeffer et al. 2005; Noguer-Dance et al. 2010; Bellemer et al. 2012). MicroRNA genes transcribed by Pol II have been found to show similar characteristics in their promoter sequence to those of coding genes transcribed by Pol II. They share the same characteristics such as CpG islands, the TATA-box, the TFIIB recognition element (BRE), the initiator element, the downstream promoter element (DPE) and the proximal sequence element (PSE) (Ozsolak et al. 2008). Data from ChIPseq experiments have shown that almost 30% of intronic microRNAs have their own promoters, located ~57kb from the TSS of their host genes (Ozsolak et al. 2008). ChIP-seq experiments for nucleosome histone marks have also identified trimethylation of Lys 4 of histone 3 (H3K4me3), histone H3 trimethylation at lysine 36 (H3K36me3) and histone 3 trimethylation at lysine 4 (H3K4) on the promoters of microRNA genes (Guenther et al. 2007). Nowadays, data from combined fields as genomics, transcriptomics, proteomics and experiments such as RNAseq, microRNA-seq, ChIPseq, GRO-seq (Global run-on assay) and nucleosome positioning analysis in several cell types from different species have been used in order to predict microRNA gene promoter mapping. Databases like FANTOM4 EEDB (Functional annotation of mouse Edge Express database) (Severin et al. 2009), MPromDb (Mammalian Promoter Database) (Sun et al. 2006), ORegAnno (Open Regulatory Annotation database) (Griffith et al. 2008), EDGEdb (differential gene expression database) (Barrasa et al. 2007) are used for the proper annotation of TSS of microRNA genes. PROmicroRNA (Marsico et al. 2013), microTSS (Georgakilas et al. 2014), miRT (Bhattacharyya et al. 2012), ACTLocater (Accessible and Conserved TFBSs Locater) (Xiao et al. 2013) are highly accurate algorithms used for microRNA TSS predictions.

1.5.7 Functional roles of microRNAs in the immune system

As previously mentioned microRNAs are characterized as guardians of the immune system (Mehta and Baltimore 2016). They are post transcriptional regulators of hematopoietic cell fate decisions (Kluiver et al. 2006). Deregulation of microRNA expression (result of either deletions of microRNA genes *per se* or deletions of processing machinery enzymes) can result in abnormal immune function, including development of severe pathologies like cancer and autoimmunity (Rupaimoole et al. 2016). MicroRNAs can control the myeloid and lymphoid cell development and function of the innate and adaptive immune system (**Figure 10**). The role of microRNAs in the innate immune system has been supported by studies on macrophages and NK cells. Macrophages are being mainly regulated by miR-155 and miR-146a which are strongly induced by nuclear factor-κB (NF-κB) and activator protein 1 (AP-1) in response to a broad range of toll like receptors (TLRs) and cytokine signals (O'Connell et al. 2007; Huang et al. 2016). In NK cells miR-181 drives early NK cell development, by enhancing Notch signaling (Cichocki et al. 2011). In T cells microRNAs control and regulate several processes such as their development (Dooley et al. 2013), activation (Grigoryev et al. 2011), differentiation (Jeker and Bluestone 2013), proliferation and the cytokine production (Weitzel et al. 2009; Fan et al. 2012). Genetic ablations of microRNA in T cells and the ablation of essential factors such as DROSHA, DICER, and DGCR8 leads to decreased survival of T cells upon activation (Muljo et al. 2005; Chong et al. 2008; Steiner et al. 2011). More specifically, conditional inactivation of DICER in the thymus, leads to a reduction of TCRαβ expressing thymocytes as well as a reduction in the $CD4^+CD8^+$ and $CD4^+$ or $CD8^+$ cells. Absence of DICER during *in vitro* differentiation towards the T_H1 and T_H2 cell lineages, a reduced proliferation, increased apoptosis rate and failure of IFNγ expression were observed (Muljo et al. 2005). Moreover depletion of DICER in FOXP3-expressing T cells, lead to increased levels of CD127, IL4, and IFNγ and loss of suppressive activity of T_{regs} in vitro (Zhou et al. 2008). Genetic ablation of DROSHA causes deregulation of T_{regs}, inability of $CD4^+$ cells to differentiate to T helper cells as well as autoimmune manifestation (Chong et al. 2008). Concluding, the above data present the necessity of microRNAs in maintaining the homeostasis of the adaptive immune system. The abundance of microRNAs in hematopoietic stem cells demonstrates the essential role of microRNAs in the immune cell lineage stabilization. Furthermore, it has been demonstrated that a high ratio of microRNA/target can reduce the expression despite transcription, by inhibiting the transcriptional "noise" and controlling the immune responses (Li et al. 2007; Bartel 2009; Jeker and Bluestone 2010). In T cells microRNAs can act as upstream or downstream regulators but also as regulated targets (Li et al. 2007).

Some of the most important microRNAs that are required for T cell development and for the normal immune function are presented below and on the **Figure 10**.

miR-181a. Bone marrow, spleen and thymus show the highest expression of miR-181a (Bartel 2009). mir-181 family consists of mir-181a, mir-181b, miR-181c and miR-181d. miR-181a1b1 cluster contains miR181a1 and miR-181b1 which are located on chromosome 1, while miR-181a2b2 cluster contains miR-181a2 and miR-181b2 which are located on chromosome 2. miR-181a1b1 is one of the most important microRNAs in cells of the adaptive immune system. miR-181-deficient mice showed severe defects in lymphoid development and T cell homeostasis associated with impaired PI3K signaling (Henao-Mejia et al. 2013). miR-181a enhances TCR signaling strength by directly targeting phosphatases (Li et al. 2007) while inhibition of miR-181a during T cell development, convert positively selected peptides into self-antigens (Ebert et al. 2009). Furthermore, the development of NKT cells is miR-181a-dependent (Fragoso et al. 2012). In addition, it has been shown that decline in miR-181a expression with age impairs T cell receptor sensitivity (Li et al. 2012).

miR-146a. It is considered as one of the most essential microRNAs in the control of hematopoiesis, immune function and cancer (Labbaye and Testa 2012). Deregulation of miR-146a expression has been linked with papillary thyroid carcinoma, cervical, ovarian and breast cancers (Perry et al. 2009). Although this microRNA is being induced as a general response in myeloid cells through TLR-2, -4, or -5 ligands, it is also expressed in T cells. As an important feedback regulator of NFκB signaling pathway, in human memory T cells miR-146a is induced by NFκB in response to TCR engagement. It targets TNF receptor associated factor (TRAF6) and Interleukin-1 receptor-associated kinase 1 (IRAK1), by creating a feedback mechanism which can control NFκB signaling (Yang et al. 2012). In microRNA-146a-deficient mice, deregulation of NFκB signaling can lead to myeloproliferation and myeloid malignancies (Zhao et al. 2011). Moreover, miR-146a is critical for the suppressor function of T_{regs}. Deficiency of miR-146a in T_{regs} cells results in a breakdown of immunological tolerance and the activation of STAT1, leading to T_H1 cell-mediated pathology (Lu et al. 2010).

miR-17-92. The polycistronic microRNA-17-92 is highly expressed in precursor T cells and B cells. miR-17-92 is composed of six members from four different seed families. miR-17-92 consists of miR-17, miR-18a, miR-19a, miR-20a, miR-19b and miR-92-1 which are found close together in a region of ~800bp located on chromosome 14. Overexpression of miR-17-92 in T cells is associated with lymphoproliferative disease

and autoimmunity and leads to death prematurely, by targeting tumor suppressor PTEN and the proapoptotic protein Bim (Xiao et al. 2008). Recently it was reported that miR-17-92 is associated with axial patterning in vertebrates (Han et al. 2015). Genetic ablation of miR-17-92 in mice, lead to death within minutes after birth due to the severe underdevelopment of the lungs and/or heart (Ventura et al. 2008). Data from deletion of the miR-17–92 cluster and its paralogues (miR-106b–25) in mice cause more severe developmental disorders compared to ablation of only the miR-17–92 locus, indicating the synergistic collaboration between these two microRNAs in order to regulate mouse embryonic development and survival (Ventura et al. 2008).

miR-155. miR-155 is the most well-studied microRNA and the most highly induced upon TCR stimulation (Vigorito et al. 2013). miR-155 is processed from a primary transcript of a long non-coding RNA called BIC and it is considered an important and pleiotropic regulator of immunity and cancer. Depletion of miR-155 results in defects in adaptive immune system (Rodriguez et al. 2007; Thai et al. 2007; Vigorito et al. 2007; O'Connell et al. 2010). miR-155 is overexpressed in several types of hematopoietic malignancies and its overexpression in mice can lead to B cell lymphoma (Tam and Dahlberg 2006). Overexpression of miR-155 promotes T_H1 differentiation *in vitro* (Thai et al. 2007; Banerjee et al. 2010). Data from experimental autoimmune encephalomyelitis (EAE) in mice have shown that miR-155-deficient mice are highly resistant to EAE probably due to a defect in T_H1 and T_H17 cells (O'Connell et al. 2010). Moreover, it has been shown that miR-155-deficient mice are resistant to collagen-induced arthritis by displaying a defect in T_H17 polarization, which demonstrates that miR-155 is essentially involved in the adaptive and innate immune reactions leading to autoimmune arthritis (Bluml et al. 2011). Further evidence, from miR-155-deficient mice and the impaired function of T_H1 and T_H17 cells, demonstrated that these mice failed to control *Helicobacter pylori* (Oertli et al. 2011). miR-155 is also highly expressed in T_{regs} whilst miR-155-deficient mice show a decreased number of thymic and peripheral T_{regs} (Lu et al. 2009).

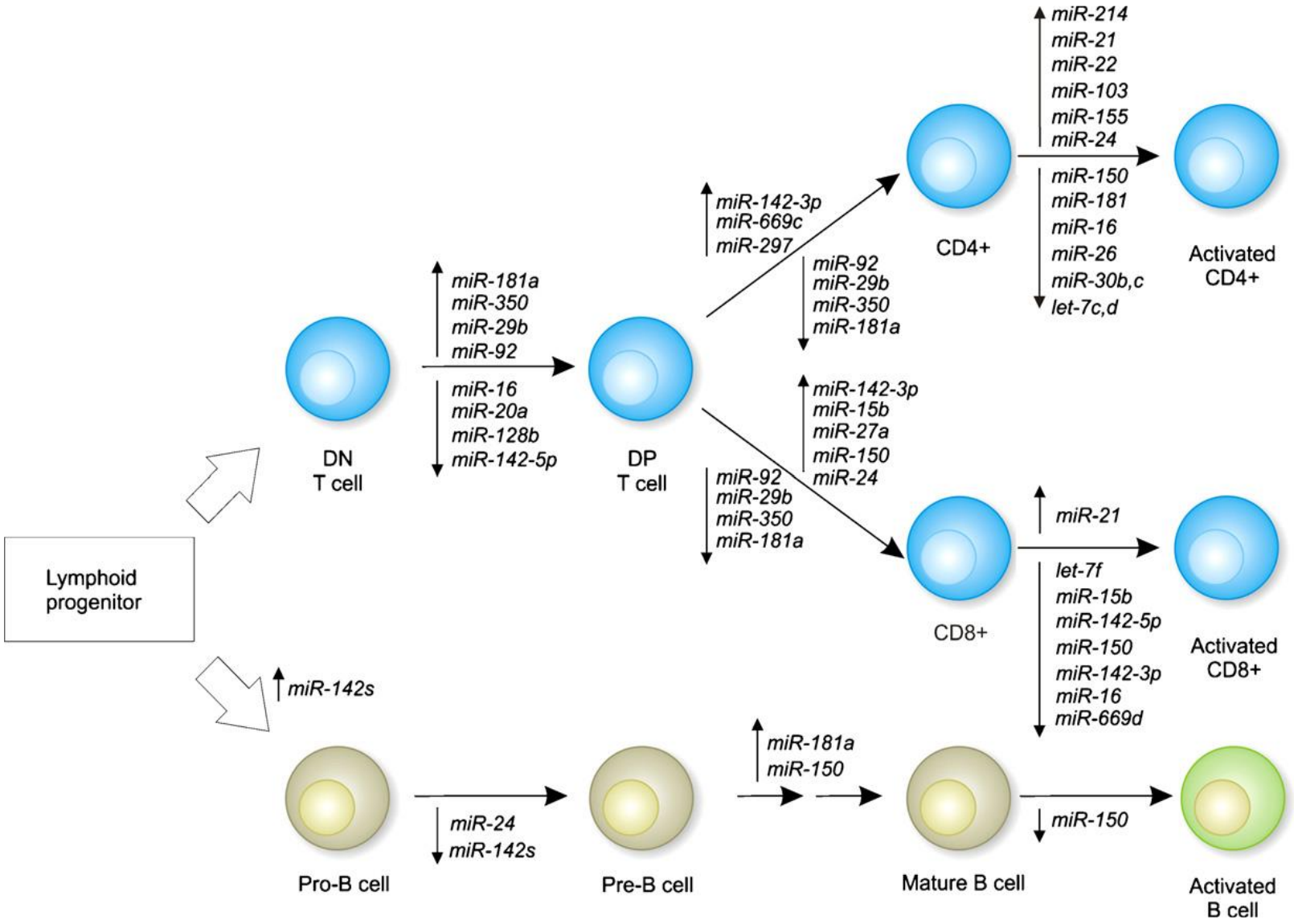

Figure 10. Involvement of microRNAs in lymphoid differentiation of B and T cells (Sonkoly et al. 2008)

1.6 Nuclear architecture: Dynamic interplay of 3D chromatin organization

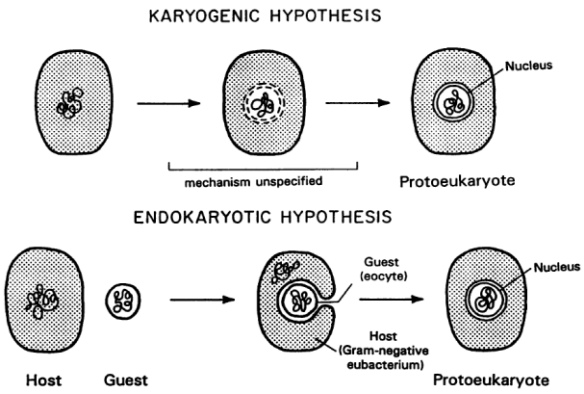

Figure 11. Depiction of first models proposed to explain the origin of the cell nucleus (Gupta and Golding 1996).

In 1996, two different hypotheses were proposed about the origin of the nucleus (Gupta and Golding 1996). The first hypothesis, termed karyogenic hypothesis, suggested that the nucleus and its enclosing membranes were gradually acquired through a segregating process (**Figure 11**). While the second hypothesis demonstrated that the cell nucleus, like the other eukaryotic organelles enclosed in double membranes (the chloroplast and mitochondrion) has probably been derived through capture by an engulfing species. Since the ER and the nuclear envelope share the same structure, it seems more possible and scientifically accepted (but not proved) that both hypotheses can be related with the evolution of the endomembrane organelles by membrane invagination to the inner site of the cell. Histone modifications, DNA methylation patterns, nuclear sub-compartments such as chromosome territory (CT), lamina associated domains (LADs) and transcription factories are conserved through distantly related eukaryotes, suggesting that these basic principles of genome organization are prevalent for all eukaryotes (Postberg et al. 2010). For the last decade the high-resolution capacity microscopic approaches in collaboration with several molecular approaches (Fiserova et al. 2017; Nozaki et al. 2017; Xu et al. 2018), based on the chromosome conformation capture (3C) related technologies (Schmitt et al. 2016), combined with methods of modeling and interpreting chromatin interactions, have revealed a better understanding of the spatial organization of chromatin structure. The organization of the chromatin in cells is driven by the short or long range intra- or inter- chromosomal interactions between different genomic loci. Interactions of these genomic loci with stable nuclear compartments such as the nuclear lamina or the nucleolus can also contribute shaping the genome (van Steensel and Dekker 2010). Nowadays in the single cell sequencing era where scientist can profile the epigenetic and transcriptomic landscape of the cells, studies have shown that spatial organization of cells can vary between individual nuclei by showing different interactions within each cell and locally constrained chromatin movements. In 2014, 4D Nucleome consortium (https://commonfund.nih.gov/4dnucleome) (a new term in the field of nuclear

organization) introduced the principles behind the three-dimensional organization of the nucleus in space and time (the 4th dimension), the role that nuclear organization plays in gene expression and cellular function, and how changes in the nuclear organization affect normal development as well as various diseases (https://commonfund.nih.gov/4Dnucleome/index). Nuclear and chromatin organization plays a crucial role in regulating cellular functions. Many studies have shown that spatial positioning of different genomic loci can be directly linked with gene expression (Fraser and Bickmore 2007; Lanctot et al. 2007), DNA repair and chromosome translocations (Roix et al. 2003; Misteli and Soutoglou 2009), replication (Gilbert et al. 2010) and X-chromosome inactivation (Nora and Heard 2010). Moreover, nuclear organization is tightly linked with diseases. Disorder of the nuclear architecture can lead to severe diseases. Mutations of the Lamin A/C genes are linked with premature aging disorders such as HGPS (Hutchinson–Gilford progeria) or atypical Werner's syndrome and several other diseases that have been characterized as laminopathies (Worman et al. 2009) (Schreiber and Kennedy 2013).

1.6.1 Functional Compartmentalization of the cell nucleus

The chromatin of the eukaryotic cells is spatially organized while the nucleus is functionally and highly subcomaptmentalized as shown in **Figure 12**. Nuclear sub-compartments play a crucial role in the organization and function of the genome. During mitosis, nuclear compartmentalization is disrupted but it is rapidly reestablished during post-mitotic nuclear reformation. Several sub-compartments have been demonstrated to play a crucial role in nuclear organization. Firstly, the transcription factories are considered as one of the most important nuclear compartments (Mitchell and Fraser 2008).The replication and transcription factories constitute "hot spots" in the nucleus where several genes aggregate in foci. These foci are fewer than the genes transcribed at the time, indicating that these few factories facilitate a huge number of genes by offering a coordinated transcriptional process. Klf-1 is a paradigm that explains how active co-regulated genes and their transcription factories collaborate. Klf-1 mediates coupling of Klf1-regulated genes at specific transcription factories in erythroid cells (Schoenfelder et al. 2010). Another important subcompartment of the nucleus is the Polycomb group protein (PcG) bodies (Sexton et al. 2007). PcG bodies in Drosophila function as a repressive environment, acting through epigenetic chromatin modifications and by regulating the nuclear organization of their target genes. Cajal bodies can modify small nuclear (snRNAs) and nucleolar RNAs (snoRNAs) and assemble the corresponding RNPs, while in PML more than a hundred proteins are being sumoylated (Pirrotta and Li 2012; Grossniklaus and Paro 2014) .

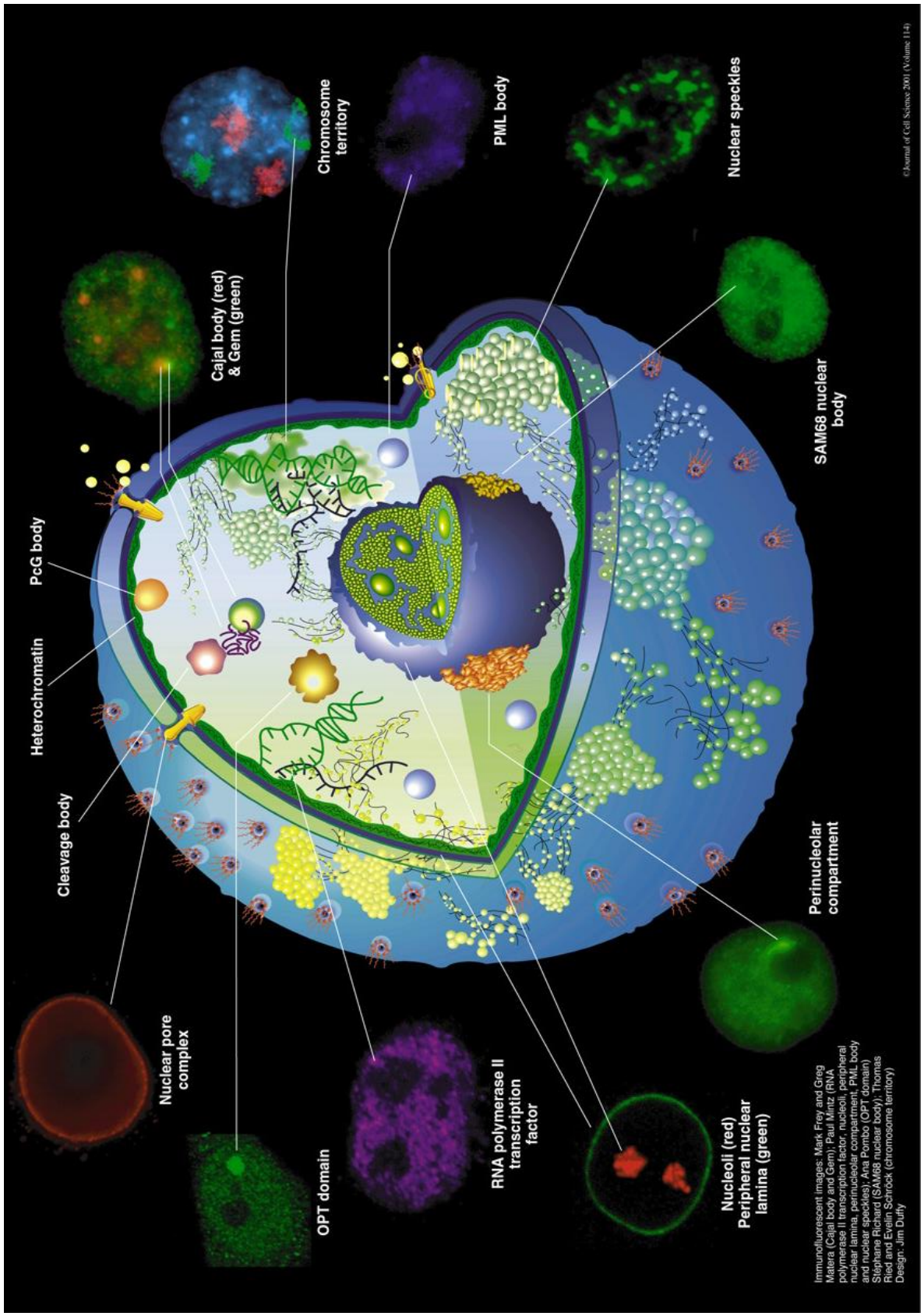

Figure 12. Nuclear domains and subcompartments (Spector

Nuclear speckles are another important sub-compartment of the nucleus which harbor components of the splicing system snRNAs, SC35, and other spliceosome components by altering the nuclear organization (Spector and Lamond 2011). Moreover, it has been shown microscopically that actively transcribed gene clusters are close to foci of transcription factories or nuclear speckles (Spector and Lamond 2011).

Except from the different sub-compartments that exist in the nucleus, the genome is also compartmentalized in two different clusters: compartment A and compartment B. Genomic loci that are clustered in compartment A are gene rich, transcriptionally active and DNAse I hypersensitive, while loci that are clustered in compartment B are gene poor, transcriptionally inactive and DNAse I insensitive (Lieberman-Aiden et al. 2009). Clustering of genomic loci to the nuclear lamina (NL), LADs, topologically associated domains (TADs), nucleolus and other subnuclear compartments such as PcG bodies in Drosophila seem to be part of the B compartment. Data from Hi-C experiments in several human and mouse cells have demonstrated that probably the nucleus is not clearly divided into sub-compartments A and B but there is a continuum between them, where chromatin regions associate with other regions that have similar transcription or activity status (Imakaev et al. 2012).

According to the hierarchical organization of the genome the first level of organization is the folding of genomes and their distribution into chromosome territories (CTs) (**Figure 13**). Within each CT, chromatin is further folded into smaller domains, termed (TADs). Each TAD can be divided into subdomains, called sub-TADS. Sub-TAD borders are also marked by the insulator CCCTC-binding protein (CTCF) and they can be folded in regulatory loops (Dekker and Heard 2015). Chromatin looping can contribute to *cis* and *trans* regulatory elements to reach gene promoters in order to regulate expression. Chromatin loops and sub-TADs are retained and delimited by chromatin insulators (CTCF), mediators and chromatin organizers such as cohesin (Phillips-Cremins and Corces 2013).

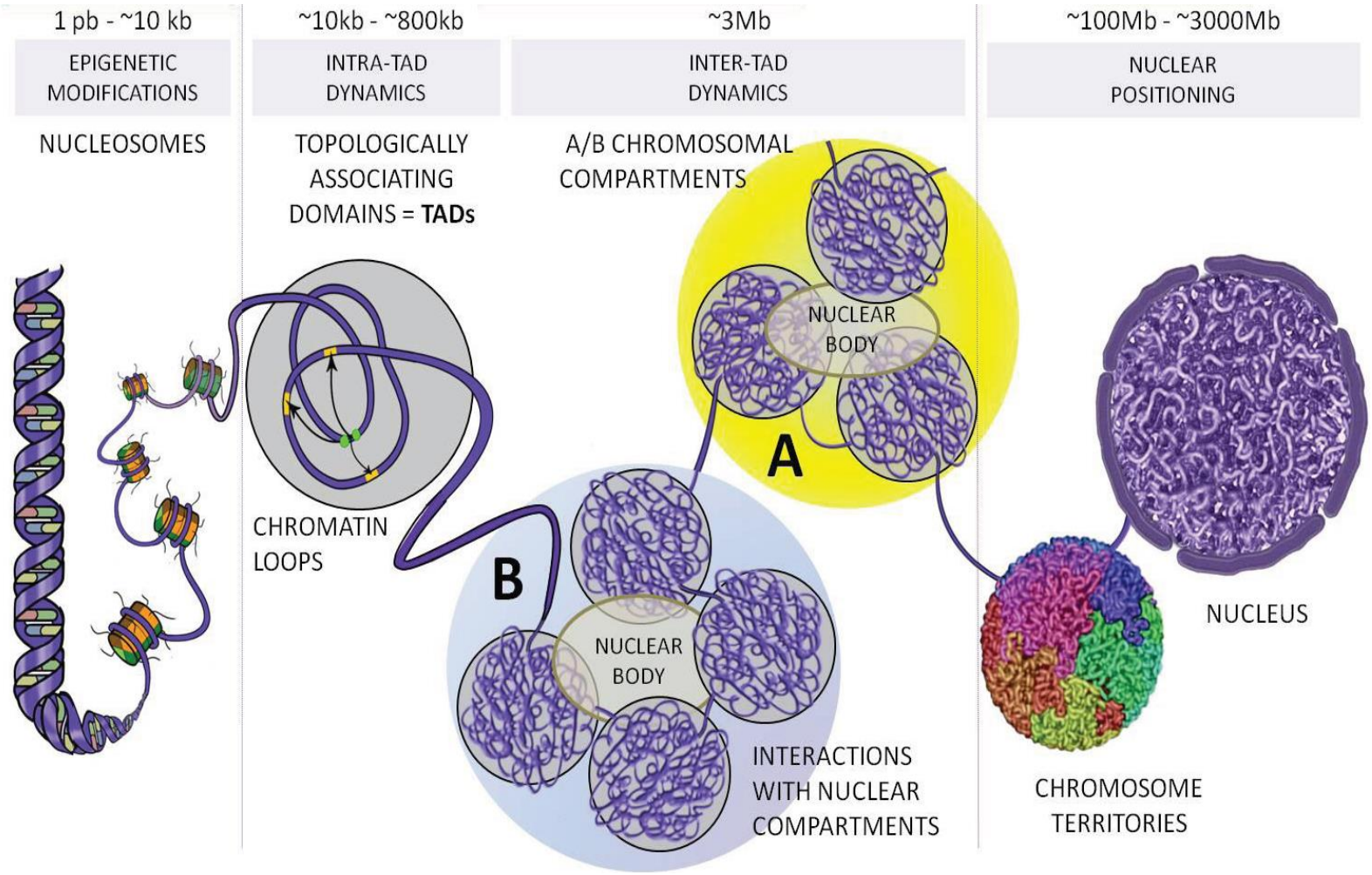

Figure 13. Scheme for the global genome organization in mammals from the megabase scale to the nucleosome level (Ea et al. 2015)

1.6.2 Principles of genome folding into chromosome territories

During most of the cell's lifespan, chromosomes occupy distinct regions in the nucleus. Chromatin is not static within these domains but is actively condensed and decondensed in a transcriptional activation dependent manner (Cremer and Cremer 2010; Sanchez-Alvarez et al. 2011). Chromosomes are located at specific subnuclear territories within the nucleus while the transcriptionally active genes may be found on their external domains (**Figure 14**) (Cremer and Cremer 2010; Bickmore 2013). Initially, the term chromosome territory (CT) was introduced by Rabl (1885) and Boveri in 1909.

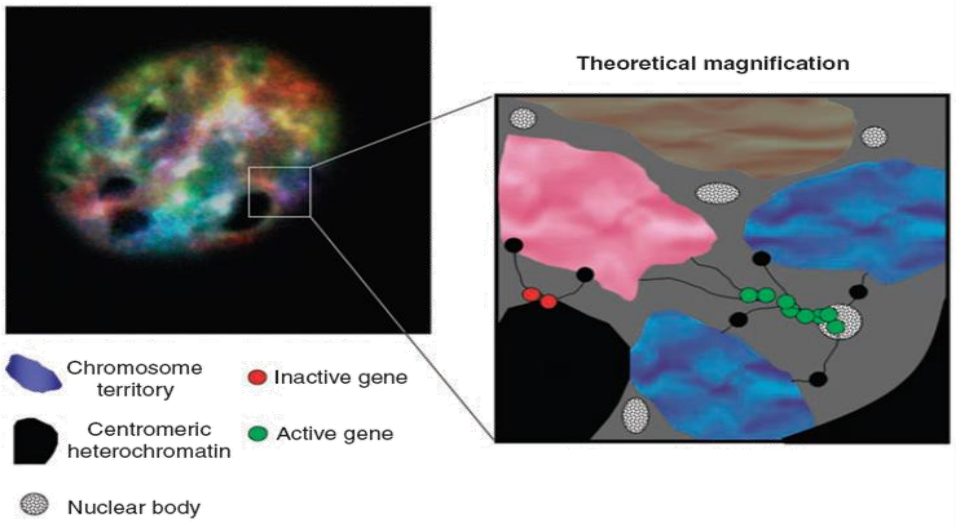

Figure 14. Simultaneous staining of mammalian chromosome territories depicting the looping out from the CT of the transcriptionally active genes

Particularly, Boveri was trying to introduce the functional and structural aspect of chromosomes as a specific unified theory of heredity, but at that time he could not prove it due to the lack of technological and experimental tools. CTs were visualized for the first time in 1985 by *in situ* hybridization method and later on the generation of specific chromosome probes led to the visualization of CT on both metaphase and 3D interphase nuclei (Cremer et al. 1984; Manuelidis 1985; Schardin et al. 1985; Cremer et al. 1988; Lichter et al. 1988; Bolzer et al. 1999).

Untill now three patterns of chromosome topology have been shown in the eukaryotic cell. During anaphase, centromeres and telomeres are positioned opposite to each other and this phenomenon is called Rabl configuration. Rabl configuration is maintained also during interphase. The radial positioning

of chromosomes (chromosomes located either at the center or at the periphery of the nucleus) was established by studies of the human lymphocyte chromosome 18 and chromosome 19 (Croft et al. 1999). Chromosome 19 (the most gene-dense human chromosome) is located towards the center of the nucleus while chromosome 18 (the least gene-dense chromosome) is located at the nuclear periphery (Croft et al. 1999; Cremer et al. 2001; Cremer et al. 2003) (**Figure 15**). The concept of relative positioning was introduced from observations where chromosomes 7, 8 and 16 were found in diametrically located positions within the interphase nucleus of human fibroblasts (Nagele et al. 1999). Spatial organization of chromosome territories is closely linked to important biological processes such as transcription, replication and cellular differentiation (Postberg et al. 2010). Chromosomes that have the same size and gene density interact in a higher rate between them, therefore, gene dense but short chromosomes gather at the center of the nucleus while gene poor chromosomes have the tendency to locate at the nuclear periphery (Lieberman-Aiden et al. 2009; Zhang et al. 2012b). So far there are no data that can confirm the relocalization of the CTs within the nucleus during the differentiation of post mitotic cells. However it has been reported that in neurons the X chromosome territory in epilepsy can be relocated in both females and males (Borden and Manuelidis 1988). Another study that reported the relocalziation of the CTs has been demonstrated in rod nuclei (Solovei et al. 2009). The rod photoreceptor nuclei of the nocturnal and diurnal mammals have a completely different chromatin organization. In nocturnals, after day 6post partum, during the terminal differentiation of rod cells the heterochromatin relocalizes at the center of the nucleus while the euchromatin locates at the nuclear periphery, in order to facilitate the night vision.

Genome wide Hi-C analysis demonstrated that genes located on the same chromosome can interact more often even if the distance between them can reach the 200Mbp linear distance compared to loci that are located to different chromosomes (Lieberman-Aiden et al. 2009; Zhang et al. 2012b). Although it has been reported that there is no difference between the distribution of the genes with higher or lower transcriptional activity within the CTs, there are few exceptions where the genes (eg. *MHC* and *EDC* loci and *HOX* gene cluster) are looping out from the CT (Williams et al. 2002; Chambeyron et al. 2005; Kupper et al. 2007).

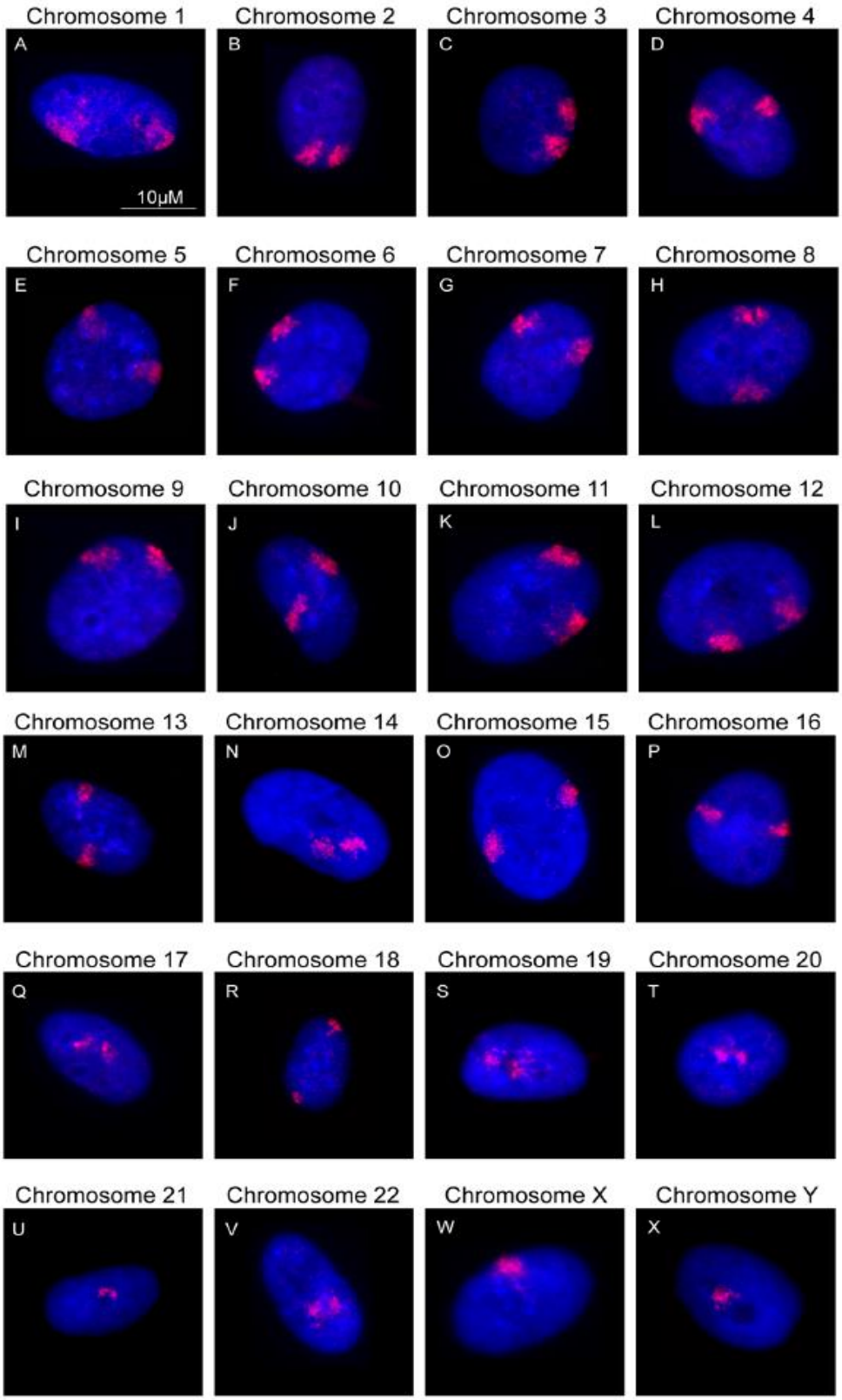

Figure 15. Subnuclear localization of all chromosomes in human dermal fibroblasts (Mehta et al. 2013)

1.6.3 Topologically Associated Domains (TADs)

Microscopically, it has been shown that within CTs smaller chromosomal domains (CD) can be observed. CDs may have a size of ~100 kb to several Mbp and usually are located between the borders of CTs (Cremer and Cremer 2010). Although since the first microscopic observation of the CT, new imaging such as super resolution microscopy provided more details regarding the organization of the CTs and CDs (Cattoni et al. 2015).

In 2002 a new methodology was introduced describing interaction between 2 loci not only with imaging methods (DNA *in situ* hybridization) but with high-resolution biochemical assay showing the interaction in 3D interphase nuclei (Dekker et al. 2002). The methodology was named Chromosome Conformation Capture (3C) and is based on the crosslinking of the chromatin, digestion of the chromatin with either 4- or 6-bp cutter restriction enzyme, ligation and at the end PCR detection of physical contact between the two genomic loci (**Figure 16 & 17A**) (Dekker 2006; Hagege et al. 2007; Comet et al. 2011; Gavrilov et al. 2013; Rao et al. 2014; Nagano et al. 2015). In order to map genomic interactions between in more than two loci, the 3C methodology was evolved in (4C) based on a 3C on Chip, circular 3C, open-ended and olfactory receptor 3C (Lomvardas et al. 2006; Simonis et al. 2006; Wurtele and Chartrand 2006; Zhao et al. 2006; Sati and Cavalli 2017). 4C requires one additional round of digestion and ligation and offering the opportunity to map one versus all genome wide interactions by providing a better resolution than the 3C (Kb to few 100Kb) (**Figure 16 & 17B**) (van de Werken et al. 2012). Both 3C and 4C are insufficient to provide more details regarding the chromatin organization of the 3D interphase nuclei due to the genomic region of interest- restriction. As a consequence, a new version of 3C was introduced, Chromosome conformation capture carbon copy (5C) where many to many genomic interactions could be mapped. 5c is an approach to study interactions between megabase sized regions and the additional steps include the design or reverse primers in the genomic regions of interest (Dostie et al. 2006; Fraser et al. 2009; Lajoie et al. 2009; Ferraiuolo et al. 2012; Phillips-Cremins et al. 2013). The use of 5C by Nora et al., introduced for the first time the fundamental and stable topologically associated domains (TAD) (**Figure 16, 17C & 18**) (Dixon et al. 2012; Nora et al. 2012; Sexton et al. 2012; Rousseau et al. 2014; Sexton and Cavalli 2015). In 2009 mapping of all in *cis* and *trans* long- or short- range genomic interactions through Hi-C was developed by Leiberman-Aiden et al., and reported the compartmentalization of the genome in active (A) and inactive (B) domains (Lieberman-Aiden et al. 2009; Nagano et al. 2013; Rao et al. 2014; Nagano et al. 2015; Sati and Cavalli 2017). Data from high-resolution 5C and Hi-C demonstrated the existence of TADs in human, mouse and Drosophila genomes (Dixon et al. 2012; Nora et al. 2012; Sexton et al. 2012).

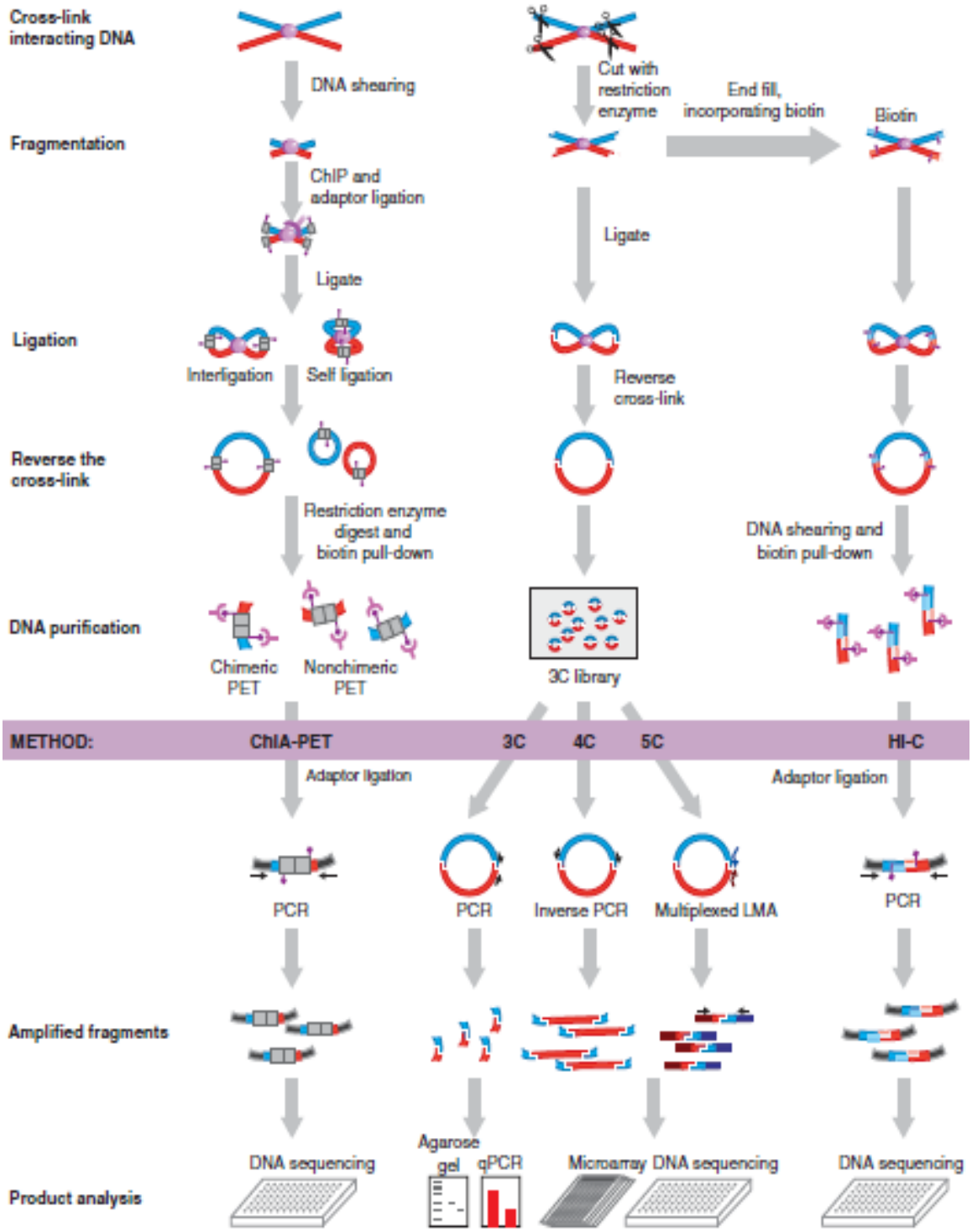

Figure 16. Schematic representation of the 3C-derived methods (Dekker and Misteli 2015).

The size of TADs may vary from tens of kb to several Mbp. In mouse the TAD size is approximately 880kb (Dixon et al. 2012). Genome domains that are located in the same TAD show higher internal interacting frequency compared to loci that are located between two different TADs (Dekker and Heard 2015). Human and mouse genomes are composed of more than 2000 TADs encompassing more than 90% of the entire genome, while in *D. melanogaster* more than 1100 TADs have been reported. As it was demonstrated by Hi-C experiments, the genomes of *Saccharomyces cerevisiae* and *Schizosaccharomyces pombe* seem to be devoid of TAD organization, while plan genomes are organized in pericentromeric regions (Duan et al. 2010; Tanizawa et al. 2010; Feng et al. 2014). TADs are conserved between mouse and human and show high similarity between different cell types. Long range chromatin interactions that abstain around 20kb are found on the same TAD (Dixon et al. 2012). Borders of TADs are also conserved as it was shown in mouse embryonic stem cells and mouse cortex as well as in Drosophila (Sexton et al. 2012). Mammalian TAD borders are rich in transcription start sites (TSS) of housekeeping genes, rich in CTCF insulator protein binding (15% of CTCF is found on TADs' border in mammals), Smc1 and Smc2 (subunits of cohesin), H3K4me3 and H3K36me (active chromatin histone marks) and Med1 and Med12 (which are subunits of the *Mediator* multiprotein complex) (Dixon et al. 2012). Since, the megabase scale TADs seem to be cross species conserved, then the organization of chromatin at the sub-megabase scale (sub-TADs) can determine and contribute to the cellular function and fate. A recent study of a high-resolution architecture map across seven genomic loci (*Oct4, Nanog, Nestin, Sox2, Klf4, and Olig1-Olig2*) in embryonic stem cells and neural progenitor cells identified around 60 sub-TADs domains (Phillips-Cremins et al. 2013). In this study it was demonstrated that cohesin and CTCF mediate long-range chromatin interactions while mediator and cohesin couple short-range chromatin interactions. In conclusion, sub-TAD organization, consisted of chromatin loops, may be linked to some cell type specific characteristics whereas TADs represent constant domains that are stable after cell activation, differentiation and development.

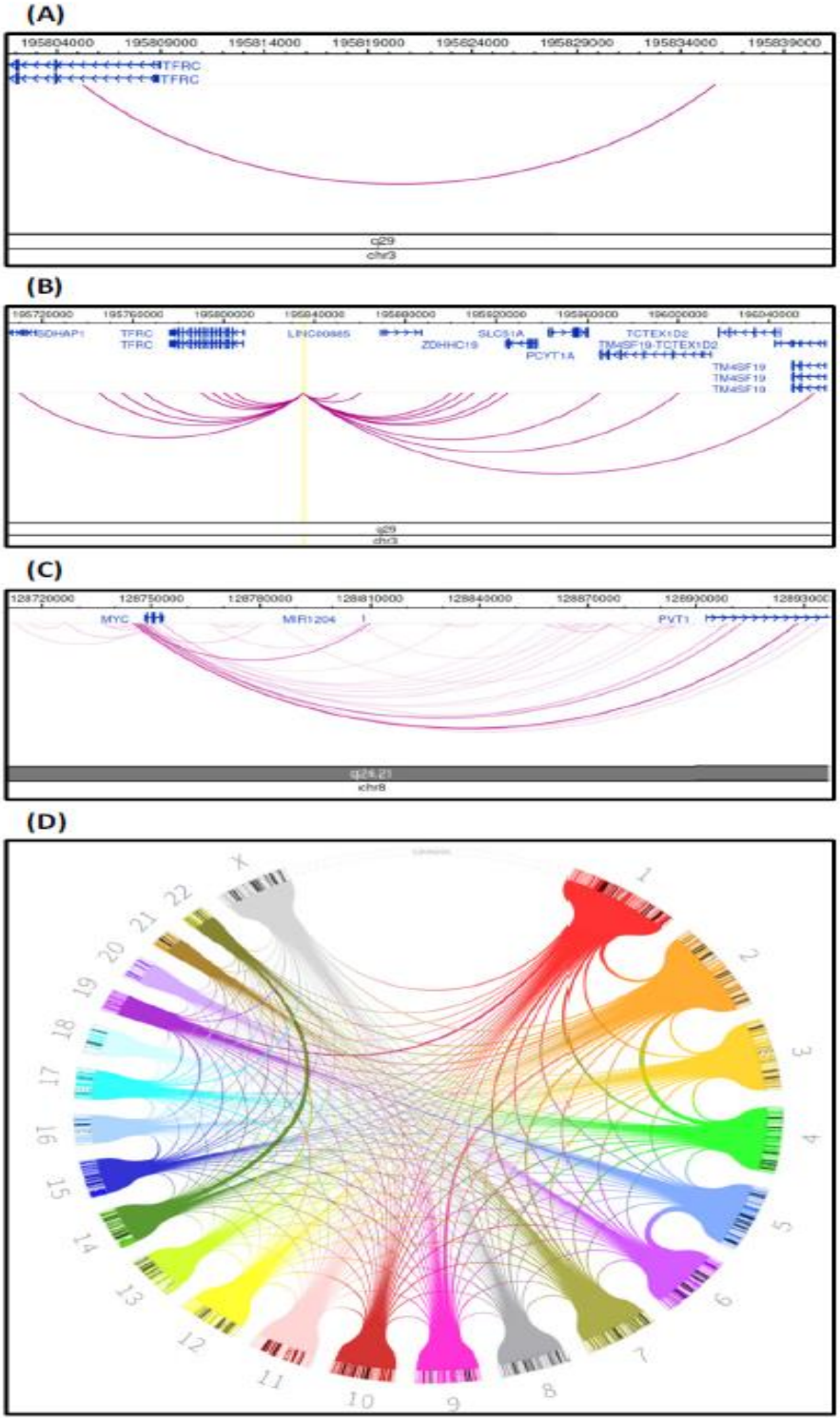

Figure 17. Visualization of 3C derived methods based. (A) 3C is used to study interactions between two genomic loci (one to one). (B) 4C is used to quantify interactions of one genomic locus vs all. (C) 5Cis used to study chromatin interactions between several genomic loci (many to many). (D) Hi-C identifies all chromatin interactions (all to all). (See et al. 2019)

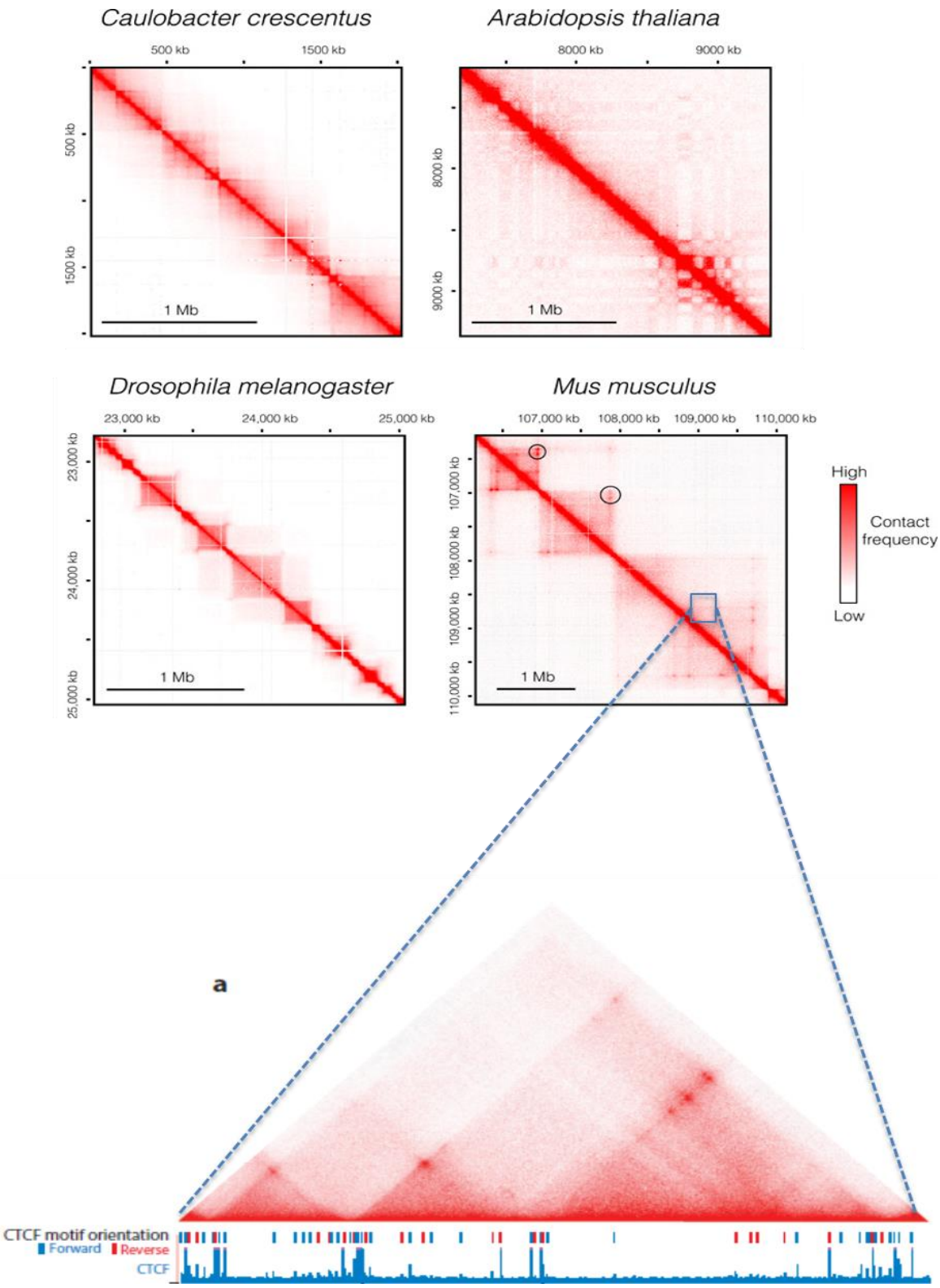

Figure 18. (*a*) High-resolution Hi-C data in four different species: *C.crescentus*, *A.thaliana*, *D. melanogaster* and *M. musculus*. Topologically associating domains (TADs) appear as triangles of high signal on the Hi-C heat map while loops appear as focal points. CTCF binding sites define TAD andsub-TAD borders (Merkenschlager and Nora 2016).

1.6.4 The role of chromatin looping in gene regulation

The regulation of gene expression includes regulatory elements that are located in large distances from the regulated genes in a linear conformation (Andersson and Sandelin 2019). In order to solve the problem of promoter-enhancer communication and to bring them to physical proximity, chromatin is organized into looped structures or chromatin hubs that connect regulatory elements to activate or repress transcription (Furlong and Levine 2018). As small proteins that recognize the DNA sequence transcription factors (TF) play an essential role in activating or repressing transcription of genes through direct or indirect binding or by recruiting the transcriptional factors at the transcription starting sites (TSS) (Chernukhin et al. 2007; Allen and Taatjes 2015; Lambert et al. 2018). Whether the TF shape the 3D structure of the nucleus or it is *vice versa* is not clear yet. Also remains unclear the frequency of chromatin looping mediated through the enhancer promoter interaction within the nucleus. Until now, several types of chromatin loops have been reported (Deng et al. 2012; Cavalli and Misteli 2013; Kim and Shendure 2019). The first model refers to intragenic loops, where the 5'- and the 3'-end of a gene join with each other to allow gene transcription, RNA Pol II recycling and retain transcriptional directionality through the direct oligomerization of the TF (**Figure 19A**) (Pant et al. 2004; Weintraub et al. 2017; Kim and Shendure 2019). The second group of chromatin loops is called enhancer promoting looping and is mediated by transcription factors that can collaborate either with the mediator complex or with chromatin organizers (**Figure 19B**) (Deng et al. 2012; Deng et al. 2014b; Love et al. 2014; Kim and Shendure 2019; Monahan et al. 2019). Another model of the TF action on the chromatin is described as phase separation (**Figure 19C**). This model suggests that interactions between intrinsically disorder regions (IDR) of the TF lead to the formation of the "condensates" or chromatin "hubs". Both *in vivo* and *in vitro* studies have reported that TF and their cofactors are highly enriched for IDR. TFs such as OCT4 and GCN4 enhance the formation of the phase separation through the Mediator linking directly the phase separation with 3D chromatin conformation and gene expression (de Wit et al. 2013; Denholtz et al. 2013; Boija et al. 2018; Cho et al. 2018; Chong et al. 2018; Sabari et al. 2018; Kim and Shendure 2019; Petrovic et al. 2019). Another model suggested is the "interaction with loop extruders" (Figure 16D). In this model the chromosome complexes (SMC) encircle the DNA and form a loop and its size can be related with the blocking of the cohesin (binding or releasing the DNA) by the CTCF. Insulator-mediated chromatin looping can gather and isolate individual loci, by keeping isolated the transcriptionally activated domain from other surrounding elements (Cavalli and Misteli 2013; Haarhuis et al. 2017; Hansen et al. 2017; Rao et al. 2017; Schwarzer et al. 2017; Ganji et al. 2018; Kim and Shendure 2019). Interactions of the TF with landmark such as nuclear

lamina has also been described (**Figure 19E**). Although nuclear lamina is considered a repressive environment, in *Saccharomyces Cerevisiae* it is generally accepted that NPCs can act as transcription factors by recruiting genes at the nuclear periphery (Light et al. 2010; Brickner et al. 2012; Brickner et al. 2019). Recent studies have reconfirmed the interaction of NPC with active genes and with super enhancers in mammals as well (Zullo et al. 2012; Baumann 2016; Ibarra et al. 2016a; Pascual-Garcia et al. 2017; D'Angelo 2018; Kim and Shendure 2019). TF can also bind to non-coding RNA through protein RNA interaction (**Figure 19F**). Long non coding RNAs, such as *Xist* or *Firre* scaffold multiple chromatin proteins and TF in order to coordinate specific functions within the nucleus (Quinodoz and Guttman 2014; Kung et al. 2015; Yang et al. 2015). Furthermore both CTCF and YY1 which are considered as genome organizers act also as TF, have also been reported to bind RNA (Sigova et al. 2015; Kim and Shendure 2019). Finally, the last model of TF action suggested is the chromatin modifications (**Figure 19G**). TF that directly bind on DNA, recruit other proteins or coactivators or chromatin remodelers that can modify DNA or histones tails (methylation and acetylation) (Spitz and Furlong 2012; O'Malley et al. 2016; Yin et al. 2017; Zhu et al. 2018; Kim and Shendure 2019). Promoters can be located proximal to genes and can initiate bidirectional transcription (Wei et al. 2011; Scruggs et al. 2015). Enhancers are located distal to protein-coding genes and may require chromatin conformational placement near regulated loci. Enhancers can also drive transcription from a position upstream of, downstream of, or within target genes (Pennacchio et al. 2013). Insulators for either gene expression or chromatin state separate heterochromatin from euchromatin and active from inactive gene expression domains while repressors can cause the expression of nearby genes (Burgess-Beusse et al. 2002; West et al. 2002; Reynolds et al. 2013). The fact that one enhancer can have more than one gene target and conversely, multiple enhancers can regulate a single gene, further highlight the need for mapping chromatin contacts, to understand the functional connectivity of regulatory elements. The most frequent interactions between promoters and sequences are found usually 120 kb upstream of TSSs (Sanyal et al. 2012). The most well studied case of long-range chromatin looping is the mammalian *β-globin* gene (Zhang and Qian 2002; Drissen et al. 2004; Bartkuhn and Renkawitz 2008; Chien et al. 2011; Deng et al. 2012; Huang et al. 2017). The *β-globin* gene locus contains several genes that are expressed sequentially and in a tissue-specific manner dependent on cell differentiation. β-globin gene locus contains an upstream locus control region (LCR) which is enriched in enhancers that regulate its expression during development by creating looping domains (Tolhuis et al. 2002). Other examples of chromatin looping include the *IFNγ-TH2* loci in CD4 T cells (Spilianakis and Flavell 2004), *MHC class I* locus (Kumar et al. 2007), *IgH* in B cells (Sayegh et al. 2005), *HOXb1* (Wurtele and Chartrand 2006) and the imprinted locus *H19–Igf2* (*Dlx5–Dlx6*) (Horike et al. 2005). All the aforementioned examples underline

the importance of chromatin looping as a general feature of chromatin architecture in eukaryotes that has several functional roles including transcription activation, repression and DNA recombination.

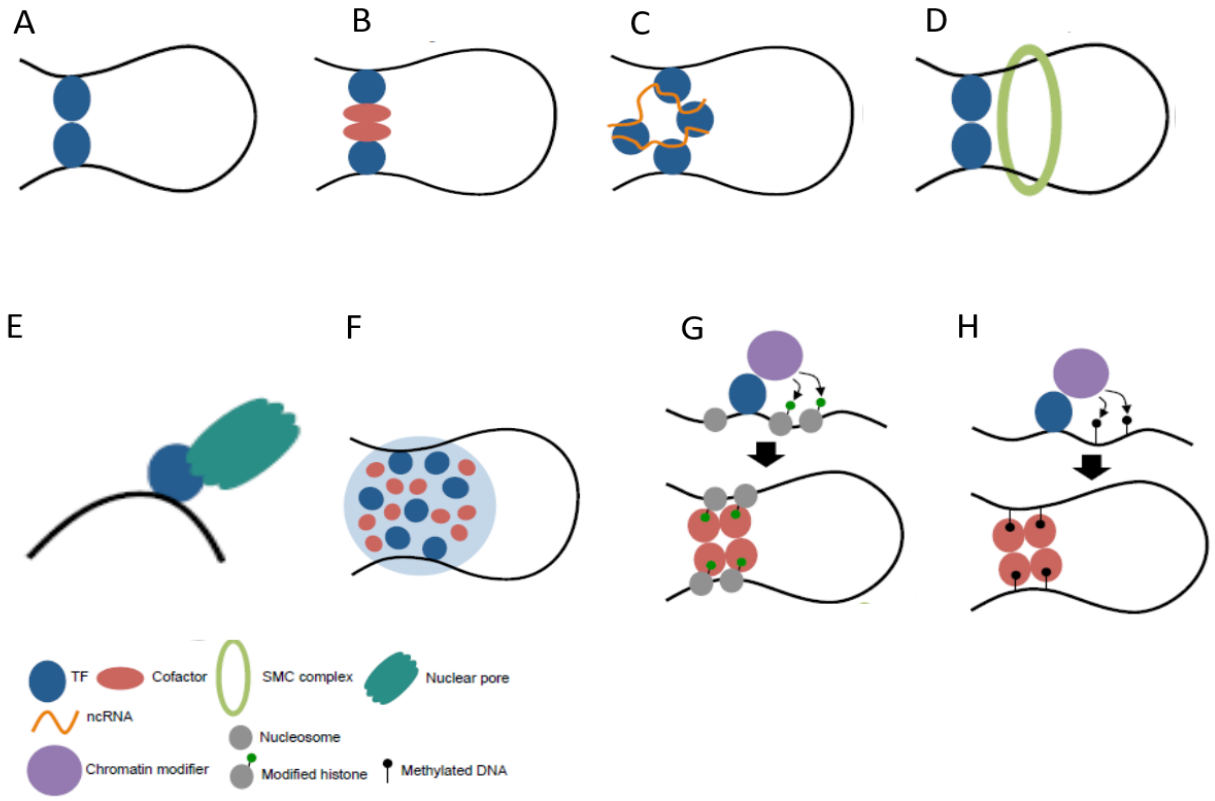

Figure 19. Modes of TF Action on 3D Genome Organization: (A) Direct oligomerization, (B) Cofactor oligomerization. (C) Condensate formation. (D) Interactions with loop extruders. (E) Interactions with nuclear landmarks such as nuclear pores. (F) Protein-RNA interactions. (G) Chromatin modifications, including histone modifications (left panel) and DNA methylation (right panel) (Kim and Shendure 2019).

1.6.5 Genome organizers

Mammalian genomes are huge and consist of billions of bases of DNA containing sufficient regulatory information to create complex organisms with thousands of cell types and considerable behavioral repertoires. Each of the 24500 genes in the human genome has likely many different regulatory regions that moderate the appropriate function of genes. Apart from nuclear sub-compartments such as the transcription factories, chromosome territories, nuclear lamina, nucleolus, nuclear speckles or paraspeckles, nuclear organization can be affected by genome or global chromatin organizer proteins

(Shachar et al. 2015). Genome organizers are factors that mediate the folding and organization of the genome inside the nucleus either by forming chromatin loops or by serving as seeding sites that anchor specific genomic loci. So far the most well-studied mammalian genome organizers are CTCF protein, cohesin, proteins of the nuclear envelope such as LaminA/C and the SATB1 protein. All these genome organizers can sequestrate tissue-specific gene regulation in an evolutionary dependent context. Therefore, the interplay of genome organizers with nuclear architecture can act as a regulatory layer of genome functions in a discrete cell fate by regulating/mediating the transcriptional activity of specific genes.

1.6.5.1 Nuclear periphery as a genome organizer

The nuclear envelope is consisted of two membranes, the inner and the outer membrane. The outer membrane is continuous with the endoplasmic reticulum while the inner membrane is associated with nuclear lamina (NL). The main structural components of nuclear lamina are the type V intermediate filament proteins Lamin A, B and C. Lamin A and C are encoded by the *LMNA* gene by alternative splicing, while Lamin B is encoded by two genes (lamin B1 by *LMNB1* and lamins B2 and B3 by *LMNB2*). Another difference between Lamin A/C and Lamin B is their expression profile. Lamin B is expressed in most cell types, while Lamin, A is expressed only after differentiation (Dittmer and Misteli 2011; Gruenbaum and Foisner 2015).

Nuclear envelope is penetrated from high molecular weight transmembrane proteins, termed nuclear pore complex (NPC), which can facilitate the transport between the nucleus and the cytoplasm. The mammalian NPC consists of 30 unique proteins called nucleoporins (Nups), which are present in multiple copies due to the eightfold stoichiometry of the complex (Otsuka and Ellenberg 2018). The nuclear lamina contains also a large variety of proteins that span the INM, called nuclear envelope transmembrane proteins (NETs), which are associated directly or indirectly with lamins (e.g., LBR, emerin, LAP2β, LEM-2)(Schirmer and Foisner 2007) (**Figure 20**). NETs mediate cell signaling, mechano-transduction, nuclear architecture, chromatin tethering and gene regulation. Composition of nuclear lamina shows cell type specificity and it depends on the differentiation stage (Worman 2012) (Korfali et al. 2012). Importantly, many studies have demonstrated that nuclear lamina can operate as an organizing "platform", by shaping and maintaining the 3D structure of the nucleus (Zuleger et al. 2011; Zheng et al. 2018; Shevelyov and Ulianov 2019). Except for the mechanical support that double lipid bilayer membrane can offer to the

nucleus, it plays a crucial role in the transport through the nuclear pore complexes (NPC) and also, serves as an anchoring point for heterochromatin. NPCs can also influence genome function and organization in a transcription-independent matter. It is believed that NPCs and lamins have divergent roles in transcriptional activation and repression, respectively.

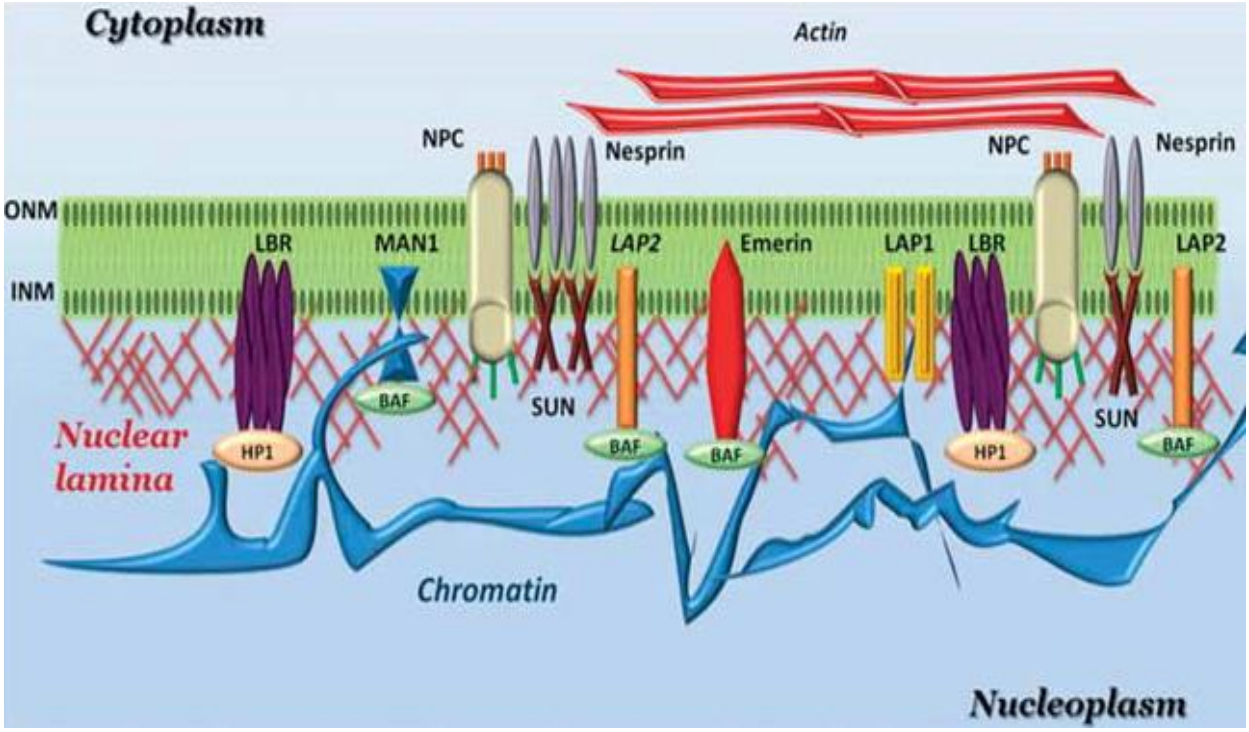

Figure 20. Structural components of the nuclear periphery (Vidal et al. 2012).

The question if lamins can be characterized as activators of repression or repressors of activation remains still unanswered. During activation and differentiation, cells can go through a chromatin shuffling in the nucleus. Genes upon their transcriptional activation are usually moving towards the center of the nucleus and genes that are going to be silenced move towards the nuclear periphery. In contrary, there are exceptions whereby genes that are being activated move from the cell interior to the periphery in order to be expressed. In yeast, inositol-3-phosphate synthase (INO1), (hexokinase 1) HXK1 and (thiol-specific antioxidant 2) TSA2 genes are relocalized to the nuclear periphery in order to be expressed (Taddei et al. 2006). In almost all eukaryotic cells heterochromatin is concentrated at the nuclear periphery while euchromatin tends to occupy more internal regions in the nucleus. As an exception, rod photoreceptors are the only cells that present an inverted chromatin organization. In rod cells, euchromatin is tethered at the nuclear periphery while heterochromatin is localized at the center of the nucleus (Solovei et al. 2009). This phenomenon is thought to be important for the light transmission properties of rod cells. The

inversion is caused by developmentally controlled silencing of expression of lamins A/C and LBR. In contrast to the genomic distribution observed in most cell types, in rod cells both active and inactive genes are found mainly at the nuclear periphery. In these cells, nuclear periphery contains high levels of transcription factors and nascent transcripts (Solovei et al. 2009). Analysis of 16 species (nine nocturnal and seven diurnal) revealed a strong correlation between the presence of such an inverted nuclear arrangement and a nocturnal lifestyle. The main functional effect of the inverse organization seems to be changes in the optical properties of the cell, which have been hypothesized to contribute to the much higher sensitivity of the rod cells of nocturnal mammals to low light levels.

So far two lamin-dependent mechanisms have been reported, regarding the tethering of heterochromatin to the nuclear periphery. The study of nuclear organization, by analyzing rod photoreceptor cells from 39 mammalian species, showed that LBR and/or lamin A/C are essential for tethering heterochromatin to the nuclear periphery. The LBR-dependent mechanism explains how LBR selectively interacts with heterochromatin, by recognizing specific modifications of histone 4 in heterochromatin formation (Hirano et al. 2012). Lamin A/C can also bind chromatin, although typically it functions as a scaffold for other chromatin-interacting proteins, in particular LEM-domain proteins. Chromatin/DNA binding by lamins is not sufficient for heterochromatin tethering, but might synergistically enhance binding. The LEM domain containing protein Lap2b is implicated in gene silencing at the nuclear periphery in mammals. It interacts with HDAC3 which promotes heterochromatin formation and the LEM domain containing protein tethers the whole complex to NE (Zullo et al. 2012). In *C. elegans*, as in mammals LEM proteins are anchored the INM, interact with lamins and bind to chromatin (Ikegami et al. 2010; Mattout et al. 2011).

Unlike NL that associates with repressed and heterochromatin regions, NPCs were shown to interact with euchromatin and active genes (**Figure 21**). NUPs are linked with chromatin organization and they can promote transcription. It has been demonstrated that NUPs can sequestrate transcriptional regulators and mobilize the repressive or active chromatin environment. Overexpression of Nup98 increases the expression of interacting genes in human neural precursor cells (Liang et al. 2013). In yeast, gene recruitment sequences (GRS) on the promoters of *INO1* and *TSA2* are responsible for the re-localization of these genes to NPCs. Inhibiting the interaction of these genes with NPCs, can lead to reduced expression levels (Taddei et al. 2006). In *D. melanogaster,* Nup153 binds to 25% of the genome in continuous domains extending between 10-500 kb and these large Nucleoporin-Associated Regions (NARs) are enriched for markers of active transcription, including high RNA polymerase II occupancy and histone H4K16 acetylation. Moreover, NUPs mediate the male-specific dosage compensation complex in *D.*

melanogaster (Vaquerizas et al. 2010). Furthermore, NUPs can affect chromatin organization by mediating the interaction between genes. In human, Nup98 binding sites are enriched for GAGA factor binding (Liang et al. 2013). In yeast, Nup-binding sites are enriched for binding of the transcription factor RAP1 and loss of NUP2 can cause spread of silencing from telomeres (Sood and Brickner 2014). Recently it was demonstrated that Nup93 and Nup153 bind super enhancer regulatory structures that drive the expression of key genes and specify cell identity. These nucleoporin-associated super enhancers localize preferentially to the nuclear periphery and the absence of Nup153 and Nup93 results in dramatic transcriptional changes of the super enhancer-associated genes (Ibarra et al. 2016b).

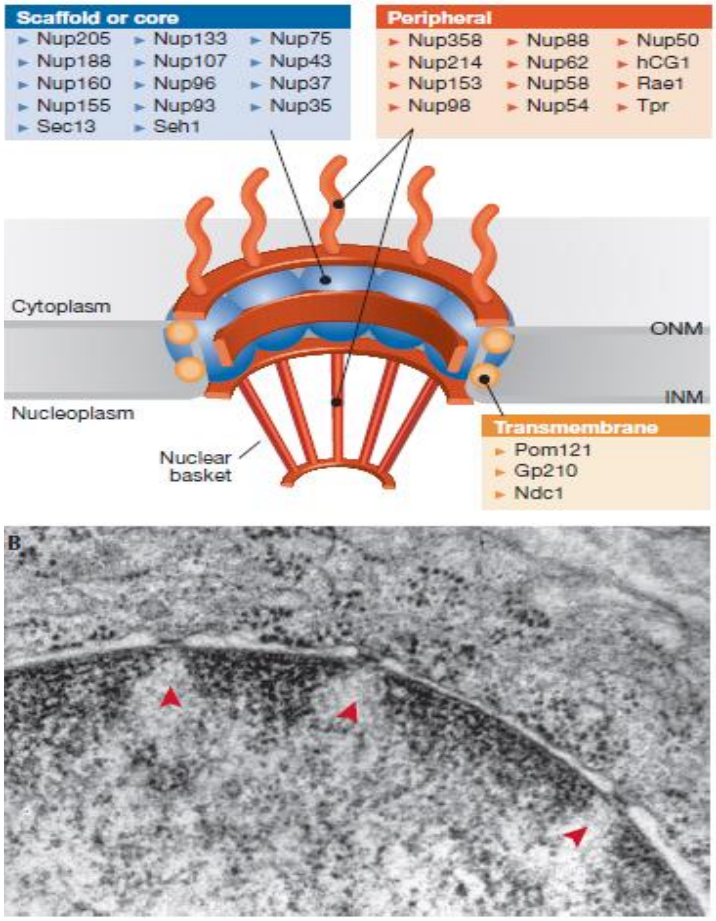

Figure 21. A) Structural components of the NPC complex. (B) Electron microscopy image depicting the NPC surrounded by euchromatin (light staining) while the dark staining shows the localization of heterochromatin (Capelson and Hetzer 2009).

1.6.5.2 Lamin Associated Domains (LADs)

Genomes of organisms that are evolutionarily distant, such as the fruit fly, mouse, and humans have large nuclear lamina–associated domains (LADs). These lamin-associated domains can vary between 0,1-10Mbp and consist around 40% of the genome. LADs were identified in 2000 by the DNA adenine methyltransferase identification (*DamID*) methodology (van Steensel and Henikoff 2000). *DamID* has the ability to map the binding sites of DNA- and chromatin-binding proteins in eukaryotes and it is based on

the fused LaminB1 protein to the bacterial Dam-methytransferase by leading to methylation of the associated genomic loci. The incorporated methylation marks are then identified by DNA sequencing and mapped onto the genome (Guelen et al. 2008). These condensed chromatin genomic loci, are AT-rich regions containing centromeric and telomeric sequences and other developmentally repressed loci, but can also include H3K4me3-marked chromatin that is found presumably unrepressed.

Major parts of LADs are conserved, although some small relocalization occurs during differentiation. Data from *DamID* experiments on different cell types showed three different groups of LADs: constitutive LADs (cLADs) as regions that are lamin-associated in all four cell types mentioned, constitutive inter-LADs (ciLADs) that are chromatin regions between LADs in all four cell types and facultative LADs (fLADs) that are regions for which LAD-status is cell type dependent (**Figure 22**) (Meuleman et al. 2013). Within cLADs, gene density reduces as the distance from the borders increases. As in TAD organization, LAD borders are also marked by binding of the CTCF insulator protein (5–10 kb outside LADs). Moreover, a discrete enrichment of promoters and CpG islands is observed outside LAD regions (Guelen et al. 2008; Meuleman et al. 2013). It is still unclear if the "intelligent" nucleus is placing the "non useful" heterochromatin and LADs to the periphery or if LADs are a result of active binding process. LADs are not static domains and during differentiation they can relocate from the periphery to the interior of the nucleus (Peric-Hupkes et al. 2010). The small movements of chromatin from the nuclear periphery can be explained by the activation of genes during differentiation and their localization to the interior of the nucleus in order to be transcribed. Except from the AT-rich elements and inactive genes, cLADs consist of gene desert and LINE elements while SINE elements are depleted in cLADS and overrepresented in ciLADs (Guelen et al. 2008). Comparing cLADs in mouse embryonic stem cells, human embryonic stem cells, fibroblasts and the human HT1080 fibrosarcoma cell line, a conservation of more than 71% of these regions is observed. cLADs between mouse, human and other metazoans such as *C. elegans* (embryos) and *D. melanogaster* (cultured embryo cells) show small differences and LADs are enriched for AT-rich elements compared to ciLADs (Ikegami et al. 2010; van Bemmel et al. 2010). Moreover, the ubiquitous DNA binding factor POU2F1 (also known as Oct1), which encompases an AT-rich DNA binding motif is localized at the nuclear periphery and binds LaminB1 (Malhas et al. 2009). Although, LaminA/C and LaminB have a different expression pattern upon differentiation, data from *DamID* experiments for LaminA/C binding in neuronal progenitor cells and astrocytes showed that ~94% of both proteins interact with the same genomic regions (Meuleman et al. 2013).

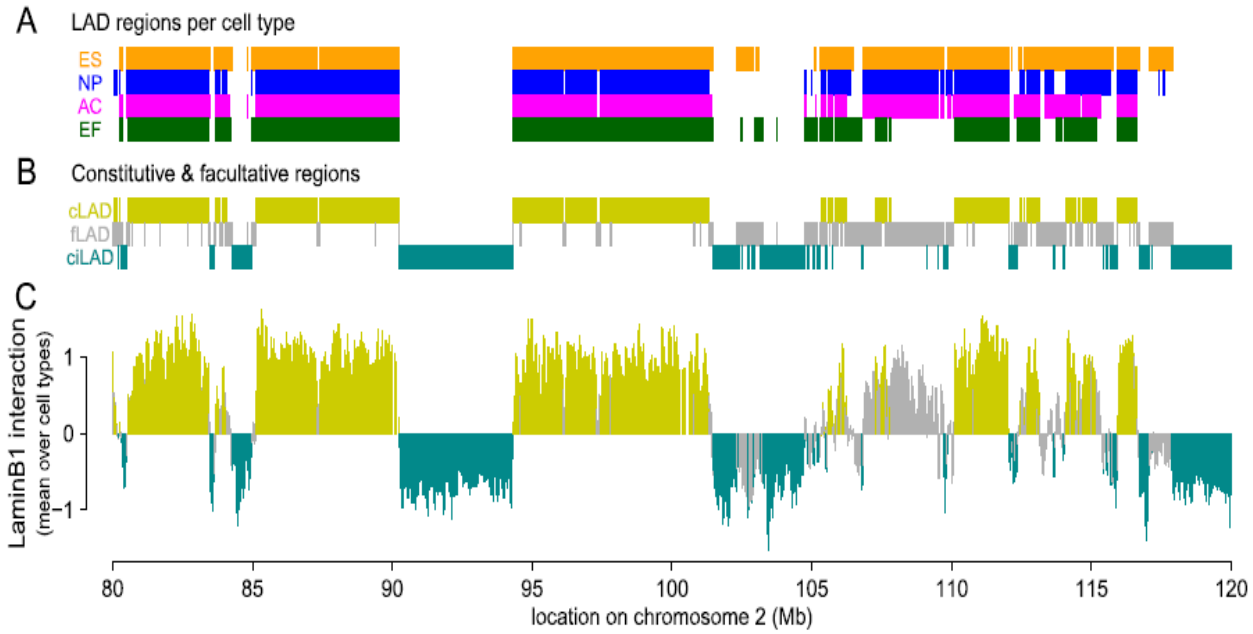

Figure 22. Depiction of genome–nuclear lamina interactions. (A) Regions classified as laminB1-interacting in mouse ESCs (orange), NPC (blue), astrocytes (pink), and MEF (dark green). (B) and (C) Regions common to all cell types are termed cLADs (mustard) and ciLADs (cyan), with dynamic regions termed fLADs (gray) (Meuleman et al. 2013).

1.6.5.3 CTCF as a genome organizer

CTCF (CCCTC-binding factor) is a highly-conserved zinc-finger multifunctional protein, which is implicated in different genomic functions and is characterized as a genome organizer. CTCF plays a crucial role in gene regulation (acting either as insulator or enhancing promoter transcription) and chromatin organization through mediating long-range chromatin interactions (**Figure 23**) (Hark et al. 2000) (Chen et al. 2008). CTCF is considered as the master weaver of genome organization (Phillips and Corces 2009). Initially, CTCF was discovered as a transcription regulator of the *c-Myc* proto-oncogene (Filippova et al. 1996). It is defined as an insulator due to its unique ability to block enhancer activity when it is located between enhancer and promoter sequences in reporter plasmids (Giles et al. 2010). The most well-studied of the CTCF insulator activity is the case of IGF2/H19 imprinted gene locus where CTCF mediates the functional regulation of promoters-enhancer communication (Beygo et al. 2013).

Apart from TAD demarcation, CTCF can also separate LAD borders (Guelen et al. 2008). CTCF sites that oversee chromatin looping are also bound by cohesin. Depletion experiments have revealed that CTCF is potentially in charge of the spatial segregation of TADs, while cohesin acts as an organizer within TADs.

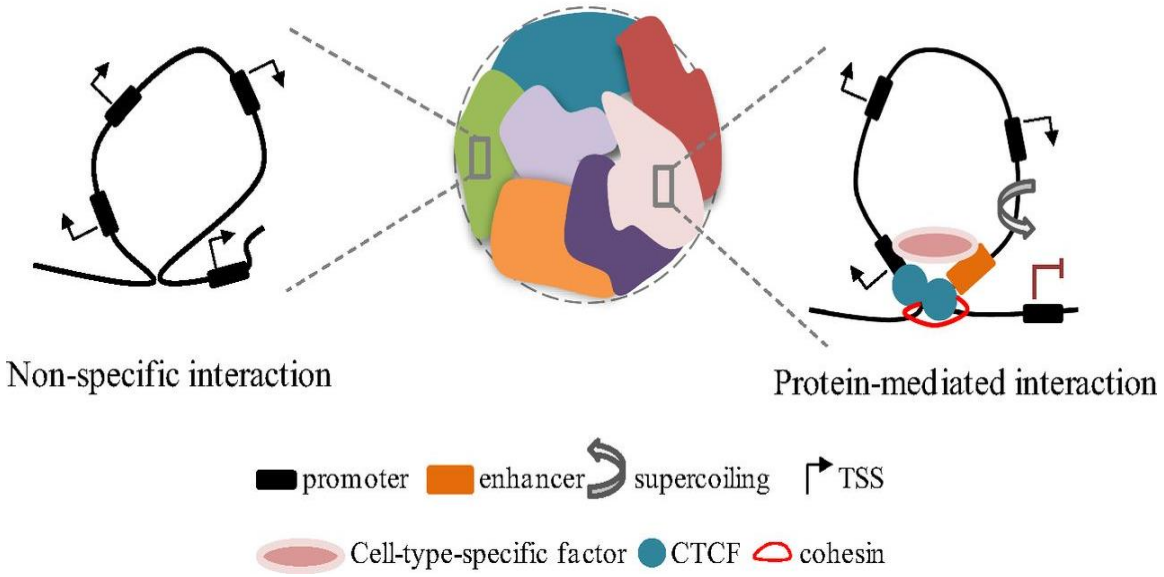

Figure 23. 3D chromatin organization mediated through genome organizers CTCF and cohesion (Baranello et al. 2014).

This can be explained by the fact that depletion of cohesin can affect the short-range chromatin interactions but not TADs formation, while depletion of CTCF affects the TADs borders and causes increased interactions between TADs which can lead to gene expression changes (Zuin et al. 2014). Recently, it was shown that chromatin looping is determined by the CTCF-binding polarity. Experimental data demonstrated that CTCF inverted binding sites (CRISPR-mediated inversion) and disengaged sites do not necessarily form new chromatin loops and cohesin recruitment to CTCF sites is independent of loop formation (de Wit et al. 2015). Moreover, ChIA-PET derived data for CTCF and RNA Pol II demonstrated that CTCF/cohesin-mediated interaction anchors, serve as structural foci for spatial organization of constitutive genes concordant with CTCF-motif orientation, whereas RNA Pol II interacts within these structures by selectively drawing cell-type-specific genes toward CTCF foci for coordinated transcription (Tang et al. 2015). Furthermore, another study reported that CTCF/PAPR1 (Poly ADP-ribose polymerase

1) complex can control circadian transcriptional activity by enhancing the interactions between circadian rhythm controlled genes and the nuclear periphery (LADs) (Zhao et al. 2015).

1.6.5.4 Cohesin as a genome organizer

Cohesin is a multiprotein complex that provides cohesion between sister chromatids during replication of DNA in S phase during cell division(Peters et al. 2008). Cohesin mediates the chromosome segregation through mitosis and meiosis and controls the integrity of genomic information passed on to the next generation (Brooker and Berkowitz 2014). In mammalian genomes, cohesin colocalizes with CTCF (Parelho et al. 2008). Apart from its function in the cell cycle, cohesin is also involved in nuclear organization and regulation of gene expression in interphase nuclei (Guillou et al. 2010; Ohlsson et al. 2010). Cohesin can control transcriptional activity by either bringing gene loci into proximity or by stabilizing the chromatin loops formed by CTCF (**Figure 24**) (Merkenschlager and Odom 2013). Moreover, cohesin has a crucial role in the post-mitotic DNA repair, is highly enriched at DNA damage sites and is extremely conserved through evolution (Strom et al. 2004; Nasmyth and Haering 2009).

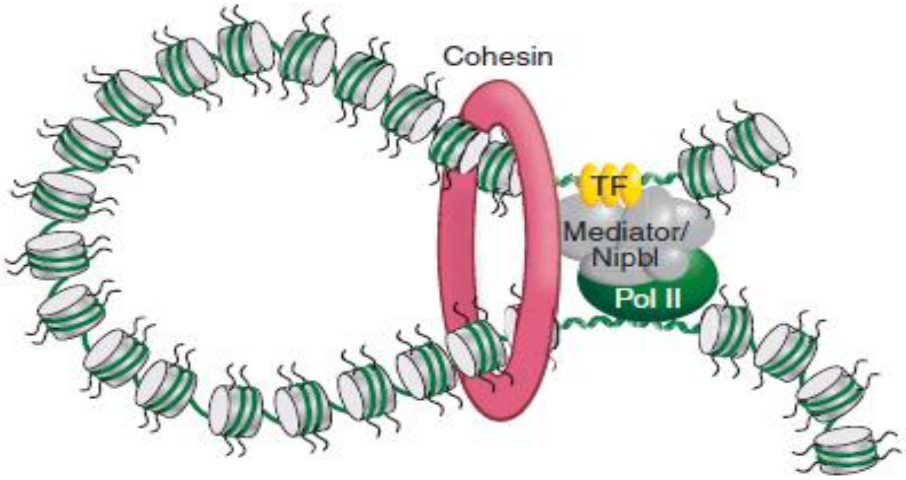

Figure 24. The long range interactions between gene promoters and enhancers are mediated through cohesion and the mediator complex. The complex of CTCF, cohesion and mediator organize the 3D structure of the mammalian genome by mediating the long range chromatin interactions (Dekker and Misteli 2015)

Genetic ablation of cohesin in *D. melanoagster* neurons cause defective axon pruning, while depletion of Rad21 (cohesin) in murine thymocytes can cease transcription and the rearrangement of the TCRα locus,

leading to defective thymocyte development (Pauli et al. 2010; Seitan et al. 2011). Furthermore, it has been reported that in human cells cohesin affects directly higher order chromatin conformation mediated through CTCF at the imprinted *IGF2-H19* locus. Depletion of cohesion led to a deregulation of the chromatin loop and affected the expression of *IGF2* locus (Nativio et al. 2009). Recent data from ChIA-PET experiments in human naïve and embryonic stem cells showed that cohesin-associated chromatin loops organize TADs in embryonic stem cells and during cell fate transitions functional changes occur within TADs (Ji et al. 2016) while another study reported that the conserved anchors of CTCF-CTCF loops are frequently mutated in cancer (Katainen et al. 2015).

1.6.5.5 SATB1 as a genome organizer

SATB1 (specific AT-rich binding protein 1) is a transcription factor that regulates T cell development and differentiation. SATB1 acts as a genome organizer and mediates the maintenance of higher-order chromatin structure. Structurally, SATB1 protein (763aa) contains a PDZ-like domain, a CUT repeat containing domain and a homeodomain as shown in **Figure 25A**. The PDZ-like domain in the N terminal region of SATB1 is necessary for its dimerization and it was shown to interact with β-catenin (Notani et al. 2010), promyelocytic leukemia (PML)(Kumar et al. 2007), HIV Tat, HDAC1 (Kumar et al. 2005) and CtBp proteins (Purbey et al. 2009). CUT domain is crucial for DNA binding and increases binding affinity. Moreover, the N-terminal region of SATB1 encompasses a ubiquitin-like domain that is implicated in its oligomerization (Wang et al. 2012). SATB1 shows a unique nuclear distribution in thymocytes that forms a "cage-like" or “aromatic” structure, circumscribing heterochromatin. This unique pattern is maintained in early stages of T_H2 cell differentiation but is abolished upon terminal T_H2 differentiation where SATB1 protein represents a diffused localization pattern inside the cell nucleus. Moreover, SATB1 can participate in a protein scaffold network (**Figure 25B**) by directly binding to specific DNA sequences, termed Matrix Attachment Regions (MARs) which are important for higher order chromatin loop formation. Upon its binding on DNA, SATB1 organizes chromatin architecture by tethering distant genomic loci into its network, facilitating their coordinated transcriptional regulation.

The fact that SATB1 is surrounding heterochromatin regions, suggests that the interchromatin space is occupied by chromatin loops containing gene dense regions with transcriptionally inactive genes (Cai et al. 2003). SATB1 binds to several gene loci to form a cluster at the stem of the chromatin loop and near

the regulatory domains of the genes. It is the constructor of the chromatin loop structure, or "loopscape", for global gene regulation that is leading to the expression of genes in a cell type specific manner.

SATB1-deficient mice have small thymi, spleen and lymph nodes and show a deregulated T cell development (Alvarez et al. 2000). The development of T cells is blocked at the DP stage and the $CD4^+$ or $CD8^+$ single positive thymocytes fail to further develop, resulting in the death of SATB1 knockout mice at the age of three weeks. Furthermore, in T cells the major histocompatibility (MHC) class I locus shows a specific loop structure, which is missing in other cell types. In T cells, SATB1 interacts with PML protein to organize the MHC class I locus into distinct higher-order chromatin-loop domain structures. IFNγ treatment and silencing of either SATB1 or PML induce dynamic reorganization of chromatin loops (Kumar et al. 2007). Another role of this genome organizer has been demonstrated in T_H2 cells. Upon differentiation of T_H2 cells, SATB1 is induced to form a transcriptionally-active chromatin structure that includes the TH2 cytokine gene locus which encompases the TH2-specific *Il4, Il5* and *Il13* genes (Cai et al. 2006). In DP cells the expression of *Rag1* and *Rag2,* is under the control of the anti-silencer element, which counteracts the activity of an intergenic silencer. It was demonstrated that SATB1 binds to the anti-silencer element (ASE) and *Rag* promoters, allowing the participation of *Rag2* in the chromatin hub and the interaction of RNA polymerase II to both the *Rag1* and *Rag2* promoters (Hao et al. 2015). As mentioned before, SATB1 regulates gene expression by recruiting histone modifiers. *In silico* analysis of the H3K9ac and H3K14ac modifications, demonstrated same binding sites with SATB1, supporting its ability to control the activation of gene expression and creating transcriptionally accessible chromatin regions in the genome (Galande et al. 2007). Interaction of SATB1 with chromatin remodelers such as ACF1, ISWI and histone deacetylase complexes can lead to inhibition of gene expression, through histone deacetylation and nucleosome remodeling (Yasui et al. 2002). Furthermore, it was shown that SATB1 is critical for $CD4^+$ T helper cell differentiation. In humans, more than 300 genes that are linked with the TH differentiation have been demonstrated to be regulate by SATB1, suggesting a crucial role in the appropriate generation and function of TH subsets (Ahlfors et al. 2010).

1.7 Chromatin organization in T cells

For the past decades the 3D organization of chromatin linked to gene expression has been an emerging field of investigation providing more details into gene regulation and expression during differentiation and development (Williams et al. 2006; Hiratani et al. 2008; Van Bortle and Corces 2012; Dixon et al. 2015;

Ricci et al. 2015; Stavreva and Hager 2015). Large number of epigenetic marks have been reported in T cells upon activation and differentiation, including histone modifications, chromatin modifiers and DNA methylation, in charge of regulating gene expression and altering chromatin organization (Zhang et al. 2012a). Interchromosomal interactions between distal regulatory DNA sequences (such as promoters, enhancers, insulators, locus control regions (LCR), non-coding sequences (CNSs)) play a crucial role in T cell differentiation and are directly correlated with gene expression levels. So far studies have tried to elucidate the role of the chromatin organization as a determinant of the T cell lineage commitment and identity (Zhang et al. 2012a; Hu et al. 2018; Issuree et al. 2018).

One of the most interesting key features during the journey of T cell development is the "resting" or quiescent phase. Upon thymocyte maturation the immature DN cells initially demonstrate a large morphology, although they became smaller with a condensed chromatin before they enter the DP phase. During this time $CD4^+$ cells show reduced levels of global transcription, low metabolic activities, reduced production of cytokines and significantly different nuclear organization and epigenetic hallmarks compared with terminally differentiated TH cells. The cells remain in quiescence phase until they encounter the TCR specific antigen, which leads to the clonal expansion of the peripheral $CD4^+$ cells. TCR activation promotes the production of IL2, with the last one activating the Stat5 through the Jak/Stat cascade (Rawlings et al. 2004). During T cell activation and differentiation, cells can go through chromatin shuffling in the nucleus. Resting lymphocytes demonstrate small nuclei, condensed chromatin with a significantly higher fraction of facultative heterochromatin compared to activated lymphocytes which have bigger nuclei containing more relaxed chromatin (Frangini et al. 2013). The quiescent phase of T cells is directly linked with epigenetic histone modifications. Cytokine promoters demonstrate hypo-acetylated histone modifications before activation (Roh et al. 2006). This chromatin condensation protects the cells from inaccurate signal activation by blocking the Stat5 to reach its targets unless there is a TCR signal that can lead to a proper activation. The condensation is required for the proper development of T cells and is mediated through condensin II complex (Rawlings et al. 2011). Chromosome relocalization is another phenomenon that has also been observed in T cells. In thymocytes during differentiation chromosome 6 shifts towards the center of $CD4^+$ cells and towards the periphery in $CD8^+$ cells (Kim et al. 2004). Chromosome 6 contains also the major histocompatibility (MHC) region at 6p21 which loops out from CT6 via large loops, in response to activation of MHC genes. A significantly increased proportion of nuclei displaying these loops were observed in B-lymphoblastoid cells and in Interferon-γ (INF-γ)-treated fibroblasts, which express the MHC genes, compared with untreated fibroblasts (Volpi et al. 2000). Multiple scientific reports have highlighted the significance of the chromatin changes during the

TCR engagement, while others studies have deciphered the chromatin accessibility changes during T cell activation (Burren et al. 2017). Despite the fact that single cell studies host technical challenges, nowadays chromatin accessibility studies are based not only DNase-seq MNase-seq NOMe-seq but also in scATAC seq, providing further details about chromatin organization (Buenrostro et al. 2015; Cusanovich et al. 2015; Jin et al. 2015; Pott 2017; Clark et al. 2018; Cusanovich et al. 2018; Lai et al. 2018). Recently, a systematic study connecting data from ssDnase-Seq, Hi-C and RNA-Seq peported that during the developmental transition from HSPC to DP cells, dynamic transformation of the chromatin takes place, where chromatin accessibility, TAD and intra TAD-organization but also the AB compartments are modified throughout the transition from DN2 to DN3 stage. The transition from DN2 to DN3 is one of the most pivotal T lineage commitment checkpoint. During the transition genes that promote multi-potency (such as *Hmga*, *Meis1*, *Lmo2*) are transfer from A compartment to B compartment, while genes that are related with maturation and selection of the T cells (such as *Bcl11b*, *Ets1*, *Tcf7*, Cd3d, and Lef1) relocate from B compartment to A compartment (Hu et al. 2018).

1.8 Long and short range chromatin associations in T cells

Chromosomal interactions (inter- or intra-) are prominent factors of the chromatin organization and biological processes, that orchestrate the gene expression. Direct physical interactions are revealed by the new techniques that enabled either the visualization (Fluorescence *In Situ* Hybridization-FISH) or sequencing of the chromatin conformation capture methods (3C, 4C, 5C, Hi-C, ChIA-PET) of the interacting chromatin domains (Spilianakis et al. 2005; Nora and Heard 2010; Dixon et al. 2012; Sexton et al. 2012; Cavalli and Misteli 2013; Chaumeil et al. 2013). As mention above, the immune system remains one of the best developmental model system to study these interactions since in most of the cases each interaction is directly linked to a physiological response. Whilst in D. melanogaster the interchromosomal associations have been widely studied (Chen et al. 2002; McKee 2004; Bateman et al. 2012) reporting transvection (pairing of homologs chromosome) to be spread widely in the genome(Mellert and Truman 2012), only few studied have reported the interchromosomal interactions in mammalian cells (Spilianakis et al. 2005; Monahan et al. 2019). One of the most studied case is the X inactivation where the LINC *Xist* (X-inactive specific transcript) covers the X chromosome in *cis* and leads to silencing (Bacher et al. 2006; Xu et al. 2006). Another example of molecularly well understood interchromosomal interaction is the expression of the olfactory receptor genes, where a single enhancer (H-enhancer) can cause the monoallelic expression of only one of the 1300 odorant receptors genes (Lomvardas et al. 2006; Clowney et al. 2012). In other studies, chromosomal interactions have been reported to be directly linked with diseases

(Thatcher et al. 2005; Koeman et al. 2008; Liu et al. 2008). Nevertheless, interchromosomal interactions have been reported in lymphocytes as well. During T cell differentiation, long range intrachromosomal interactions control the regulation of cytokine genes. For instance, the ectopic expression of the β-globin locus control region (LCR) was reported to interact with the active globin genes within the active chromatin Hub, demonstrating a mammalian trans activation (although in low frequencies) (Carter et al. 2002; Tolhuis et al. 2002; Vieira et al. 2004; Noordermeer et al. 2011).

In T cells one of the most well studied functional interchromosomal association between genes located in different chromosomes was reported for the *Th2* locus (consisted of Interleukin 4 (*Il4*), interleukin 5 (*Il5*) and interleukin 13 (*Il13*) and their LCR located on chromosome 11) and IFNγ (chromosome 10) in naïve $CD4^+$ cells. Upon T cell activation the interaction is dissociated and the cells are differentiated into TH1 or TH2 lineage, suggesting that when these two loci interact the genes are repressed. The later was also confirmed by genetic ablations of the Th2 locus, that directly affected the expression of INF-γ (Spilianakis et al. 2005; Williams et al. 2010). Subsequent studies validating the significance of the long range chromatin interactions in T cells, based on ChIA-PET strategy in human primary resting $CD4^+$ cells have also documented the long range chromatin interactions, where among the 6520 long-distance chromatin interactions, 2067 enhancers were identified to interact with 1619 promoters and enhance their expression. In the same report RUNX1 gene (located on chromosome 21) was found to interact with six enhancers, while another important locus for the T cell development, VAV1 locus (located on chromosome 19-known to contain a rich network of multiple enhancer and promoters) was found to interact with four potential enhancers (Chepelev et al. 2012). Additionally, long range chromatin intrachromosomal interaction have been reported for IFNg-IFNgR1 gene loci in CD4+ and TH1 cells. IFNg is the master regulator of the TH1 differentiation. *IFNg* gene and *IFNgR1* gene are both positioned in chromosome 10 separated by a region of 98.5Mb. DNA FISH combined with 3C experiments demonstrated that the *Ifnγ R1* gene promoter comes in close proximity with the *Ifnγ* gene in order to be monoallelically expressed in both $CD4^+$ and TH1 cells. The interaction is CTCF mediated and independent of active transcription in each cell type (Deligianni and Spilianakis 2012). Similarly, it was also demonstrated that upon differentiation of naive $CD4^+$ into TH1 cells, the *cis* interaction of the *IFNγ* locus is mediated by cohesion (Hadjur et al. 2009). Another example of long range chromatin interactions in T cells was reported on the expression of IL-21 in $CD4^+$ cells. IL21 is an essential pleiotropic cytokine that is produced in actvated CD4 cells and can promote differentiation through TH17 and TfH. IL21 expression is upregulated in a STAT3- and NFAT dependent manner, by an enhancer element that is located in a conserved noncoding sequence 49kB upstream of the IL-21 gene (Park et al. 2016). Furthermore, it has

also been shown that in double positive (DP) thymocytes and single positive naive T cells, where the CD8 locus was activated upon intrachromosomal interactions between the CD8α promoter and the CDβ gene. Such an interaction was only observed in low levels in B cells (where the CD8 locus is not activated)(Ktistaki et al. 2010). All the above data accentuate the importance and the necessity of the dynamic long range chromatin interaction during T cell development and underline how these events can affect 3D chromatin conformation in subsequent T cell lineages upon activation and differentiation.

MATERIALS AND METHODS

Ethics

All experimental design and procedures presented in this study, were conducted according to Greek national legislations and institutional policies upon ethical committee approval. Mice were cared for and managed within the Institute of Molecular Biology (IMBB) Core Facility (**https://www.imbb.forth.gr/imbb-people/en/animal-house**) following Institute guidelines based on the Greek ethical committee of animal experimentation, approved by the General Directorate of Veterinary Services, Region Crete (license number: EL91BIO-02).

2.1 Isolation and *in vitro* differentiation of murine CD4$^+$ T cells

Thymocytes were isolated from four week old C57BL/6 mice. Peripheral lymphocytes were obtained from axillary and popliteal lymph nodes and spleens of 5-6-week-old C57BL/6 and conditional knockout mice (SATB1). CD4$^+$ T cells were isolated from the mixed population by positive selection conducted with CD4 magnetic MicroBeads and MACS separation columns (**Figure 26**). Mouse embryonic stem cells JM8A3 N.1 (derived from C57BL/6N mice, feeder independent) were cultured in Dulbecco's Modified Eagle's Medium supplemented with 15% fetal bovine serum, 1% L-Glutamine, 1% penicillin and streptomycin, 3mM CHIR99021, 1µm PD0325901, 500 U/ml leukemia inhibitory factor and 100 µM β-mercaptoethanol.

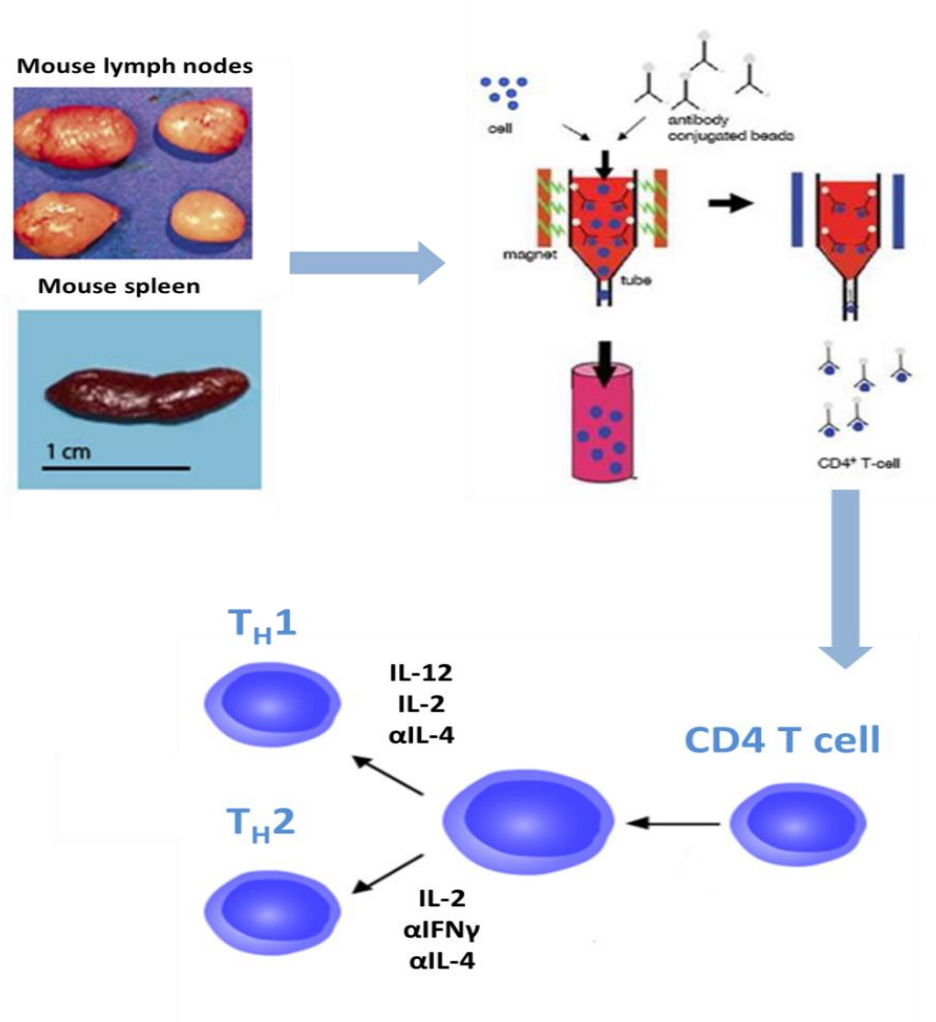

Figure 26. Schematic representation of Isolation and *in vitro* differentiation of mouse CD4 T cells.

2. 2 Isolation of peritoneal macrophages

For peritoneal macrophage isolation 10- week old C57BL/6 mice were intraperitoneally injected with 2 ml of 4% w/v thioglycollate medium diluted in 1X Phosphate-Buffered Saline (PBS). Four days after the injection the mice were sacrificed and washed intraperitoneally with 15 ml filtered saline. Following the peritoneal lavage the cells were centrifuged at 1500 rpm for 5 minutes and resuspended in fresh Dulbecco's Modified Eagle's Medium (DMEM) supplemented with 10% fetal bovine serum, 2mM L-Glutamine, 1X penicillin and streptomycin under sterile conditions. The cells were seeded on culture dishes and incubated under 5% CO_2 at 37°C for at least 24 hours before any experimental treatment. Macrophages isolated with this protocol were characterized by advanced cellular adhesion under culture conditions and expression of the integrin alpha (CD11b or Mac-1) surface marker as tested with Immunofluorescence experiments described below.

2.3 Cell culture

For cell culture, all the cell-sorting procedures were carried out under sterile conditions. Differentiation of naive $CD4^+$ T cells was carried out by stimulation with plate-bound αCD3 and αCD28 antibodies. Cells were cultured under 5% CO_2 at 37°C in CLICK's medium supplemented with 100μg/ml Penicillin/Streptomycin, 0.05mM β-mercaptoethanol, 2mM L-Glutamine and 25mM HEPES for five days. Cells were cultured at 1,5-2×10^6 cells/well in 12-well plates. For T_H1 cell differentiation, the medium was supplemented with 20 units/ml IL-2, 3.5 μg/ml IL-12 and 10 mg/ml IL-4. For T_H2 cell differentiation we used 20-50 units/ml of IL-2, 10 μg/ml IL-4 and 10 mg/mlIFNγ). Restimulation of terminally differentiated T_H1 and T_H2 cells was carried out with αCD3 antibody for one hour. Cell identity upon opposing conditions of differentiation was further assessed by qRT-PCR experiment for the expression of *Il4* and *Ifnγ* genes.

2.4 Total RNA Isolation

In order to check the pri-microRNA expression in T cells, RNA was isolated using the TRI-REAGENT following the manufacturer's instructions. Firstly cells were isolated, stimulated (when necessary), counted and added to 1ml TRI-REAGENT. For 1ml of Trizol reagent a total number of $1x10^6$ cells was used. Cells were lysed with Trizol reagent for 5 minutes at room temperature. 0.2ml chloroform was added to the lysate and then vortexed and centrifuged at 14000 rpm for 20 minutes at 4°C. The RNA containing aqueous phase was collected and precipitated. RNA was precipitated using 1/10 of the reaction volume CH3COONa 3M pH 5.2, two volumes of 100% ethanol and 0,25 μg/μl of linear acrylamide. Samples were centrifuged for 20 minutes at 4°C and the RNA pellets were washed with 75% ethanol and reconstituted in 30 μl DEPC-treated H_20

2.5 Reverse Transcription and *c*DNA synthesis

In total 1 μg of DNase I treated RNA was used for reverse transcription reactions using an Oligo d(T) primer and M-MuLV Reverse Transcriptase, following the manufacturer's instructions. 10% of the cDNA produced was used for quantitative PCR (qPCR) using the SYBR Green PCR Master mix according to the manufacturer's instructions. The thermal cycler used for the aforementioned reactions was an Opticon2 DNA Engine (MJ Research) creating standard curves. Reactions were performed in triplicate for statistical evaluation. The results were normalized over *Hprt1* mRNA levels. The primer sets used for pri-microRNA quantitation are provided in **Table 1**.

MIR gene	Forward primer 5'→3'	Reverse primer 5'→3'
miR-181a1b1	GCTGAAGACAGAACCGCAAA	AGTTAAACCGAGAAACGGCG
miR-181a2b2	GACCGTTGACTGTACCTTGG	AGGCCACAGGACTGTATCTTG
miR-150	GCAACAACTCCAGCTTCTCC	TGATCTGCTTGAACCCCTGT
miR-181c	GGCAAGTTCTTGGATAACTGGAG	TTGCAGGGGCTGCGTTTT
miR-142	GAAGAATCCCCGTGGACAGA	CCCAAGTATCAGGGGTCAGG
miR-146a	GCCAGCCCTGTAAAAACACA	TCTTCGCTGGGATTATGGGG
miR-17/92	TCCATAGTTGTGTTTGCAGCC	AAGTAAATAGCAGGCCACCATC
miR-155	ACCCTGCTGGATGAACGTAG	CATGTGGGCTTGAAGTTGAG
miR-let7e	TTCTGGTCTCCCATCAATCC	CAGAGAAGACACCCCAGCTC
Hprt1	GTCCCAGCGTCGTGATTAGC	TTCCAAATCCTCGGCATAATG

Table 1. Primer sets utilized for pri-microRNA quantitation.

2.6 Western blot

Protein extract

Thymocytes were isolated, washed with 1xPBS and centrifuged at 1400rpm for 5 minutes. The pellet was retained and the washing step was repeated. A total of $400x10^6$ cells were incubated in lysis buffer (50 mM Tris-HCl, pH 8, 170 mM NaCl, 0.5% Nonidet P-40, 50mM NaF (Serine/Threonine phosphatases), 1mM PMSF and 1x Complete Protease Inhibitors for 40 minutes on ice under agitation and followed by centrifugation at 14000rpm for 15 minutes at 4^oC. Protein concentration of the cell lysate was determined by the Bradford Assay.

Bradford assay

The Bradford Assay is a dye-binding assay in which a differential color change of a dye occurs in response to various concentrations of protein. The absorbance maximum for an acidic solution of Coomassie ® Brilliant Blue G-250 dye shifts from 465nm to 595nm when binding to protein occurs and it binds to primarily basic and aromatic amino acid residues, especially arginine. The 5x Protein Assay Dye Reagent Concentrate was diluted with deionized water and filtered through Whatman paper to remove particulates. Three different dilutions of the protein extract were used (1:1, 1:10 and 1:100) and protein extract samples were assayed in triplicate. Five dilutions (1mg/µl, 800ng/µL, 400ng/µL, 200ng/µL, 100ng/µL and 50ng/µL) of Bovine serum albumin (BSA) were used in order to calculate the concentration of the protein extracts. All samples (standard protein and protein extract) were incubated at room temperature for at least 5 minutes to increase the absorbance. The absorbance was measured at 595 nm and the final concentration of the protein was conducted from the standard curve, which has been constructed based on the measurements of the BSA protein. In total, 30µg of protein extract were used for the western blot assay.

For the denaturation of the proteins, 5x Laemmli buffer (10% SDS, 50% Glycerol, 100mM Tris pH 6.8, 80mM β-mercaptoethanol or DTT, 0.05% w/v Bromophenol blue) was used and samples were boiled at 95°C for 5 minutes. Protein extracts were subjected to SDS-PAGE. The Stacking gel: 4.5% of Acrylamide/Bis, 0,1% SDS, 0.125 M TRIS-HCl, 2 mM EDTA pH 8.8, 0.08% APS and 0.04% TEMED) gather the proteins of each sample in a very thin layer before they are separated and the Separating gel: (8-12% of Acrylamide/Bis, 0,1% SDS, 0.375 M TRIS-HCl, 2 mM EDTA pH 8.8, 0.04% APS and 0.04% TEMED) in which the proteins ultimately separate based on their apparent molecular weight. Initially, the voltage used was

35V until the dye reached the separation gel and then a voltage of 150V was used to separate the proteins. Next proteins were transfered under wet conditions for 16 hours. The gel, the filter paper and fiber pads were incubated in transfer buffer (Tris 48mM, glycine 39mM, SDS 1.3mM, methanol 20%) for 15 minutes. The transfer was conducted under continuous stirring of the buffer solution at 4°C. Confirmation of the successful transfer was performed by staining the membrane with Ponceau-S (0,2%).

Figure 27. Illustration of prepared stack for protein transfer during Western blot assay.

The immunoassay is a technique that allows the detection of proteins that have been transferred to a nitrocellulose membrane with the aid of a specific antibody against the protein of interest. The technique is based on the detection of the protein being transferred by adding a secondary antibody conjugated with horseradish peroxidase (HRP). The HRP reacts with exogenously added substrate and emits luminescence or gives typical reaction color. The nitrocellulose membrane was incubated for 20 minutes in blocking buffer (5% milk dissolved in 1xPBS-0.1% Tween-20) in order to block the binding sites of membrane proteins and to avoid nonspecific binding of the antibody. The nitrocellulose membrane was then rinsed with 1xPBS-0.1% Tween-20 for 10 minutes to remove the residual blocking buffer. The membrane was incubated overnight at 4°C with the primary antibody (dilution: anti-DROSHA 1/1000, anti-SATB1 1/5000). After the incubation with the primary antibody, the membrane was rinsed three times with 1xPBS-0.1% Tween-20 at room temperature, under continuous agitation for 10 minutes. Then the secondary antibody was added for one hour at room temperature (dilution: 1/20.000 rabbit HRP). The ECL substrate is a highly sensitive non-radioactive, enhanced luminol-based chemiluminescent substrate for the detection of horseradish peroxidase (HRP). The ECL Western Blotting Substrate detects picogram amounts of antigen and with the use of photographic or other imaging methods visualizes the presence of HRP. Firstly, the substrate was prepared by mixing equal parts of the Peroxide Solution and the Luminol

Enhancer Solution provided by the manufacturer. The membrane was incubated for one minute at room temperature. The solution was removed and the membrane was placed in a film cassette. An X-ray film was placed on top of the membrane and exposed for 1 minute by using the AGFA Curix 60 Film Processor.

2.7 Bacterial Artificial Chromosome (BAC) clone culture

Nine murine BAC clones (8 clones for microRNA genes and *TNFα*) (see **Table 2**) were used in order to prepare probes for DNA-FISH. All BAC clones were purchased from BACPAC Resources Centre - CHORI in the form of bacterial glycerol stocks. Firstly, each BAC clone was streaked onto Petri dish plates with custom-made LB media containing 12.5μg/ml chloramphenicol and incubated for approximately 24 hours, upside down in a 37°C incubator. A single colony was selected and inoculated into 1 ml liquid LB media (supplemented with 12.5 μg/ml chloramphenicol). After overnight incubation at 37^0C, 1ml of each liquid culture was used for BAC DNA isolation and PCR reconfirmation of the proper sequence integration in each corresponding BAC clone. For BAC DNA isolation the cells were spun for 1 min at 6000 rpm at room temperature. The pellet was resuspended by vortexing in 100 μl ice cold P1 solution (50mM Tris, pH8, 10mM EDTA pH 8 and 400 ng/μl RNase A). An equal volume of P2 solution (0.2 NaOH, 1% SDS) was added to the pellet in order to lyse the cells, incubated at room temperature for 5 minutes and neutralized with P3 solution (3M KoAc pH 5,5) for 5 minutes on ice. Upon centrifugation at 14.000 rpm for 10 minutes at RT the supernatant was collected and the BAC DNA was precipitated with 2,5 volumes of 100% ethanol. The DNA preparations were further centrifuged at 14.000 rpm for 10 minutes at 4^0C. The DNA pellet was washed with 75% ethanol and reconstituted in 30 μl ddH_20. The concentration and the purity of the isolated BAC DNA were determined with both spectrophotometric assay (Nanodrop) and agarose gel electrophoresis. For BAC DNA reconfirmation, PCR reactions were performed. Each reaction was prepared in a final volume of 50 μl containing 5μl DNA, 2 mM MgCl, 0.4 mM dNTPs, 10 pmol of each forward and reverse primer and 2.5 U Taq polymerase. The PCR cycles were as following: the initial incubation at 94°C for 5 min, 40 cycles of denaturing (94°C for 40 sec), annealing (60°C for 40 sec) and extension (72°C for 36 sec) and the final extension at 72°C for 10 min. The PCR products were then analyzed by electrophoresis of the products on 1.5% TBE agarose gel. The primer sets used in this assay are listed on **Table 3**.

Genomic locus	Location	BAC clone
miR-181a1b1	chr.1	RP24-71D3
miR-181a2b2	chr.2	RP24-128E22
miR-150	chr.7	RP24-246G23
miR-181c	chr.8	RP24-368F14
miR-142	chr.11	RP24-376D9
miR-146a	chr.11	RP23390G172
miR-17/92	chr.14	RP23-7L16
miR-155	chr.16	RP24-278G19
miR-let7e	chr.17	RP24-308G19
***LT/TNF* locus**	chr.17	RP23-446C22

Table 2: The murine BAC clones used for the preparation of DNA-FISH probes

microRNA gene	Forward primer 5'→3'	Reverse primer 5'→3'
miR-181a1b1	CTGAAGACAGAACCGCAAAGC	AAACGGCGTTAATACCCC
miR-181a2b2	CAACAGCAGTGGTCCTTAGAA	CCTTTGCTTCAGGAAACTTGT
miR-150	CAGGTTTGGCCTACATACA	TATCATGATCTGCTTGAACCC
miR-181c	TCACAACCCACCGACAACAAT	CTCTCCCAACTCCAGTTATCC
miR-142	CGCTCTCTCGAATGCACGTC	AATTAGAGCCAAAGGTAGAGG
miR-146a	AGGAGGAATAGGCGTTGAGG	CTGGGACACAAGATAGGCAAGT
miR-17/92	AGGCTTACATGTGTCCAATTT	ATGCCAGAAGGAGCACTTAG
miR-155	TTGGCCTCTGACTGACTCC	CATGTGGGCTTGAAGTTGAGA
miR-let7e	AAAGAAACAAGAAGACGGAC	ATCCCTTAGAGAAGACAATCTG

Table 3: Primers used for the reconfirmation of BAC clones

2.8 3-D DNA Fluorescence *in situ* hybridization (3D DNA-FISH)

Cell preparation

Cells were seeded on sterile glass coverslips and restimulated (T_H1 and T_H2 with aCD3 for one hour). Cells were then fixed with 4% PFA in 1X Phosphate-Buffered Saline (PBS) for 12 minutes, permeabilized with 0.5% Triton X-100 for 5 minutes, rinsed with 1xPBS and incubated in 20% glycerol in 1xPBS for 30 minutes. After three freeze-thaw cycles in liquid nitrogen, the cells were incubated in 0,1N HCl for four minutes. Finally, the cells were rinsed with 2xSSC (for 20xSSC: 3M NaCl, 0.3M Sodium citrate) and stored in 70% ethanol at 4°C.

Probe preparation for hybridization

100ng from each DNA probe and 1μg mouse COT-1 DNA were lyophilized using the Concentrator plus for 15 minutes at 45°C. The pellet was resuspended in 5μl de-ionized formamide and incubated at 37°C for one hour. Probe DNA was further denatured at 95°C for 5 minutes and then mixed thoroughly with 5μl of 2x hybridization buffer (4xSSC, 20% Dextran sulfate, 50 mM Sodium Phosphate).

Cell preparation for hybridization

Cells were dehydrated with four washes of increasing ethanol concentrations (70%, 80%, 95% and 100%). The glass coverslips were briefly air-dried and then incubated with denaturation buffer (70% deionized formamide, 2xSSC, pH7, pre-warmed at 73°C) for 5 minutes at 73°C. The cells were again dehydrated in increasing concentrations of ice-cold ethanol. Hybridization: each probe was placed separately on a glass microscope slide and the cell-spotted side of the coverslip was flipped on top of the hybridization buffer, sealed with rubber cement and incubated at 74°C for 4 minutes for T_H1 and T_H2 cells, at 72°C for 5 minutes for CD4 cells and at 73°C for 5 minutes for thymocytes. The hybridization step continued for 12-16 hours in a humidified hybridization chamber at 37°C. After the completion of hybridization, washing steps were performed to eliminate the background noise in the imminent imaging procedure. The coverslips were washed three times with 2xSSC, once with 1xPBS and then left to dry off water residuals. The coverslips were then mounted on ProLong Gold anti-fade reagent supplemented with DAPI for nuclear DNA staining.

Plasmid constructions for RNA FISH probes

RNA FISH probes were specifically constructed to detect the primary microRNA (pri-miR) transcript. The first step included the creation of eight different 1kb DNA fragments cloned into TOPO® TA vectors. The purified BAC DNA was used as a template for the 1kb sequence amplification. The primer pairs used for PCR amplification are listed on **Table 4**. The isolated fragments were cloned into a TOPO® TA vector and transformed DH5a strain of E.coli cells by heat shock at 42°C for 90 seconds. Transformed bacteria were plated on solid LB medium containing 100 μg/ml ampicillin and 50 μg/ml of X-Gal, β-galactosidase substrate and incubated at 37°C overnight. After blue-white selection, white colonies further inoculated liquid LB cultures for small-scale plasmid DNA isolation and cloning efficiency verification through restriction enzyme digestion. The restriction sites of the TOPO® TA vector in use are cited in **Figure 28**. After screening all the aforementioned clones, larger LB cultures followed in order to isolate the recombinant plasmids, have them sequenced and use them for RNA FISH probe preparation. Plasmid DNA isolated was phenol-chloroform purified and biotinylated using either the Biotin Nick Translation kit or the Biotin NT labeling following the manufacturer's instructions.

microRNA gene	Forward primer 5'→3'	Reverse primer 5'→3'
miR-181a1b1	CATGCGTCCTTGCAGTTCTTT	GGATAACGGGGCAGGAAGTA
miR-181a2b2	GTGAGAGACCCAACAGCAG	CCTGGAGCAGTACTTCCGTA
miR-150	CTAGGCTCTCAGGCAGTGTT	GTCCTGGGACAGAGCAAAGA
miR-181c	GGTCGATGGTTTGTCTGAGC	GCAGGAGTTTCACACAAGCA
miR-142	GCCATTTCTGCCAACACACT	CCCCAGGCTGTGTCTTAGTC
miR-146a	AGCACTGTCAACCTGACACA	GGACCAGCAGTCCTCTTGAT
miR-17/92	ACTTCTGGCTATTGGCTCCT	AACTTCACCTAAGCCCCCAC
miR-155	CGGTTTGTGAGTCCCCAAAG	ATGTCAGTCGAGAATGGCCG
miR-let7e	CACCCTCCCTACTTCTGGTC	AAAGGAACCAGGAGATGCCT

Table 4. Primer sets used for PCR amplification

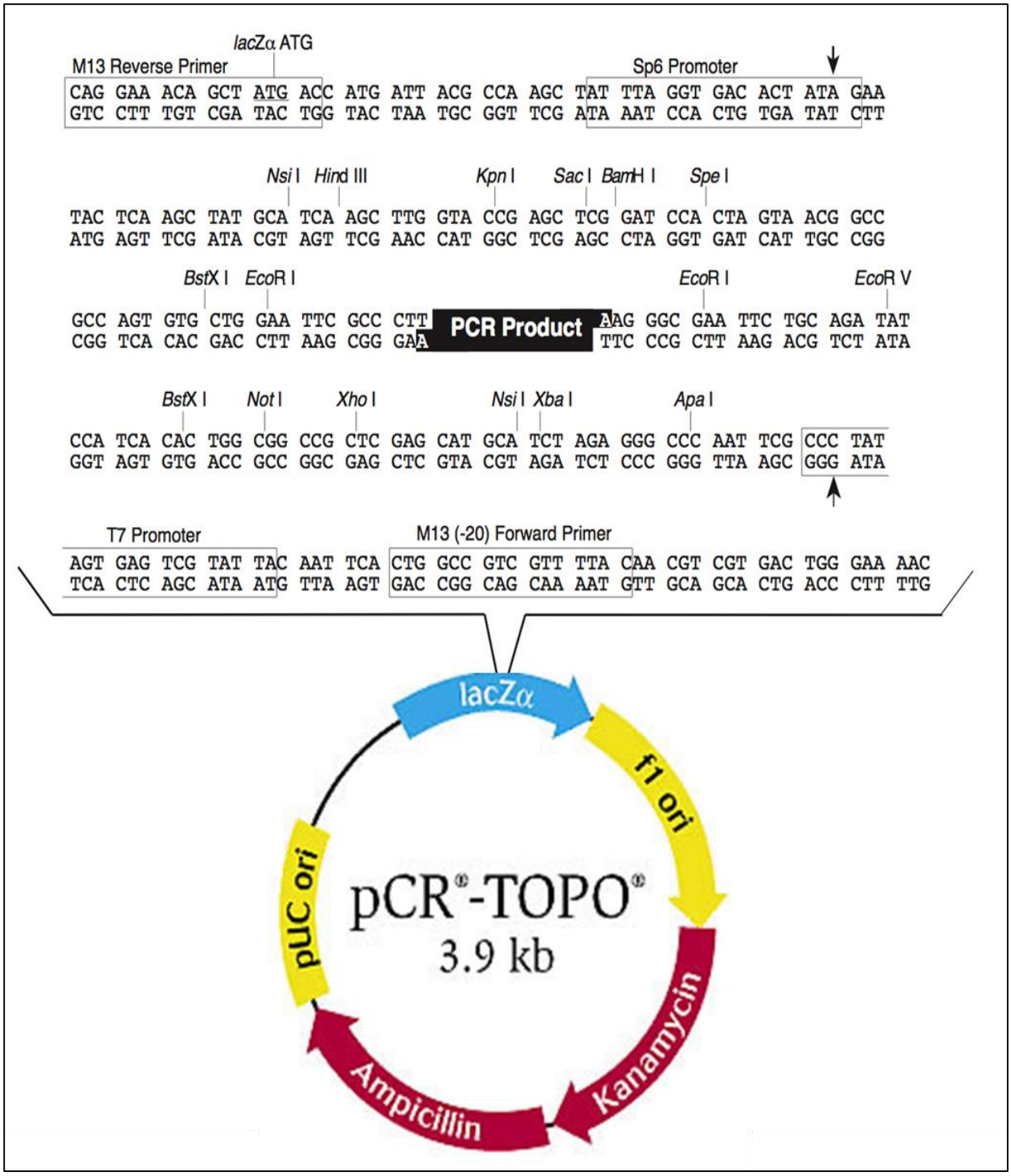

Figure 28. Schematic representation of the 3973 nt pCR®II- TOPO® cloning vector containing: LacZα gene: bases 1-589, M13 Reverse priming site: bases 205-221, Sp6 promoter: bases 239-256, Multiple Cloning Site: bases 269-383, T7 promoter: bases 406-425 M13 (-20), Forward priming site: bases 433-448, f1 origin: bases 590-1027, Kanamycin resistance ORF: bases 1361-2155, Ampicillin resistance ORF: bases 2173-3033, pUC origin: bases 3178-3851. (https://tools.thermofisher.com/content/sfs/vectors/pcriitopo_map.pdf)

2.9 RNA-DNA Fluorescence *in situ* hybridization (RNA-DNA FISH)

Cell preparation

All the buffers and solution used for the RNA-DNA FISH experiments were RNAse free. Initially cells were seeded on sterile glass coverslips as previously described. Cells were then transferred on ice and washed with ice cold 1X Phosphate-Buffered Saline (PBS) twice. For the cytoplasm removal, cells were treated for either 2.5 minutes (thymocytes and CD4) and 3 minutes (T_H1 and T_H2 cells) with cytoskeletal buffer (CSK) containing 100 mM NaCl, 300 mM sucrose, 3 mM MgCl2, 10 mM PIPES, 0.5% Triton X-100, 1mM EGTA, and 2 mM vanadyl-ribonucleoside complex. Cells were then fixed with 4% PFA in 1xPBS for 10 minutes, washed three times with 70% ethanol and stored in 70% ethanol at -20°C until use.

Probe preparation for hybridization

100ng from each probe, 1µg mouse COT-1 DNA and 20 µg yeast transfer RNA were lyophilized using a SpeedVAc (vacuum concentrator) for 15 minutes at 45°C. The pellet was resuspended in 5µl de-ionized formamide and incubated at 37°C for one hour. Probe DNA was further denatured at 95°C for 10 minutes and then thoroughly mixed with 5µl of 2x hybridization buffer (4xSSC, 20% Dextran sulfate, 2mg/ml acetylated BSA, 50 mM Sodium Phosphate).

Cell preparation for hybridization

Cells were sequentially dehydrated with four washes of increasing ethanol concentrations (70%, 80%, 95% and 100%) and briefly air-dried. Hybridization: each probe was placed separately on a glass microscope slide and the cell-spotted side of the coverslip was flipped on top of the hybridization buffer, sealed with rubber cement and incubated for 4 minutes at 73°C. The hybridization step continued for 12-16 hours in a humidified hybridization chamber at 37°C. The steps following hybridization, important for the signal amplification of pri-microRNA transcripts, were conducted using the TSA Biotin System kit according to the manufacturer's instructions. Specificity of RNA FISH probes was verified with hybridization upon RNase treatment of cells. For RNase A treatment, the cells were incubated with 100µg/ml RNaseA for at least 30 minutes prior to hybridization.

2.10 Immunofluorescence

Cells were isolated, stimulated as previously described and seeded on sterile glass coverslips. Cells were fixed in freshly prepared 2% PFA for 10 minutes at RT, permeabilized with 0.5% v/v Triton X-100/1xPBS for 5 minutes and rinsed with 1xPBS. Cells were blocked in 1% w/v BSA/1xPBS for 30 minutes at RT, incubated with the primary antibody for one hour at RT in a dark and humidified chamber, rinsed three times in 1xPBS, incubated with the secondary antibody for 45 minutes at RT in a dark and humidified chamber, rinsed three times with 1xPBS and left to air-dry off water residuals. Finally, the coverslips were mounted with ProLong Gold antifade reagent supplemented with DAPI for nuclear DNA staining.

Antibodies

- DROSHA Rabbit anti-mouse: Abcam, ab12286
- LAMINA/C Rabbit anti-mouse: Abcam, ab108922
- LAMINB1 Goat anti-mouse: Santa Cruz, sc-6217
- DGCR8 Rabbit anti-mouse: Abcam, ab36865
- p-PolII Rabbit anti-mouse: Santa Cruz, sc-13583
- SATB1 Goat anti-mouse: Santa Cruz, sc-5990

2.11 Immunofluorescence combined with DNA FISH

Cell preparation for IF/DNA FISH

Cells were seeded on sterile glass coverslips, and stimulated as previously described. Cells were fixed in freshly prepared 2% PFA for 10 minutes at RT, permeabilized with 0.5% v/v Triton X-100/1xPBS for 7 minutes and rinsed with 1xPBS. Cells were then blocked in 1% w/v BSA/1xPBS for 30 minutes at RT, incubated with the primary antibody for one hour at RT in a dark and humidified chamber, rinsed three times in 1xPBS, incubated with the secondary antibody for 45 minutes at RT in a dark and humidified chamber and rinsed three times with 1xPBS.

Probe preparation for hybridization

100ng from each DNA probe and 1µg mouse COT-1 DNA were lyophilized using the Concentrator plus for 15 minutes at 45°C. The pellet was resuspended in 5µl de-ionized formamide and incubated at 37°C for one hour. Probe DNA was further denatured at 95°C for 10 minutes and then thoroughly mixed with 5µl of 2X hybridization buffer (4xSSC, 20% Dextran sulfate, 2mg/ml acetylated BSA, 50 mM Sodium Phosphate).

Cell preparation for hybridization

Cells were dehydrated with four washes of increasing ethanol concentrations (70%, 80%, 95% and 100%). The coverslips were briefly air-dried and then incubated with denaturation buffer (70% de-ionized formamide, 2xSSC, pH7, pre-warmed at 73°C) for 5 minutes at 73°C. The cells were again dehydrated in increasing concentrations of ice-cold ethanol. Hybridization: each probe was placed separately on a glass microscope slide and the cell-spotted side of the coverslip was flipped on top of the hybridization buffer, sealed with rubber cement and incubated at 72°C (CD4 cells), at 73°C (thymocytes) and at 74°C (T_H1 and T_H2 cells) for 4 minutes. The hybridization step continued for 12-16 hours in a humidified hybridization chamber at 37°C. After the completion of hybridization, washing steps were performed to eliminate the background noise in the imminent imaging procedure. The coverslips were washed three times with 2xSSC, once with 1xPBS and then left to dry off water residuals. The coverslips were then mounted on ProLong Gold antifade reagent supplemented with DAPI for nuclear DNA staining.

2.12 Immunofluorescence combined with RNA-DNA FISH

Cell preparation for IF/RNA-DNA FISH

All the buffers and solution used for the IF combined with RNA-DNA FISH experiments were RNAse free. Cells were seeded on sterile glass coverslips, and stimulated as previously described. Cells were fixed in freshly prepared 4% PFA for 10 minutes at RT, permeabilized with 0.5% v/v Triton X-100/1xPBS for 7 minutes (thymocytes, CD4, T_H1, T_H2 and BMDMs) and rinsed with 1xPBS. Cells were then blocked in 1% w/v BSA/1xPBS for 30 minutes at RT, incubated with the primary antibody for one hour at RT in a dark and humidified chamber, rinsed three times in 1xPBS, incubated with the secondary antibody for 45 minutes at RT in a dark and humidified chamber and rinsed three times with 1xPBS.

Probe preparation for hybridization

100ng from each probe, 1µg mouse COT-1 DNA and 20 µg yeast transfer RNA were lyophilized using the Concentrator plus for 15 minutes at 45°C. The pellet was resuspended in 5µl de-ionized formamide and incubated at 37°C for one hour. Probe DNA was further denatured at 95°C for 10 minutes and then mixed thoroughly with 5µl of 2x hybridization buffer (4xSSC, 20% Dextran sulfate, 2mg/ml acetylated BSA, 50 mM Sodium Phosphate.

Cell preparation for hybridization

Cells were sequentially dehydrated with four washes of increasing ethanol concentrations (70%, 80%, 95% and 100%) and briefly air-dried. Hybridization: each probe was placed separately on a glass microscope slide and the cell-spotted side of the coverslip was flipped on top of the hybridization buffer, sealed with rubber cement and incubated for four minutes at 73°C. The hybridization step continued for 12-16 hours in a humidified hybridization chamber at 37°C. After the completion of hybridization, washing steps were performed to eliminate the background noise in the imminent imaging procedure. The coverslips were washed three times with 2xSSC, once with 1xPBS and then left to dry off water residuals. The coverslips were then mounted with ProLong Gold antifade reagent supplemented with DAPI for nuclear DNA staining.

2.13 Chromosome Painting combined with DNA FISH

Cell fixation and DNA BAC probe preparation was performed as for the DNA-FISH experiments. FITC-labeled Paint of mouse chromosome 11 and 17 was warmed at 37°C, added to the probe mix with 10µl of chromosome paint hybridization buffer and incubated at 37°C for 10 minutes. Probes were denatured for 10 minutes at 70°C, followed by a 30 minutes incubation at 37°C. Cells were dehydrated using an ethanol series (twice with 70% EtOH for 2 minutes, twice with 90% EtOH for 2 minutes and once with 100% EtOH for 5 minutes at RT) and briefly dried at 37°C. The coverslips were then incubated with denaturation buffer (70% de-ionized formamide, 2xSSC, pH7, pre-warmed at 73°C) for 5 minutes at 73°C. Cells were again dehydrated in increasing concentrations of ice-cold ethanol (twice with 70% EtOH for 2 minutes, twice with 90% EtOH for 2 minutes and once with 100% EtOH for 5 minutes at RT) and briefly air-dried. Hybridization: each probe was placed separately on a glass microscope slide and the cell-spotted side of

the coverslip was flipped on top of the hybridization mix, sealed with rubber cement and incubated at 72°C (CD4), at 73°C (thymocytes) and at 74 (T_H1 and T_H2 cells) for 4 minutes. The hybridization step continued for 12-16 hours in a humidified hybridization chamber at 37°C. After the completion of hybridization, washing steps were performed to eliminate the background noise in the imminent imaging procedure. The coverslips were washed three times with 2xSSC, once with 1xPBS and then left to dry off water residuals. The coverslips were then mounted with ProLong Gold antifade reagent supplemented with DAPI for nuclear DNA staining.

2.14 a-Amanitin treatment

In order to block transcription, a-Amanitin, an RNA Polymerase II inhibitor was used. Thymocytes, CD4 and T_H2 cells were treated with Click's medium supplemented with 50μg/ml a-amanitin and 20-50 U/ml IL-2 for 6 hours at 37°C. A second group with the same cell subtypes (thymocytes, CD4 and T_H2) was used as a control. Cells were rinsed with 1xPBS, seeded on sterile glass coverslips, stimulated and prepared for RNA/DNA FISH experiments and qPCR assays as previously described.

2.15 Microscopy and quantitative 3D image analysis

FISH and IF signals were examined on a Leica TCS SP8 confocal microscope unit. Using a 63× objective, images of ~35 optical sections were captured with a step of 250nm and acquired at different λs. A 405nm laser was used to excite and detect DAPI staining, a 561-nm laser was used to excite and detect Alexa Fluor 568, a 488-nm laser was used to excite and detect Alexa Fluor 488 and a 633nm laser was used to excite and detect Alexa Fluor 647 in separate sequence to avoid bleed through in different channels. Images were analyzed with the use of Volocity software (Perkin Elmer). The Volocity 3D Visualization module has the ability to visualize, identify, quantify and separate objects between them (ex. nuclei and DNA-FISH or IF signals) as shown in **Figure 29**. Ecxept from the ability to position the viewing point either outside or inside the 3D object, Volocity can determine the distances between nuclear sub-compartments from 3D reconstructed images. Volocity can determine the volume of the cells and distinguish the distances between the center of the fluorescent signal (alleles) and the edge of the nucleus as defined by DAPI staining. All distances between microRNA gene alleles were determined from the center of the two alleles until the edge of the cell borders, for all DNA, RNA FISH and IF experiments.

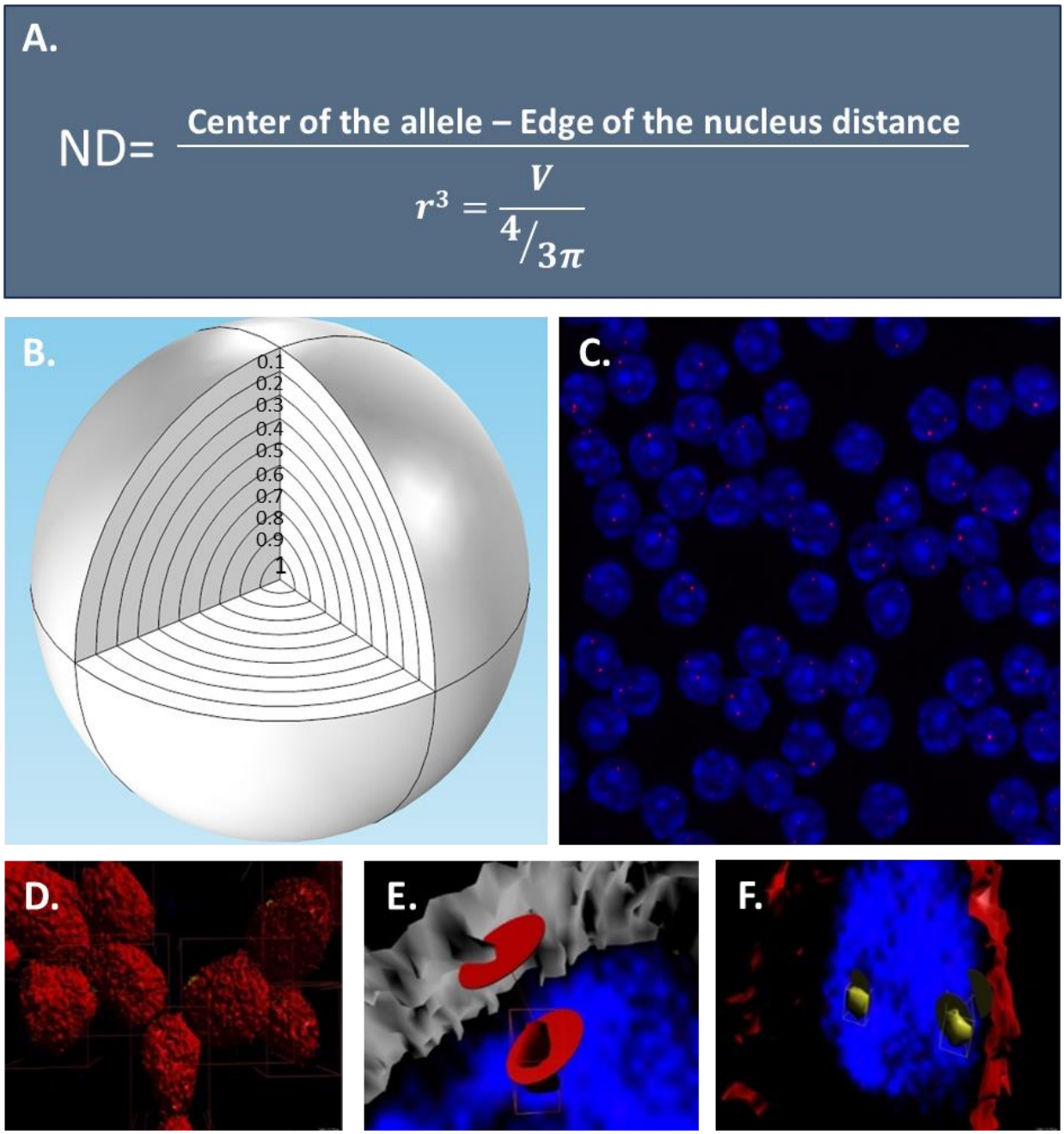

Figure 29. A) Equation used for the calculation of cell volume. B) 3D distance measurements conducted with Volocity 3D Image Analysis Software were normalized, in 10 homocentric shells for each allele from *miR* genes and TNFα. ND=1 defines the maximum distance, whereas ND=0 defines the minimum distance of an allele from the nuclear periphery. C) Confocal microscopy image representing hybridization of a *mirR* gene (red) in thymocytes (DAPI staining blue). D, E and F present confocal microscopy images deconvoluted with the Volocity software from 3D DNA FISH experiments.

The absolute distances were normalized by the cell radius, which was determined by the equation shown in **Figure 29B**. In order to analyze and visualize the normalized distances, we clustered them in 10 isocentric circles of equal area (0-0.1, 0.1-0.2, 0.2-0.3, 0.3-0.4, 0.4-0.5, 0.5-0.6, 0.6-0.7, 0.7- 0.8, 0.8-0.9,

0.9-1) as presented in **Figure 29B**, where 0 and 1 are determined as nuclear periphery and nuclear center respectively. The aforementioned measurements have only been performed for images depicting nuclei with two signals (alleles) and having an intact 3D architecture. Moreover, only nuclei showing similar volumes between different biological replicates were used in order to avoid experiments with swollen nuclei. For all cell types under investigation, at least 200 nuclei were analyzed per each DNA and RNA FISH experiment. Furthermore, positions of microRNA genes relative to LMNB1 were also determined through the analysis of 3D datasets using Volocity. microRNA gene and LMNB1 colocalization was determined either by juxtaposition and a partial overlap of red and green pixels or a complete overlap between red and green pixels (red: DNA FISH probes and green: LMNB1). The distances of DNA-FISH signals from the nuclear periphery were analyzed by two independent investigators.

2.16 Statistical analysis

The statistical significance of distances (between alleles and the cell periphery) but also of gene relocalization during differentiation was assessed using the non-parametric two tailed Kolmogorov-Smirnov (KS) test. The analysis was performed by the SPSS Statistics software. When a D value [maximum distance of the cumulative distribution functions (CDF) of the two samples] was attributed above zero (0<D<1) and a p value was equal to or lower than the significance level of 0,05 then the distributions were considered *as* significantly different. In that case it was considered that the null hypothesis of the two distributions in comparison being similar, was rejected. All graphs presented in this thesis have been designed by using the SigmaPlot and GraphPad Prism 6 software. The reported *p* and *D* values were calculated with the XL-STAT and GraphPad Prism 7 software package. Welch's T-test was used to test significant differences between microRNA within and outside of cLADs. Pearson r was used to study the linear correlation between microRNA within or outside cLADs and gene density. Pearson's r was used to measure the linear correlation between two variables. The coefficient varies from −1 _ *r* _ 1. where a r = 1 was a perfect positive correlation, r = -1 was perfect negative correlation and *r* _ ±0.7 was strong, *r* = ±0.5 − 0.7 was moderately strong and *r* = ±0.3 − 0.5 was weak and *r* = ±0 − 0.3 was no linear relation. Quantitative differences for all qPCR assays were presented as a mean of the triplicates with standard deviation (±SD). For data presentation, graphs were designed using GraphPad Prism 7 and Sigma Plot Software.

2.17 Bioinformatic analysis of microRNA cLAD/ciLAD co-localization characterization and distance distribution assessment

Datasets used for the analysis of microRNA cLAD/ciLAD co-localization: mouse pre-microRNA gene coordinates were downloaded from miRBase (Release 21) for four different species (mouse: Mus musculus, human: Homo sapiens, fly: Drosophila melanogaster, worm: Caenorhabditis elegans). LAD coordinates for the same species were obtained from published DamID experiments in human (Guelen et al. 2008), mouse(Peric-Hupkes et al. 2010), fruit fly (Pickersgill et al. 2006) and worm (Ikegami et al. 2010) respectively. For the mouse genome we obtained constitutive LAD domains through comparison of four different tissues (Peric-Hupkes et al. 2010). For the same genome and from the same experiments we obtained the constitutive inter-LAD (ciLAD) domains, termed as the regions that constitute domains intervening defined LADs in the aforementioned tissues studied. Coordinates for both microRNA and cLAD/ciLAD were converted to hg19 (human), mm9 (mouse), dm3 (fly) and ce10 (worm). Protein coding gene coordinates were obtained from the UCSC Genome Browser under the RefSeq catalogues of Genes and Gene Prediction Tracks. For human and mouse genomes we made use of EBI's Expression Atlas to define constitutive protein coding genes. Human constitutive genes were called the ones which were designated as highly expressed in at least 80% of the 32 studied tissues, while tissue-specific ones were called on the basis of the corresponding percentage being less than 10%. For the mouse genome as only 6 tissues were available we only called constitutive genes the ones belonging to the top 10% of expressing genes in all 6 tissues. Analysis of microRNA overlap with cLAD and ciLAD: overlap enrichment analysis was conducted as follows. The total overlap percentage between microRNA gene loci and cLAD/ ciLAD was calculated through the intersection of the two coordinate files, using BEDTools (Quinlan and Hall 2010) intersect function. The enrichment of the observed overlap was calculated as the ratio over an expected value obtained through a simple calculation of intersection, based on the genome coverage percentage of each of the two coordinates. Following this analysis, enrichment values greater than 1 correspond to a greater overlap than the one expected by chance, indicative of co-localization preference. Values below 1 are indicative of an avoidance of colocalization preference. The significance of the enrichment values was calculated in all cases on the basis of a permutation test as previously described (Andreadis et al. 2014). The microRNA gene coordinates were shuffled in the genome in random positions, keeping the distribution of sizes and number of elements unchanged and the observed overlap was calculated. This process was repeated for 1000 such permutations and p-values were set as the ratio of times an overlap

as big (or as small) as the initial one was found in the total number of trials (N = 1000). In cases where not even a single random permutation yielded such a high (or low) overlap value, p-value was set to be boundary (for instance, if a cLAD was 100 kb and a microRNA gene locus was lying >100 kb upstream or downstream of its closest boundary, the microRNA gene was discarded from the analysis). We then scaled the obtained distances by dividing over the cLAD/ciLAD size in order to accommodate the variability in domain sizes. In this way, a microRNA gene locus could either: a) lie within the domain and thus be no farther than half the domain size from its closest boundary, or b) lie outside of the domain and thus, by definition, not farther than one full domain length. As there is no reason to assume a directional effect that distinguishes between the domain boundaries or upstream/downstream localization, we took all distances within the domains as positive and all distances from outside the domain as negative. In this way the scaled microRNA-cLAD/ciLAD distances were defined in a range of [-1, 0.5], with -1 being the farthest possible element outside the domain, 0 being the boundary and 0.5 being the farthest possible towards the center of the domain.The software named LADiMIR was used for the spatial analysis of microRNA genes and lamina associated domains (LADs) and to explore the microRNA/LADs colocalization and genomic context. Perl programming language was used for all analytical purposes and algorithms, where data visualization and user interface where created using the web programming tools: HTML, CSS and JavaScript. The platform used to run the software was an Intel(R) Core(TM) i7-4500 CPU @ 1.80GHz 2.40 GHz, 8.00 GB of RAM, with a 64-bit Windows 10 home operating system. Strawberry Perl for MS windows v.5.20.3.2 (64bit) was used as a Perl environment. All datasets where obtained from independent sources. LAD data have occurred from *DamID* experiments in four different species *Mus musculus, Homo sapiens, Caenorhabditis elegans* and *Drosophila melanogaster*. LAD data were acquired from their original publication, LMNB1 in *Mus musculus* (assembly mm9) from (Peric-Hupkes et al. 2010), for *C.elegans* (ce10) (Ikegami et al. 2010), for *D.melanogaster* (dm3) from (van Bemmel et al. 2010) and for LMNB1 from *Homo sapiens* (hg19) was taken from (Guelen et al. 2008). A USSC genome browser tool called LiftOver, was used in order to convert mouse mm9 assembly to mm10 and human hg19 to hg38, by using default parameters. All micro-RNA data were acquired from miRbase.org and gene sets where obtained from the Ensemble database. Two main algorithms where created to first identify microRNA/cLAD colocalization and second to generate microRNA gene genomic context. microRNA genes where conceived to be in one of three states: 1) fully within LAD, 2) partially (both shared the same classification), and 3) outside LAD.

2.18 Analysis of microRNA and mRNA loci overlaps with nucleoporins

An overlap analysis was performed in a way similar to the one described for the cLAD/ciLAD regions. This time the compared coordinates were the ones of protein-coding and microRNA gene loci against the nucleoporin peaks as provided by publicly available datasets.

2.19 Enrichment of DGCR8 signal in microRNA against mRNA gene loci

Data were compared as distributions of mean signals for the two types of genes. An aggregate score analysis was conducted through the calculation of average signal values over the genomic regions defined by the gene loci in the following way. DGCR8 signal provided as bigWig scores were extracted for regions corresponding to the coordinates of a microRNA or mRNA gene locus and then an arithmetic mean was calculated for each locus. A mean aggregate DGCR8 score was thus corresponding to the gene body of each locus. BigWig score aggregation was performed with the use of a suitably adjusted script which implements the bigWigSummary UCSC utility.

2.20 RNA/GRO-seq analysis

Depending on the dataset used in each analysis, either normalized gene counts (RPKM) or continuous signal values (in the case of GRO-seq) were implemented. In the case of RNA-seq RPKM values were assigned to each gene that was included in the public dataset. For GRO-seq, provided as continuous scores in the form of bigWig files, we calculated a mean aggregate score along the region that corresponded to each locus' coordinates as described above.

2.21 GEO accession numbers of datasets used for comparative-analyses:

Method used	GEO
LaminB1 DamID-seq	GSE8854
LaminB1 DamID-seq	GSE17051
LaminB1 DamID-seq	GSE5089
LEM-2 ChIP-seq	GSE25933
RNA-seq	GSM2095053
RNA-seq	GSM2095060
RNA-seq	GSM1120730
RNA-seq	GSM1120731
RNA-seq	GSM1120732
RNA-seq	GSM940701
GRO-seq	GSE27037
NUP 153 DamID-seq	GSE64008
NUP-98 ChIP-seq	GSE48996
NUP-93 DamID-seq	GSE87831
DGCR8 ChIP-seq	GSM2389981

Table 5. GEO numbers used for comparative analysis

2.22 Chromatin Immunoprecipitation (ChIP)

ChIP was performed on sonicated chromatin prepared from thymocytes and TEPMs using standard procedures. Chromatin was prepared from 4×10^6 cells. Cells were fixed in fixation buffer (50 mM HEPES-KOH pH 7,5, 100 mM NaCl, 1 mM EDTA pH 8, 0,5 mM EGTA, pH 8, 1% formaldehyde) for 10 minutes. The fixation reaction was quenched by the addition of 125 mM glycine for 5 minutes on ice under agitation. Fixation was followed by cell lysis (10mM TrisHCl pH 7.5, 10mM NaCl, 3mM $MgCl_2$, 0.5% NP40, 1mM PMSF) for at least 15 minutes. Then the cells were centrifuged at 2000g for 5 minutes at 4^0C twice. Lysates were resuspended in sonication buffer (50mM Hepes pH 8.0, 150mM NaCl, 5mM EDTA pH 8.0, 0.5mM EGTA pH 8.0, 0.3% SDS, 0.1% Na-deoxycholate, 1mM PMSF).

Chromatin shearing: 1ml of chromatin was sonicated on ice to produce 300-800 bp chromatin fragments as shown in **Figure 29** by using the Covaris S220 Focused-ultra sonicator instrument. Chromatin was sonicated for 15 minutes with the length of the intervals being 60 seconds on/10 seconds off. The instrument's parameter settings used by default were Peak value at 140, Duty factor value at 5.0 and cycles/burst value at 200. 10µl of the sheared soluble chromatin solution was used in order to check the shearing efficiency and the rest was kept at 4°C.

Shearing efficiency: 10µl of chromatin were added to lysis buffer (50mM Tris pH8, 10mM EDTA pH8, 0.2M NaCl, 1% SDS) and incubated at 65°C for 4 hours. 100mg/ml RNase A was added to the sample and incubated at 37°C for one hour and then the sample was proteolysed with 20mg/ml proteinase K at 55°C for two hours. DNA was recovered upon Phenol-Chloroform extraction and ethanol precipitation.

Immunoprecipitation (IP): before each IP the sheared soluble chromatin solution was firstly centrifuged at 14.000 rpm for 5 minutes at 4°C 1/100 of the sheared chromatin was isolated and stored at -20°C in order to be used as an input control. For each IP 2 µg chromatin was diluted in ChIP dilution buffer (10mM Tris pH 8.0, 1mM EDTA pH 8.0, 100mM NaCl, 1% Triton-X, 1mM PMSF) to a final volume of 3mL so that the concentration of SDS was reduced (0,1% final). Chromatin was incubated with 10 µg of antibody and IgG (normal mouse IgG). Prewashing of protein G-Dynabeads was repeated three times in ice cold 0,01% Tween-20/ 1xPBS and finally pre-blocked for 30 minutes at 4°C with 1% BSA/1xPBS. The sample was then centrifuged at 14.000 rpm for 5 minutes at 4°C in order to avoid aggregates. Per each IP sample 100µl beads were added, incubated for four hours under rotation at 4°C in order to bind the specific chromatin-antibody complexes. Upon IP, the beads were washed twice with high salt buffer (20mM Tris pH=8,

500mM NaCl, 2mM EDTA, 0.1% SDS, 1% Triton X-100, 1mM PMSF), low salt buffer (20mM Tris pH=8, 150mM NaCl, 2mM EDTA 0.1% SDS 1% Triton X-100, 1mM PMSF) and lithium chloride buffer (10mM Tris pH=8, 250mM LiCl, 2mM EDTA,1% NP-40, 1mM PMSF). The beads were washed at 4°C under rotation in 1ml of each washing buffer for three minutes. At the end, the beads were resuspended in 250 µl Elution buffer (50 mM Tris-HCl pH 8, 10 mM EDTA, pH 8, 1% SDS) and crosslinks were reversed overnight at 65°C. After de-crosslinking, beads were removed and the eluents were isolated and diluted with TE buffer (10mM Tris-HCl pH 8, 1mM EDTA pH 8). Input and bound fractions were treated with 100mg/ml RNase A at 37°C for one hour and then with 20mg/ml proteinase K at 55°C for three hours. The precipitated DNA was purified using the Qiagen PCR clean-up kit (Qiagen, UK). The Purified DNA was resuspended in 20µl ddH20 and its concentration was determined with a Qubit fluorometer by using the Qubit® dsDNA HS assay kit.

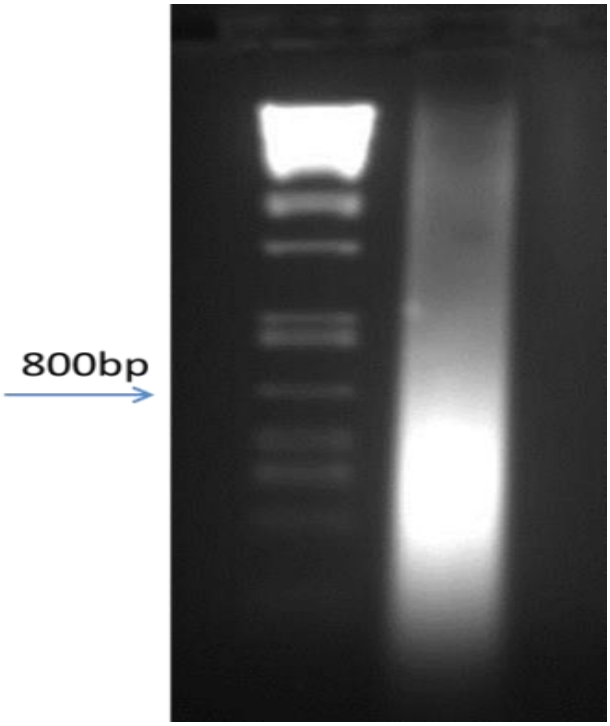

Figure 29. Depiction of thymocytes derived sheared chromatin (200-800bp) upon sonication for 15 minutes with a Covaris instrument.

qPCR evaluation of ChIP experiment: The primer sets used for ChIP DNA evaluation were based on previous publications from ChIP-on-chip experiments for DROSHA. T cells specifically expressed pre-miR sequences were used as positive control regions, whilst as negative control regions pre-miR sequences of non-expressed microRNAs or non-expressed coding gene sequences in T cells (Morlando et al. 2008;

Gromak et al. 2013). The primer sets used in ChIP assays are presented in **Table 6**. The qPCR reaction was carried out with 4 µl DNA, 0.4 µM each forward and reverse primer and 1×SYBR Jump-Start reaction mix in a total volume of 20 µl. PCR cycles were set on and run through Opticon 1/2 program (MJ Research) connected to a PCR cycler. Each PCR cycle consisted of the initial activation of Taq polymerase at 94°C for 2 minutes, 40 cycles of denaturing (94°C for 30 seconds), annealing (60°C for 30 seconds) and extension (72°C for 30 seconds). The fluorescence intensity was indicated at 75, 78, 80 and 82°C after each cycle. The analysis of resulting C(t) values was performed using the Opticon1/2 software. The amplification threshold was set to 0.1, at which PCR amplification curves were still in a linear range on a logarithmic scale. C(t) values for samples and those for serial dilutions of input DNA were read at this point. Standard calibration curves were generated by plotting C(t) values against log (arbitrary DNA concentration). This represented a linear correlation between C(t) and log(DNA concentration) with R^2 value >0.95. The arbitrary DNA concentration of each sample was calculated using equations generated from the calibration curves. The resulting DNA concentration of samples was normalized against input.

	micro RNA gene	Forward primer 5'→3'	Reverse primer 5'→3'
Positive control regions	*miR-155*	TGAAGGCTGTATGCTGTTAATGC	ATGCTAACAGGTAGGAGTCAGTC
	miR-146a	GCTATCCCAGCTGAAGAACTGA	TCTGAGAACTGAATTCCATGGGTTA
Negative control regions	*miR-17/92*	TCCATAGTTGTGTTTGCAGCC	AAGTAAATAGCAGGCCACCATC
	Olfr 303	GGGCCACAGAAGTTTAGCTG	CGCCCTCTGCATTACTCAC

Table 6. qPCR primer sets used on precipitated DNA from DROSHA ChIP experiment in thymocytes.

2.22.1 Chromatin Immunoprecipitation sequencing (ChIP-seq) library preparation and bioinformatics analysis

The library preparation for ChIPseq experiments was carried out in the Greek Genome Center (GGC) of Biomedical Research Foundation of Academy of Athens (BRFAA) according to the manufacturer protocol as described (Ford et al. 2014). Briefly, 10-20ng of Immunoprecipitated Chromatin DNA was incubated with T4 DNA polymerase Klenow Fragment and T4 DNA Polynucleotide Kinase in order to generate blunt ends. Treatment of blunt-ended DNA fragments with Klenow (3' to 5') exonuclease in the presence of ATP resulted in the addition of a single 'A' nucleotide to the 3' ends of the DNA fragments. Illumina adapters bearing a single-base 'T' overhang ligated with the A-tailed DNA in the presence of DNA ligase. In order to convert the Y-shaped adapters to linear dsDNA the ligated fragments were 5 cycles PCR-amplified. The PCR products were purified and size-selected (200-500bps) by agarose gel electrophoresis. The accurate number of PCR cycles that was required for equal enrichment of each sample was defined by qPCR. The template size distribution of each final PCR-amplified DNA library was estimated using an Agilent Bioanalyzer DNA 1000 chip while its DNA concentration was quantitated using the Qubit® dsDNA HS Assay Kit. A 1.8 pM pool of equal represented DNA libraries was loaded and sequenced to Nextseq 500 platform using Illumina NextSeq® 75 c kit. Single-end 85 bp reads for Drosha IP and Input from thymocytes and peritoneal macrophages were generated with NextSeq500 in the GGC. All ChIPseq data were aligned to the mouse genome version NCBI-37/mm9 with the use of bowtie2 (version 2.1.0) and «--very-sensitive» parameter. Samtools (version 0.1.19) (Langmead and Salzberg 2012) were used for data filtering and file format conversion. The MACS (version 1.4.2) algorithm (Zhang et al. 2008) was used for peak calling with input as control. Gene annotation and genomic distribution of the peaks identified by MACS was performed with bedtools (Quinlan and Hall 2010) and graph representation (heat maps) of the tag read density around TSS was performed with the seqMiner (version 1.3.3) software (Ye et al. 2011). ChIPseq data have been deposited in the Short Read Archive (SRA) under the accession codes SRPXXXX1.

Reagents

Product name	Company	Catalog number
a-Amanitin	Sigma	A2263
Acetylated BSA	Ambion	AM 2614-G1
Biotin Nick Translation kit	ROCHE	11 745 824 910
Biotin NT labelling kit	Jena Biosciences	PP-310-BIO16
CD4 MicroBeads	Miltenyi Biotech L3T4	130-49-201
CHIR99021	SELLECKCHEM	SI263
CLICK's medium	SIGMA	C5572
COT-1 DNA	Invitrogen	18440-016
DAPI	Invitrogen, Molecular Probes	P-36931
DEPC-treated water	Ambion	AM9922
Dextran sulfate	Millipore	S4030
DGCR8 Rabbit anti-mouse	Abcam	ab36865
DNase I	New England Biolabs	M0303L
DROSHA Rabbit anti-mouse	Abcam	ab12286
Dulbecco's Modified Eagle's Medium	GIBCO	41966
Fetal bovine serum	GIBCO	10270
Formamide	Ambion	AM9342
HEPES	BIOSERA	LM-S2030/100
IL-12 (p70)	BD Pharmingen	554592
IL-2	BD Pharmingen	550069
IL-4	R&D	MAB 404
LAMINA/C Rabbit anti-mouse	Abcam	ab108922
LAMINB1 Goat anti-mouse	Santa Cruz	sc-6217
leukemia inhibitory factor	CHEMICON	ESG 1107 ESGRO LIF
L-Glutamine	GIBCO	15030

Product name	Company	Catalog number
Luminol Enhancer Solution	Thermo Fischer	32106
MACS separation columns	Miltenyi Biotech LS	130-042-401
M-MuLV Reverse Transcriptase	NEB	M0253S
Mouse COT-1 DNA	Invitrogen	18440-016
PFA 16% aqueous solution	Electron Microscopy Sciences	30525-89-4
PD0325901	SELLECKCHEM	S1036
Penicillin and streptomycin	GIBCO	15140122
p-PolII Rabbit anti-mouse	Santa Cruz	sc-13583
Protein Assay Dye Reagent Concentrate	BIO-RAD	500-0006
Purelink PCR purification kit	Invitrogen	K31001
RNaseA	Qiagen	151045750
Anti-SATB1	Santa Cruz	SC-5990
Spectrum Orange/Green dUTP	Abbott Molecular	02N33-050/02N32-050
SYBR Green PCR Master mix	Applied Biosystems	4309155
TOPO® TA vector	Invitrogen	10351-021
TOPO® TA vectors	Invitrogen	45-0640
TRI-REAGENT	SIGMA	T9424
TSA Biotin System	Perkin Elmer	NEL700A001K
Vanadyl-ribonucleoside complex	NEB	S1402S
Vysis Nick Translation kit	ABBOT	07J00-001
XMG1.2	R&D	MAB 4851
Yeast transfer RNA	Ambion	AM 7119
αCD-28	R&DMAB	4831
αCD3	R&D MAB	484
β-mercaptoethanol	SIGMA	63689

RESULTS

To unravel the mechanistic aspects of microRNA gene transcriptional regulation we studied the expression profile and subnuclear organization of microRNA gene loci in murine T lymphocytes. All experiments presented in this thesis were conducted in four distinct T cell subtypes: thymocytes, CD4, T_H1 and T_H2 cells. Upon differentiation of CD4 cells under the proper conditions, cells were re-stimulated for one hour as previously described.

In consideration of the complete and appropriate differentiation into T_H1 and T_H2 cells, upon every single differentiation experiment the terminally differentiated cells were analysed for the expression of specific cytokine genes by qPCR. For T_H1 cells, we analyzed the expression levels of the *Ifnγ* cytokine gene, while for T_H2 cells the expression of the *Il4* gene (**Figure 30**). According to the published literature, T_H1 cells posses high steady state mRNA levels of *IFNγ*, T_H2 cells express high levels of *IL-4* while naïve CD4 cells do not express any of these cytokine genes.

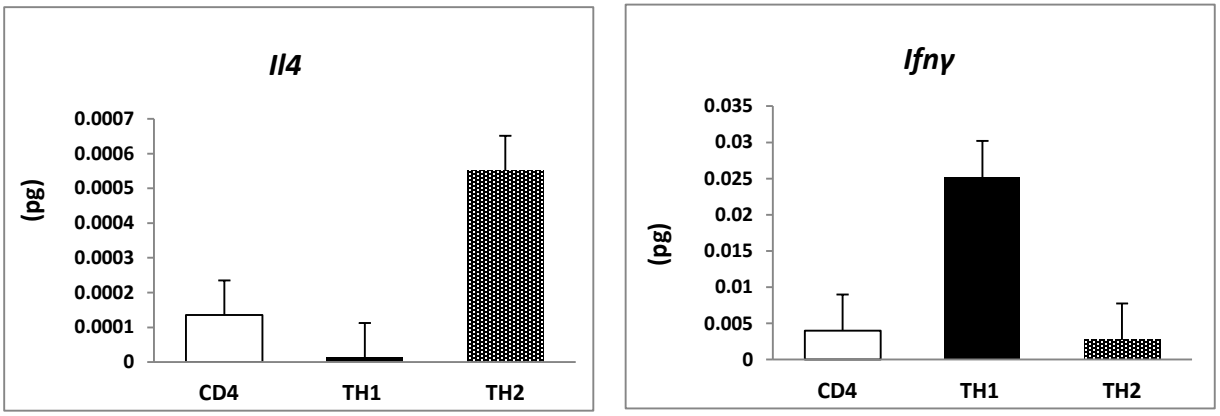

Figure 30. Quantitative analysis of *Ifnγ* and *Il-4* cytokine gene expression in distinct T cell lineages before and after differentiation as deduced by qRT-PCR.

3.1 Detection of primary-microRNA transcripts in T cells

Quantitative PCR was used to detect the pri-microRNA levels in thymocytes, CD4, T_H1 and T_H2 cells. Total RNA was extracted for all cell types (for T_H1 and T_H2 cells upon restimulation of terminally differentiated cells with anti-CD3 antibodies for one hour). Reverse transcription of every cell type provided the cDNA needed for qPCR. Pri-microRNA transcripts were normalized to the housekeeping gene *Hprt1* mRNA levels.

We detected higher expression levels, across all tested microRNAs, in differentiated cells (T_H1 and T_H2) in comparison to the other cell types (thymocytes and CD4 cells) (**Figure 31**). *miR-17-92* was the only microRNA gene for which we detected a lower expression in differentiated cells, which can be explained by the fact that *miR-17-92* is highly expressed during thymocytes development. Relatively uniform pattern of low expression in thymocytes exhibited *miR-181a1b1*, *miR-181c*, *miR-146a* and *miR-155*. On the contrary, *miR-181a2b2*, *miR-17-92* and *miR-142* showed high expression in thymocytes. T_H1 cells showed a microRNA profile quite similar with those of T_H2 cells. *miR-181-a1b1*, *miR-181c*, *miR-181a2b2* and *miR-142* were highly expressed in both T_H1 and T_H2 cells. Expression of *miR-155* in CD4 and T_H1 cells was highly expressed compared to thymocytes and T_H2 cells with more than an 8.5-fold difference.

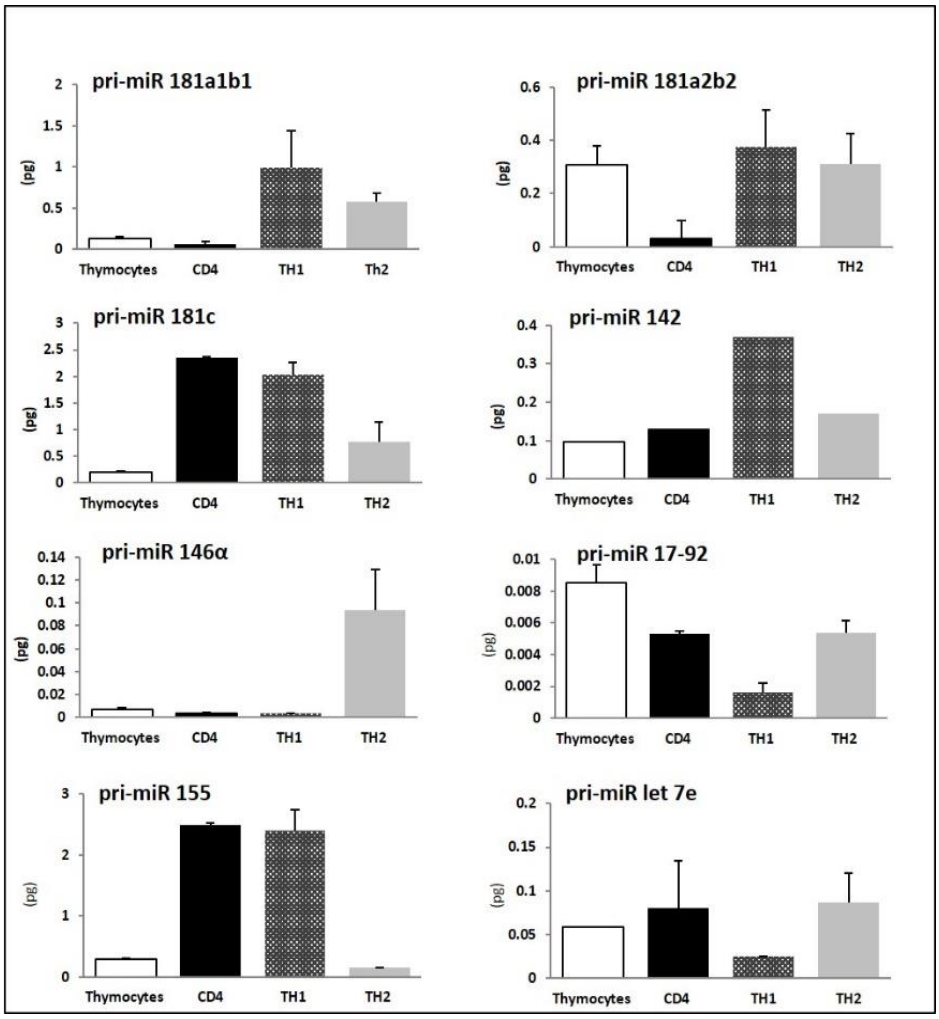

Figure 31. Quantification of pri-microRNA expression levels in distinct T cell lineages before and after differentiation.

3.2 Single cell analysis of primary-microRNA gene expression

To study the primary-microRNA gene expression profile at the single cell level, we performed RNA/DNA-FISH experiments in three-dimensionally preserved cell nuclei. Eight microRNA gene loci (*miR-181a1b1*, *miR-181a2b2*, *miR-181c*, *miR-142*, *miR-146a*, *miR-17-92*, *miR-155* and *miR-let7e*) were selected which are expressed during the murine lymphoid cell development. Experiments were performed in thymocytes, CD4, T_H1 and T_H2 cells. Fluorescently labeled probes were used to hybridize with the nascent endogenous microRNA loci with simultaneous hybridization of BAC DNA probes to the corresponding gene locus. The 3D RNA/DNA-FISH method that we used allowed us to study the subnuclear localization of genes in relation to the nuclear space, and it permitted the maintenance of the three-dimensional structure of the cell. By using this method, we could simultaneously detect the newly synthesized mRNA transcript as well as the DNA of the two alleles.

1kb biotinylated DNA FISH probes (as previously described) were used for the detection of the nascent microRNA transcript. To confirm whether the fluorescent signals that we visualized were not an artifact, such as hybridization with the genomic DNA, but was due to the hybridization of the DNA FISH probe with the nascent RNA, we treated the cells with RNase-A treatment before the hybridization. In the presence of RNase-A, the nascent RNA was eliminated and only DNA FISH signals could be detected as presented in **Figure 32**. The absence of the RNA signals in the RNase-A treated cells confirmed that the signals from the non-treated cells were undoubtedly due to nascent microRNA expression.

Moreover, to confirm that the microRNA signals were not due to the cloning vector sequence hybridization we also performed RNA-DNA FISH experiments by hybridizing with the labeled cloning vector without any inserts as shown in **Figure 32**.

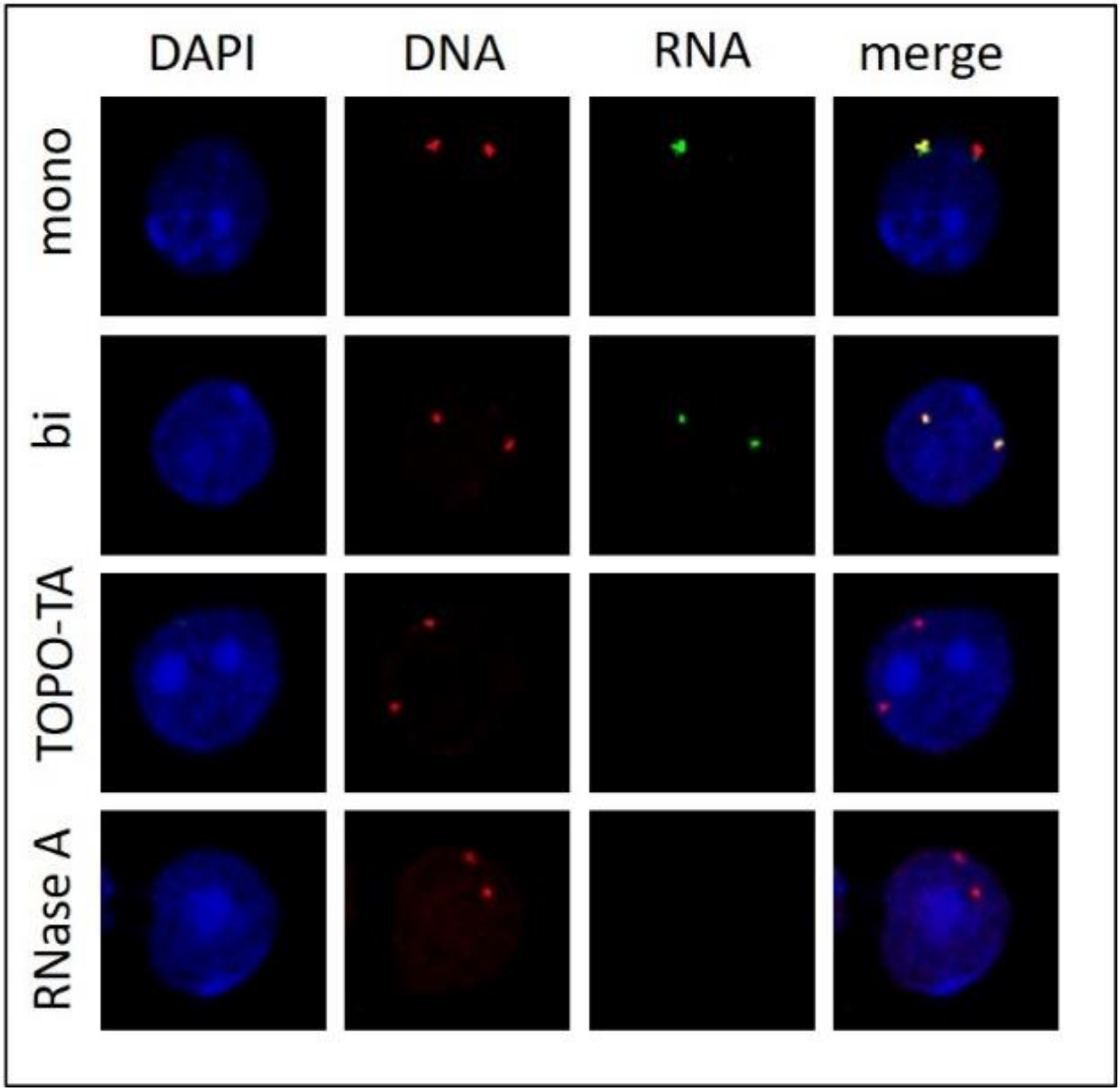

Figure 32. Representative confocal microscopy images of RNA-DNA FISH experiments for microRNA gene loci (DNA - red) with the respective nascent pri-microRNA transcript (green) in thymocytes (DNA counterstained with DAPI-blue). The upper two panels depict mono- and biallelically expressing cells. The third panel presents RNA-DNA hybridization with the TOPO-TA cloning vector while the last row depicts RNA-DNA FISH hybridization after RNAse-A treatment of the cells.

3.3 microRNA genes are monoallelically expressed in T cells

To assess, at the single cell level, the allelic expression profile of microRNA genes in T cells, we performed RNA-DNA FISH experiments in mouse thymocytes, $CD4^+$, T_H1 and T_H2 cells. Biotinylated DNA FISH probes were utilized to detect the newly synthesized pri-microRNA transcript.

Cells were isolated as described in the Materials and Methods section. Experiments were repeated twice for each cell type and more than 150 cells were analyzed for each independent experiment. RNA-DNA FISH experiments were conducted in CSK (CytoSKeletal buffer)-treated cells in order to remove the cytoplasm and enhance probe penetration to the complementary nascent microRNA in the nucleus. Only microRNA signals colocalized with the respective microRNA gene locus (DNA) were evaluated and processed for downstream analysis considering that only these signals were the newly synthesized primary transcripts of the microRNA genes as shown in **Figure 34**. Moreover, all the images shown in **Figure 34**, are presented from a single focal plane, although extensive z-stack images were recorded to analyze a 3D single cell.

As summarized in **Figure 35** the RNA-DNA FISH experiments in mouse T cells indicate a profound tendency for monoallelic microRNA gene expression. microRNAs are **mostly monoallelically expressed in thymocytes, $CD4^+$, T_H1 and T_H2 cells.** In thymocytes we found that 40% of the cells express *miR-181a1b1* and *mir-146a* in a monoallelic manner, while more than 20% of thymocytes monoallelically expressed *miR-181a2b2*, *miR-181c*, *miR-142* and *miR-17-92*. Biallelic expression in thymocytes was extremely low with less than 3-5% of the cells expressing *miR-181a1b1*, *miR-181*, *miR-146a* and *miR-17-92* in a biallelic manner. Biallelic expression of *miR-181a2b2*, *miR-142*, *miR-155* and *miR-let 7e* in thymocytes was almost not detected by the RNA-DNA FISH methodology.

CD4 cells exhibited a totally different expression profile of microRNA genes compared to thymocytes. More than 25% of CD4 cells monoallelically expressed *miR-181a2b2*, *miR-142*, *miR-146a* and *miR-17-92*, while less than 10% of the cells showed monoallelic expression for *miR-181c*, *miR-155* and *miR-let-7e*. Less than 5% of CD4 cells showed a biallelic expression of *miR-142*.

On the contrary, the biallelic expression of microRNA genes after differentiation was different compared with thymocytes and CD4 cells. More than 20% of the T_H1 cells expressed *miR-181a1b1*, *miR-181a2b2*, *miR-142*, *miR-17-92* and *miR-155* monoallelically. Our experiments showed that *miR-146a* is highly

monoallelically transcribed in T_H1 cells, whilst the biallelic expression was less than 5% in T_H1 cells. Furthermore, the biallelic expression of the other microRNA genes under investigation was almost not detected in T_H1 cells.

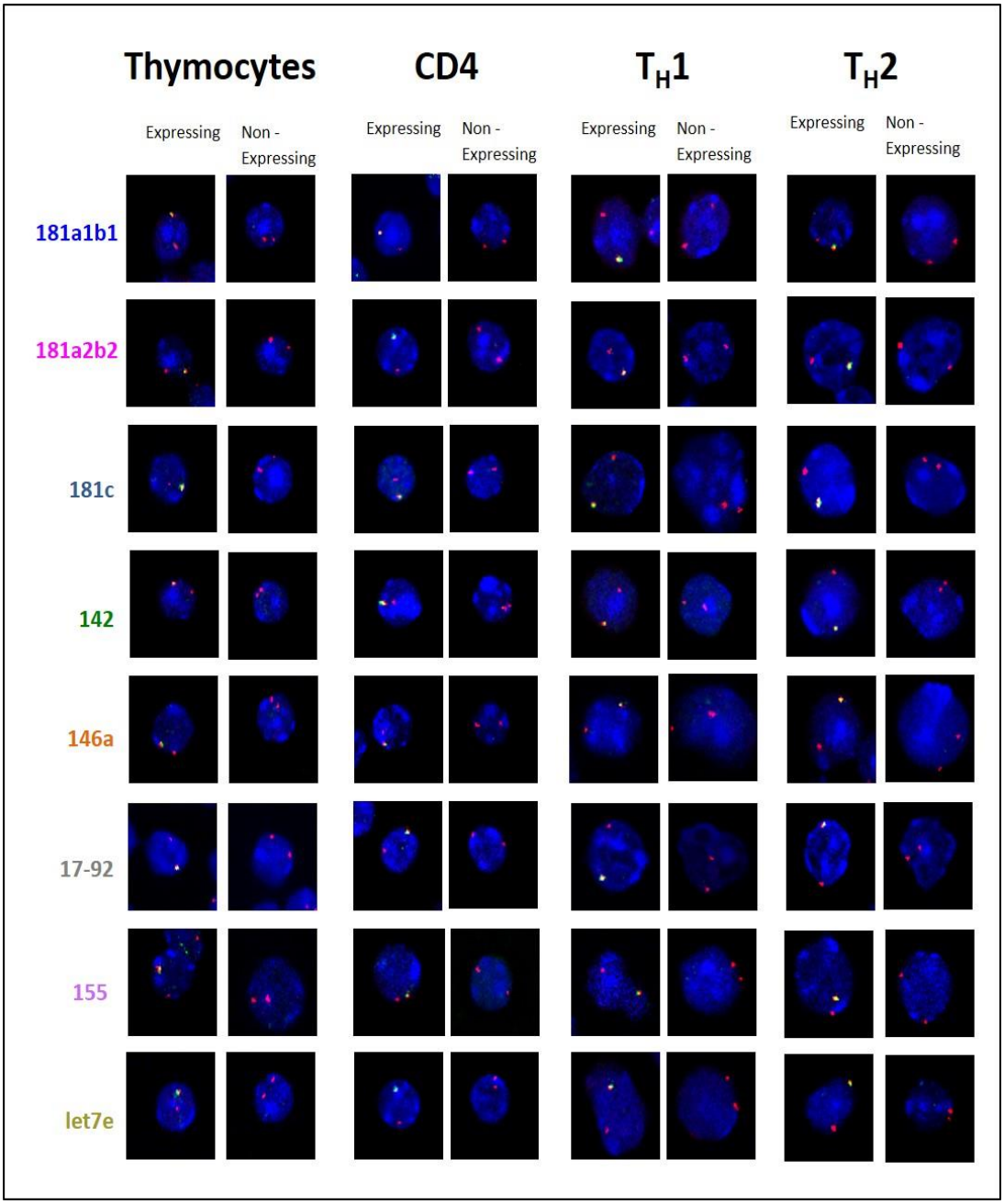

Figure 34. Representative confocal microscopy images of RNA-DNA FISH experiments for microRNA genes in thymocytes, CD4, T_H1 and T_H2 cells. DAPI (blue) staining of the nucleus indicate the presence of DNA, microRNA genes probes labeled with Spectrum orange (red) were hybridized to the two alleles of every microRNA gene and the DNA biotinylated probe (green) was used to detect the nascent microRNA transcript. The first column for every cell type depicts the expressing cells while the second column depicts non-expressing cells from the same experiment.

T_H2 cells demonstrated high expression of all microRNA genes under investigation. *miR-181a2b2*, *miR-142*, *miR-17-92*, *miR-181c* and *miR-155* were expressed in higher levels (40% of the cells) inT_H2 cells when compared with the other subtypes of T cells. Less than 10% of the cells exhibited biallelic expression for *miR-181a1b1*, *miR-181a2b2*, *miR-142*, *miR-17-92*, *miR-181c* and *miR-155* while *miR-146a* didn't show any biallelic expression. miR-let7e was not expressed in T_H2 cells. In general, differentiated T cells demonstrated higher expression and higher frequency of biallelic expression when compared to undifferentiated cells (thymocytes and naïve cells).

The higher frequency of monoallelically expressed microRNA gene alleles is due to the low expression levels of primary microRNA transcripts and not due to imprinting. These results are in line with bioinformatic predictions regarding the allelic expression profile of both microRNA genes and coding genes and does not seem to be affected by neighboring gene transcription status (**Figure 36, 37** & **Table 7**).

Therefore, we conclude that the eight microRNA genes we have studied are mainly monoallelically expressed in the early stages of T cell development (thymocytes) and peripheral CD4 cells. Upon terminal differentiation of peripheral CD4 cells into the T_H1 and T_H2 cell lineages the expression of microRNA genes remains monoallelic although a low fraction of cells also exhibits biallelic expression.

The 3D RNA-DNA FISH experiments demonstrated that most of the microRNA genes showed a tendency to avoid localization towards the center of the cell nucleus. Therefore, our next aim was to study the subnuclear localization of microRNA genes by means of DNA FISH analysis.

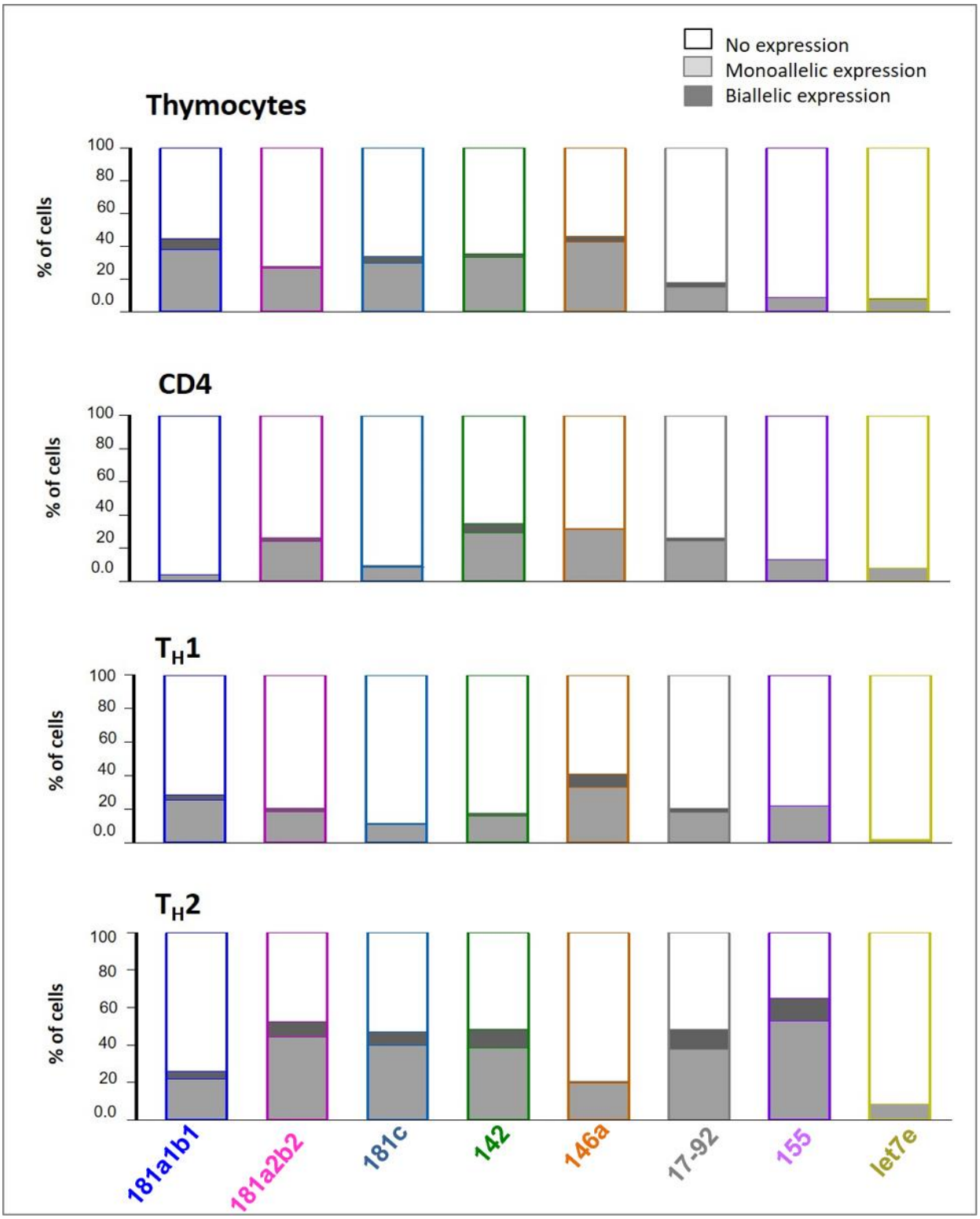

Figure 35. microRNA allelic expression profile in thymocytes, CD4, T_H1 and T_H2 cells.

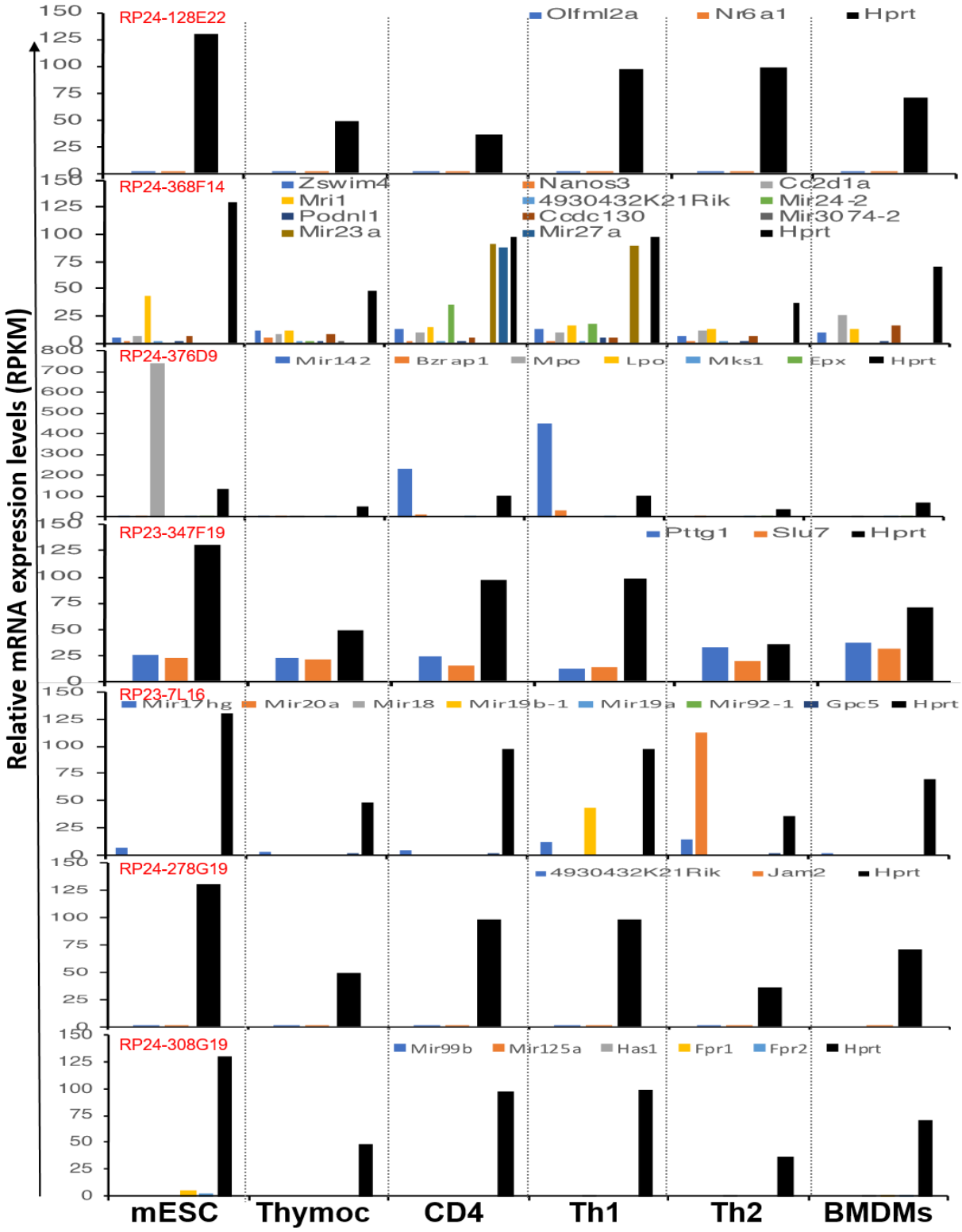

Figure 36. Bar graphs depicting the relative mRNA levels of both coding and non-coding genes flanking each of the eight microRNA genes under study in each BAC clone. RPKM (Reads Per Kilobase per Million) values calculated from publicly available RNA-seq datasets for the six cell types indicated.

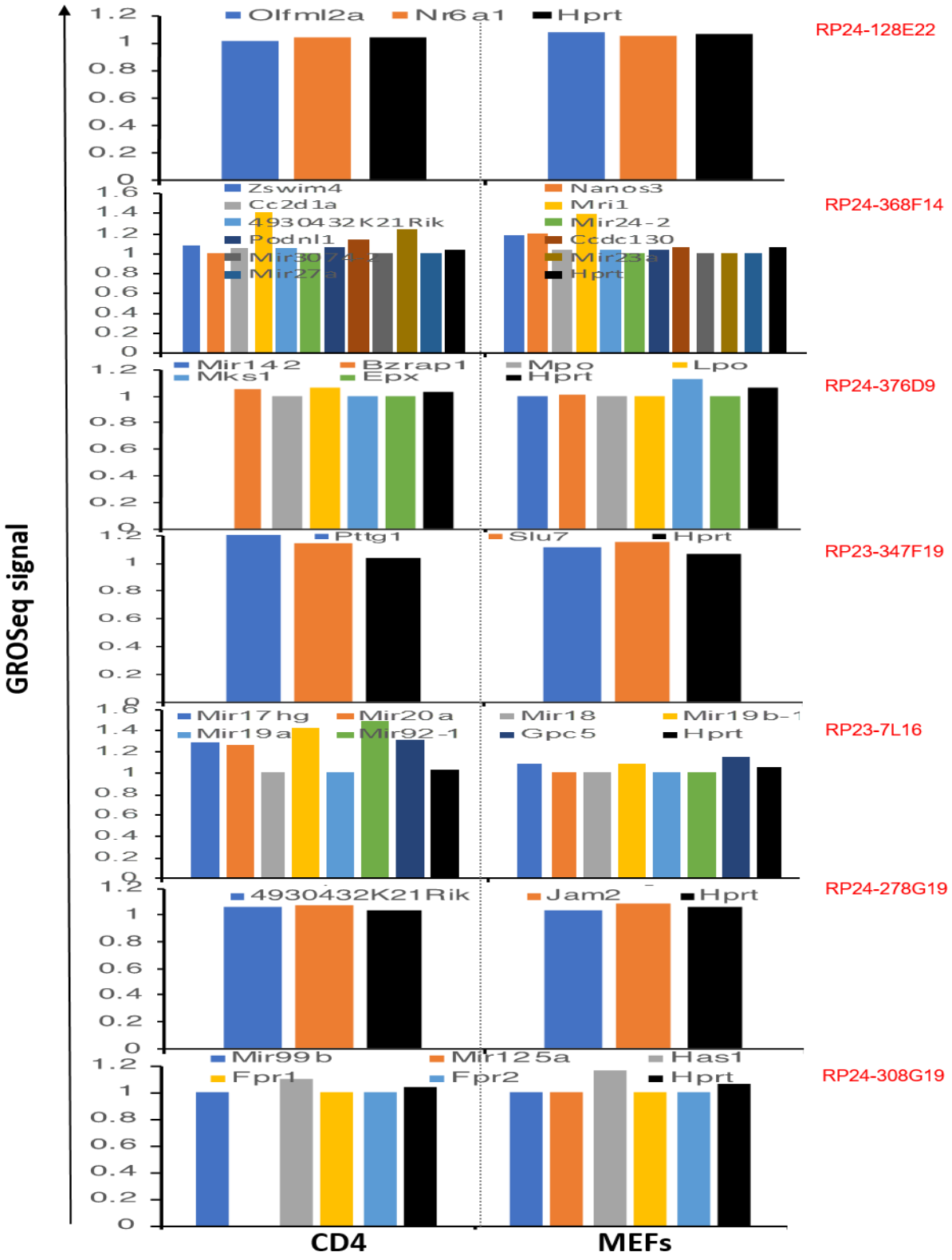

Figure 37. Nascent transcription of the genes as in (A) as deduced from aggregate score analysis of publicly available GRO-seq data in CD4$^+$ T-cells and mouse embryonic fibroblasts (MEFs)

miR	Chr	BAC clone	BAC clone Coordinates	miR coordinates	Other genes
miR-181a1/b1	1	RP24-71D3	137,857,577 - 138,069,947	a1:137,966,455-137,966,541 b1:137,966,639-137,966,718	
miR-181a1/b1	2	RP24-128E22	38,773,611 - 38,951,434	a2: 38,852,735-38,852,810 b2: 38,853,830-38,853,918	Nr6a1, Olfml2a,
miR-181c	8	RP24-368F14	84,109,833 - 84,296,280	84,178,873-84,178,961	Podnl1, Cc2d1a, 4930432K21Rik, Nanos3, mir181-d, Zswim4, Ccdc130, Mri1, Mir24-2, Mir27a, Mir3074-2, Mir23a
miR-142	11	RP24-376D9	87,718,667 - 87,882,764	87,756,864-87,756,927	mir142, Supt4a, Bzrap1, Mir142b, Mpo, Lpo, Mks1, Epx,
miR-146a	11	RP23-347F19	43,271,828 - 43,471,844	43,374,397 - 43,374,461	Pttg1, Slu7,
miR-17-92	14	RP23-7L16	114,948,625 - 115,140,014	115,043,671-115,043,754	Mir17hg, Mir20a, Mir18, Mir19b-1, Mir19a, Mir92-1, Gpc5
miR-155	16	RP24-278G19	84,640,010 - 83,813,137	84,714,140-84,714,204	4930529L06Rik, Mir155hg, Jam2,
miR-let7e	17	RP24-308G19	17,766,734 - 17,911,549	17,830,352 - 17,830,444	Spaca6, Mir99b, Mir125a, Gm36907, Has1, Fpr1, Fpr2,

Table 7. Monoallelic expression (blue), biallelic expression (red), undetermined (black), according to "dbMAE: the database of autosomal monoallelic expression"**. ASSEMBLY USED FOR COORDINATES:** GRCm38.p3 (C57BL/6J) (Savova et al. 2016).

3.4 Peripheral localization of microRNA gene loci in T cells

Transcriptional regulation of microRNA genes is critical to the development, selection and differentiation of T cells, therefore we examined their subnuclear localization during this process.

In order to study the subnuclear localization of microRNA gene loci in relation to the cell nuclear space, we performed 3D-DNA Fluorescence *in situ* hybridization (3D DNA FISH) experiments. Hybridizations were performed using thymocytes, CD4, T_H1 and T_H2 cells according to the protocol described in Materials and Methods section, by maintaining the 3D structure of the cells. The distance between the center of the allele (DNA FISH signal) from the edge of the cell nucleus (considering DNA counterstaining with DAPI) was calculated with the use of the Volocity software. All the distances were normalized to the volume of the cell nucleus (ND: normalized distance). To avoid any statistical errors or artifacts each experiment was conducted at least twice and more than 200 nuclei were analyzed per individual experiment. The positions of microRNA genes were classified in 10 isocentric shells where a normalized distance with a value of ND=0 denotes the localization of a gene allele to the nuclear periphery and a normalized distance with a value of ND=1 denotes the localization of a gene allele to the nuclear center (**Figure 38**).

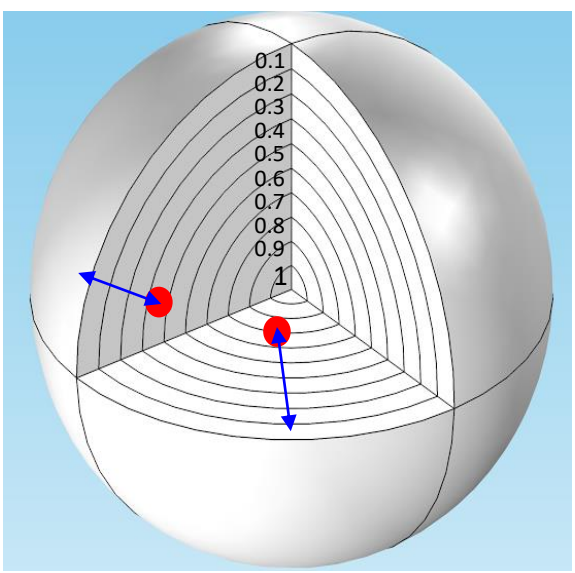

$$\mathbf{ND} = \frac{Allele - Nuclear\ periphery}{Radius}\ \mu m$$

Figure 38. A Normalized distance was calculated by dividing the absolute distance between the center of the signal from the edge of the nucleus (as defined by DAPI counterstaining) with the radius of each nucleus.

Our 3D-DNA FISH experiments demonstrated that in all T cell types the eight microRNA gene loci under study exhibited a peripheral localization in the cell nucleus. microRNA gene loci demonstrated a completely different allelic distribution when compared with the *Tnfα* locus, which exhibited an internal distribution.

Thymocytes demonstrated a peripheral distribution of the eight microRNA genes, with most alleles located at the external shell clusters. The peripheral clusters ND=0-0.1 included more than 40% of all microRNA gene alleles. A low percentage of *Tnfα* alleles (15%) located at the 0-0.1 ND cluster, whereas the higher percentage (50%) of alleles gathered at the 0.1-0.2 ND cluster (**Figure 39A**).

$CD4^+$ cells exhibited a conserved pattern of peripheral localization for microRNA genes as in thymocytes. Similarities were observed with the external clusters 0-0.1 and 0.1-0.2 containing more than 60% of total alleles of all microRNA genes under investigation. Interestingly, the distributional pattern of *Tnfα* alleles showed some differences comparing with thymocytes. In CD4 cells the higher percentage of alleles in the external clusters 0-0.1 was only 20% while most of the *Tnfα* alleles located at the more internal clusters 0.6-0.7 (**Figure 40A**).

Terminally differentiated T_H1 and T_H2 cell populations exhibited an even higher peripheral microRNA gene alleles localization when compared with undifferentiated cells such as thymocytes and $CD4^+$ cells. In T_H1 cells the external cluster 0-0.1 included more than 45% of the total microRNA gene alleles. Although *Tnfα* displayed different kinetics in T_H1 cells by being relocated to the interior of the nucleus, the highest percentage (40%) of *Tnfα* alleles in T_H1 cells located in the internal clusters 0.3-0.4 (**Figure 41A**).

T_H2 cells demonstrated a similar pattern of localization for the microRNA gene alleles. All microRNA genes under investigation were located at the peripheral cluster, with the external cluster 0-0.1 including 40% of the total alleles. On the contrary, *Tnfα* alleles presented a more internal nuclear distribution with the external cluster 0-0.1 containing only 25% of the alleles (**Figure 42A**).

In conclusion, most of the microRNA genes under study are located at the nuclear periphery. The distribution of microRNA gene alleles in T cells encompassed the ND clusters of 0.1-0.5. Comparing the microRNA gene alleles subnuclear localization with that of the *Tnfα* gene we observed that in all cell types *Tnfα* gene alleles exhibited an internal localization pattern with a quite lower percentage of alleles located at the nuclear periphery.

No relocalization for microRNA gene loci was observed when we compared thymocytes to peripheral CD4 cells. In undifferentiated cells (thymocytes and $CD4^+$), the *Tnfα* gene locus exhibited an expanded distribution of alleles up to the internal 0.7 ND cluster. When T cells underwent differentiation, a higher peripherization of gene loci was observed. As mentioned in the introduction, T cells have a very particular

nuclear organization. At the naïve stage the chromatin of T cells is very compact and these immature cells are being in a quiescent state. The activation of T cells can lead to chromatin decompaction and relocalization of genes. Upon differentiation, most microRNA gene loci were re-localized towards the nuclear periphery. Before differentiation, an average of ~50% of microRNA gene alleles were localized in the nuclear periphery, whereas after differentiation this percentage increased to ~60%.

Although the kinetics of microRNA genes showed a peripheral relocalization during differentiation, the control locus *Tnfα* also exhibited interesting kinetics. In T_H1 cells, *Tnfα* was relocalized towards the center of the nucleus with the ND cluster of 0.3-0.4 including the highest fraction of alleles. In T_H2 cells, the *Tnfα* allele distribution was similar to $CD4^+$ cells.

To test the randomness of microRNA genes subnuclear distributions we used the non-parametric Kolmogorov Smirnov (KS) normality test. The statistical analysis was performed with the use of the IBM SPSS19 statistical analysis software. The distributions were considered significantly different when attributed a D (maximum distance of the cumulative distribution functions (CDF) of the two samples) value above zero ($0<D<1$) and a p value equal to or lower than the significance level of 0,05. In that case, it was considered that the null hypothesis of the two distributions in comparison being similar was rejected. The KS test demonstrated that the normalized distances of microRNA gene loci under investigation have a similar distribution pattern between them while the control locus *Tnfα* has a different pattern for all cell types analyzed (thymocytes, CD4, TH1 and TH2 cells) (**Figures 39-42**). In addition, cumulative frequency curves displayed that the distribution of microRNA gene alleles ND values is clearly different from the distribution of *Tnfα* gene alleles ND values in thymocytes, $CD4^+$, TH1 and TH2 cells (**Figures 39-42**).

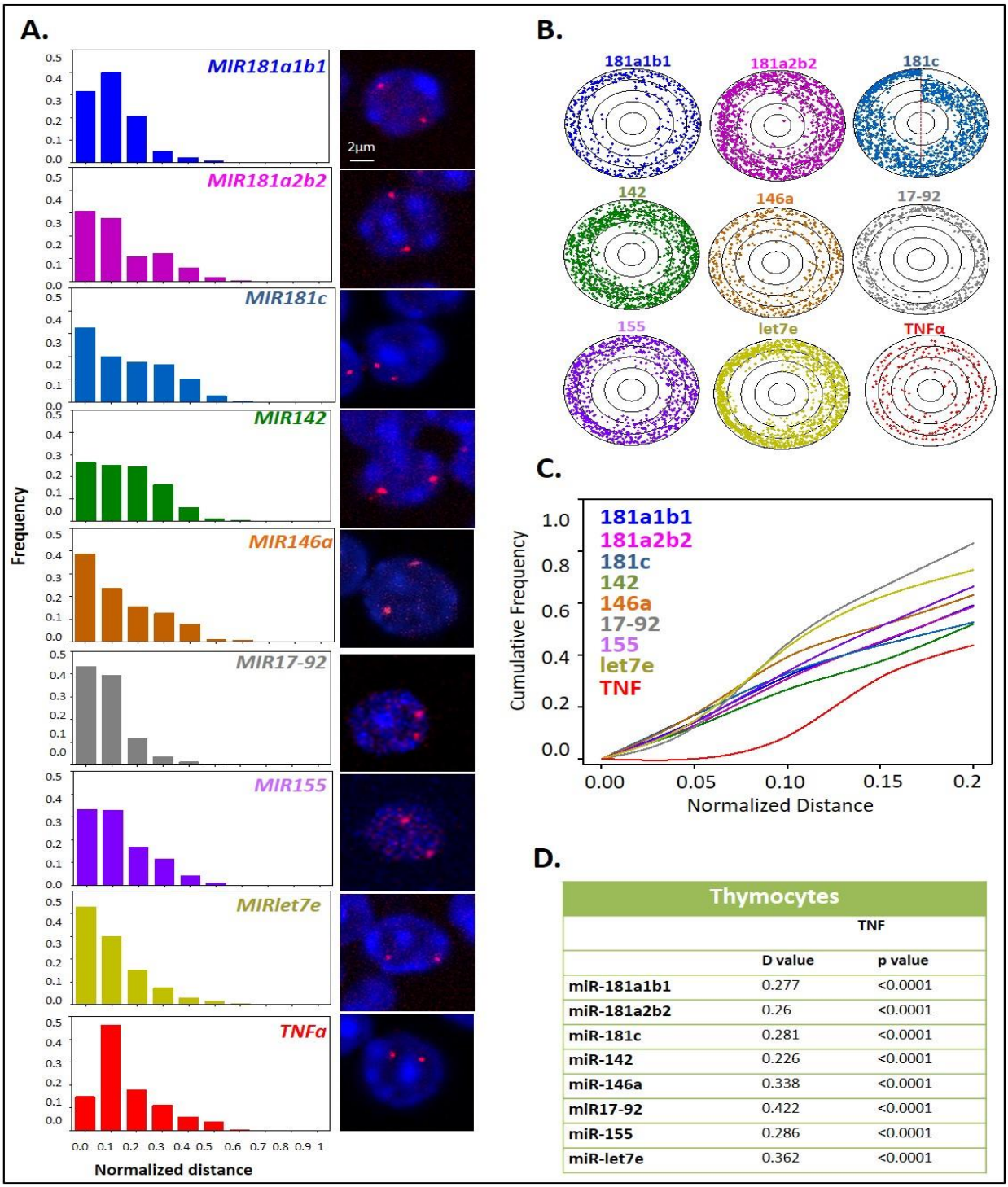

Thymocytes		
	TNF	
	D value	p value
miR-181a1b1	0.277	<0.0001
miR-181a2b2	0.26	<0.0001
miR-181c	0.281	<0.0001
miR-142	0.226	<0.0001
miR-146a	0.338	<0.0001
miR17-92	0.422	<0.0001
miR-155	0.286	<0.0001
miR-let7e	0.362	<0.0001

Figure 39. A) Distribution of microRNA gene alleles ND values in thymocytes and confocal microscopy images with representative DNA FISH experiments for eight microRNA genes and the *Tnfα* control locus (scale bar: 2µm). B) 2D-Polar plots subdivided in 5 concentric circles showing the peripheral distribution of microRNA gene alleles in thymocytes. C) Cumulative frequency curves of microRNA and *Tnfα* gene alleles ND values in thymocytes. D) Kolmogorov-Smirnov test of distributions between microRNA genes and *Tnfα* in thymocytes. The p values for the KS test statistics are indicated (**$p < 0.05$).

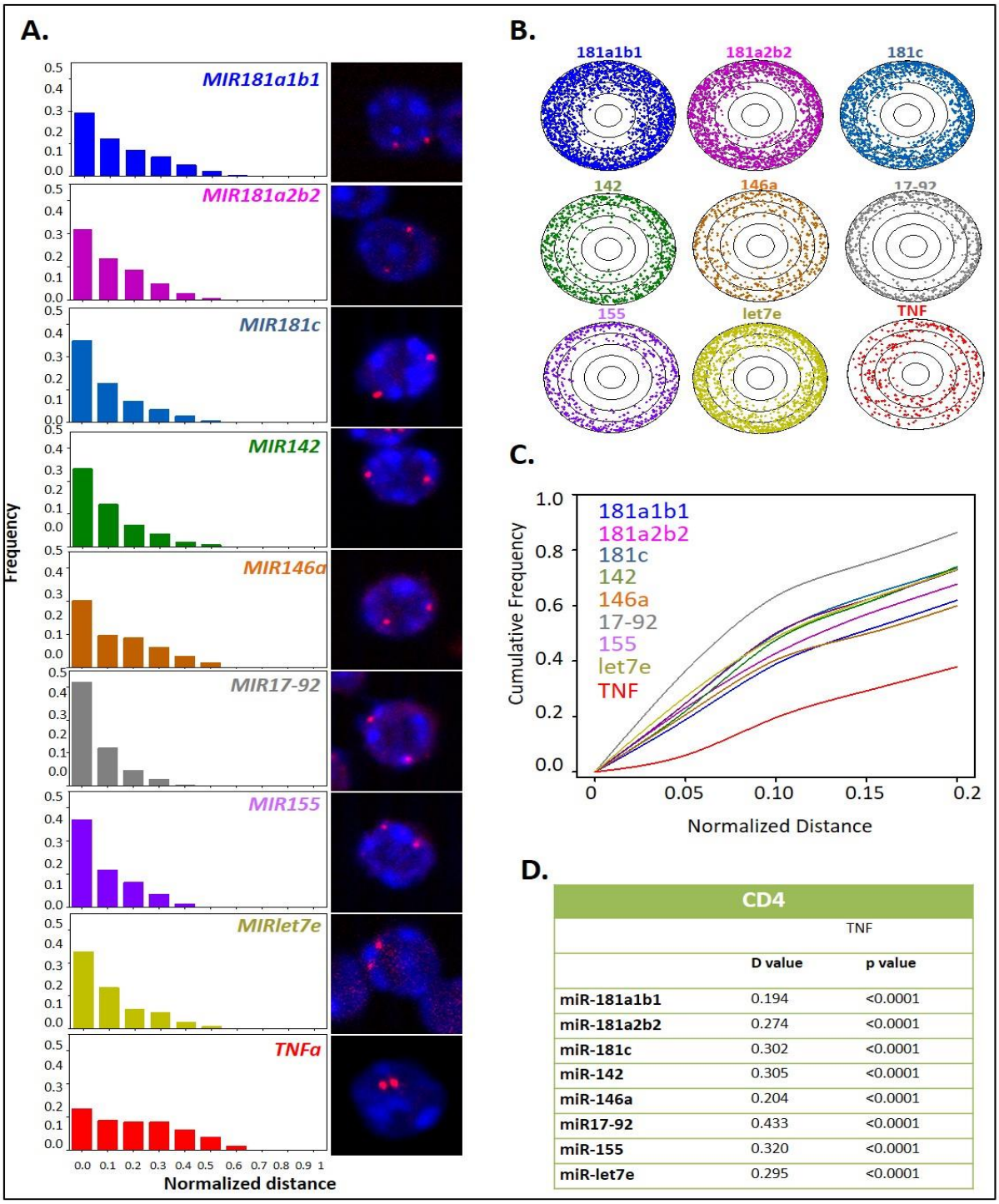

CD4		
	TNF	
	D value	p value
miR-181a1b1	0.194	<0.0001
miR-181a2b2	0.274	<0.0001
miR-181c	0.302	<0.0001
miR-142	0.305	<0.0001
miR-146a	0.204	<0.0001
miR17-92	0.433	<0.0001
miR-155	0.320	<0.0001
miR-let7e	0.295	<0.0001

Figure 40. A) Distribution of microRNA gene alleles ND values in CD4 cells and representative confocal microscopy images of DNA FISH experiments for 8 microRNA genes and the control locus *Tnfα* (scale bar: 2µm). B) 2D-Polar plots subdivided in 5 concentric circles showing the peripheral distribution of microRNA genes in CD4 cells. C) Cumulative frequency curves for microRNA and *Tnfα* gene alleles ND values in CD4 cells. D) Kolmogorov-Smirnov test for the distribution of ND values between microRNA and *Tnfα* gene alleles in CD4 cells. The p values for the KS test statistics are indicated (**p < 0.05).

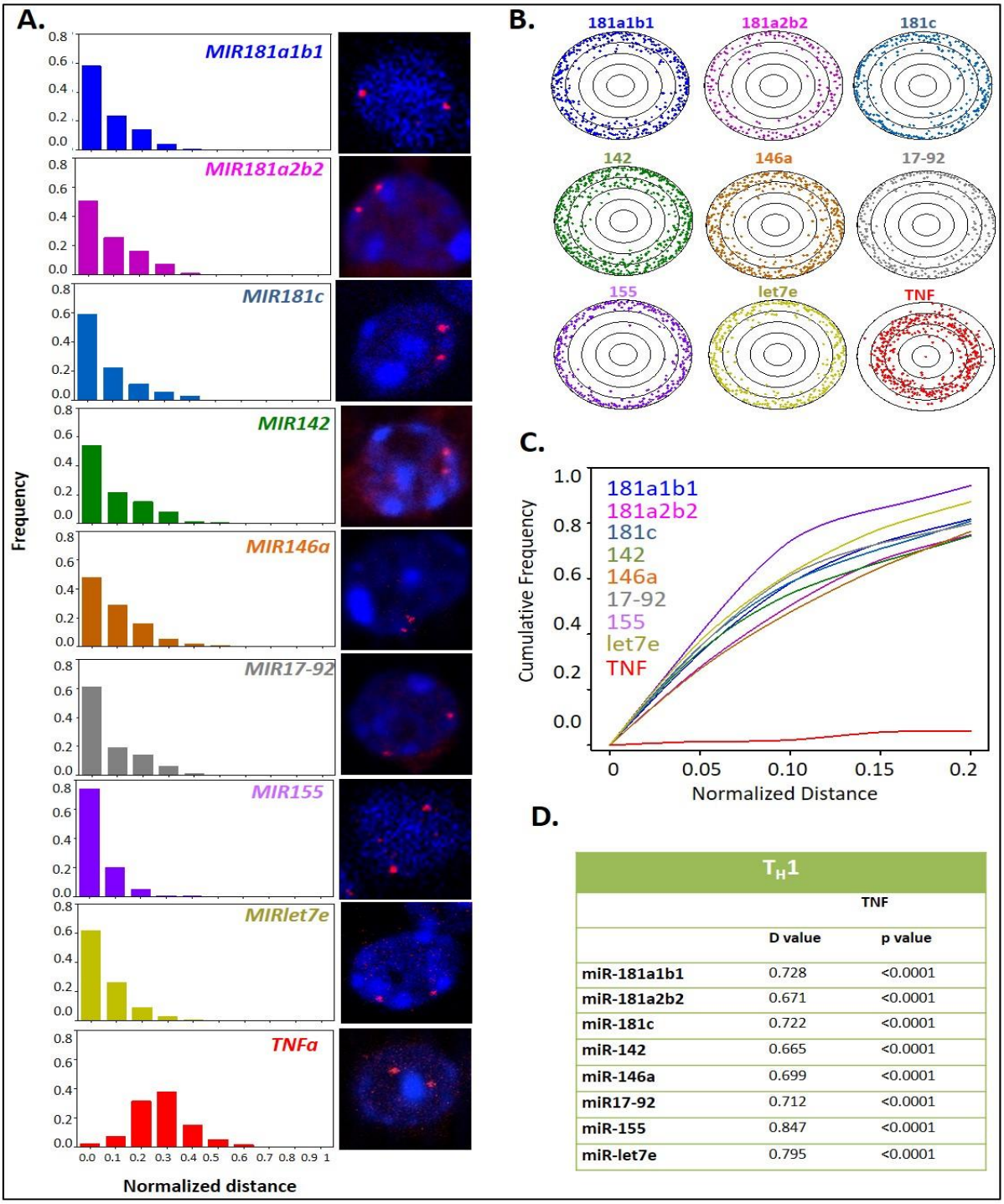

T_H1		
	TNF	
	D value	p value
miR-181a1b1	0.728	<0.0001
miR-181a2b2	0.671	<0.0001
miR-181c	0.722	<0.0001
miR-142	0.665	<0.0001
miR-146a	0.699	<0.0001
miR17-92	0.712	<0.0001
miR-155	0.847	<0.0001
miR-let7e	0.795	<0.0001

Figure 41. A) Distribution of microRNA gene alleles ND values in T_H1 cells and representative confocal microscopy images of DNA FISH experiments for 8 microRNA genes and the control locus *Tnfα* (scale bar: 2µm). B) 2D-Polar plots subdivided in 5 concentric circles showing the peripheral distribution of microRNA genes in T_H1 cells. C) Cumulative frequency curves for microRNA and *Tnfα* gene alleles ND values in T_H1 cells. D) Kolmogorov-Smirnov test for the distribution of ND values between microRNA and *Tnfα* gene alleles in T_H1 cells. The p values for the KS test statistics are reported (**$p < 0.05$).

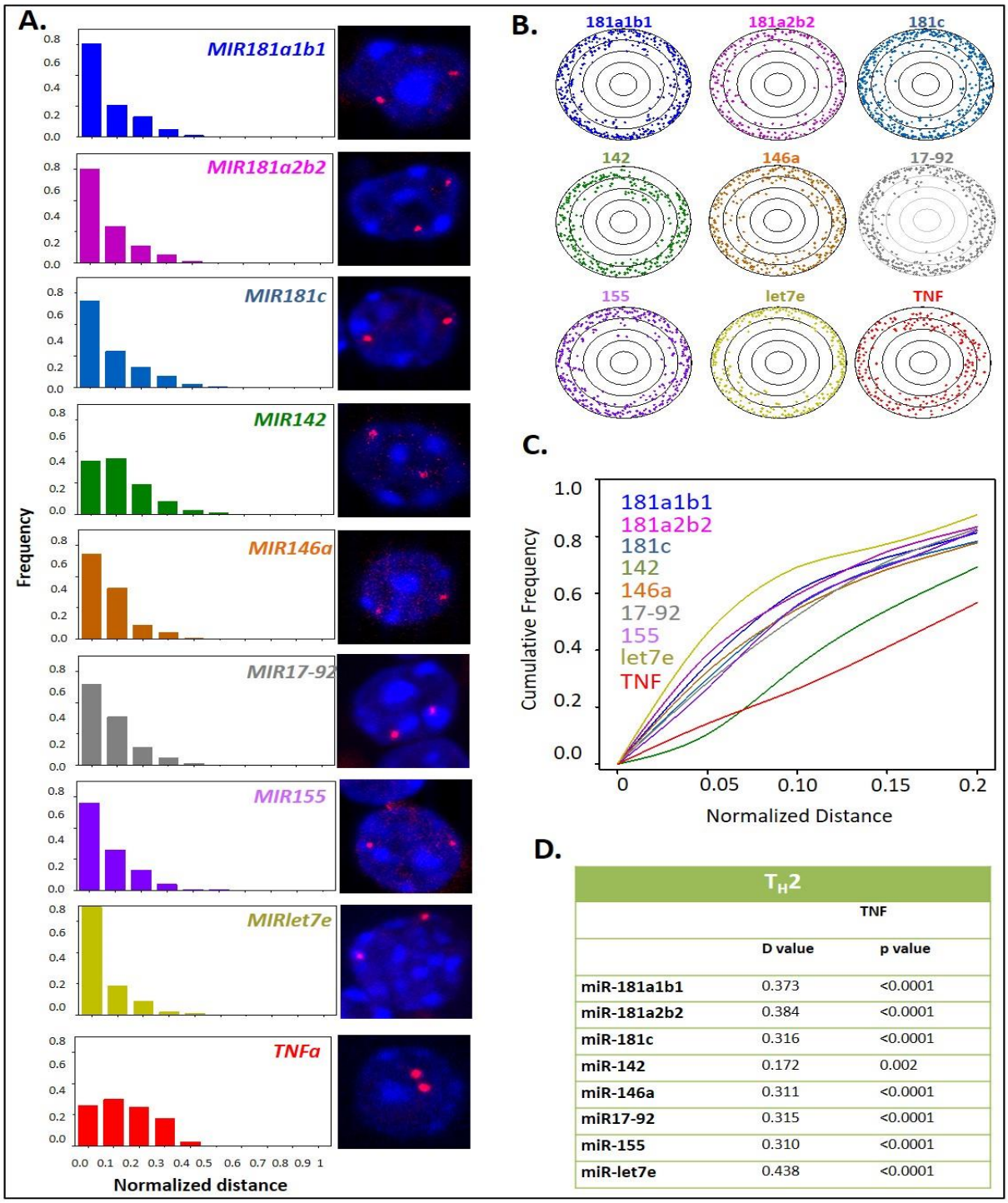

T_H2		
	TNF	
	D value	p value
miR-181a1b1	0.373	<0.0001
miR-181a2b2	0.384	<0.0001
miR-181c	0.316	<0.0001
miR-142	0.172	0.002
miR-146a	0.311	<0.0001
miR17-92	0.315	<0.0001
miR-155	0.310	<0.0001
miR-let7e	0.438	<0.0001

Figure 42. A) Distribution of microRNA gene alleles ND values in T_H2 cells and representative confocal microscopy images of DNA FISH experiments for 8 microRNA genes and the control locus *Tnfα* (scale bar: 2µm). B) 2D-Polar plots subdivided in 5 concentric circles showing the peripheral distribution of microRNA genes in T_H2 cells. C) Cumulative frequency curves for microRNA and *Tnfα* gene alleles ND values in T_H2 cells. D) Kolmogorov-Smirnov test for the distribution of ND values between microRNA and *Tnfα* gene alleles in T_H2 cells. The p values for the KS test statistics are reported (**$p < 0.05$).

3.5 microRNA gene loci colocalize with proteins of the nuclear periphery

In order to experimentally test whether the peripheral distribution of the investigated microRNA gene loci was attributed to a dynamic interplay with the nuclear lamina, as already described for coding genes (Zhao et al. 2015), we performed 3D-DNA FISH in concert with immunofluorescence experiments. As already described in the introduction, the filamentous structure of nuclear lamina apart of its role in maintaining the nuclear structural integrity, it is also implicated in the nuclear positioning of chromatin and transcription regulation. The major structural components of the nuclear lamina in mammals are the intermediate filament proteins Lamin A/C (LMNA/C), LMNB1, and LMNB2. Nuclear lamina also provides a scaffold for organizing nuclear pore complexes (NPCs), which has been reported to have many gene regulatory functions. Therefore, we isolated and differentiated $CD4^+$ T cells in order to examine the colocalization of microRNA gene loci with nuclear periphery proteins.

Firstly, we showed that LMNB1 and LMNA/C are colocalized in T cells, by means of co-immunofluorescence experiments. As previously mentioned lamins are not expressed in all cell types. At the embryonic state, Lamin A/C is merely expressed, while Lamin B is highly expressed. In thymocytes both lamins are expressed and greatly colocalize as shown in **Figure 43A**. For this reason, we decided to perform the subsequent 3D immune-DNA FISH experiments presented below by immunofluorescence staining for LMNB1.

Transcriptionally active genes at the nuclear periphery are often associated with the nuclear pore complex (NPC). Except from LMNB1 and LMNA/C, we also investigated the colocalization of microRNA genes with Nuclear Pore Complexes (NPC). Our experiments were repeated twice and more than 150 cells were analyzed for every single hybridization. Immuno-DNA FISH experiments were performed for all T cell subtypes according to the protocol described in the Materials and Methods section. Proteins of the nuclear periphery such as LMNB1 and NPCs were used to study the potential colocalization of microRNA genes with the nuclear periphery. According to all the 3D immuno-DNA FISH experiments we conclude that microRNA genes are not colocalized and do not show any tendency of proximity with NPCs in thymocytes. This can be explained by the fact with a mix of all eight labeled BAC probes detecting the discrete microRNA gene loci failed to reveal a colocalization of microRNA gene loci with NPCs at the nuclear periphery (**Figure 43E**). that in contrast with lamins there is not a continuum between the NPCs as shown in **Figure 43C**. DNA FISH analysis

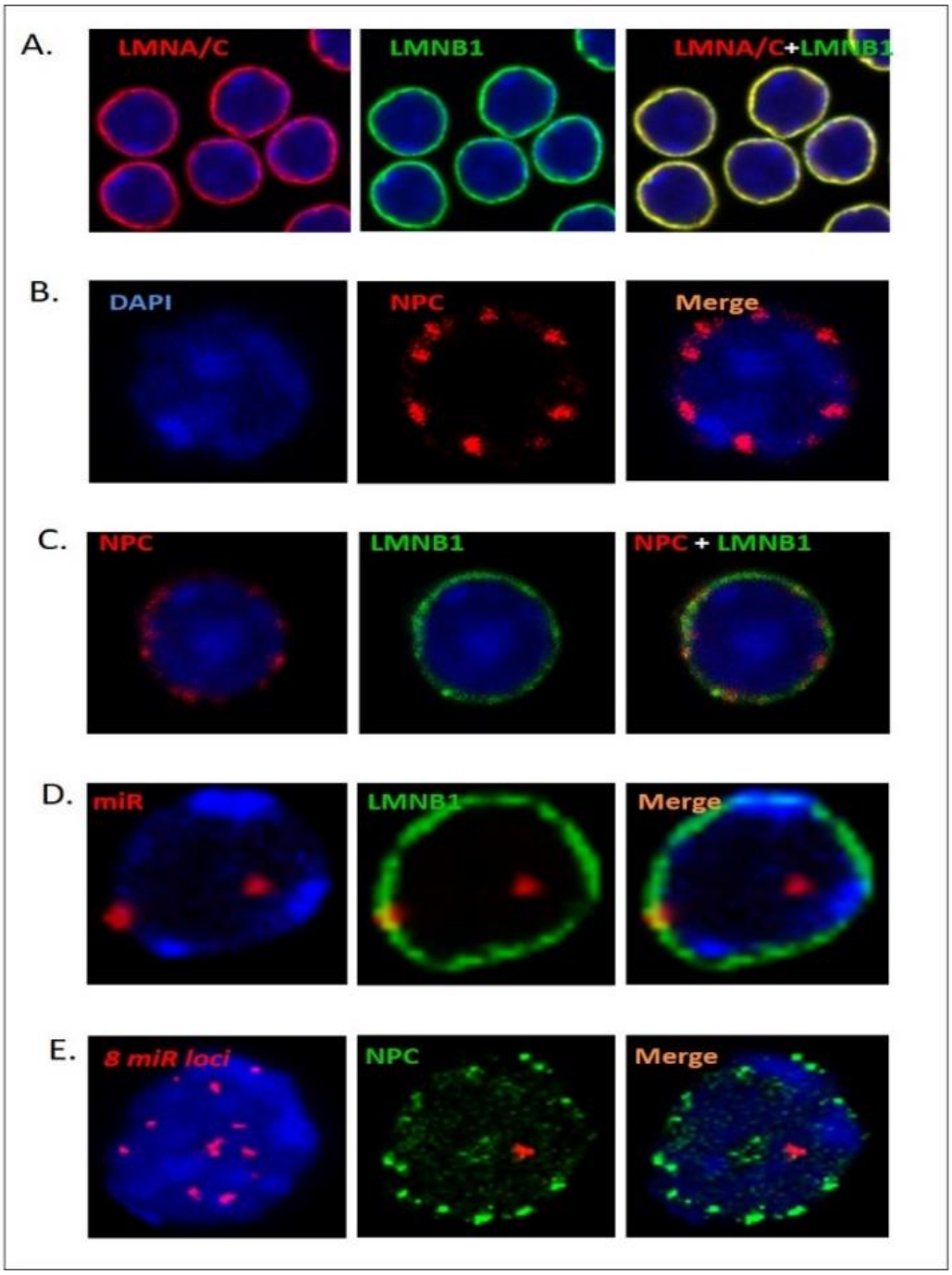

Figure 43. A) Confocal microscopy images showing the colocalization of LMNA/C (red) and LMNB1 (green) proteins in thymocytes (DNA counterstained with DAPI - blue). B) NPCs (red) localization in thymocytes (DNA counterstained with ToPro3 - blue). C) Confocal microscopy images that show the colocalization of NPCs (red) and LMNB1 protein (green) in thymocytes (DNA counterstained with DAPI - blue). D) Immuno-DNA FISH with hybridization to a single microRNA gene (red) and simultaneous LMNB1 staining (green) in thymocytes (DNA counterstained with DAPI - blue). E) Immuno-DNA FISH experiment with hybridization to all eight microRNA gene loci and simultaneous LMNB1 staining in thymocytes (DNA counterstained with DAPI - blue). The first image of each horizontal panel shows merged z-stacks while the second and the third image of each panel depicts a single z-stack section.

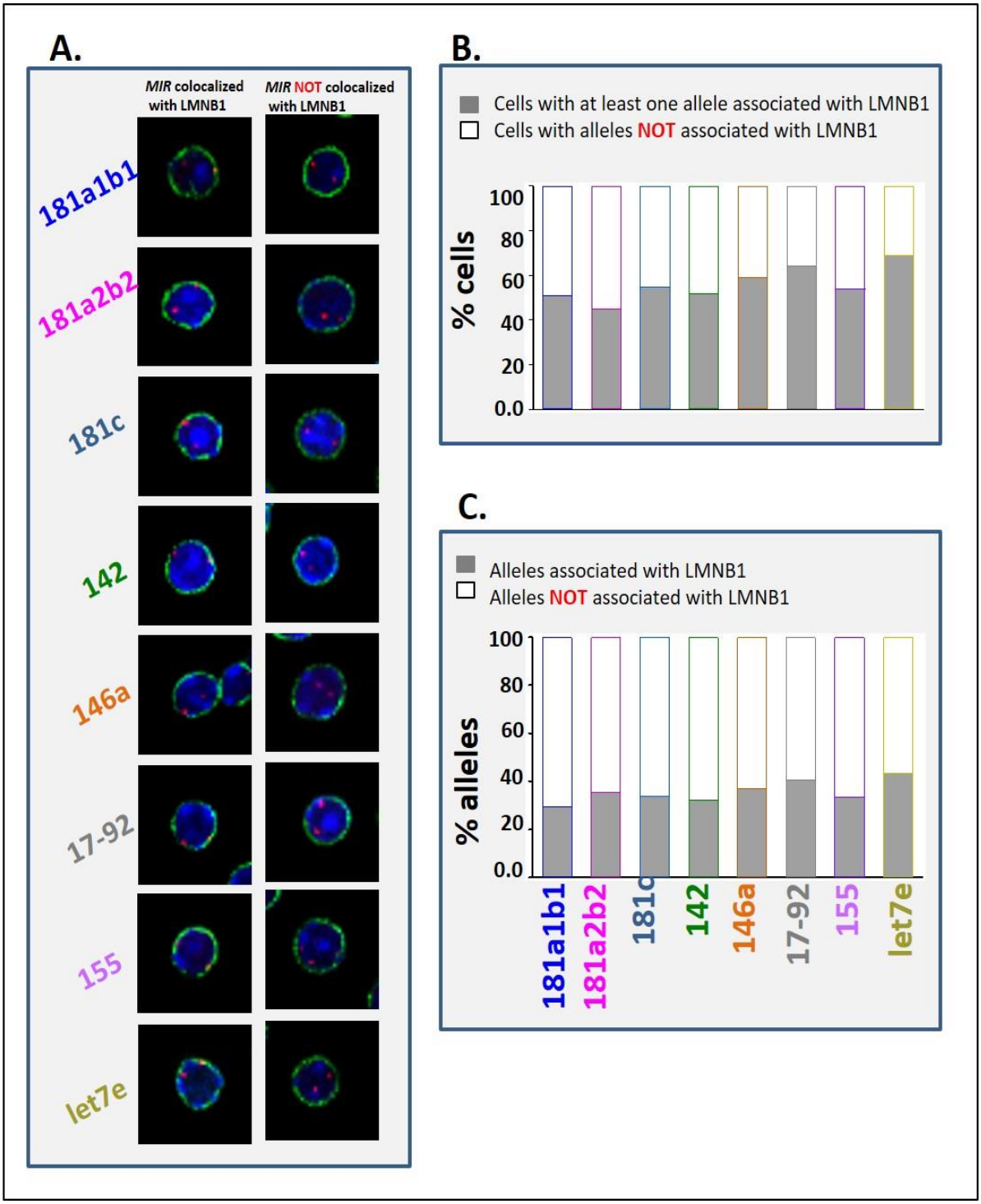

Figure 44. A) Confocal microscopy images from 3D Immuno-DNA FISH experiments for microRNA genes and LMNB1 in thymocytes. The first column depicts cells with at least one microRNA gene allele being colocalized with LMNB1, whilst the second column depicts microRNA gene alleles not colocalized with LMNB1. All the images presented are from single z-stack sections. B) Diagram showing the percentage of thymocytes having at least one microRNA gene allele colocalized with LMNB1. C) Diagram presenting the percentage of alleles colocalized with LMNB1.

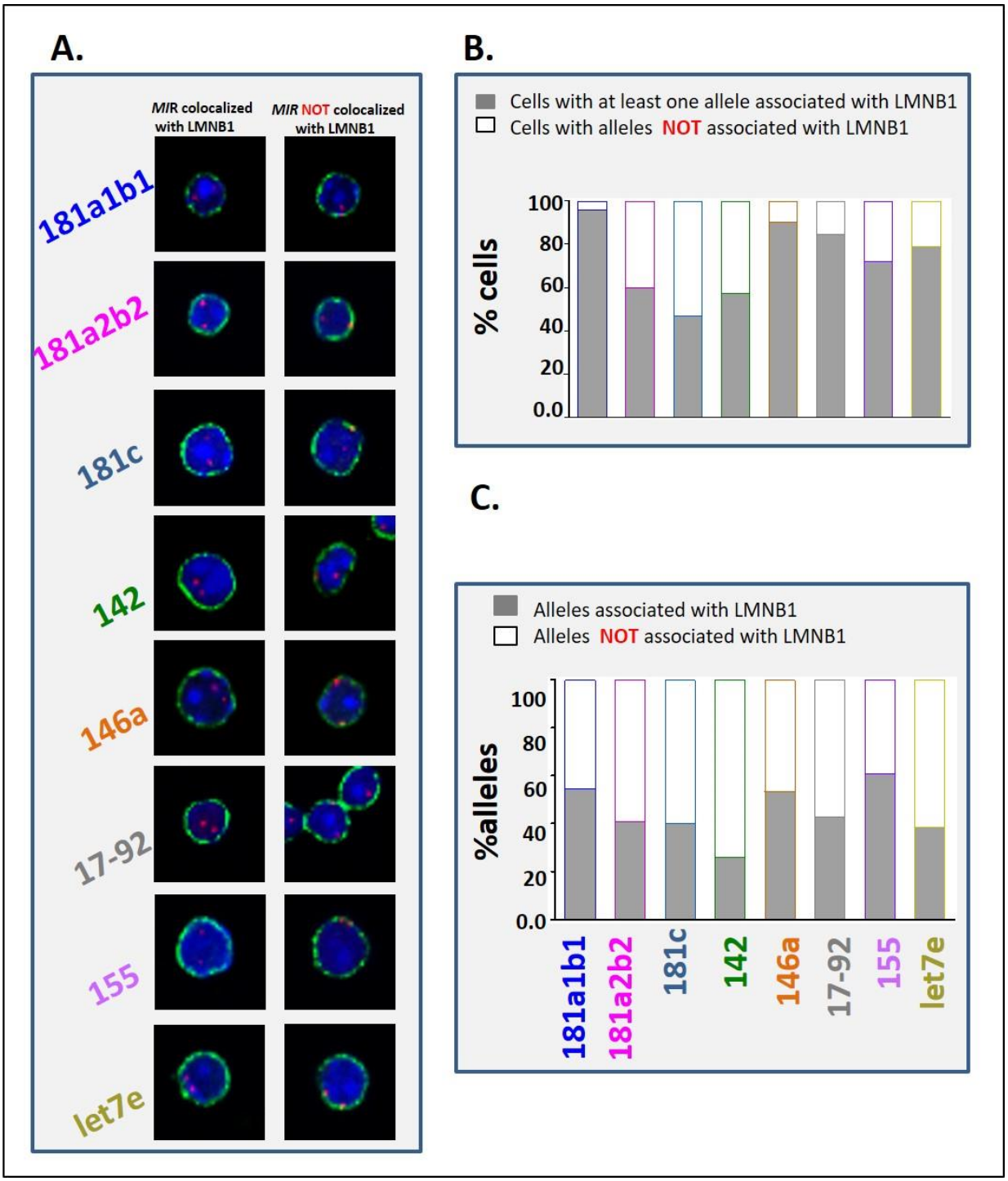

Figure 45. A) Confocal microscopy images from 3D Immuno-DNA FISH experiments for microRNA genes and LMNB1 in CD4 cells. The first column depicts cells with at least one microRNA gene allele being colocalized with LMNB1, whilst the second column depicts microRNA gene alleles not colocalized with LMNB1. All images presented are from single z-stack sections. B) Diagram showing the percentage of CD4 cells having at least one allele colocalized with LMNB1. C) Diagram presenting the percentage of alleles colocalized with LMNB1.

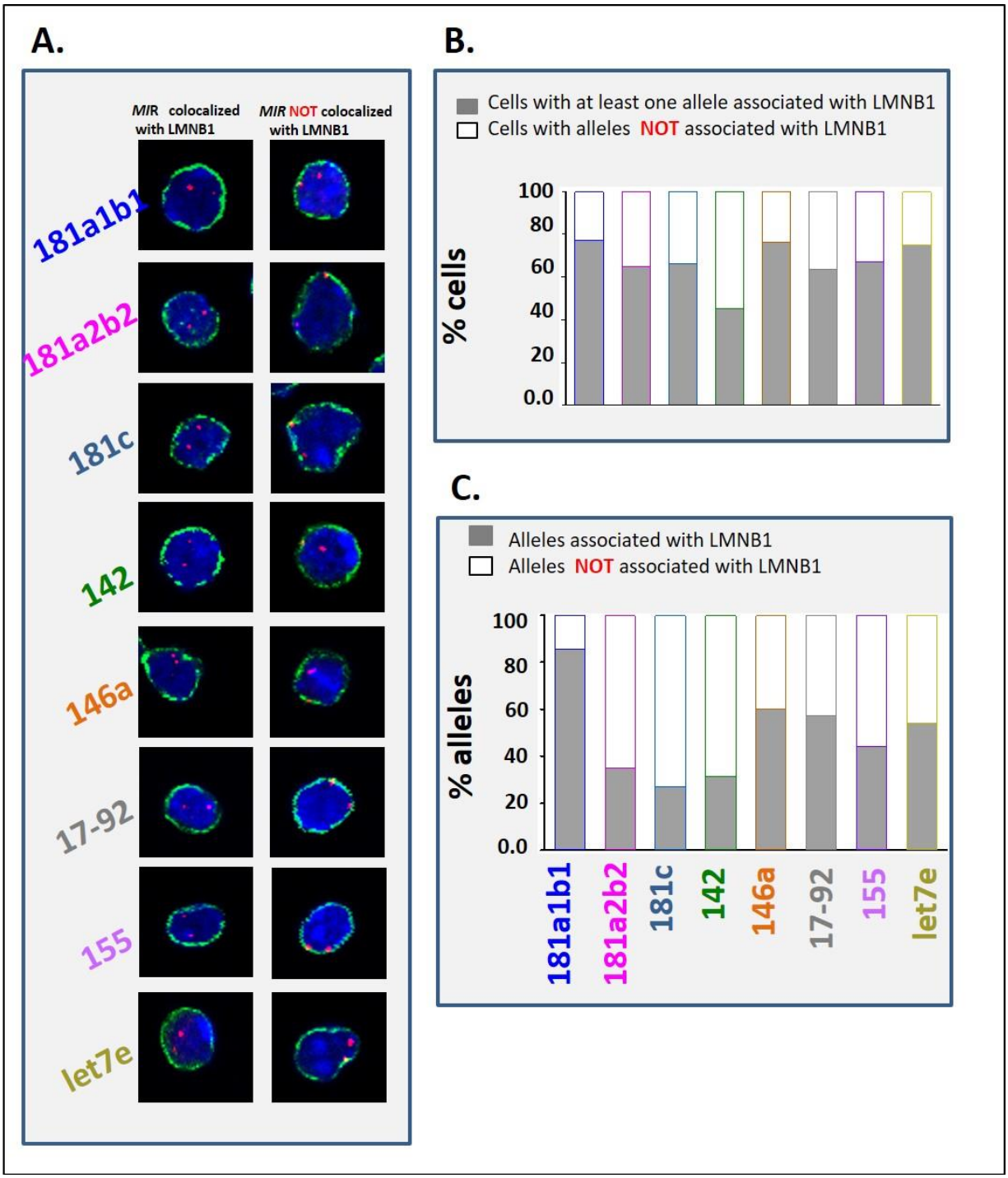

Figure 46. A) Confocal microscopy images from 3D Immuno-DNA FISH experiments for microRNA genes and LMNB1 in TH1 cells. The first column depicts cells with at least one microRNA gene allele being colocalized with LMNB1, whilst the second column depicts microRNA gene alleles not colocalized with LMNB1. All images presented are from single z-stack sections. B) Diagram showing the percentage of T H1 cells having at least one allele colocalized with LMNB1. C) Diagram presenting the percentage of alleles colocalized with LMNB1.

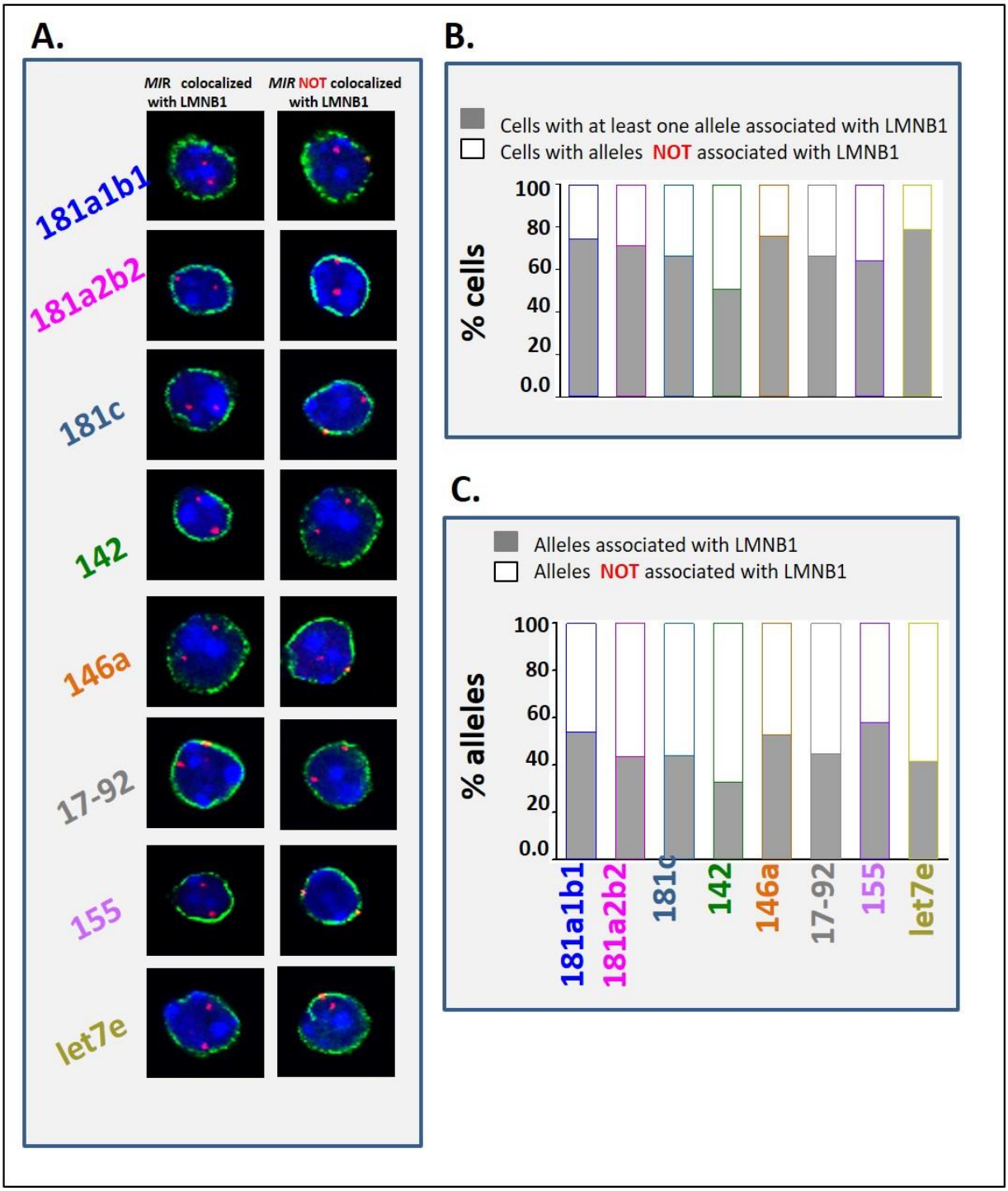

Figure 47. A) Confocal microscopy images from 3D Immuno-DNA FISH experiments for microRNA genes and LMNB1 in T_H2 cells. The first column depicts cells with at least one microRNA gene allele being colocalized with LMNB1, whilst the second column depicts microRNA alleles not colocalized with LMNB1. All images presented are from single z-stack sections. B) Diagram showing the percentage of T_H2 cells having at least one allele colocalized with LMNB1. C. Diagram presenting the percentage of alleles colocalized with LMNB1.

On the contrary, 3D immuno-DNA FISH experiments in T cells demonstrated that microRNA gene loci were colocalized with LMNB1 in T cells (**Figure 43D**). 3D immuno-DNA FISH experiments demonstrated that in thymocytes (**Figure 44A**) more than 50% of the cells display at least one microRNA gene allele colocalized with LMNB1 (**Figure 45B**). $CD4^+$ cells exhibited higher levels of colocalization of microRNA genes with LMNB1 (**Figure 46B**). Except from *miR-181c* (which was colocalized with LMNB1 in only 40% of the cells) for the rest of the microRNA genes more than 60% of the CD4 cells displayed at least one allele colocalized with LMNB1. During activation and differentiation of T cells towards the T_H1 and T_H2 cell lineages, the fraction of alleles colocalized with LMNB1 increased. In both cell types, in over 50% of the cells at least one microRNA gene allele colocalized with LMNB1 (**Figures 47B & 48B**). These findings are in agreement with our previous DNA FISH results, where we found a higher tendency for perinuclear localization of microRNA genes upon differentiation, which can explain the higher fraction of these genes colocalized with nuclear lamina proteins.

Based on the previous results, we concluded that the microRNA gene loci under study localize in the nuclear periphery in close proximity to the nuclear lamina, irrespectively of their transcription status. Therefore, we questioned whether microRNA genes colocalize with NPCs. Such an interaction of NPCs with euchromatin could promote transcription and control chromatin organization as previously reported (Breuer and Ohkura 2015; Starling 2017; D'Angelo 2018). Although we couldn't show any correlation between NPCs and microRNA genes by means of IF-DNA-FISH, we next analyzed publicly available ChIP-seq data for NUP153, NUP93 and NUP98 (GEO numbers are provided in the corresponding Materials and Methods information section). We found that microRNA gene loci were significantly enriched, compared to coding genes, for NUP153 and NUP93 proteins (**Figure 48**). While NUP153 and NUP93 displayed similar results, this was not the case for NUP98 where we did not observe any significant enrichment between microRNA gene loci and mRNAs. Based on these results we conclude that nuclear pore proteins may be implicated in tethering microRNA gene loci to the nuclear periphery.

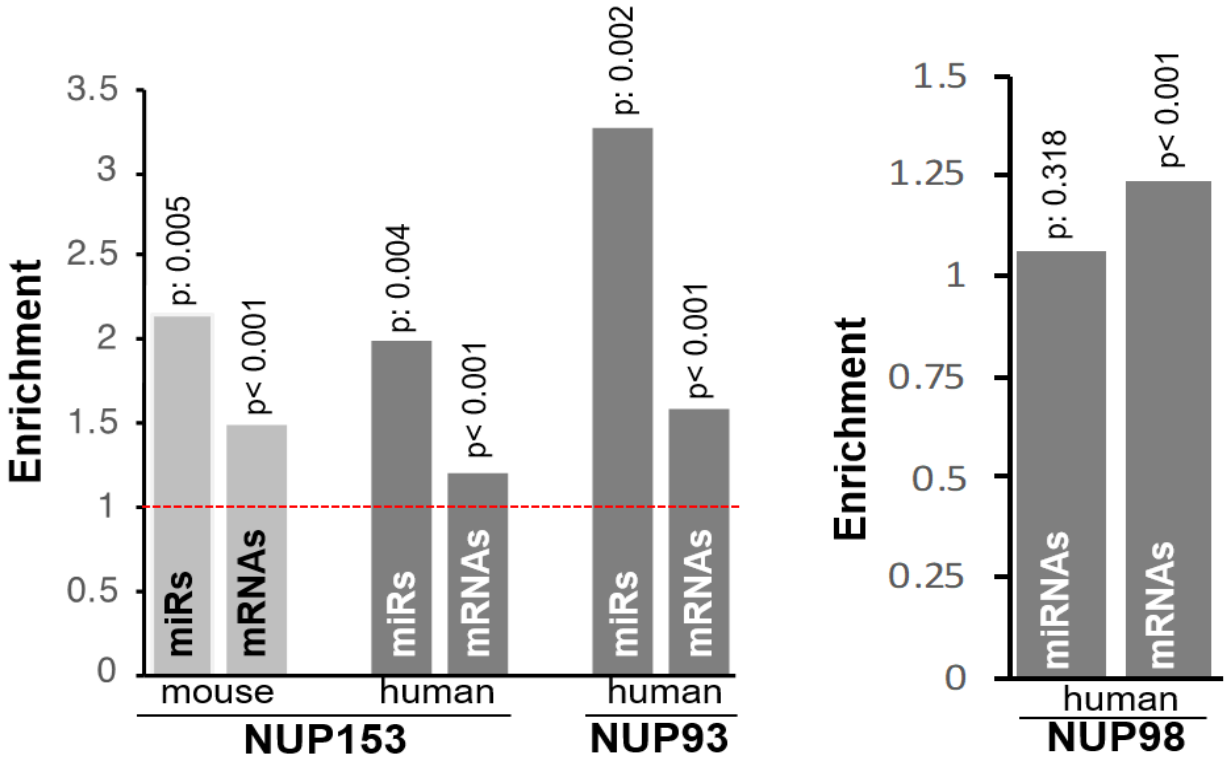

Figure 48. Assessment of overlap tendencies between a) microRNA and b) protein coding mRNA gene loci with peaks corresponding to human and mouse nucleoporins. Enrichment of colocalization was calculated as observed over expected ratios of overlaps between the compared genomic regions. Pvalues were calculated on the basis of 1000 random permutations of the peaks' regions. Values <0.001 indicate not one out of 1000 permutations had a value as high as the observed.

3.6 Peripheral localization of microRNA gene loci in murine ESCs

Based on the consistency of our findings regarding the perinuclear positioning of microRNA genes tested, we next investigated whether this preferential localization constitutes an immune cell specific phenomenon or has been established in earlier developmental stages in a manner that excludes the tested microRNA genes from internal nuclear positions. To answer that, we examined the allelic distribution of microRNA gene loci in mouse embryonic germline competent cells (ESCs) JM8.4. As mentioned in the introduction, lymphoid hematopoietic progenitor cells leave the bone marrow and they migrate to the thymus to develop in discrete T cell lineages. After that, a series of rearrangements occur to the TCR genes and thymocytes go through positive and negative selection. During the aforementioned migration from the bone marrow to the thymus and later to the secondary lymphoid organs such the spleen and the lymph nodes, T cells encompass specific gene expression programmes accompanied by major chromatin reorganization and gene positioning alteration. The eight microRNA and the *TNFα* gene loci were used for 3D-DNA FISH experiments performed in ESCs. A total number of 150 cells were analyzed for each gene. In ESCs the microRNA gene alleles were mostly located to the nuclear periphery as deduced by the distribution of alleles ND values between the clusters ND=0.0-0.1. More than 80% of the alleles were positioned at the nuclear periphery occupying the external cluster of ND=0.0-0.1 (**Figure 49**). Interestingly, the *Tnfα* locus also demonstrated a perinuclear localization in ESCs with 80% of the gene alleles ND values included in the ND cluster of 0.0-0.1. Our results indicated that similarly to T cells, ESCs demonstrate a perinuclear localization of microRNA gene loci, with no relocalization observed between ESCs and T cells before or after differentiation. In contrary the *Tnfα* locus demonstrated different kinetics in ESCs and T cell subtypes, localized towards the nuclear center in T cells and in the nuclear periphery in ESCs.

Since the perinuclear localization of specific microRNA genes is conserved between ESCs and upon development in T cells, we conclude that the localization of microRNA genes at the nuclear periphery may not be a random phenomenon but it is reveals a link between 3D chromatin organization and microRNA gene expression.

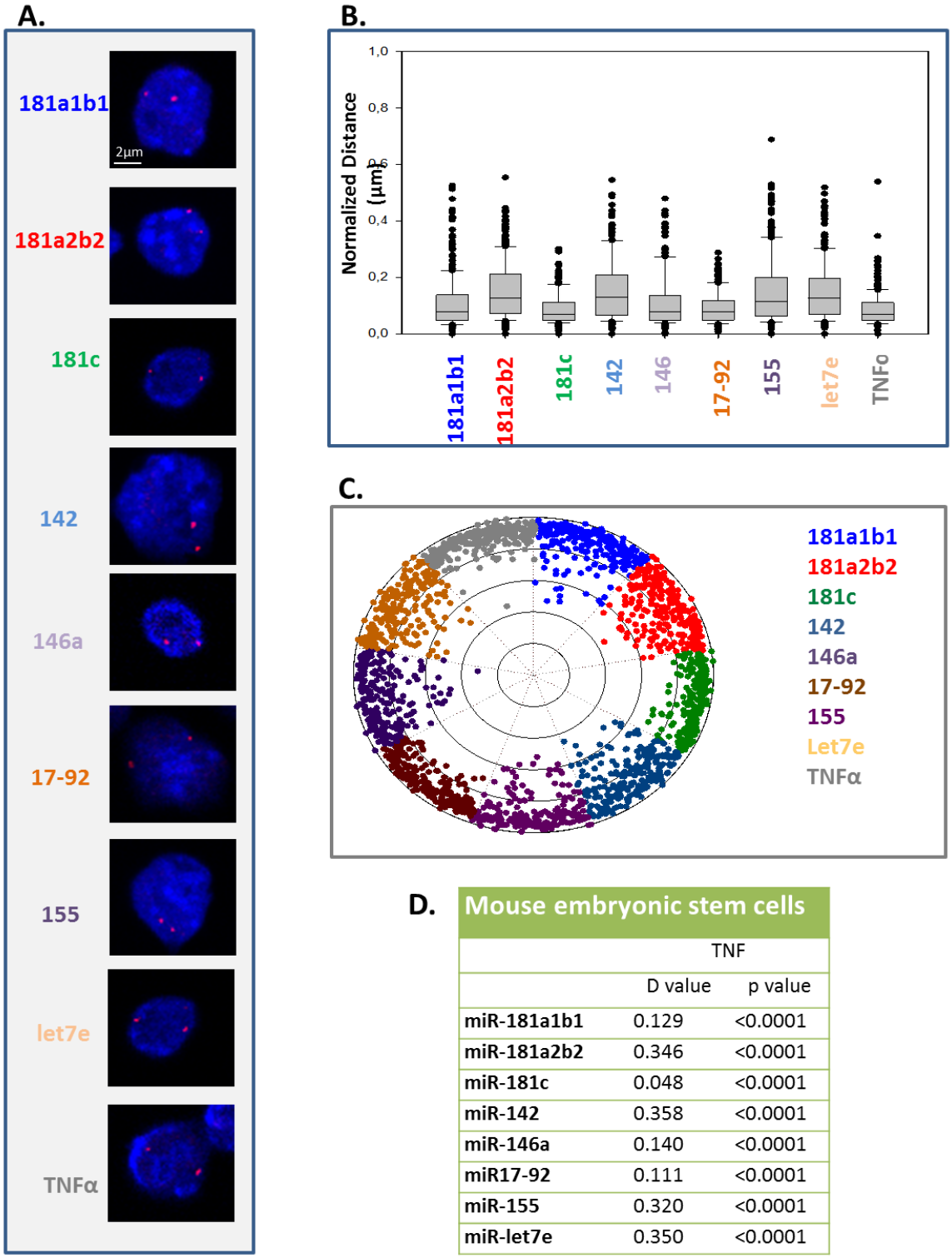

D.

Mouse embryonic stem cells		
	TNF	
	D value	p value
miR-181a1b1	0.129	<0.0001
miR-181a2b2	0.346	<0.0001
miR-181c	0.048	<0.0001
miR-142	0.358	<0.0001
miR-146a	0.140	<0.0001
miR17-92	0.111	<0.0001
miR-155	0.320	<0.0001
miR-let7e	0.350	<0.0001

Figure 49. A) Representative confocal microscopy images from 3D DNA FISH experiments for the eight microRNA and *Tnfα* gene loci (red) in ESCs (DNA counterstained with DAPI - blue). B) Box plot diagram depicting the distribution of microRNA and *Tnfα* gene alleles ND values in ESCs. Black line within the box defines the median of the ND values calculated. C) Polar plot for the gene alleles ND values distribution in ESCs. D) KS test for the distribution of gene alleles ND values for microRNA and *Tnfα* gene loci in ESCs.

3.7 Association of eight microRNA genes with LAD domains

Collectively our previous experiments demonstrated a perinuclear localization of microRNA gene loci and a colocalization with nuclear lamina proteins. Therefore, we further questioned if there is any connection between microRNA gene loci with the Lamin Associated Domains (LADs).

LADs are long chromosomal regions associated with lamin proteins as deduced by chromatin precipitation and subsequent next generation sequencing experiment. Such domains can vary in length between 0.1-10Mbp and consist around 40% of the eukaryotic genome. LADs are highly conserved between species and genes localized within these regions are generally transcriptionally inactive (Guelen et al. 2008). Although it was reported that LADs are gene poor domains, it was also reported that genes before transcriptional activation lose their respective nuclear lamina association, or they gain nuclear lamina association when they are no longer expressed. This illustrates the necessity for increasing our understanding regarding the functional roles of these large domains in genome organization.

DamID experiments provided us with data about LADs in four different murine cell types: mouse embryonic stem cells (ECs), mouse embryonic fibroblasts (MEFs), neuronal progenitor cells (NP) and astrocytes. In order to check if microRNA gene loci colocalize with LADs, we analyzed the extended genomic region of 2 Mb encompassing the primary transcript of each of eight microRNA gene locus under study in four cell types. Constitutive LADs (cLADs) are lamin-associated regions in all four cell types (ECs, NPs, astrocytes and MEFs) while constitutive inter-LADs (ciLADs) are chromatin regions between LADs in all four cell types mentioned. This analysis revealed that microRNA and *Tnfα* gene loci are located between cLADs and within ciLADs. (**Figure 50**). These data are in agreement with our previous results from RNA-DNA FISH experiments. The microRNA genes under investigation are transcribed at the nuclear periphery and they avoid the “inactive” cLAD area.

These results lead to the conclusion that the nuclear periphery can affect genome organization by tethering active chromatin domains and functioning as a transcriptionally active environment for microRNA gene expression.

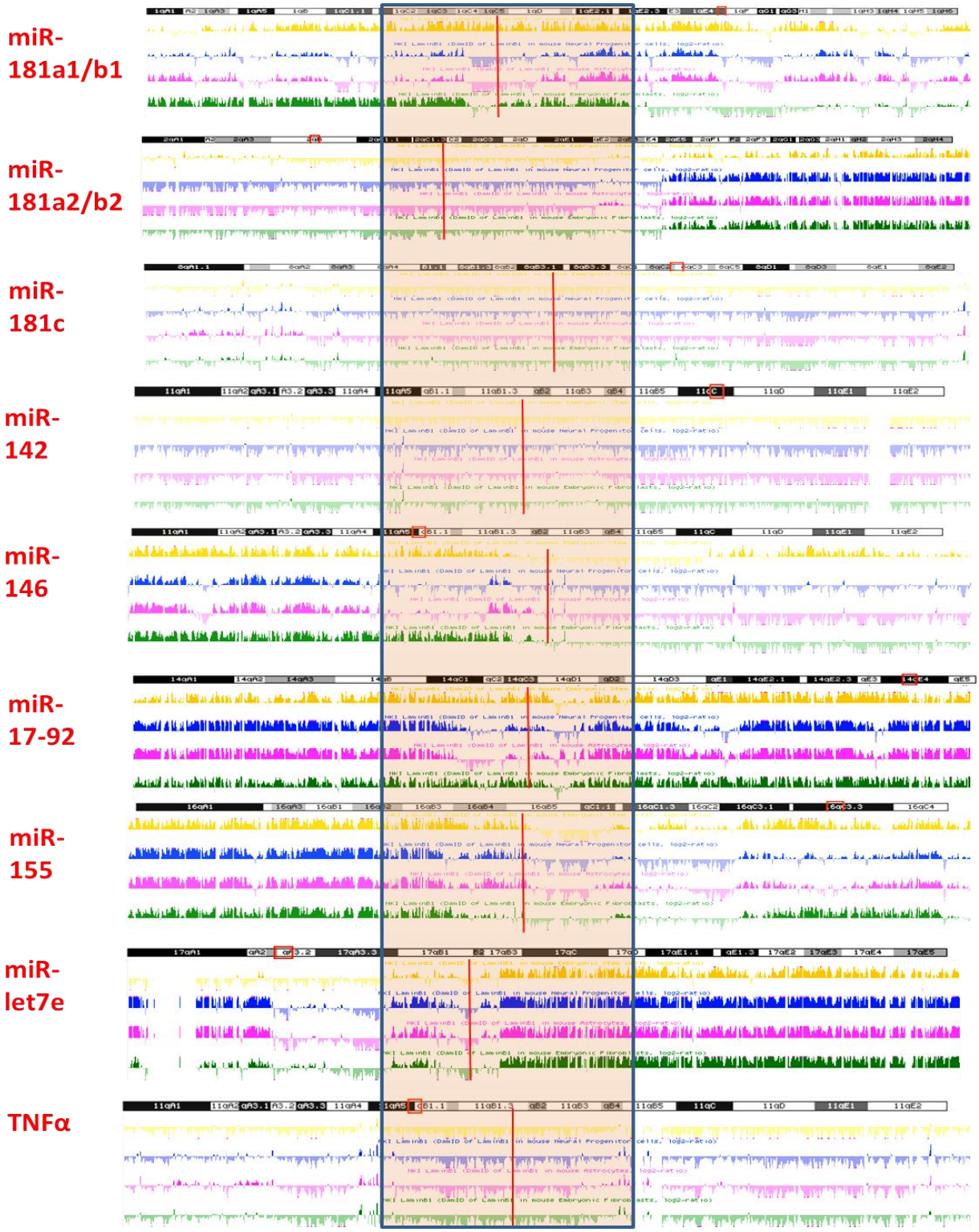

Figure 50. *In silico* analysis of eight microRNA genes and LADs in four distinct cell types: mouse embryonic stem cells (yellow), mouse neuronal progenitor cells (blue), mouse astrocytes (pink) and mouse embryonic fibroblasts (green). An area of 2Mbp was chosen to show the distribution of LADs upstream and downstream of a microRNA gene. The last row depicts the analysis for the *Tnfα* locus.

3.8 Conserved localization of microRNA genes within ciLADs

Based on the previous results, that eight microRNA genes are located within cilADs and considering the fact that LADs are cross species conserved (Meuleman et al. 2013), we next wondered if this tendency of microRNA genes to avoid cLADs is immune specific microRNA-related or it's a random phenomenon. In order to answer this question, we checked for association of all murine microRNA genes with LAD domains. Our analysis revealed that not only the microRNA genes under investigation but almost all murine microRNA genes and coding genes were located within ciLADs domains (**Figure 51**). Subsequently, we questioned whether the observed perinuclear localization of microRNA gene loci reflected their localization in proximity to the borders of ciLADs. Our analysis revealed that *miR-181a2b2*, *miR-17-92*, *miR-155* and *miRlet7e* were localized closer to the ciLAD boundary, whereas *miR-181c*, *miR-142* and *Tnfα* gene loci were localized towards the center of their corresponding domains. When the comparative analysis was scaled up to all the murine microRNA genes annotated in the miRbase, we found that microRNA gene loci did not exhibit a distinct tendency of localization towards either the border or the center of ciLAD/cLAD compartments. microRNA genes located proximal to cLADs were positioned far from the corresponding boundaries, whereas ciLAD-associated microRNA genes were preferentially positioned within the domain, exhibiting a slight preference towards the center of the domain.

Based on these observations we next checked for association of all microRNA with LADs in four different organisms *Homo sapiens, Mus musculus, Drosophila melanogaster and Caenorabditis elegans*. LADs coordinates were taken from the work of the van Steensel laboratory and the coordinates of microRNA genes were taken from the microRNA database, miRBase. A software developed in our laboratory, named LADiMIR (described in the Materials and Methods section) was used to investigate the location of all microRNA genes annotated in the miRBase (until March 2016) in relation to LAD localization, in four different species (*Homo sapiens, Mus musculus, Drosophila melanogaster and Caenorabditis elegans*). (**Figure 52A**)

We found significant depletion of microRNAs in LAD for all studied species with the exception of *C. elegans* were a depletion (Enrichment Value=0.91) was not deemed significant (p-value=0.11). The same trend was found to exist for protein-coding genes, albeit to a lesser extent in all studied species, with enrichment values being <1 but always higher than the corresponding ones for microRNAs. This may indicate an increased tendency for microRNAs to avoid LAD although one cannot discard biases in the definition and

mapping of microRNAs. Interestingly, we observed an even more striking differential enrichment between constitutive and tissue-specific genes for both human and mouse, with constitutive genes strongly avoiding LADs to an extent that surpasses the one of microRNAs.

More specifically, in ***H. sapiens*** we found that from 1881 pre-miR genes annotated in miRBase only 340 are located within cLAD while the rest are located between cLADs (or within ciLADs) (**Figure 53A**). microRNA genes display a tendency to avoid the constitutive LAD domains in *H. sapiens*. Chromosome X displayed the highest number of microRNA genes localized within a cLAD region, (54 out of 118 microRNAs) while chromosome 19, which demonstrates the highest gene density, contains the highest number of microRNA genes outside cLADs. In *H. sapiens*, gene density ranges from around 4-9 genes/Mbp to 24.6 genes/Mbp such as on chromosome 19 (**Figure 53B**). The number of microRNA genes within cLADs generally decreases with increasing gene density and as a result only 19% of microRNA genes lie within cLAD regions in humans. To test whether the two groups, microRNAs within and outside of cLADs, are significantly different, we used Welch's T-test where the t =-7.0884 and $p = 8.7e^{-8}$. Furthermore, Pearson's correlation between microRNA genes within cLADs and gene density and also correlation between microRNA genes outside cLADs and gene density showed that these two groups are significantly different. In *H. sapiens* we noticed a weak negative correlation between gene density and microRNAs lying inside cLADS with an r = -0.2003 and a strong correlation r = 0.711 for microRNAs to be outside (**Figure 53C & 53D**). The number of microRNA genes within cLADs decreased slightly with increased gene density and microRNA genes outside cLADs increased with gene density. Genes within cLAD regions are generally transcriptionally inactive and cLAD–genome interactions are highly conserved, therefore a trend for microRNA genes within cLADs to have a weak linear correlation would not be counterintuitive.

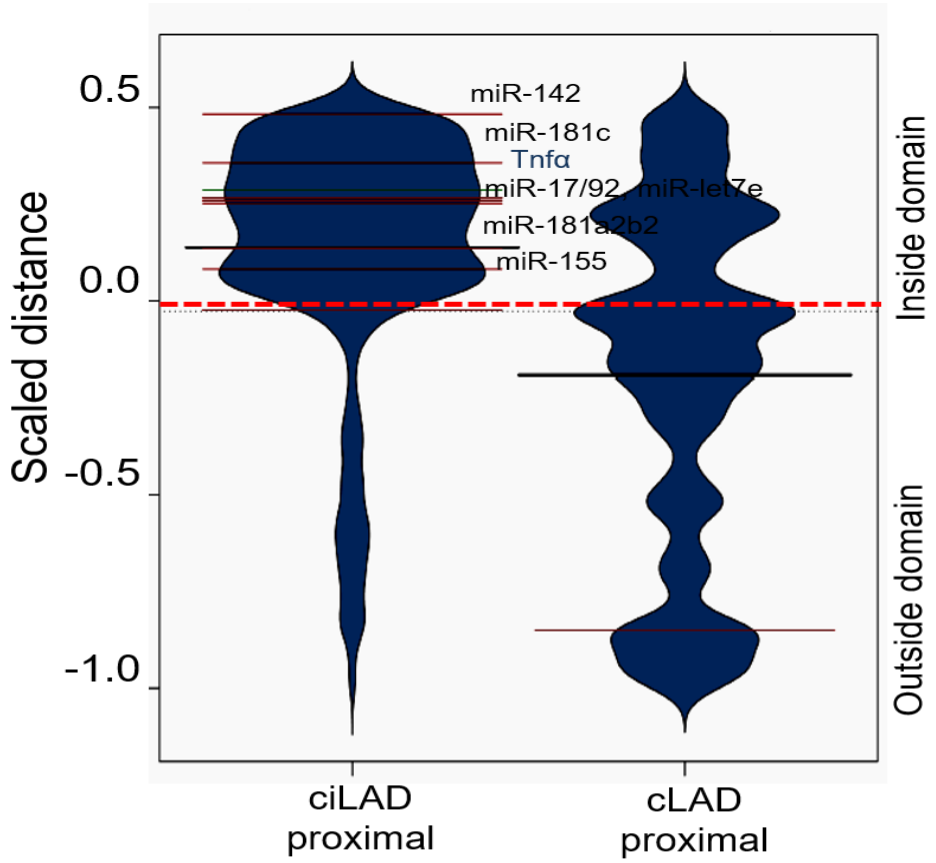

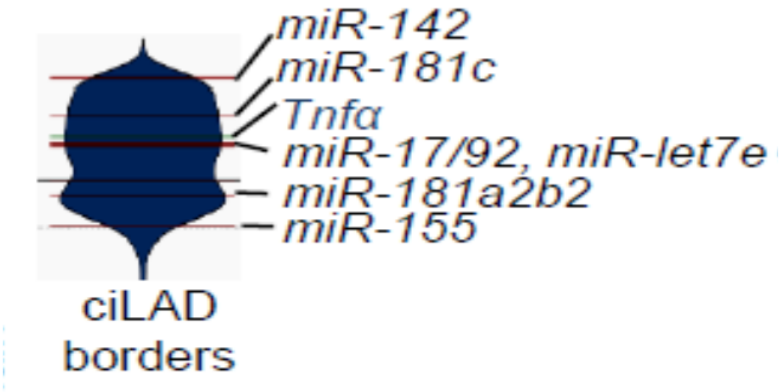

Figure 51. Beanplots portraying the scaled distance distribution of microRNA genomic sequences to their most proximal ciLAD/cLAD regions. Red lines represent the microRNA genes under study, whereas the green line corresponds to TNFα locus. Small but interesting tendencies for the localization of microRNA sequences either towards the centers of ciLADs, or at the cLAD/ciLAD boundaries are observed and recapitulated by the Wilcoxon rank-sum test (pvalue <= 10e-90).

A.

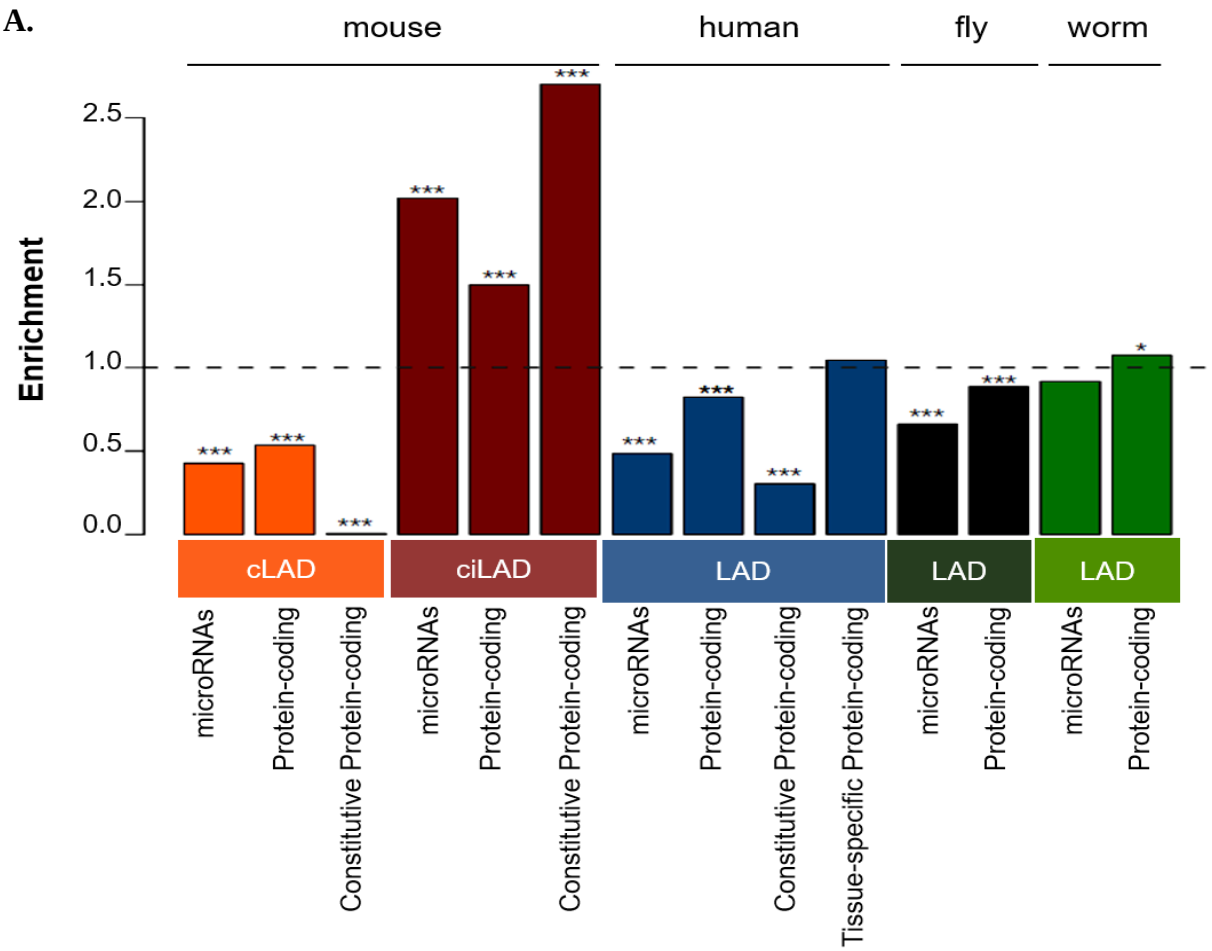

B.

Comparison	Enrichment	p-value
Mouse mir in cLADs	0.427	0.001
Mouse mir in ciLADs	2.020	0.001
Mouse protein Genes in cLADs	0.534	0.001
Mouse protein Genes in ciLADs	1.499	0.001
Mouse constitutive Genes in cLADs	0.002	0.001
Mouse constitutive Genes in ciLADs	2.705	0.001
Human mir in LADs	0.483	0.001
Human protein Genes in LADs	0.825	0.001
Human constitutive Genes in LADs	0.302	0.001
Human tissue-specific Genes in LADs	1.045	0.131
Fly mir in LADs	0.659	0.001
Fly protein Genes in LADs	0.888	0.001
Worm mir in LADs	0.918	0.110
Worm protein Genes in LADs	1.074	0.064

Figure 52. A). Enrichment values of microRNA and protein-coding genes within and outside LAD regions. Permutation *p*-values are depicted as ***:<0.001, **:<0.01 and *:<0.05 respectively, and calculated on the basis of 1000 permutations. B). Enrichment values and significance for miR/protein-coding genes against LAD/iLADs for four different species

For ***M. musculus*** LADiMIR analysis showed that similarly to *H. sapiens*, microRNA genes are located between cLADs. From a total number of 1187 microRNA genes, 1028 resided outside cLADs while 150 microRNA genes were located within cLADs (**Figure 54A**). Therefore, only 14% of the microRNA genes are classified as within cLAD regions and the rest of them are positioned within ciLADs. Interestingly, chromosome 2 displayed an unusually high number of microRNAs inside cLADs. Chromosome 2 contains 78 microRNA genes within cLADs from a total of 147 microRNA genes. Chromosome 2 contains a cluster of microRNAs that spans an area of around 50.000bp. A Welch's T-test was also performed on the data and gave a t score of t=-7.8772 and a $p = 1.67e^{-9}$. Pearson's correlation for microRNAs within cLADs displayed an r = 0.0677, a very weak positive correlation, and for microRNA genes outside of cLADs its r = 0.3193 indicating a weak positive correlation (**Figure 54C & 54D**). Finally, the mouse gene density also presented many similarities with human gene density, although it was slightly higher, averaging 8.4 genes/Mpb as compared to 7.4 genes/Mbp in *H. sapiens* (**Figure 54B**). In conclusion, for the mouse genome, since ciLADs do contain genes that are being expressed at the periphery, this is in agreement with our previous results from DNA FISH experiments showing microRNA genes expressed when located at the nuclear periphery. Since the majority of microRNA genes in *M. musculus* was found within ciLADs we questioned if there were any differences between intergenic and intragenic microRNA gene localization. *In silico* analysis of all intragenic and intergenic microRNA genes revealed that there is a small enrichment of intragenic over intergenic microRNA genes within ciLADs (data not shown). This can be explained by the fact that the same analysis for protein coding genes showed that they are also overrepresented in ciLADs. Although comparing the protein coding genes with microRNA genes there was a small enrichment of microRNA genes within ciLADs, in both cases there was a tendency to avoid cLAD domains (data not shown).

D. melanogaster demonstrated a similar pattern as observed in humans and mice, with only 25% of microRNAs located within cLAD regions (**Figure 55A**). Gene density compared with *H. sapiens* and *M. musculus* was higher with an average of 100 genes/Mpb (**Figure 55B**). In order to check for differences between microRNA genes within and outside cLADs, Welch's T-test was performed and a t-score of -2.756 and a p-value of 0.03323 were obtained. The null hypothesis was rejected suggesting that there is a significant difference between the two groups. Pearson's correlation for microRNA genes within cLADs displayed a very strong positive correlation with an r = 0.6534. Surprisingly microRNA genes outside of cLADs displayed also strong positive correlation with an r r = 0.8269 (**Figure 55C & 55D**). Comparing the Pearson's correlation tests (microRNA genes located within or outside cLADs) between *H. sapiens, M. musculus* and *D. melanogaster*, we notice that only *D. melanogaster* showed a strong correlation. This can

be explained by the size of the genome of *D. melanogaster*, having only six chromosomes with higher gene density when comparing with *H. sapiens* and *M. musculus*.

C. elegans was the only organism that presented a different distribution pattern of cLAD and ciLAD containing microRNA genes, when compared with *H. sapiens, M. musculus* and *D. melanogaster*. In *C. elegans*, 47% of the microRNA genes were located within cLADs (**Figure 56A**). *C. elegans* demonstrated the highest gene density with 200 genes/Mpb, which can be attributed to the genome size of this organism, which has only six chromosomes (**Figure 56B**). Welch's T-test gave a t-score of -0.467 and a p-score of 0.6536, suggesting that there was not a significant difference between microRNA genes within and outside cLADs. A Pearson's correlation test for both groups was strongly negative. microRNA genes within cLADs displayed an r = -0.6094 and microRNA genes outside cLADs displayed an r = -0.4298, suggesting that the number of microRNA genes within and outside cLADs decrease with increased gene density (**Figure 56C & 56D**).

Collectively, from the data obtained for all four organisms, we conclude that *H. sapiens* and *M. musculus* show similar tendency of weak correlation for microRNA genes located within ciLADs and strong for microRNA genes located outside cLADS. On the other hand, *D. melanogaster* and *C. elegans* demonstrate a higher gene density and share the tendency of having strong correlation for microRNA genes within and outside of cLADs, respectively.

Homo sapiens

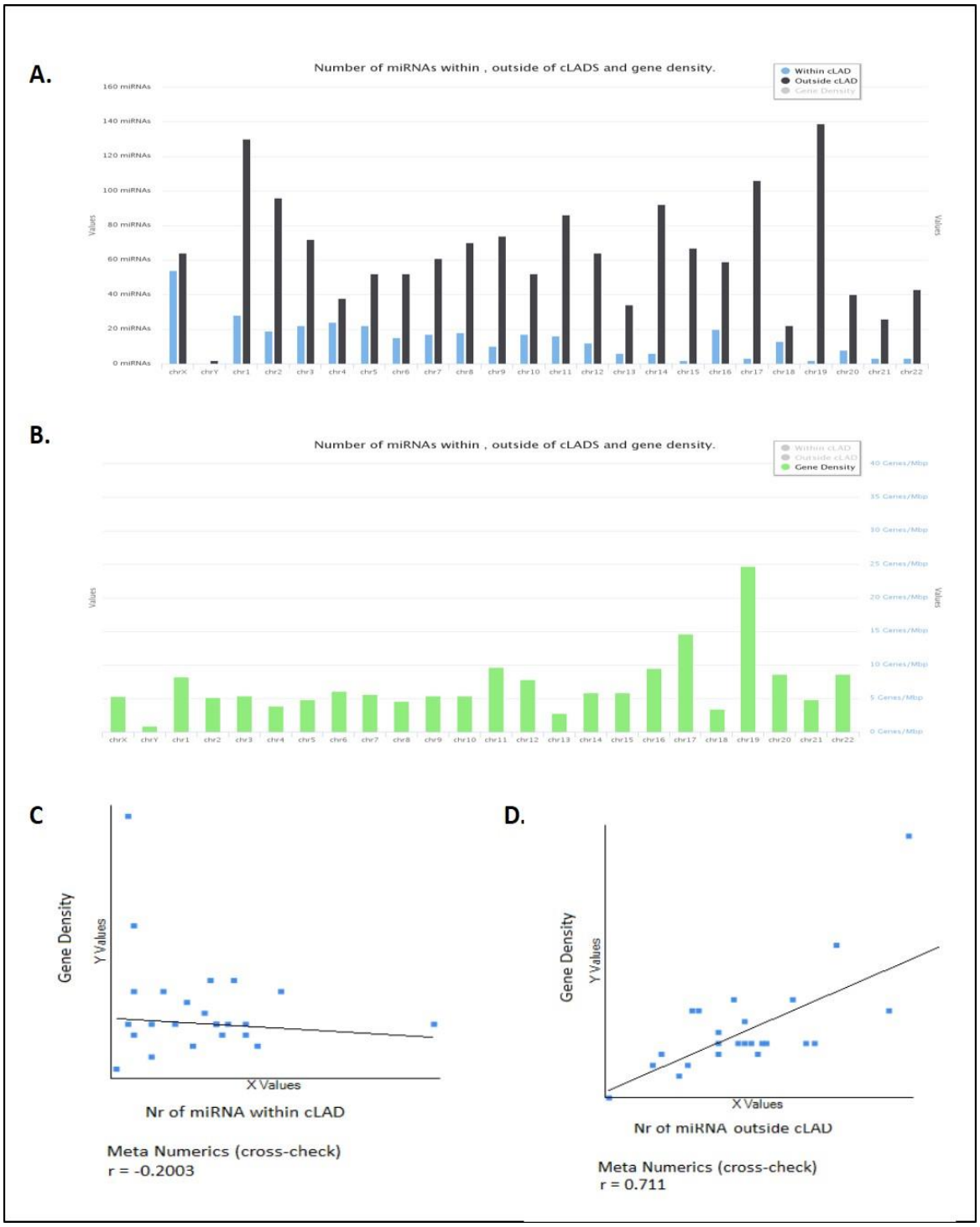

Figure 53. A) Diagram representing the number of microRNA genes located within and outside cLADs in *H. sapiens*. B) Diagram showing the gene density for each chromosome in *H. sapiens*. C) Pearson's correlation between microRNA genes within cLADs and gene density. D) Pearson's correlation between microRNA genes outside cLADs and gene density.

Mus musculus

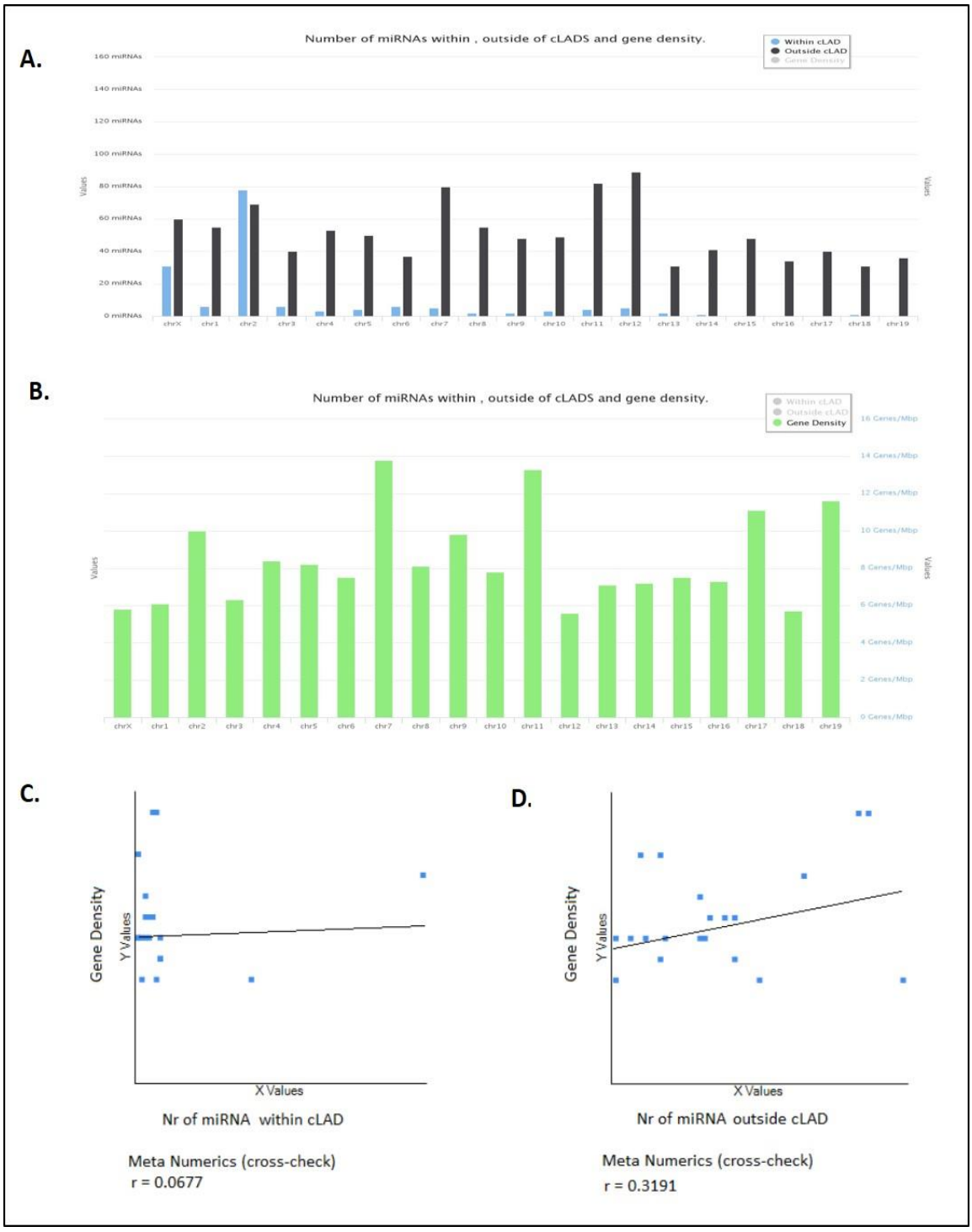

Figure 54. A) Diagram representing the number of microRNA genes within and outside cLADs in *M. musculus* B) Diagram showing the gene density for each chromosome in *M. musculus*. C) Pearson's correlation between microRNA genes within cLADs and gene density. D) Pearson's correlation between microRNA genes outside cLADs and gene density.

D. melanogaster

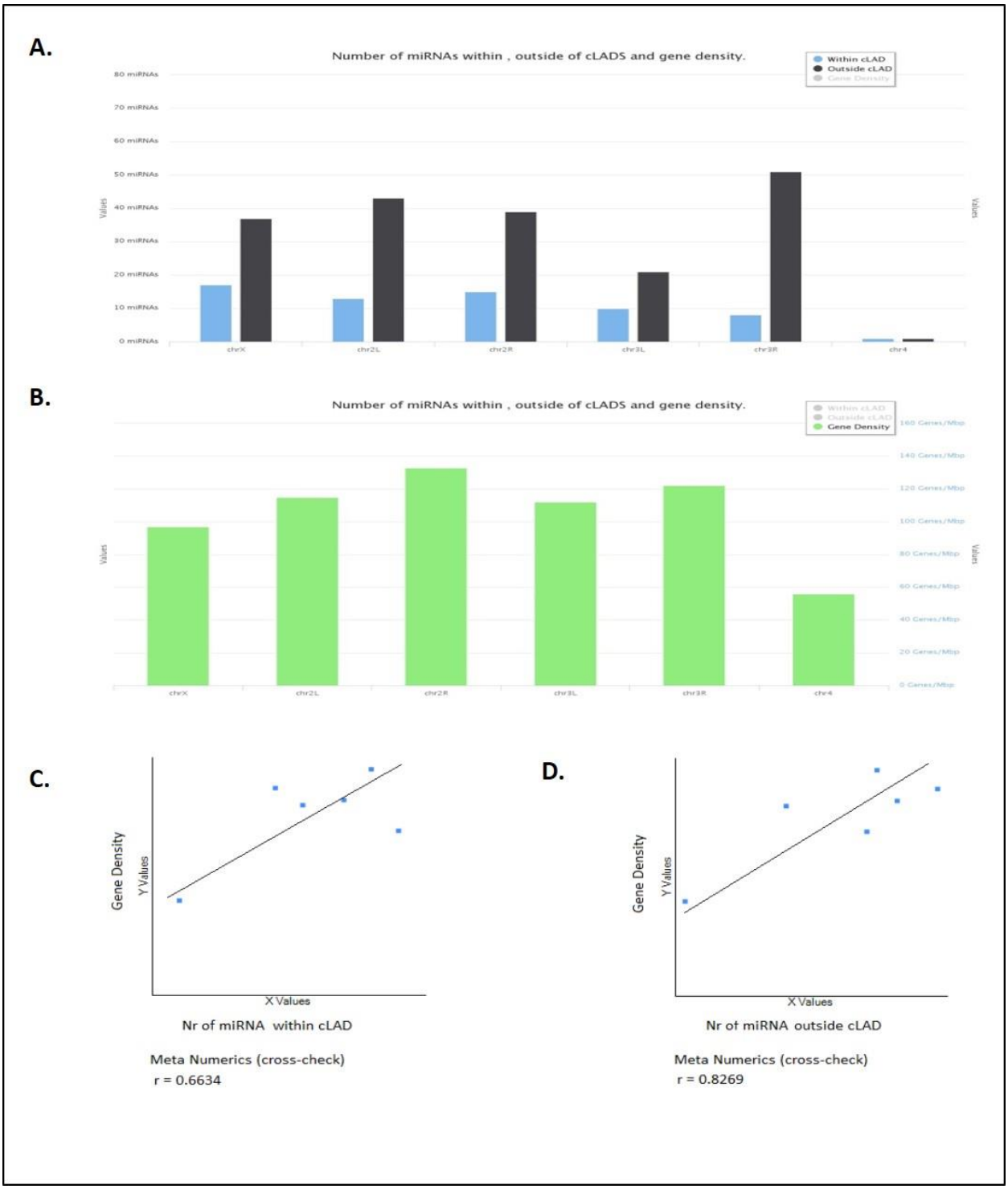

Figure 55. A) Diagram representing the number of microRNA genes within and outside cLADs in *D. melanogaster* B) Diagram showing the gene density for each chromosome in *D. melanoagster*. C) Pearson's correlation between microRNA genes within cLADs and gene density. D) Pearson's correlation between microRNA genes outside cLADs and gene density.

C. elegans

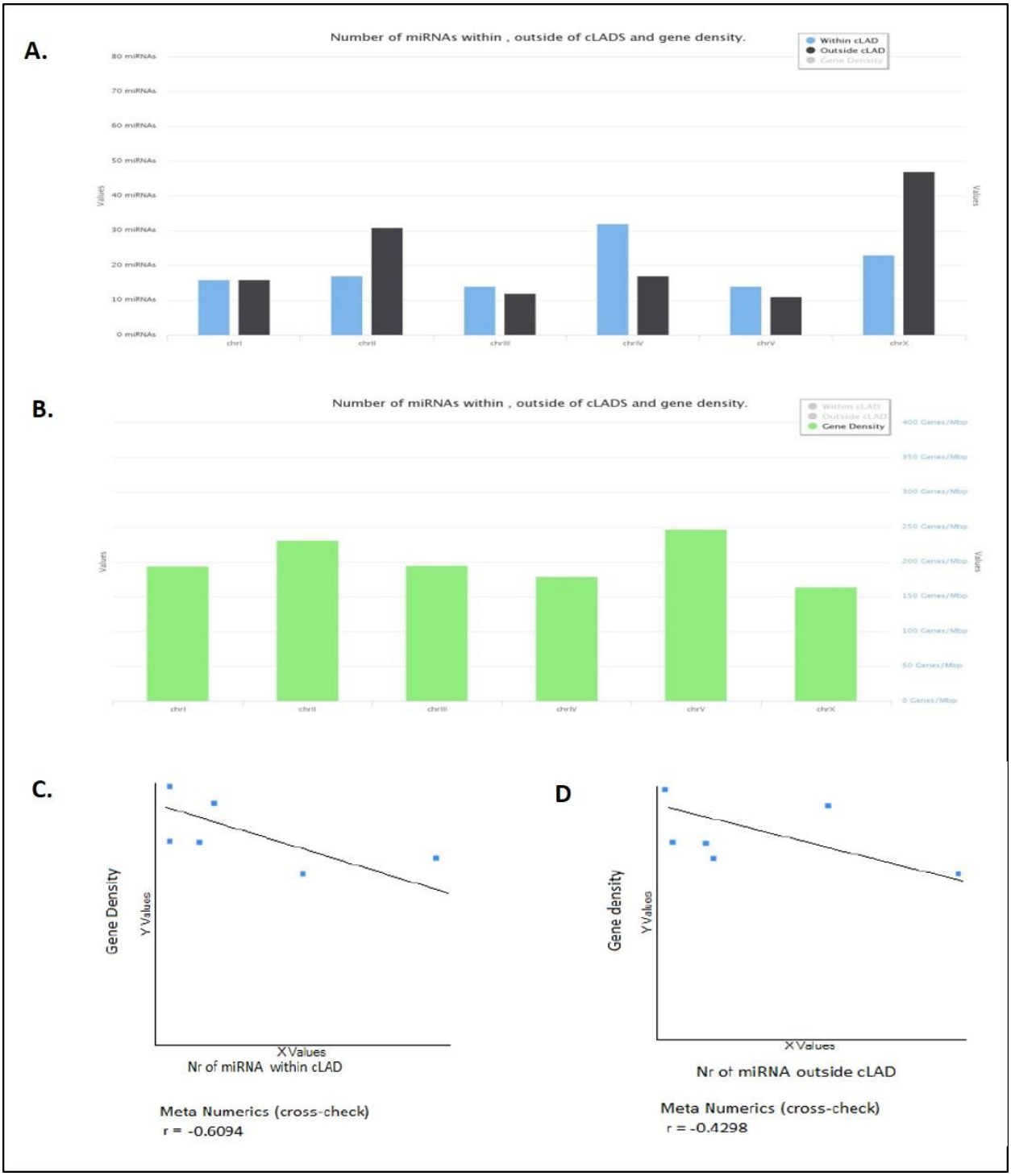

Figure 56. A) Diagram representing the number of microRNA genes within and outside cLADs in *C. elegans* B) Diagram showing the gene density for each chromosome in *C. elegans*. C) Pearson's correlation between microRNA genes within cLADs and gene density. D) Pearson's correlation between microRNA genes outside cLADs and gene density.

3.9 Preferential localization of microRNA genes in respect to their chromosome territories (CTs) in T cells

Chromosome territories (CT) are considered as important nuclear sub-compartments where they can define the position of many genes. Since the microRNA genes under investigation displayed a peripheral localization, we next wondered what could be the relationship of microRNA gene localization to their respective chromosome territories. Therefore we performed 3D DNA FISH experiments for microRNA gene loci in combination with chromosome painting. As previously mentioned, the *Tnfα* and *miR-let7e* gene loci are located on mouse chromosome 17 (CT17). Chromosome painting with DNA FISH experiments on thymocytes and CD4 cells showed that CT17 in thymocytes displays a perinuclear localization. Both CT17 and *miR-let-7e* were located at the periphery of the nucleus (**Figure 57A**). Interestingly, *Tnfα* was looping out of its corresponding chromosome territory and localized to the nuclear interior. These findings are in agreement with our data regarding the localization of the *Tnfα* gene locus to the nuclear interior that we previously demonstrated by 3D-DNA FISH experiments (**Figure 57A**). We next decided to study *miR-146a* which is highly expressed in T cells. *miR-146a* and *TH2* locus (which was used as a control) are both located on chromosome 11. 3D-DNA FISH experiments in thymocytes, for the *TH2* locus demonstrated a more internal nuclear localization pattern when compared with the distribution of *miR-146a* (**Figure 57B & 57C**). When we compared the distribution of alleles from the *TH2* locus with the distribution of *miR-146a* we noticed that the *TH2* alleles displayed a localization preferentially to the nuclear center. The percentage of TH2 alleles located at the nuclear periphery (ND cluster 0.0-0.1) was only 30%, while for *miR-146a* it was 50% of the alleles. The results from 3D DNA FISH experiments combined with chromosome painting (CT11) and double DNA FISH (*TH2* and *miR-146a* gene loci) showed that CT11 displayed a perinuclear localization. Similarly, to CT17, CT11 demonstrated a polarization, where *miR-146α* was located on the external border of CT11 and the *TH2* gene locus alleles were looping out from the chromosome territory to the center of the nucleus (**Figure 57D**).

In conclusion, 3D DNA FISH experiments combined with chromosome painting reconfirmed the perinuclear localization of microRNA genes and further indicated that the whole CT is localized to the nuclear periphery. A polarization of control loci and microRNA genes was observed within the peripheral CT, with the control locus trying to "escape" from the CT (looping out) and placed in more internal clusters and the microRNA gene remaining at the periphery.

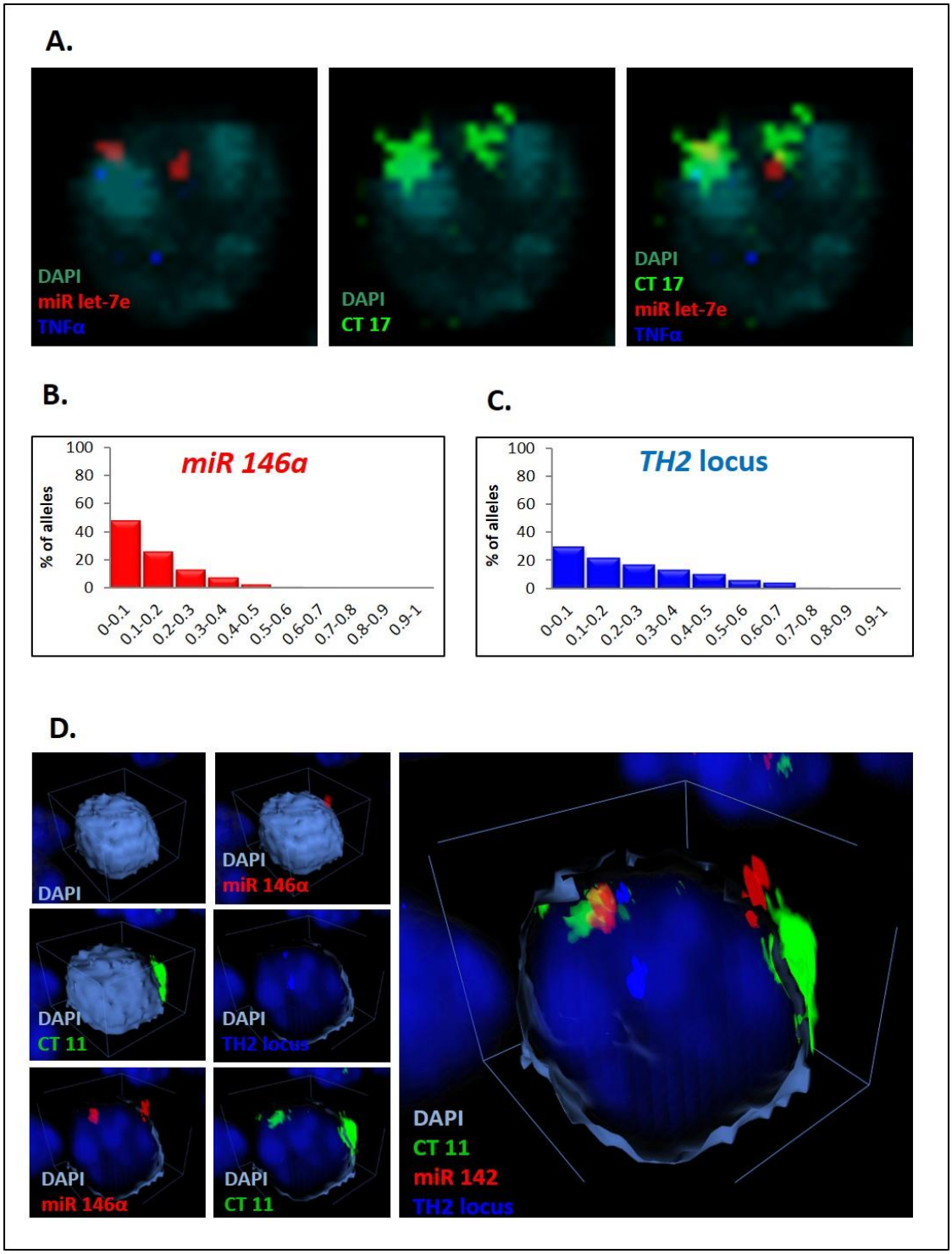

Figure 57. A) Confocal microscopy images of single z-stack sections from 3D DNA FISH experiments combined with chromosome painting in thymocytes. Chromosome painting for CT17 (green), miR let-7e (red), *Tnfα* (blue) and DAPI staining (light blue). B) and C) *miR-146α* and TH2 gene alleles ND values distribution in thymocytes. D) Deconvoluted single z-stack sections of confocal microscopy images from chromosome paints and double DNA FISH (*TH2* locus and *miR-146α*) experiments in thymocytes. Chromosome painting of CT 11 (green), *miR-146α* (red), *TH2* locus (blue) and DAPI staining (light blue).

3.10 Peripheral localization of microRNA genes is independent of transcriptional activity

Since our previous results demonstrated that microRNA genes can be transcribed irrespective of their perinuclear localization, we next wondered if the peripheral localization is related to transcription *per se* and how transcription could affect localization. As mentioned before, T cells have a particular chromatin organization and during development and differentiation a whole shuffling of the chromatin is observed (Kim et al. 2004; Spilianakis et al. 2005; Ktistaki et al. 2010; Rawlings et al. 2011). Although, it is well established in the literature that upon transcriptional activation genes may re/localize at the interior of the nucleus (Chuang et al. 2006; Schneider and Grosschedl 2007; Dillon 2008), this is not a general observation in the case of T cells. During CD4 and CD8 cell development, the whole CT6 is being relocated either to the periphery or the center of the nucleus respectively and transcribed. So the periphery of the nucleus is not necessarily a repressive environment for transcription in CD4 cells. Therefore, we next questioned what would be the effect in microRNA subnuclear localization in T cells if we blocked transcription.

Transcription factories are considered as crucial compartments of the nucleus since they can control nuclear organization by "supervising" the chromatin location for active genes. It is known that inhibition of the initiation of transcription may lead to release of RNA Pol II foci and decrease chromatin associations between active genes (Mitchell and Fraser 2008; Chakalova and Fraser 2010). Controversially, inhibition of elongation of transcription did not affect the proximity between active genes within the transcription factories of RNA Pol II, indicating that absence of transcription does not affect transcription factories (Razin et al. 2007). In order to check whether the eight microRNA genes under study are affected from transcription inhibition, we conducted 3D-DNA FISH experiments in thymocytes, CD4 and T_H2 cells, upon treatment with α-amanitin for 6h. α-amanitin can bind the RNA Pol II enzyme and inhibit transcription. It binds with high specificity and high affinity (K_i = 3–4 nM) near the catalytic active site of RNA Pol II. It establishes a conformation of the enzyme that prevents nucleotide incorporation and translocation of the transcript. The effect of a-amanitin is irreversible because it triggers degradation of Rpb1, the largest RNA Pol II subunit.

Transcription in thymocytes, CD4 cells and T_H2 cells was inhibited after 6 hours of α-amanitin treatment. The efficiency of transcription inhibition was confirmed by both qRT-PCR and RNA FISH for all the cell

types under investigation (**Figure 58B-58C**). Treated and untreated cells were prepared for DNA FISH experiments as described in the Materials and Methods section. microRNA genes that were highly expressed as deduced from our prior RNA-DNA FISH experiments were selected for study from each cell type. 120 cells were analyzed for each cell type. The analysis indicated that in T cells the inhibition of transcription does not affect the microRNA gene allelic distribution (**Figure 58A**).

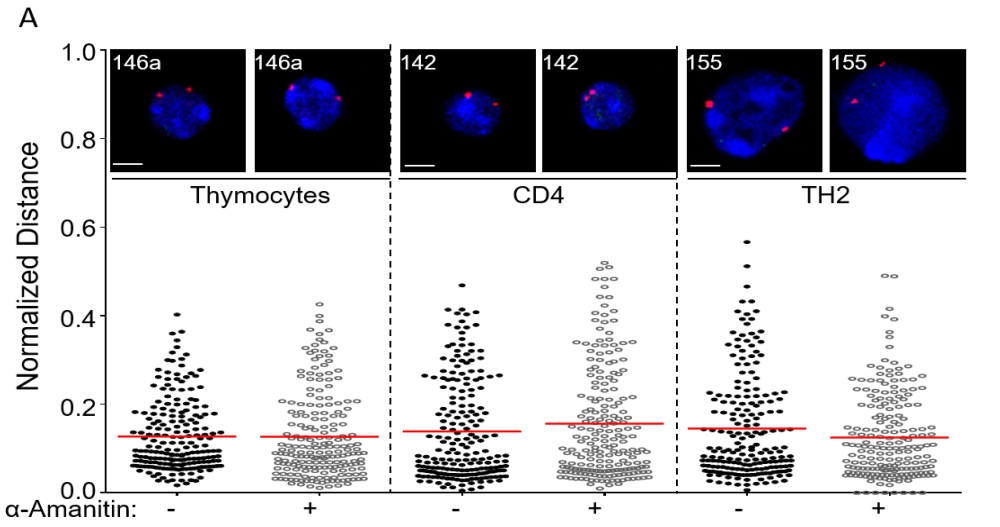

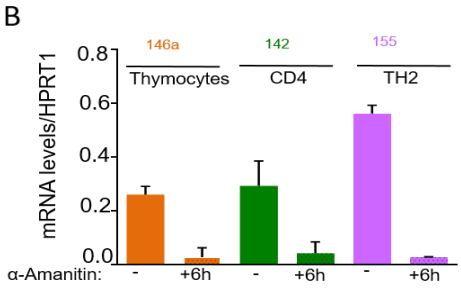

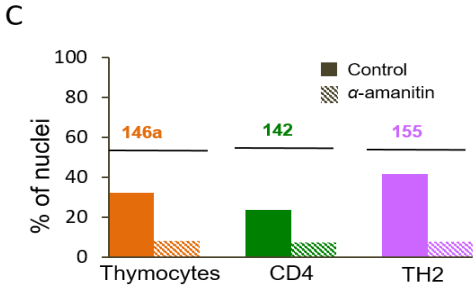

D

	+ 6h α-amanitin	
	D value	*P* value
Thymocytes	0.125	0.081
CD4 cells	0.105	0.208
TH2 cells	0.106	0.196

Figure 58. a-amanitin mediated transcription inhibition in T cells. A) confocal microscopy images from single z-stack sections in thymocytes, CD4 and T_H2 cells (hybridized with miR146a, miR-142 and miR-155 respectively). B) Gene alleles ND values distribution of treated and untreated cells. The red line depicts the median of the distribution for the alleles analyzed. The y-axis depicts the Normalized Distance values of microRNA gene alleles. X-axis: Untreated (-) and α-amanitin treated (+6h) cells for 6 hours.

In thymocytes, inhibition of transcription did not alter the gene allelic distribution of *miR-146a* and 47% of the gene alleles located at the nuclear periphery in untreated cells compared to 51% of the gene alleles

in a-amanitin treated cells. 46% of the alleles for miR-142 in untreated CD4 cells were located at the nuclear periphery (ND= 0.0-0.1) compared to 53% of the gene alleles being perinuclear in α-amanitin treated cells. In T_H2 cells 48% of miR-155 gene alleles were perinuclear in untreated cells compared to 51% in treated cells (**Figure 58A**). Furthermore, Kolmogorov Smirnov (KS) analysis of the normalized distances for each population displayed a non-significant difference before and after *α*-amanitin treatment of cells (KS test: p-value=0.052, 0.122 and 0.390 for thymocytes, CD4 and T_H2 cells for untreated and treated cells respectively) (**Figure 58D**). We also performed the same experiments for a cLAD-located gene [Developmentally-regulated GTP-binding protein 1 (*Drg1*)] in both ES cells and thymocytes. Our results indicated that trancription inhibition did not cause any statistically significant relocalization of *DRG1* alleles towards the nuclear interior in either of the two cell types (**Figure 59A & 59B**)

In conclusion, the *α*-amanitin-dependent inhibition of active transcription did not affect the perinuclear localization of either the ciLAD-located microRNA genes, nor the cLAD-located control coding gene (*Drg1)*.

A

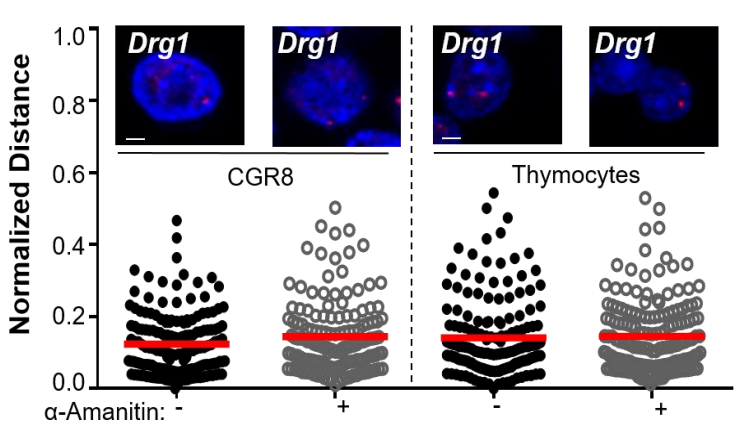

B

	+ 6h α-amanitin	
	D value	*P* value
CGR8	0.152	0.049
Thymocytes	0.095	0.438

Figure 59. Scatter plot indicating the ND distribution of the cLAD localized *Drg1* gene before and after α-amanitin treatment of CGR8 mouse embryonic stem cells and thymocytes. Number of nuclei assessed: CGR8/(-)α-amanitin n=170, CGR8/(+)α-amanitin n=144, thymocytes/(-)α- amanitin n=158, thymocytes/(+)α-amanitin n=164.

3.11 Nuclear lamina is not a repressive environment for the transcription of microRNA genes in T cells

Proteins of the nuclear lamina participate in the regulation of transcription including the direct binding to transcription factors and induction of epigenetic histone modifications (Shaklai et al. 2007; Dechat et al. 2010). In mammals nuclear lamina can act as a repressive environment for the transcription for many genes while in yeast, the nuclear periphery is comprised of at least two sub-compartments, a permissive compartment involving nuclear pore complexes (NPCs) that facilitate gene expression and a repressive compartment consisting of foci of silencing factors and (Reddy et al. 2008).

Our immuno-DNA FISH experiments demonstrated a high frequency of microRNA gene alleles colocalized with LMNB1 in T cells and according to our RNA FISH data we showed that these microRNA genes are transcribed at the nuclear periphery. We next questioned if nuclear lamina could affect the expression of microRNA genes that are colocalized with LMNB1. In order to investigate the repercussions of microRNA gene colocalization with the nuclear lamina and its effect on the allelic microRNA gene expression profile, we performed IF-RNA/ DNA FISH (for the pri-microRNA and the gene locus) and assessed the frequency of micro- RNA gene alleles that were actively expressed and were either colocalized or not with the nuclear lamina, We performed Immuno/RNA-DNA FISH experiments in thymocytes hybridizing with different expressing microRNA genes and staining for LMNB1. More specifically microRNA genes that are expressed in thymocytes were selected: *miR-181a1b1*, *miR-181c*, miR-17-92 and *miR-155*.

Our results indicated that microRNA gene alleles that are colocalized with LMNB1 are also transcribed as shown in **Figure 60B**. *miR-181a1b1*, *miR-181c*, and *miR-17-92* which are highly expressed in thymocytes and *miR-155* which demonstrated a lower expression (as indicated previously by qPCR and RNA FISH experiments) didn't show any significant differences of the expressing alleles colocalized with LMNB1 (**Figure 60A**). In four microRNA genes studied there was no tendency of expressing alleles to avoid or prefer the nuclear lamina (LMNB1). Moreover, we repeated the same experiment with 2 other microRNA genes (data not shown) and the results were similar. Almost, 50% of the expressing alleles tend to be colocalized with LMNB1. The latter was also confirmed by the fact that we did not detect any differences between expressing and not expressing alleles by analyzing the distance from the nuclear periphery in all cell types **(Figure 61).** Our analysis showed that there is not a tendency of the expressing alleles to relocate to more internal or the non-expressing alleles relocating to more external nuclear areas or *vice versa*. The same results were obtained for undifferentiated and differentiated cells (**Figure 61**). Furthermore, in T_H1

and T_H2 cells, where microRNA genes are highly transcribed, there were no differences between the distribution of expressing or not expressing alleles in relation to the nuclear periphery. Small differences were observed but not statistically significant.

In conclusion, despite the fact that most mammalian genes found at the periphery are not transcriptionally active, nuclear lamina is not a repressive environment for eight microRNA genes in T cells.

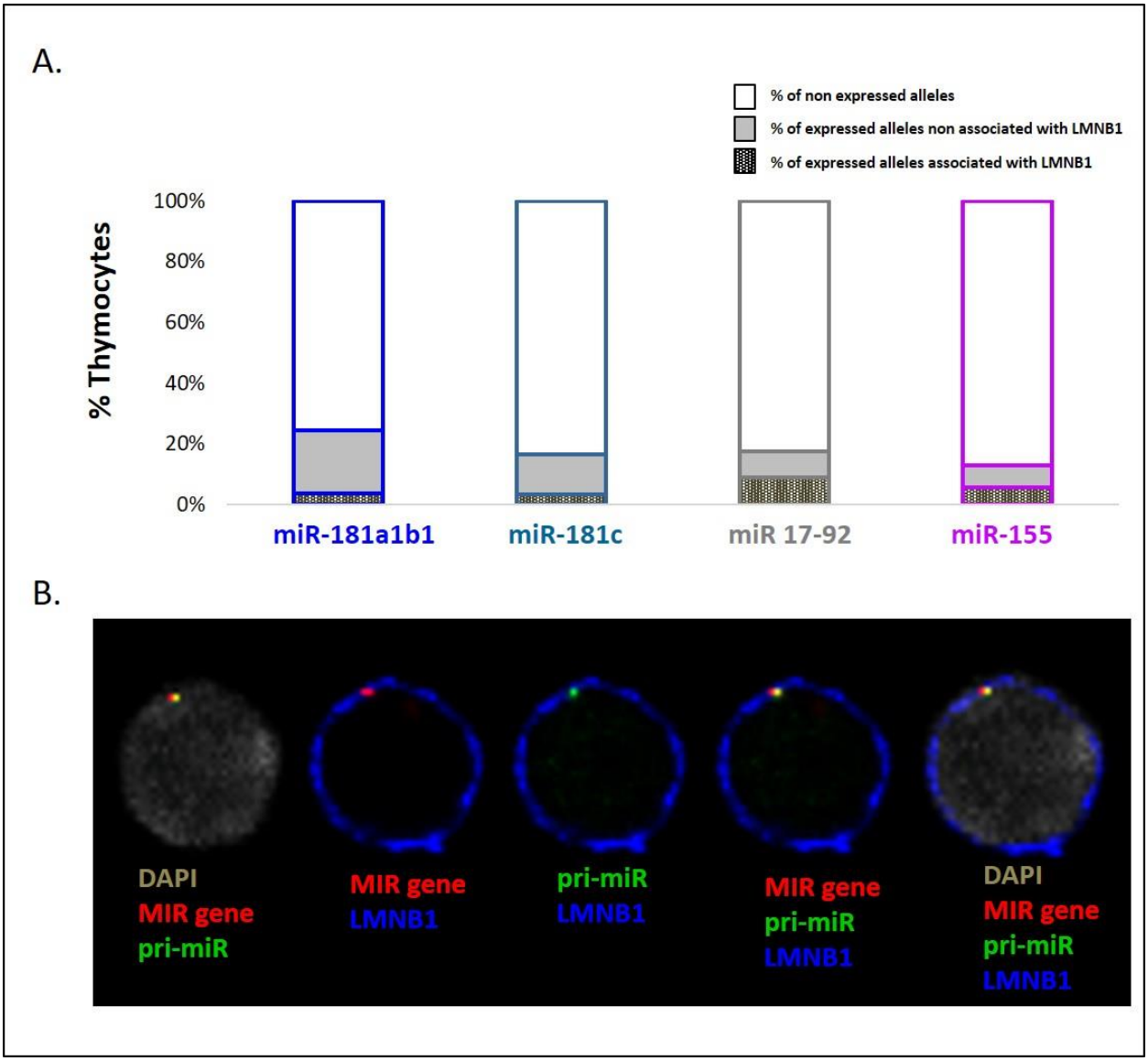

Figure 60. A) Diagram depicting the percentage of expressed microRNA gene alleles colocalized with LMNB1 in thymocytes. Number of nuclei assessed: thymocytes n = 705, Scale bar 2µm.B) Confocal Single z-stack microscopy images from Immuno/RNA-DNA FISH experiments displaying the colocalization of expressed (green) microRNA gene alleles (red) with Lamin-B1 in thymocytes. microRNA genes (red), pri-miR RNA (green), LMNB1 (blue) and DAPI staining (grey).

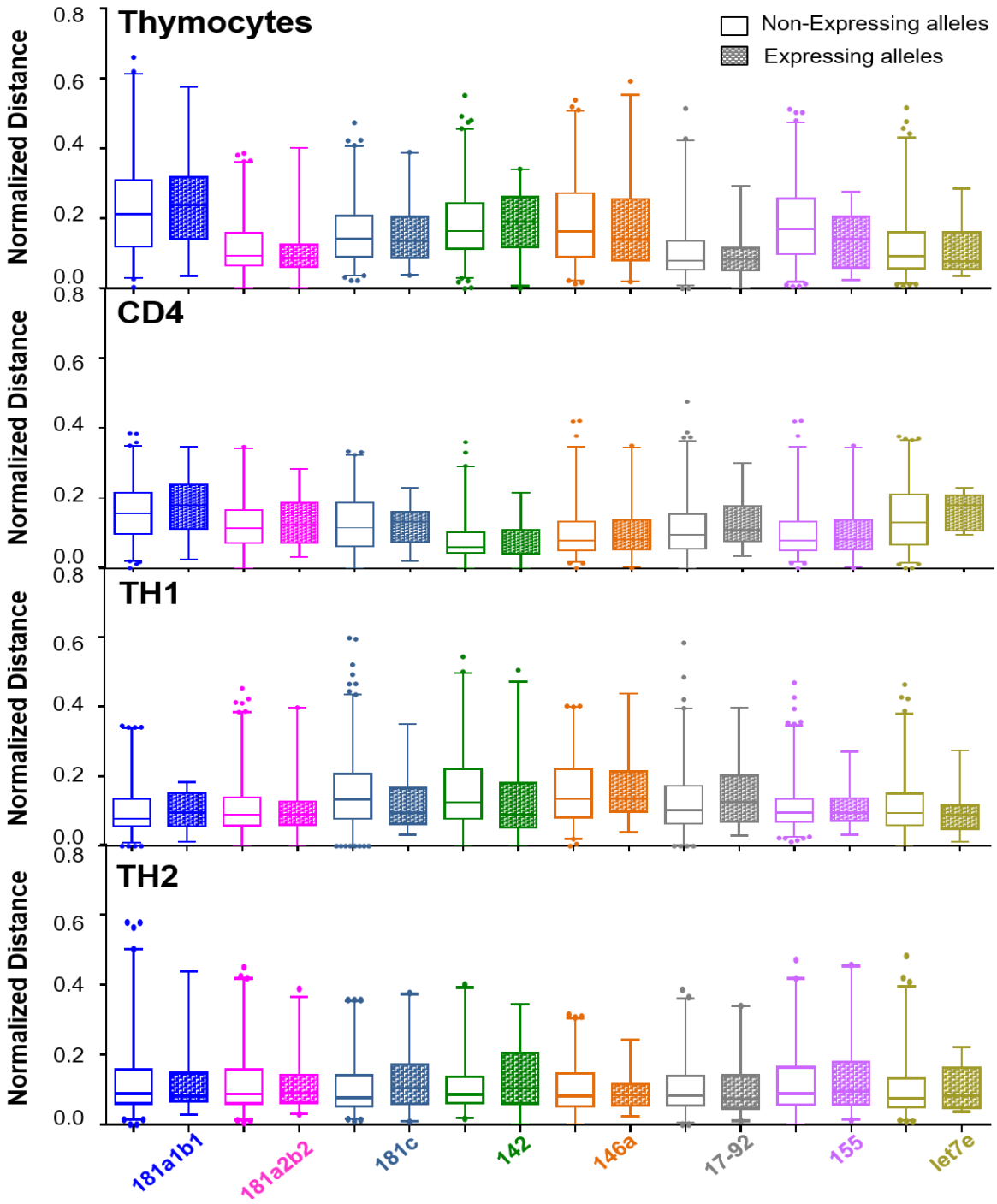

Figure 61. Distribution of non-expressing and expressing gene allele ND values. The normalized distances (y-axis) indicated in each box plot for each microRNA gene are characterized by their median. 95% of the ND values are included within the whiskers of each box plot, whereas single allele outliers (remaining 5% of total NDs) are indicated in the vicinity outside the whiskersFor each microRNA gene, the filled box represents the ND values distribution of expressed microRNA gene alleles while the empty box refers to the non-expressing alleles. For all distributions miR let-7e was used as a control since it is not expressed in T cells. Total number of alleles analyzed for each dataset were n=623, n=807, n=497, n=472 for thymocytes, CD4+, TH1 and TH2 cells, respectively

3.12 Peripheral localization of the Microprocessor complex

DROSHA, apart from being part of the microRNA biogenesis pathway, can also have noncanonical functions, such as acting as a transcription factor for protein-coding genes (Burger and Gullerova 2015; Kim et al. 2017; Pong and Gullerova 2018). Previous reports have corroborated DROSHA binding to both coding gene promoters and pre-microRNA flanking sequences during transcriptional activation of human genes via direct interaction with the phosphorylated form of RNA Polymerase II (Morlando et al. 2008). Chip-on-chip experiments have reported that DROSHA binds promoters of coding genes via direct interaction with the phosphorylated form of RNA Polymerase II (p=Pol II) (Gromak et al. 2013). DROSHA binds on the transcription start site (TSS) of several human genes (160 coding genes) by interacting with RNA Pol II CTD in a transcription dependent manner. Based on these findings, we next questioned whether the peripheral localization of microRNA genes was Microprocessor-dependent. Firstly, we studied the expression of DROSHA protein complexes by means of Western blot and IF assays in several cell types (ESCs, thymocytes, $CD4^+$, TH1 and TH2). Interestingly, we noticed that in thymocytes, DROSHA presented a peripheral localization with a specific speckled structure. Next, we calculated the frequency of cells depicting a perinuclear distribution of DROSHA in murine ESCs, thymocytes, $CD4^+$, T_H1 and T_H2 cells (**Figure 62A - 62E**). Cells were analyzed with the use of Volocity software and the nuclear periphery was defined as the edge of DNA staining with DAPI. The distribution of DROSHA protein complexes was perinuclear in all cell types examined. More specifically, ESCs, thymocytes and $CD4^+$ cells demonstrated more than 55% of DROSHA foci located at the nuclear periphery (ND clusters 0.0-0.1). While in differentiated T_H1 and T_H2 cells the percentage of DROSHA signals located at the nuclear periphery increased to ~70% (**Figure 62I**). This peripherization of DROSHA upon differentiation was similar to the kinetics that microRNA gene loci displayed in T cells. The same pattern and perinuclear localization was observed for the Microprocessor protein DGCR8, while co-immunofluorescence (co-IF) experiments for DROSHA and LMNB1 reconfirmed the perinuclear localization with the two proteins colocalized (**Figure 62G & 62H**) We next investigated whether peripheral DROSHA was colocalized with active chromatin at the nuclear lamina, serving as a possible mechanism controlling gene expression at the nuclear periphery. Our immunofluorescence experiments in thymocytes supported the colocalization between the perinuclear DROSHA protein complexes and active RNA Polymerase II foci (**Figure 62J**).

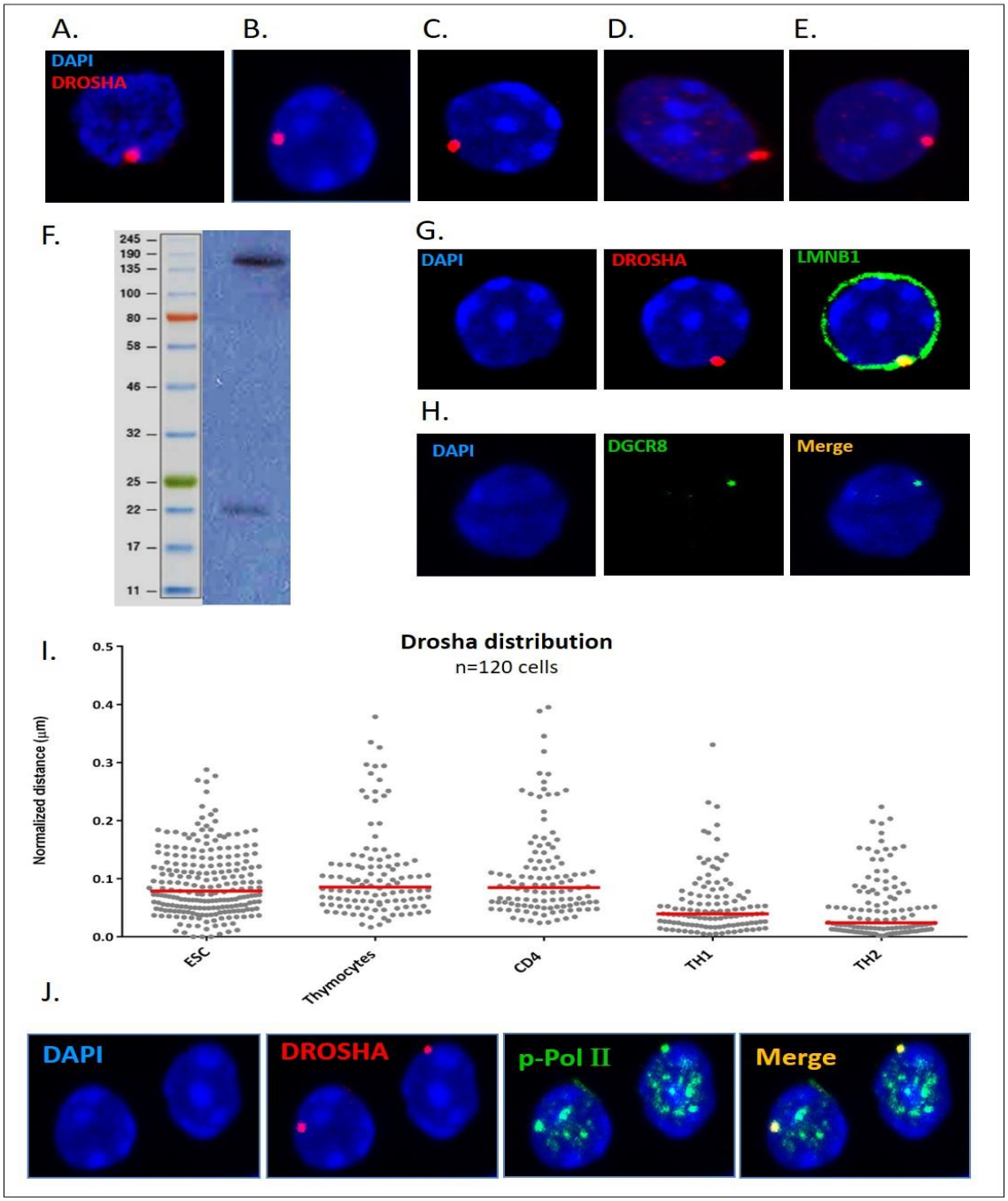

Figure 62. Perinuclear localization of DROSHA and colocalization of the microprocessor complex with active chromatin. Single z-stack sections of confocal microscopy images from IF experiments of DROSHA staining in A) ESCs, B) thymocytes, C) CD4, D) TH1 and E) TH2 cells. DROSHA (red), DAPI (blue). F) DROSHA protein expression in thymocytes. I) ND of DROSHA foci from the nuclear periphery normalized with the nuclear radius. Scatter plot for the ND distribution of DROSHA foci from the nuclear periphery in ESC, thymocytes, $CD4^+$, TH1 and TH2 cells. The red line depicts the median of the alleles analyzed. For every cell type 120 cells were analyzed with the Volocity software. J) Immunofluorescence assay displaying the colocalization of DROSHA foci with phosphorylated RNA Pol II in thymocytes. DROSHA (red), p-Pol II (green), DAPI (blue).

Since eight microRNA gene loci and DROSHA foci displayed a perinuclear localization in T cells and the DROSHA/DGCR8 protein complex binds on TSSs of human intragenic *miR-330* (Gromak et al. 2013), we next questioned whether DROSHA binds on the TSSs of the microRNA genes under investigation. To answer this, we performed DROSHA ChIP-seq experiments in thymocytes and murine thioglycolate elicited peritoneal macrophages (TEPMs). Two separate ChIP-seq experiments were performed and the analysis indicated low binding of DROSHA on chromatin. Both cell types displayed only a few DNA binding sites (75 peaks for thymocytes and 84 peaks for TEPMS) (**Figure 63**).

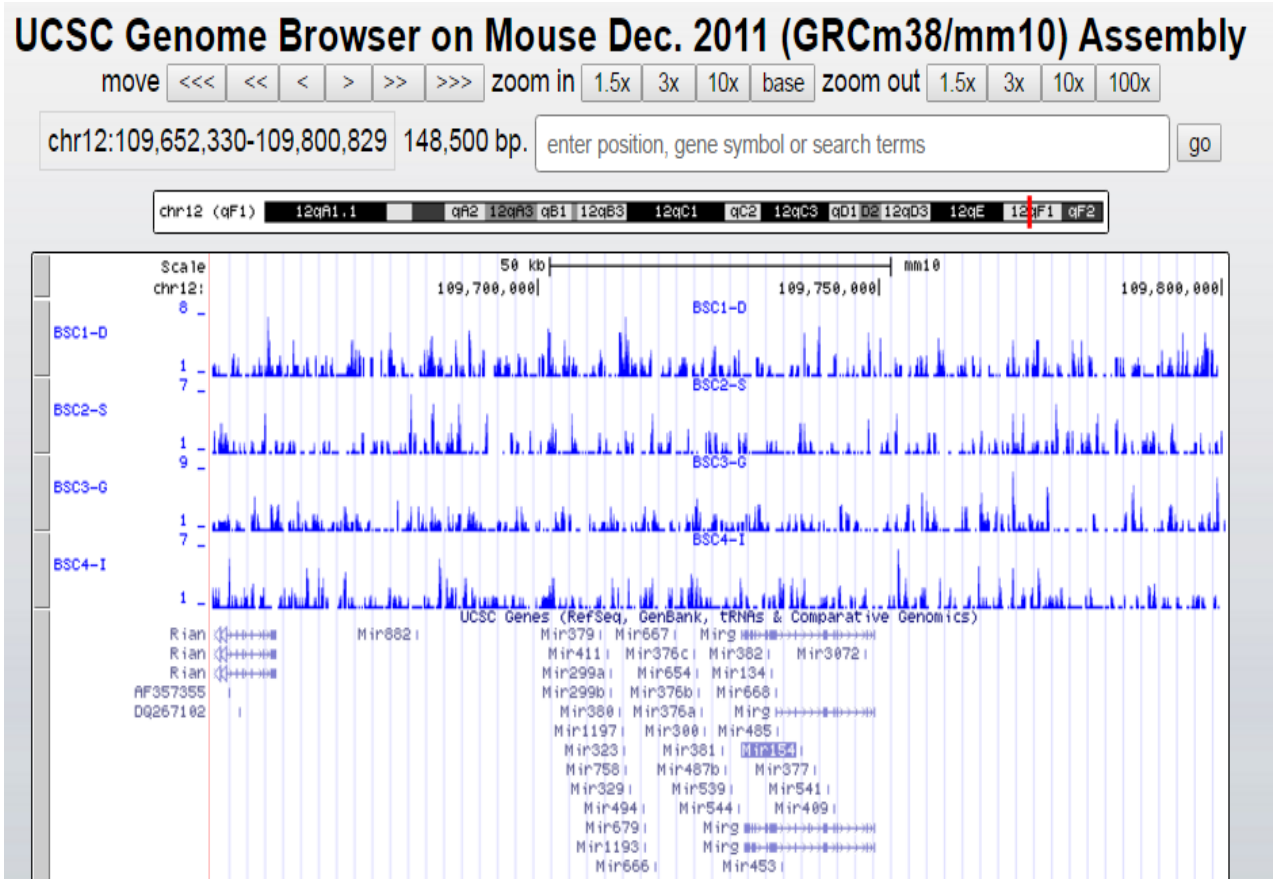

Figure 63. Results from DROSHA ChIP-seq experiments in thymocytes. Depiction of DROSHA bindings on microRNA cluster that are located on murine chromosome 12. The first row shows the binding of DROSHA in the chromatin while the third and the fourth lines represent the IgG control and the input respectively.

Since our previous results could not attribute the peripheral positioning of microRNA gene loci to DROSHA protein, we investigated the implication of DGCR8 protein in the perinuclear localization of microRNA gene loci. As previously reported both DROSHA and DGCR8 form the microprocessor complex which acts co-transcriptionally to cleave pri-microRNAs during transcription (Morlando et al. 2008; Gromak et al. 2013; Nojima et al. 2015). Published DGCR8 ChIP-sequencing experiments demonstrated enrichment of DGCR8 binding in microRNA gene-associated super-enhancers (Suzuki et al. 2017). To this end, we performed an aggregate score analysis of the aforementioned publicly available datasets (GEO number and details are provided in the corresponding Supplemental information section) and uncovered a subtle yet significant enrichment of DGCR8 binding on microRNA gene loci compared to coding genes (**Figure 64**). These results suggest that peripheral positioning of microRNA gene loci might be linked to the Microprocessor complex in a DGCR8-dependent manner.

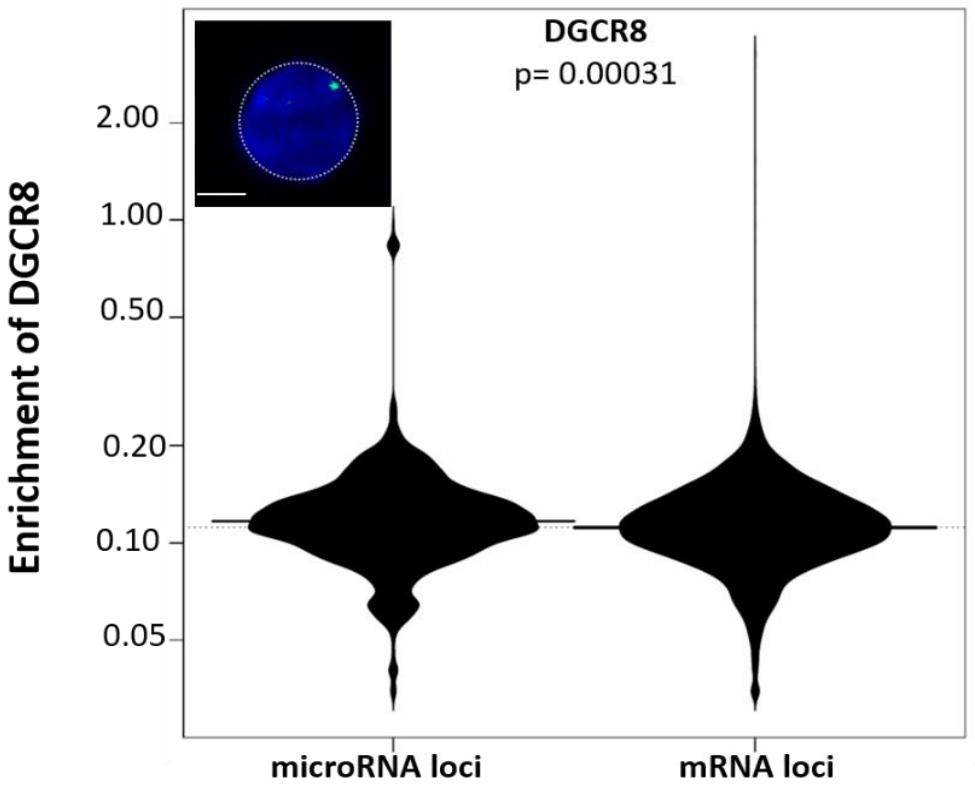

Figure 64. Confocal microscopy images from IF experiments for DROSHA (red) and DGCR8 (green) proteins in thymocytes (DNA counterstained blue). Single z-stack sections of confocal microscopy images from IF experiments of DROSHA staining in A) ESCs, B) thymocytes, C) CD4, D) TH1 and E) TH2 cells. DROSHA (red), DAPI (blue). F) DROSHA protein expression in thymocytes. I) Distribution of ND values for DROSHA foci in ESCs, thymocytes, CD4, T_H1 and T_H2 cells from IF experiments. The red line depicts the median of the alleles analyzed. For every cell type 120 cells were analyzed with the Volocity software. J) Single z-stack sections of confocal microscopy images from co-IF experiments of DROSHA and p-Pol II in thymocytes. DROSHA (red), p-Pol II (green), DAPI (blue).

3.13 Ablation of the BACH1 transcriptional regulator does not affect the expression or peripheral localization of microRNA genes

Cell type specific transcription factors may be implicated in gene positioning and spatial chromatin organization (Levantini et al. 2011; Hao et al. 2015; Shachar et al. 2015). BACH1 is a transcription factor highly expressed in the bone marrow and was characterized as an architectural transcription factor mediating chromatin interactions among Maf recognition elements-MAREs (Igarashi et al. 1998). Additionally, *Bach1* deletion has a significant impact on lymphoid- and myeloid-mediated inflammatory responses (So et al. 2012) and its binding is enriched on microRNA gene promoters (Jeong et al. 2016). To investigate whether the ablation of BACH1 could affect either the subnuclear localization, or the allelic expression profile of microRNA genes, we performed DNA FISH experiments in both wild type (wt) and *Bach1-/-* thymocytes and analyzed the subnuclear distribution of *miR-155* gene alleles, which we previously found to localize in the nuclear periphery. Our analysis in *Bach1-/-* reconfirmed the peripheral localization of *miR-155* and *miR-146a* gene alleles in thymocytes that was not statistically different between wild type (wt) and *Bach1-/-* cells (**Figure 65A-D**).

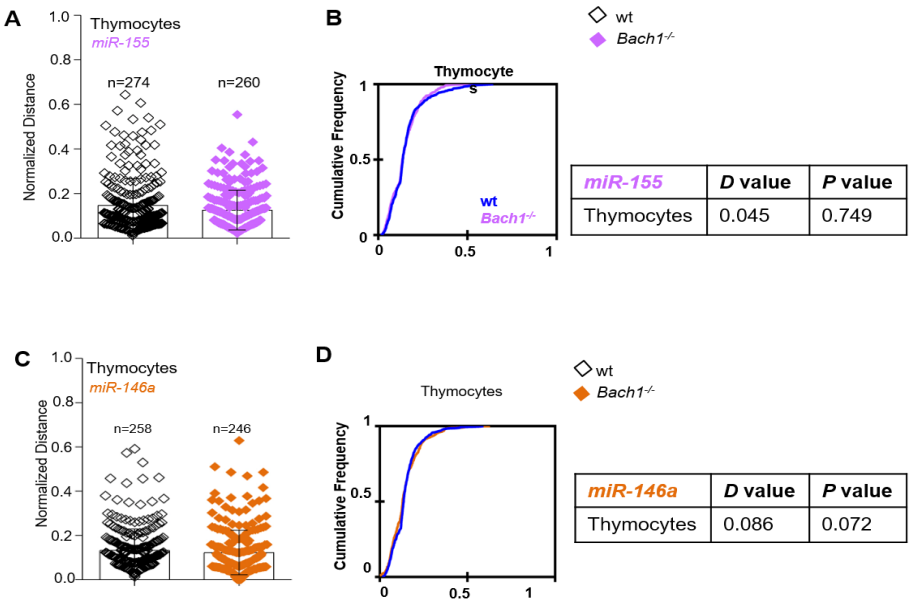

miR-155	*D* value	*P* value
Thymocytes	0.045	0.749

miR-146a	*D* value	*P* value
Thymocytes	0.086	0.072

Figure 65. A) *miR-155* gene alleles distribution in wild type (wt) and *Bach1-/-* thymocytes. (B) Cumulative frequency graphs and KS-test for the comparison of *miR-155* gene alleles distribution in wt versus *Bach1-/-* thymocytes (C) *miR-146α* gene alleles distribution in wt and *Bach1-/-* thymocytes. (D) Cumulative frequency graphs of *miR-146α* gene alleles NDs in wt and *Bach1-/-* thymocytes. KS-test analysis results are portrayed on the table.

3.14 The genome organizer SATB1 affects the localization of microRNA genes

SATB1 is a cell-type specific 'genome organizer' responsible for chromatin organization and gene positioning in T cells. The SATB1 subnuclear localization displays a particular pattern in thymocytes, forming an aromatic ring or "cage-like" structure surrounding heterochromatin (**Figure 66A**). As an important regulator of nuclear architecture, that anchors specialized DNA sequences onto its cage-like network, SATB1 recruits chromatin remodeling/modifying protein complexes to control gene transcription. Since chromatin architecture is believed to be an important regulator of gene activation or silencing, we next questioned if the perinuclear localization of the eight microRNA gene loci under study is SATB1-dependent in T cells.

To examine if SATB1 affected the perinuclear positioning of microRNA genes we generated a knockout mouse model in which the second exon of the SATB1 gene was conditionally deleted in $CD4^+$ cells. More specifically, the SATB1 conditional knockout (cKO) mouse was created by crossing the *Satb1* floxed allele (*Satb1*$^{fl/fl}$ mice) with transgenic mice expressing the Cre recombinase under the control of the CD4 gene promoter. As in the case of *Satb1* null mice, *Satb1* cKO mice demonstrated severe impairment of thymocytes development. Interestingly, the number of thymocytes and the peripheral CD4 cells in the *Satb1* cKO mouse was reduced when compared to wild type littermates. Moreover, the differentiation of $CD4^+$ cells to T_H1 and T_H2 cells was impaired and the expression of signature cytokine genes was deregulated. *Satb1* cKO-derived CD4 cells displayed a 4-fold increase of *Ifnγ* mRNA expression and 8.5-fold increase of *Il4* expression when compared to WT CD4 cells (**Figure 66B & 66C**). Expression of both *Ifnγ* and *Il4* genes was impaired in differentiated cells (2-fold decrease of *Ifnγ* mRNA expression in T_H1 cells and 7-fold decrease of *Il4* gene expression in T_H2 cells).

Since the differentiation of CD4 cells onto the T_H1 and T_H2 cell lineages was defective, we performed DNA FISH experiments only in thymocytes and $CD4^+$ cells of WT and *Satb1* cKO. DNA FISH experiments in *Satb1* cKO thymocytes demonstrated a differential subnuclear positioning of most microRNA gene loci that are under investigation. *miR-181a2b2* gene alleles were relocated toward the interior of the nucleus, while *miR-181c*, *miR-142*, *miR-146a*, *miR-155* and *miR-let-7e* gene alleles were relocated towards the nuclear periphery. The alleles of *miR-181a1b1* did not display any relocalization in the absence of SATB1 protein. The control *Tnfα* gene locus displayed a minor relocalization towards the nuclear interior (**Figure 67A**). The differences detected in gene locus positioning observed for the microRNA and the control *Tnfα* gene

loci in *Satb1* cKO compared to wt cells is statistically significant ($p<0.05$) (**Figure 67B**). On the contrary, in $CD4^+$ cells, four microRNA genes, *miR-181a1b1*, *miR-181a2b2*, *miR-17-92* and *miR-155* did not display any relocalization in the absence of SATB1 protein. *miR-181c* and *miR-142* were relocated towards the nuclear interior while *miR-146a* and *miR-let-7e* were relocated towards the nuclear periphery. Interestingly, the control *Tnfα* locus was relocalized towards the nuclear periphery (**Figure 67C**). Furthermore, the aforementioned repositioning of all gene loci observed in *Satb1* cKO mice compared to wt was statistically significant (**Figure 67D**).

Data obtained from transmission electron microscopy (TEM) experiments for WT and *Satb1* cKO thymocytes demonstrated that in the absence of SATB1 the compartmentalization of heterochromatin and euchromatin is disturbed. Moreover, in the absence of SATB1, we observed relocalization of euchromatin towards the nuclear periphery, loss of the perinuclear heterochromatin and a dispersed pattern of heterochromatin within the nucleus (**Figure 67E & 67F**).

In conclusion, genetic ablation of SATB1 causes deregulation of the chromatin in T cells, and also affects the cytokine expression and the in vitro differentiation of $CD4^+$ cells. Moreover, the absence of SATB1 led to repositioning of all microRNA gene loci under investigation and the control locus *Tnfα.*

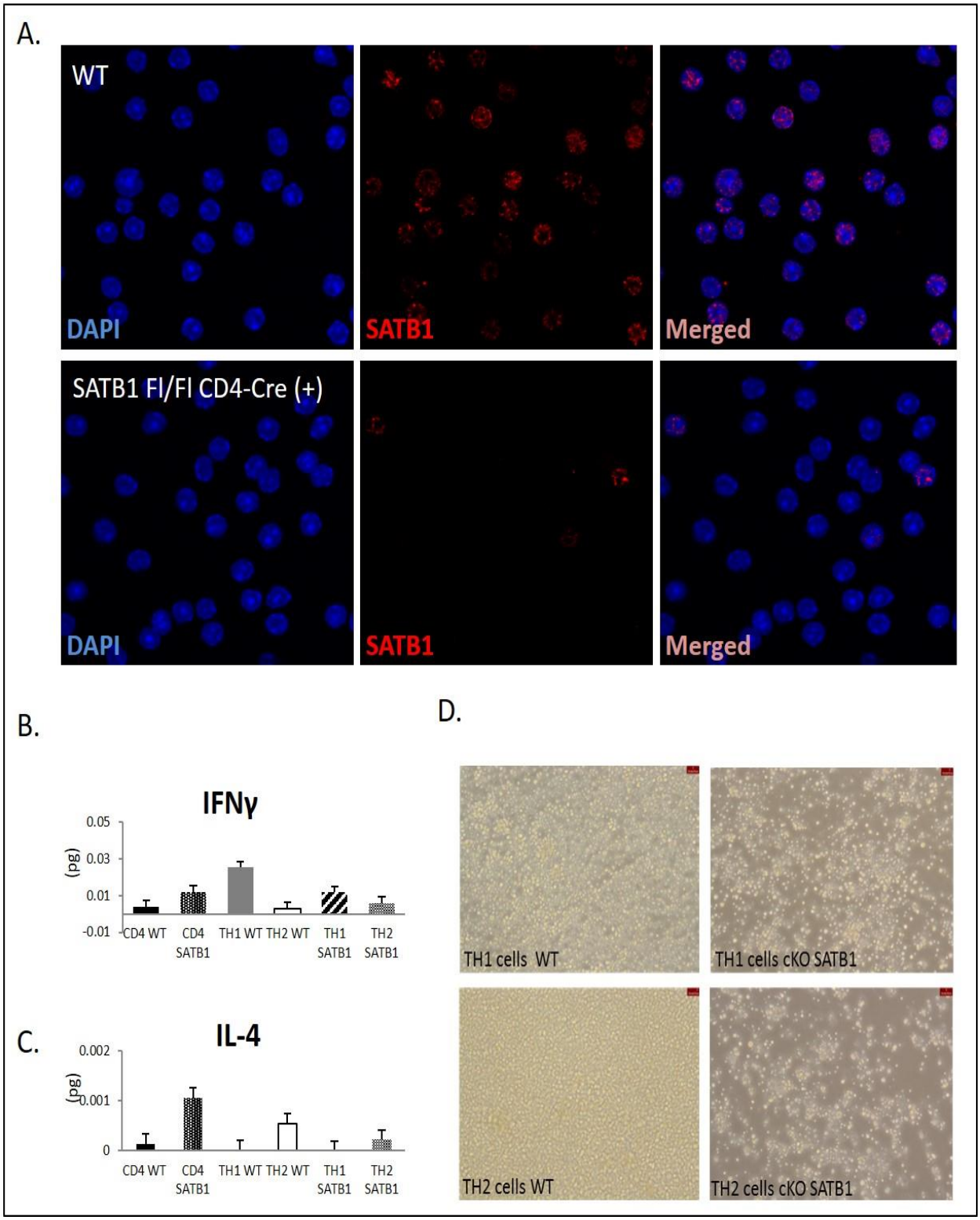

Figure 66. A) Confocal microscopy images from IF experiments in wt and *Satb1* cKO thymocytes. SATB1 (red), DAPI staining (blue.) B) and C) Quantitation of *Ifnγ* and *Il4* cytokine gene expression levels in distinct T cell lineages before and after differentiation analyzed by qRT-PCR in WT and *Satb1* cKO. D) Images from Olympus IX 50 inverted microscope and a Plan 20x lense depicting cells in culture under T_H1 and T_H2 differentiation conditions.

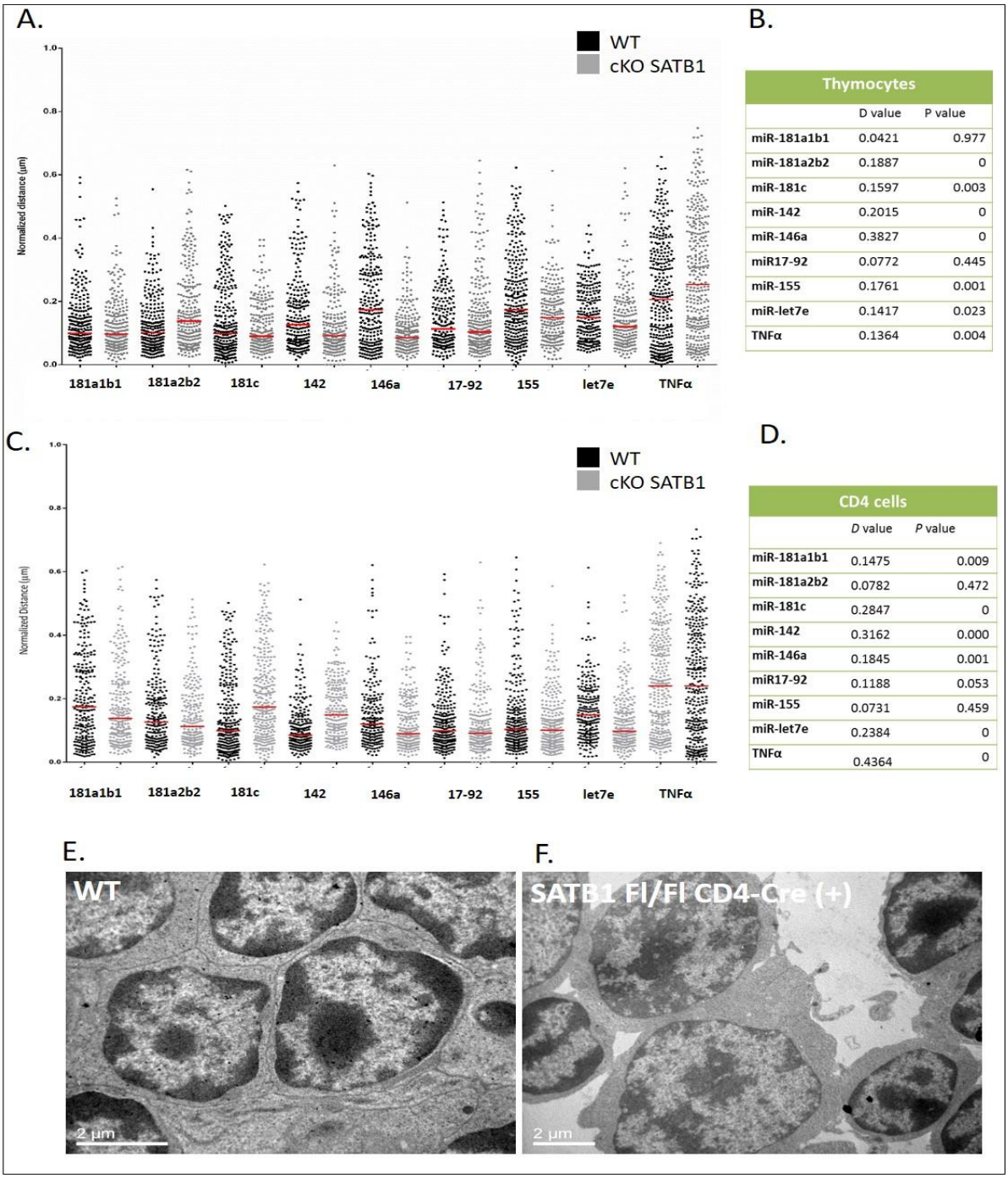

Thymocytes	D value	P value
miR-181a1b1	0.0421	0.977
miR-181a2b2	0.1887	0
miR-181c	0.1597	0.003
miR-142	0.2015	0
miR-146a	0.3827	0
miR17-92	0.0772	0.445
miR-155	0.1761	0.001
miR-let7e	0.1417	0.023
TNFα	0.1364	0.004

CD4 cells	*D* value	*P* value
miR-181a1b1	0.1475	0.009
miR-181a2b2	0.0782	0.472
miR-181c	0.2847	0
miR-142	0.3162	0.000
miR-146a	0.1845	0.001
miR17-92	0.1188	0.053
miR-155	0.0731	0.459
miR-let7e	0.2384	0
TNFα	0.4364	0

Figure 67. A) Scatter plot graph displaying the gene alleles ND values distribution for microRNA genes and *Tnfα* in thymocytes of WT and *Satb1* cKO. *The red line depicts the median of each distribution. B)* Kolmogorov-Smirnov test for the randomness of distributions between microRNA and *Tnfα* gene loci in WT and *Satb1* cKO thymocytes. C) Scatter plot showing the gene alleles ND values distribution of microRNA and *Tnfα* genes in WT and *Satb1* cKO CD4 cells. *The red line depicts the median of each distribution. D)* Kolmogorov-Smirnov test for the randomness of distributions between microRNA and *Tnfα* genes in WT and *Satb1* cKO CD4 cells. E) and F) Transmission electron microscopy images of thymic sections in WT and *Satb1* cKO mice.

DISCUSSION

Our data reveal a peripheral subnuclear localization of eight immune cell specific microRNA genes and Microprocessor during development and differentiation in discrete cell lineages, suggesting a link between the 3D chromatin architecture and the localization of microRNA gene loci. Although there is a plenty of evidence about the role of the non-coding genome on the nuclear organization, most of the studies show the direct or non-direct effect of the long non-coding RNA in shaping the chromatin structure. This is the first study which tries to link the small non-coding RNA with nuclear organization and more specifically with the nuclear periphery. Our data demonstrate that the distribution of eight microRNA genes has implications for nuclear structure and we discuss our findings in relation to the model of nucleus that is functionally compartmentalized.

Nowadays thousands of microRNAs have been discovered and more are expected to be discovered. These small non-coding RNAs serve as "hubs" of gene regulatory networks. A single microRNA can target many genes while multiple microRNAs can regulate a single gene (Wu et al. 2010). Although the role of small non coding RNA in transcription and translation has been reported, there are also data showing the role of microRNA genes in heterochromatin formation (Kim et al. 2008). In this study, we demonstrated that eight immune specific microRNA genes (*miR-181a1b1, miR-181a2b2, miR-181c, miR-142, miR146a, miR-17-92 and miR-let-7e*) are highly transcribed upon activation of T cells. MicroRNA have been characterized as guardian of the immune system and are arguably important during T cell activation and differentiation (Dooley et al. 2013). Our experiments showed that the expression levels of *miR-181-a1b1, miR-181-a2b2, miR-181c, miR-142, miR -146a, miR-17-92 and miR-155* increase after the activation of the CD4 cells. This is in agreement with published data demonstrating the importance of expression of microRNA genes during T cell activation and differentiation (Sonkoly et al. 2008). Moreover, a series of studies have assessed the impact of the microRNA network in T cell developments through knocking out different microRNA genes and key biosynthesis enzymes: DICER, DROSHA, and DGCR8 in T cells and T-cell subsets. These studies have painted a consistent picture of the relative importance of the microRNA network throughout key developmental and functional checkpoints in T cell development (Weiner 2001; Thai et al. 2007; Chong et al. 2008; Banerjee et al. 2010).

Here we report microRNA expression profile for diverse T cell subsets before and after stimulation. In order to find the allelic expression profile of microRNA genes that were under investigation, an optimized single-molecule RNA FISH method for the quantitation of primary transcripts was utilized (Zeng et al. 2015). Our data showed that microRNA genes are expressed mainly monoallelically in thymocytes, CD4 cells, T_H1 and T_H2 cells. Upon activation microRNA genes show low levels of biallelic expression in T_H1 and

T_H2 cells. According to the Geneimprint database (http://www.geneimprint.com/site/home) till now only twenty-eight microRNA genes in *M. musculus* have been annotated and only two of them show biallelic expression. Data from uniparental disomy revealed that most of the microRNA genes are transcribed monoallelically. This can be explained by the fact that almost all microRNA genes annotated at the gene imprint database, are located at the imprinted locus on chromosome 12 (Zhu and Paul 2010). Therefore, this is the first study which shows the expression profile of eight immune specific microRNA in murine T cells. The above study provides substantial information on the allelic expression profile of eight microRNA genes implicated in the regulation of the adaptive immune responses. We have attributed the monoallelic expression pattern to the moderate expression levels of these genes (Deng et al. 2014a; Reinius and Sandberg 2015) and excluded the potential of imprinting for the aforementioned loci, since low frequency biallelic expression was detected in cell populations with maximal pri-microRNA expression, following T cell receptor (TCR) activation of $CD4^+$ T cells. Although monoallelic expression has been reported for a wide range of coding genes (Reik and Walter 2001; Reinius and Sandberg 2015) it has also been documented for the non-coding genome (Lee 2000; Tian et al. 2010) such as for imprinted microRNA gene clusters found both on mouse and human chromosomes (Seitz et al. 2004; Noguer-Dance et al. 2010). In parallel, the preference for the monoallelic expression of microRNA genes could be attributed to differential methylation of regulatory elements controlling gene expression.

Our data also demonstrated that microRNA genes have a peripheral localization independent of their transcriptional activation in T cells. Quiescent naïve CD4 cells have significantly different nuclear organization and epigenetic hall marks compared with terminally differentiated TH cells. Naive, quiescent T cells have small nuclei with a significantly higher fraction of facultative heterochromatin compared with differentiated TH cells which show bigger nuclei containing more relaxed chromatin (Rawlings et al. 2011). Quiescent resting lymphocytes also show greatly reduced levels of transcription compared with activated lymphocytes (Frangini et al. 2013). Terminally differentiated, post-mitotic cells differ from quiescent cells in that their exit from the cell cycle is irreversible. The differentiated post-mitotic cells that have been studied so far, have a variety of chromosomal arrangements that may relate to the different functions of the cells. Centromeres are repositioned from a preferentially external distribution in undifferentiated cells to a more preferential peripheral position in differentiated T_H1 and T_H2 cells. Our results demonstrate that despite the significant spatial genome reorganization that occurs during differentiation of T cells, eight microRNA gene loci remain peripheral and show non-significant peripherization or relocalization of microRNA genes upon differentiation of T cells.

Relationship between dynamic genome organization and single gene regulation is highly complexed (Kim et al. 2004). Although there are numerous publications indicating that active gene transcription is found in interior of the nucleus (Chuang et al. 2006; Schneider and Grosschedl 2007) (Dillon 2008), at the same time several studies have shown that periphery can also be an "active environment". The "gene gating" hypothesis, introduced by Blobel in 1985, supported the idea that compact chromatin associates with the nuclear lamina, while expanded transcribable genes associate with the nuclear pore complex, facilitating the nuclear export of RNA (Blobel 1985). In contrast to findings of localization of inactive chromatin at the nuclear periphery, nowadays it has been found that several dynamically regulated genes are recruited to the nuclear periphery when activated (Finlan et al. 2008; Kumaran and Spector 2008; Zuleger et al. 2013; Harr et al. 2015). Nuclear periphery is not a repressive environment in T cells not only for microRNA genes but also for coding genes. During differentiation of thymocytes, *CD8* gene relocate to the periphery in CD8 cells (Kim et al. 2004). These findings are in agreement with our results. Contrary to the prevailing notion that the nuclear periphery is a repressive compartment, in *Saccharomyces cerevisiae,* it has been reported that nuclear pore components Nic96, Nup116, Nup2, Nup60 and the karyopherin Xpo1, Cse1, and Kap95 are associated with highly transcribed genes at the periphery. (Casolari et al. 2004). Moreover, in the same organism, it has been reported that activation of *INO1* (a target gene of the unfolded protein response (UPR), which encodes inositol 1-phosphate synthase) takes place at the nuclear membrane (Brickner and Walter 2004). Transcriptional activity at the periphery is not mainly a yeast phenomenon. In vertebrates the DNAse I sensitive chromatin preferably localizes at the nuclear periphery (Hutchison and Weintraub 1985). The nuclear lamina promotes telomere aggregation and centromere peripheral localization during senescence of human mesenchymal stem cells (Raz et al. 2008). Moreover, in mammalian cells beta-globin expression begins at the nuclear periphery prior following the relocalization to the interior of the cell (Ragoczy et al. 2006). All these data reported, are in agreement with our findings, that the nuclear lamina is not a repressive environment for the expression of microRNA genes. All the above studies are in agreement with our results regarding the transcriptional activity of the nuclear periphery. Our analysis indicated that in both naive, non-stimulated cells, but also in TCR-activated CD4+ T cells, microRNA genes localize in the nuclear periphery, irrespectively of their transcriptional activity or differentiation status. The role of the nuclear periphery in gene expression control still remains unclear. Nowadays, the capacity of high-resolution capacity imaging approaches (Fiserova et al. 2017; Nozaki et al. 2017; Xu et al. 2018) in concert with chromosome conformation capture (3C)-based technologies (Schmitt et al. 2016), combined with modeling for interpreting chromatin interactions, or tethering loci to specific nuclear compartments (Wang et al. 2018) provides strong support in deciphering the exact role of the nuclear periphery during

development. Although accumulating evidence supports the notion that gene transcription might be linked with repositioning into the nuclear interior (Chuang et al. 2006; Schneider and Grosschedl 2007; Dillon 2008), several studies have shown that nuclear periphery can also be a transcriptionally "active environment" (Kim et al. 2004; Ragoczy et al. 2006; Zhao et al. 2015). Despite the fact that transcription-induced relocalization of protein-coding genes or lamina associated enhancers (Zink et al. 2004; Wiblin et al. 2005; Ragoczy et al. 2006; Ktistaki et al. 2010; Robson et al. 2017) were shown to precede the actual transcription-mediated responses in the murine immune system (Spilianakis et al. 2005; Ktistaki et al. 2010; Rawlings et al. 2011; Deligianni and Spilianakis 2012) we have not observed such relocalization of microRNA gene loci before and after activation/differentiation of T cells. It still remains unresolved whether transcription actually controls directly chromatin organization and gene repositioning or *vice versa*. It has been reported that chromatin loops (Mitchell and Fraser 2008) and contacts between regulatory DNA elements and genes in the β-globin locus were unaffected upon transcription inhibition. These reports are in line with our findings in which transcription inhibition did not affect the localization of microRNA genes nor caused a repositioning in T cells.

Perinuclear positioning of microRNA genes was not affected by changes in chromatin conformation during murine development. Our results in ESCs support that subnuclear localization of these microRNA gene loci is conserved between embryonic stem cells and terminally differentiated immune cells.In contrary, the protein-coding *Tnfα* gene locus altered its subnuclear localization during development, relocalizing at the nuclear periphery in ESCs. However, the unique and intriguing chromatin landscape of ESCs has been well documented (Chen et al. 2004; Meshorer and Misteli 2006; Meshorer 2007; Gangaraju and Lin 2009), with their nuclear periphery being at the same time a transcriptionally permissive and repressive compartment (Luo et al. 2009). Core pluripotency genes expressed in ESCs, such as *Sox2*, *Nanog* and *Oct4* avoid peripheral localization (Jost et al. 2011), whereas up-regulated genes such as *Ptn*, *Sox6*, and *Nrp1* relocate from the nuclear periphery to the nuclear center during ESC differentiation (Peric-Hupkes et al. 2010; Therizols et al. 2014). Many repressive H3K27-me3 and active epigenetic marks (H3K4-me3 and H3K36-me3) localize to the periphery of ESC (Luo et al. 2009). In ESCs, chromatin is globally decondensed, enriched in active histone and contains a fraction of loosely bound architectural chromatin proteins (Meshorer and Misteli 2006). When cells differentiate, regions of condensed heterochromatin form, silencing histone marks accumulate, and structural chromatin proteins become more stably associated with chromatin (Gangaraju and Lin 2009). Nuclear architecture at the ESCs shows fewer and larger foci of heterochromatin, small nuclear speckles, larger nucleoli, an ill-defined nuclear lamina (LMNa is not expressed) while PML bodies remain similar after differentiation (Chen et al. 2004). All the above reports

are in line with our findings, where *miR-17-92* cluster, which is perinuclearly localized from embryonic stem cells to differentiated myeloid cells, was highly expressed in mESCs (Hadjimichael et al. 2016).

Our comparative analysis of DamID-derived sequencing data revealed that microRNA genes are preferentially positioned outside constitutively-repressed LAD regions in *M. musculus* and this localization pattern is conserved among four different species (*H.sapiens*, *M. musculus*, *C.elegans* and *D.melanogaster*). LADs contain AT rich gene poor domains (Guelen et al. 2008) and are also enriched for marks such as histone 3 Lys9 dimethylation (H3K9me2), which is a mark of heterochromatin and silent genes. During differentiation, constitutive LADs (cLADs) remain associated with the lamina, whereas facultative LADs (fLADs) become detached as the genes that they contain become active (Guelen et al. 2008). Regions of open chromatin, in which genes are actively transcribed, loop out into the interior of the nucleus. After mitosis, some LADs relocate to the periphery of the nucleolus in the following G1 phase of the cell cycle, although the mechanism underlying this remains unclear (Spector and Lamond 2011). We also documented that both microRNA genes and protein-coding genes display the same preference to avoid cLAD localization. This can be explained by the fact that in human and mouse 50% of the microRNA genes are intragenic, which means that their transcription is mediated through the hosting genes, while the rest of the microRNA are intergenic. These results are also compatible with our immuno-RNA-DNA FISH analysis, showing that microRNA genes are actively transcribed even when colocalized with Lamin-B1. This is in line with previous reports documenting transcriptionally active gene loci in concert with ciLAD-localization (Peric-Hupkes et al. 2010; Akhtar et al. 2013). Conclusively, our results are in accordance with reports showing that the frequency of gene colocalization with the nuclear lamina can be locus-specific (Kind et al. 2015) and that in general microRNA gene colocalization with the nuclear lamina is not associated with attenuated pri-microRNA transcription.

The chromosome painting experiments combined with DNA FISH reported a polarization of microRNA genes and the control genes located on the same chromosome. We reported that *miR-let-7e* and *miR-146a* are placed on the external edge of the CTs while the control loci *TH2* and *Tnfa* are found on the internal edge and loop out from the CTs to the interior of the nucleus. These findings are in line with data showing the sub-nuclear localization of CTs. Chromosomes 17 and 11 are peripheral in mouse and human fibroblasts (Croft et al. 1999). There is also evidence that in human dermal fibroblasts only chromosomes 14, 19, 20, 21 and 22 show an internal localization while the rest of the chromosomes are located at the periphery of the cells (Mehta et al. 2013). Moreover, it has been demonstrated that in thymocytes during

differentiation chromosome 6 shifts towards the center in $CD4^+$cells and towards the periphery in $CD8^+$cells (Kim et al. 2004). Chromosome 6 contains also the major histocompatibility (MHC) region at 6p21 which loops out from the CT6 on large loops, in response to activation of MHC genes. A significantly increased proportion of nuclei displaying these loops were observed in B-lymphoblastoid cells and in Interferon-γ (INF-γ)-treated fibroblasts, which express the MHC genes, compared with untreated fibroblasts (Volpi et al. 2000). Moreover it has been demonstrated that during differentiation and development, the *HOX* gene cluster loops out from the CT in order to be transcribed (Williams et al. 2002; Chambeyron et al. 2005; Kupper et al. 2007). Consequently, CTs may be considered as genome organizers, where different CTs may have a specific probability to be influenced by the nuclear periphery, both at the individual and population level. Given this dynamic (affecting CTs and gene loci) the nuclear periphery may be considered as an organizer of the entire genome, and not specifically of the chromatin at the nuclear periphery.

Transcription inhibition (α-amanitin 50μg/ml) did not affect the localization of microRNA genes in thymocytes, $CD4^+$ and T_H2 cells while the expression levels of microRNAs genes were severely reduced. Although there are many genes relocated at the center of the nucleus after being activated, our loci demonstrated small re-localization after α-amanitin treatment that were not statistically significant. As assessed by 4C technology, it has been demonstrated that inhibition of transcription does not affect chromatin loops. Treatment with 5,6-Dichlorobenzimidazole 1-β-D-ribofuranoside (DRB) (inhibition of transcription elongation) of fetal liver cells, didn't affect the associations between distal expressed genes *Hbb-b1* and *Eraf* (25 Mb apart) as well as *Eraf* and *Uros* (5 Mb apart) which are located on chromosome 7 (Mitchell and Fraser 2008). Furthermore, inhibition of transcription in primary erythroid cells, demonstrated that contacts between regulatory DNA elements and genes in the β-globin locus are unaffected and the locus still interacts with the same genomic regions elsewhere on the chromosome (Palstra et al. 2008). If the correlation between transcription and chromatin organization is a cause or consequence still remains unclear. The β-globin when activated and is repositioned from the nuclear periphery to the nuclear interior (Ragoczy et al. 2006), while *CFTR* after being activated is relocate to the interior locations in the nucleus (Cordes and Srivastava 2009). In other cases, the re-localization takes place first and then the transcription starts. Initial observations that highly transcribed genes tend to colocalize seemed to suggest that gene activation required DNA repositioning to transcriptionally active regions, termed transcription factories (Rottiers and Naar 2012; Chen et al. 2013). Later studies showed that genes regulated by similar transcription factors can colocalize in 3D space when they are transcribed

(Ceribelli et al. 2012). However, other studies did not observe transcription downregulation by repositioning different DNA regions to the lamina (Smalheiser and Torvik 2005).

Studies in *S. cerevisiae* and *D. melanogaster* indicated that active transcription occurs in the NPC vicinity, causing chromatin recruitment to the nuclear periphery (Casolari et al. 2004; Vaquerizas et al. 2010; Buchwalter et al. 2019). In addition to nuclear transport, NUP153 and NUP93 are considered as gene expression regulators since they control cell type specific gene expression transcriptional programs (Ibarra et al. 2016a; Toda et al. 2017). Depletion of NUP153 does not affect nuclear transport, though it induces changes in gene transcription (Jacinto et al. 2015). DamID experiments reported that these nucleoporins interact with ciLAD domains and bind to SE in U2OS and IMR-90 cells (Ibarra et al. 2016a). These findings are in accordance with our observations regarding the transcriptionally active microRNA genes at the nuclear periphery. In addition, NUP98 also regulates gene expression (Liang et al. 2013). It has been reported that in *D. melanogaster* NUP98 interacts with transcriptionally active developmental and cell cycle associated genes in the nucleoplasm (Kalverda et al. 2010). This nucleoporin is characterized as a more dynamic molecule that can detach from the nuclear periphery and bind to promoters at a distance from the NPC (Franks et al. 2017). This is in accordance with our findings suggesting no significant differences in NUP98 binding between the peripheral microRNA loci and all the protein-coding genes. Therefore, a potential explanation for the perinuclear localization of microRNA gene loci might be their interaction with NPCs.

Mammalian microRNA gene transcription is initiated in the cell nucleus by either RNA Polymerase II (Pol II) or RNA Polymerase III (Pol III) and it may yield a several kb (pri-microRNA) transcript that is co-transcriptionally processed to an ~70 bp premature RNA (pre-microRNA) by the Microprocessor complex [comprised by DROSHA and DiGeorge syndrome critical region gene 8 (DGCR8) proteins] (Cai et al. 2004; Lee et al. 2004a; Kim and Kim 2007; Morlando et al. 2008; Winter et al. 2009). Since we next demonstrated that microRNA genes and Microprocessor are located at the nuclear periphery, we hypothesized that Microprocessor could also be a mechanism explaining the peripheral location by direct or indirect binding on TSSs of microRNA genes. According to our data both DROSHA and DGCR8 show a peripheral distribution in murine ESCs, thymocytes, CD4 cells, T_H1 and T_H2 cells. It has also been shown that DROSHA cleavage occurs during transcription acting on both independently transcribed and intron-encoded microRNAs (Lee and Dutta 2009). Except from acting as a scissor at the microRNA biogenesis pathway, DROSHA can act also as a transcription factor by binding to p-pol II at transcription starting sites of coding genes (Fitzgerald and Caffrey 2014). Moreover, it has been reported that the recognition of intron-containing C19MC pri-microRNAs by Microprocessor occurs in proximity to their transcription sites.

Peripheral chromosome 19 microRNA cluster (C19MC) harbors 46 highly related pre-microRNAs processed from the repeated introns of the RNA Pol-II-transcribed non-protein coding C19MC-HG (host-gene) pri-microRNA transcripts. Live imaging experiments demonstrated that newly synthesized C19MC pri-microRNAs attract a large fraction of the Drosha– DGCR8 complex (Bellemer et al. 2012). The result from our DOSHA Chip-seq experiments didn't reveal a correlation between peripheral position of microRNA genes and Microprocessor. However another study reported that both DROSHA and DGCR8 bind to a microRNA super-enhancer (SE) to boost microRNA processing (Suzuki et al. 2017). These data agree with our findings, in which we observe enrichment of DGCR8 binding in the microRNA genes compared to protein coding genes, further supporting the potential role of DGCR8 as a microRNA gene positioning factor.

SATB1 can act as a repressor or activator for different genes. It organizes cell type–specific nuclear architecture by anchoring specialized DNA sequences and recruiting chromatin remodeling factors to control gene transcription. There is evidence that SATB1 packages densely looped transcriptionally active chromatin for coordinated expression of TH2 locus (Allen et al. 2004). Moreover it has been reported that in the absence of SATB1 thymocytes development is affected, peripheral CD4 cells are activated and there is an autoimmune manifestation (Kondo et al. 2016). In this study, we reported that SATB1 can affect the localization but also the expression of microRNA genes in T cells. Ablation of SATB1 leaded to a deregulation in expression of microRNA genes and other genes as proved by RNA-seq (data not shown) but also it caused a shuffling on the compartmentalization of the chromatin. Moreover, the deregulation in expression was also verified by qPCR experiments which reported that in thymocytes and CD4 cells gene expression is also being deregulated (data not shown). The depletion of such an abundant looping factor leaded to deregulation of chromatin organization and gene expression in T cells. Other control experiment should also follow, so the observed repositioning events can be classified as specific and not due to indirect, global effects on nuclear organization. This can be explained by the fact that in the cKO SATB1 mice there is a high deregulation of the chromatin and gene expression and the differences in relocalizations are an outcome of the pleiotropic genome organization. This interpretation is in line with data from IP-MS experiments in our lab (data not shown) which revealed interactions of SATB1 with several gene positioning factors such as HNRNPK, EP400, KlF4A, CHAF1B, AKAP8L, EHHADH, TRIM28 and SATB2. These factors were recently classified as positioning determinants based on the fact that their absence leaded to relocalization of both several endogenous peripheral and internal genomic loci (Shachar et al. 2015).

Ultimately, the peripheral positioning of microRNA gene loci might also represent an evolutionary aspect of chromatin organization. cLAD domains are enriched for LINE (Long Interspersed Elements) sequences (Meuleman et al. 2013) and the evolution of microRNA genes is speculated to descent from transposable elements integrated into the genome (Borchert et al. 2011; Roberts 2014). Next-generation sequencing and computational comparative analyses of small RNAs have demonstrated that sequence homology is more frequent for MITEs (Miniature Inverted-repeat Transposable Elements) and DNA transposons and less prevalent for LTR (Long Terminal Repeat) or non-LTR retrotransposons (SINEs, LINEs) or satellite repeats, supporting the notion of microRNA gene derivation from transposable elements (Borchert et al. 2011; Tempel et al. 2012). Additionally, it was documented that in human $CD4^+$ cells, HIV-1 integrates preferentially in regions of the eukaryotic genome found at the nuclear periphery, in proximity to nuclear pores, avoiding the heterochromatic LAD regions in order to facilitate the transcriptional regulation of the viral genome (Marini et al. 2015). These findings provide additional evidence for the evolutionary denouements of peripheral localization and reconfirm the subnuclear positioning of the microRNA genes observed in our study.

In conclusion, our report elucidates the interplay between subnuclear localization of micro- RNA gene loci and their transcriptional regulation in the murine innate and adaptive immune system, providing valuable additional knowledge of chromatin organization and gene regulation at the nuclear periphery.

While a few years ago, the question of how eukaryotic genomes are organized within the cell nucleus was a new field of study, nowadays it is believed that nuclear organization might explain different aspect of genome function. Genome-wide molecular studies and single cell studies have revealed that chromatin organization and gene expression are tightly linked by offering functional insight for many phenomena observed within the nucleus. The aim of nuclear organization field is to understand the 3D organization–function relationships within the cell nucleus on all levels, from molecules to entire genomic and epigenomic landscapes. The 4th dimension of the genome is the time and this includes all the reorganization of the 3D structure upon environmental changes, cell–cell interactions and tissue organization during cell differentiation, reprogramming, and aging. Mapping the genome structure in undifferentiated and differentiated cells (i.e. from embryonic stem cells and terminally differentiated cells) can provide a better understanding of the correlation between the disruption of nuclear architecture and how this can lead to disease. The non-coding genome and its role in chromatin organization and gene expression is also offering information on how to decipher the nuclear architecture. These considerations clearly show that much work remains to be done in order to understand how the spatial organization of

genomes relates to their function. The study of subnuclear localization of chromosomes and gene loci upon differentiation as reported here should provide a useful tool to address this fundamental aspect of genome function. Moreover, other cell single-cell analysis to track the location of individual genes in the periphery and the interior of the cell should follow to reveal the positioning of genome regions in individual living cells. Studies that can dictate the promoters of the microRNA genes and possible interaction of those promoters with peripheral proteins would be a supportive mechanism for all the above observations. Moreover, the decoding of the nuclear periphery and the study of expressing genes that lay at the nuclear periphery will provide as a better understanding of how nuclear periphery contributes to the genome architecture and to the integrity of gene expression.

REFERENCES

Adolfsson J, Mansson R, Buza-Vidas N, Hultquist A, Liuba K, Jensen CT, Bryder D, Yang L, Borge OJ, Thoren LA et al. 2005. Identification of Flt3+ lympho-myeloid stem cells lacking erythro-megakaryocytic potential a revised road map for adult blood lineage commitment. *Cell* **121**: 295-306.

Ahlfors H, Limaye A, Elo LL, Tuomela S, Burute M, Gottimukkala KV, Notani D, Rasool O, Galande S, Lahesmaa R. 2010. SATB1 dictates expression of multiple genes including IL-5 involved in human T helper cell differentiation. *Blood* **116**: 1443-1453.

Akhtar W, de Jong J, Pindyurin AV, Pagie L, Meuleman W, de Ridder J, Berns A, Wessels LF, van Lohuizen M, van Steensel B. 2013. Chromatin position effects assayed by thousands of reporters integrated in parallel. *Cell* **154**: 914-927.

Aliahmad P, Kaye J. 2008. Development of all CD4 T lineages requires nuclear factor TOX. *The Journal of experimental medicine* **205**: 245-256.

Allen BL, Taatjes DJ. 2015. The Mediator complex: a central integrator of transcription. *Nature reviews Molecular cell biology* **16**: 155-166.

Allen E, Xie Z, Gustafson AM, Sung GH, Spatafora JW, Carrington JC. 2004. Evolution of microRNA genes by inverted duplication of target gene sequences in Arabidopsis thaliana. *Nature genetics* **36**: 1282-1290.

Allman D, Sambandam A, Kim S, Miller JP, Pagan A, Well D, Meraz A, Bhandoola A. 2003. Thymopoiesis independent of common lymphoid progenitors. *Nature immunology* **4**: 168-174.

Alvarez JD, Yasui DH, Niida H, Joh T, Loh DY, Kohwi-Shigematsu T. 2000. The MAR-binding protein SATB1 orchestrates temporal and spatial expression of multiple genes during T-cell development. *Genes & development* **14**: 521-535.

Andersson R, Sandelin A. 2019. Determinants of enhancer and promoter activities of regulatory elements. *Nature reviews Genetics*.

Andreadis C, Nikolaou C, Fragiadakis GS, Tsiliki G, Alexandraki D. 2014. Rad9 interacts with Aft1 to facilitate genome surveillance in fragile genomic sites under non-DNA damage-inducing conditions in S. cerevisiae. *Nucleic acids research* **42**: 12650-12667.

Axtell MJ, Westholm JO, Lai EC. 2011. Vive la difference: biogenesis and evolution of microRNAs in plants and animals. *Genome biology* **12**: 221.

Babiarz JE, Ruby JG, Wang Y, Bartel DP, Blelloch R. 2008. Mouse ES cells express endogenous shRNAs, siRNAs, and other Microprocessor-independent, Dicer-dependent small RNAs. *Genes & development* **22**: 2773-2785.

Bacher CP, Guggiari M, Brors B, Augui S, Clerc P, Avner P, Eils R, Heard E. 2006. Transient colocalization of X-inactivation centres accompanies the initiation of X inactivation. *Nature cell biology* **8**: 293-299.

Banerjee A, Schambach F, DeJong CS, Hammond SM, Reiner SL. 2010. Micro-RNA-155 inhibits IFN-gamma signaling in CD4+ T cells. *European journal of immunology* **40**: 225-231.

Barrasa MI, Vaglio P, Cavasino F, Jacotot L, Walhout AJ. 2007. EDGEdb: a transcription factor-DNA interaction database for the analysis of C. elegans differential gene expression. *BMC genomics* **8**: 21.

Bartel DP. 2009. MicroRNAs: target recognition and regulatory functions. *Cell* **136**: 215-233.

-. 2018. Metazoan MicroRNAs. *Cell* **173**: 20-51.

Bartel DP, Chen CZ. 2004. Micromanagers of gene expression: the potentially widespread influence of metazoan microRNAs. *Nature reviews Genetics* **5**: 396-400.

Bartkuhn M, Renkawitz R. 2008. Long range chromatin interactions involved in gene regulation. *Biochimica et biophysica acta* **1783**: 2161-2166.

Bateman JR, Johnson JE, Locke MN. 2012. Comparing enhancer action in cis and in trans. *Genetics* **191**: 1143-1155.

Baumann K. 2016. Nuclear organization: NUP-tial binding to super-enhancers. *Nature reviews Molecular cell biology* **17**: 738-739.

Bellemer C, Bortolin-Cavaille ML, Schmidt U, Jensen SM, Kjems J, Bertrand E, Cavaille J. 2012. Microprocessor dynamics and interactions at endogenous imprinted C19MC microRNA genes. *Journal of cell science* **125**: 2709-2720.

Bending D, De la Pena H, Veldhoen M, Phillips JM, Uyttenhove C, Stockinger B, Cooke A. 2009. Highly purified Th17 cells from BDC2.5NOD mice convert into Th1-like cells in NOD/SCID recipient mice. *The Journal of clinical investigation* **119**: 565-572.

Berezikov E. 2011. Evolution of microRNA diversity and regulation in animals. *Nature reviews Genetics* **12**: 846-860.

Berezikov E, Chung WJ, Willis J, Cuppen E, Lai EC. 2007. Mammalian mirtron genes. *Molecular cell* **28**: 328-336.

Beygo J, Citro V, Sparago A, De Crescenzo A, Cerrato F, Heitmann M, Rademacher K, Guala A, Enklaar T, Anichini C et al. 2013. The molecular function and clinical phenotype of partial deletions of the IGF2/H19 imprinting control region depends on the spatial arrangement of the remaining CTCF-binding sites. *Human molecular genetics* **22**: 544-557.

Bhattacharyya M, Das M, Bandyopadhyay S. 2012. miRT: a database of validated transcription start sites of human microRNAs. *Genomics, proteomics & bioinformatics* **10**: 310-316.

Bickmore WA. 2013. The spatial organization of the human genome. *Annual review of genomics and human genetics* **14**: 67-84.

Bilic I, Koesters C, Unger B, Sekimata M, Hertweck A, Maschek R, Wilson CB, Ellmeier W. 2006. Negative regulation of CD8 expression via Cd8 enhancer-mediated recruitment of the zinc finger protein MAZR. *Nature immunology* **7**: 392-400.

Blobel G. 1985. Gene gating: a hypothesis. *Proceedings of the National Academy of Sciences of the United States of America* **82**: 8527-8529.

Bluml S, Bonelli M, Niederreiter B, Puchner A, Mayr G, Hayer S, Koenders MI, van den Berg WB, Smolen J, Redlich K. 2011. Essential role of microRNA-155 in the pathogenesis of autoimmune arthritis in mice. *Arthritis and rheumatism* **63**: 1281-1288.

Bohnsack MT, Czaplinski K, Gorlich D. 2004. Exportin 5 is a RanGTP-dependent dsRNA-binding protein that mediates nuclear export of pre-miRNAs. *Rna* **10**: 185-191.

Boija A, Klein IA, Sabari BR, Dall'Agnese A, Coffey EL, Zamudio AV, Li CH, Shrinivas K, Manteiga JC, Hannett NM et al. 2018. Transcription Factors Activate Genes through the Phase-Separation Capacity of Their Activation Domains. *Cell* **175**: 1842-1855 e1816.

Bolzer A, Craig JM, Cremer T, Speicher MR. 1999. A complete set of repeat-depleted, PCR-amplifiable, human chromosome-specific painting probes. *Cytogenetics and cell genetics* **84**: 233-240.

Borchert GM, Holton NW, Williams JD, Hernan WL, Bishop IP, Dembosky JA, Elste JE, Gregoire NS, Kim JA, Koehler WW et al. 2011. Comprehensive analysis of microRNA genomic loci identifies pervasive repetitive-element origins. *Mobile genetic elements* **1**: 8-17.

Borchert GM, Lanier W, Davidson BL. 2006. RNA polymerase III transcribes human microRNAs. *Nature structural & molecular biology* **13**: 1097-1101.

Borden J, Manuelidis L. 1988. Movement of the X chromosome in epilepsy. *Science* **242**: 1687-1691.

Branco MR, Pombo A. 2006. Intermingling of chromosome territories in interphase suggests role in translocations and transcription-dependent associations. *PLoS biology* **4**: e138.

Breuer M, Ohkura H. 2015. A negative loop within the nuclear pore complex controls global chromatin organization. *Genes & development* **29**: 1789-1794.

Brickner DG, Ahmed S, Meldi L, Thompson A, Light W, Young M, Hickman TL, Chu F, Fabre E, Brickner JH. 2012. Transcription factor binding to a DNA zip code controls interchromosomal clustering at the nuclear periphery. *Developmental cell* **22**: 1234-1246.

Brickner DG, Randise-Hinchliff C, Lebrun Corbin M, Liang JM, Kim S, Sump B, D'Urso A, Kim SH, Satomura A, Schmit H et al. 2019. The Role of Transcription Factors and Nuclear Pore Proteins in Controlling the Spatial Organization of the Yeast Genome. *Developmental cell* **49**: 936-947 e934.

Brickner JH, Walter P. 2004. Gene recruitment of the activated INO1 locus to the nuclear membrane. *PLoS biology* **2**: e342.

Brooker AS, Berkowitz KM. 2014. The roles of cohesins in mitosis, meiosis, and human health and disease. *Methods in molecular biology* **1170**: 229-266.

Buchwalter A, Kaneshiro JM, Hetzer MW. 2019. Coaching from the sidelines: the nuclear periphery in genome regulation. *Nature reviews Genetics* **20**: 39-50.

Buenrostro JD, Wu B, Litzenburger UM, Ruff D, Gonzales ML, Snyder MP, Chang HY, Greenleaf WJ. 2015. Single-cell chromatin accessibility reveals principles of regulatory variation. *Nature* **523**: 486-490.

Burger K, Gullerova M. 2015. Swiss army knives: non-canonical functions of nuclear Drosha and Dicer. *Nature reviews Molecular cell biology* **16**: 417-430.

Burgess-Beusse B, Farrell C, Gaszner M, Litt M, Mutskov V, Recillas-Targa F, Simpson M, West A, Felsenfeld G. 2002. The insulation of genes from external enhancers and silencing chromatin. *Proceedings of the National Academy of Sciences of the United States of America* **99 Suppl 4**: 16433-16437.

Burren OS, Rubio Garcia A, Javierre BM, Rainbow DB, Cairns J, Cooper NJ, Lambourne JJ, Schofield E, Castro Dopico X, Ferreira RC et al. 2017. Chromosome contacts in activated T cells identify autoimmune disease candidate genes. *Genome biology* **18**: 165.

Cai S, Han HJ, Kohwi-Shigematsu T. 2003. Tissue-specific nuclear architecture and gene expression regulated by SATB1. *Nature genetics* **34**: 42-51.

Cai S, Lee CC, Kohwi-Shigematsu T. 2006. SATB1 packages densely looped, transcriptionally active chromatin for coordinated expression of cytokine genes. *Nature genetics* **38**: 1278-1288.

Cai X, Hagedorn CH, Cullen BR. 2004. Human microRNAs are processed from capped, polyadenylated transcripts that can also function as mRNAs. *Rna* **10**: 1957-1966.

Cai Y, Zhou Q, Yu C, Wang X, Hu S, Yu J, Yu X. 2012. Transposable-element associated small RNAs in Bombyx mori genome. *PloS one* **7**: e36599.

Calin GA, Dumitru CD, Shimizu M, Bichi R, Zupo S, Noch E, Aldler H, Rattan S, Keating M, Rai K et al. 2002. Frequent deletions and down-regulation of micro- RNA genes miR15 and miR16 at 13q14 in chronic lymphocytic leukemia. *Proceedings of the National Academy of Sciences of the United States of America* **99**: 15524-15529.

Capelson M, Hetzer MW. 2009. The role of nuclear pores in gene regulation, development and disease. *EMBO reports* **10**: 697-705.

Carter D, Chakalova L, Osborne CS, Dai YF, Fraser P. 2002. Long-range chromatin regulatory interactions in vivo. *Nature genetics* **32**: 623-626.

Casolari JM, Brown CR, Komili S, West J, Hieronymus H, Silver PA. 2004. Genome-wide localization of the nuclear transport machinery couples transcriptional status and nuclear organization. *Cell* **117**: 427-439.

Cattoni DI, Valeri A, Le Gall A, Nollmann M. 2015. A matter of scale: how emerging technologies are redefining our view of chromosome architecture. *Trends in genetics : TIG* **31**: 454-464.

Cavalli G, Misteli T. 2013. Functional implications of genome topology. *Nature structural & molecular biology* **20**: 290-299.

Cazalla D, Xie M, Steitz JA. 2011. A primate herpesvirus uses the integrator complex to generate viral microRNAs. *Molecular cell* **43**: 982-992.

Ceribelli A, Satoh M, Chan EK. 2012. MicroRNAs and autoimmunity. *Current opinion in immunology* **24**: 686-691.

Chak LL, Okamura K. 2014. Argonaute-dependent small RNAs derived from single-stranded, non-structured precursors. *Frontiers in genetics* **5**: 172.

Chakalova L, Fraser P. 2010. Organization of transcription. *Cold Spring Harbor perspectives in biology* **2**: a000729.

Chambeyron S, Da Silva NR, Lawson KA, Bickmore WA. 2005. Nuclear re-organisation of the Hoxb complex during mouse embryonic development. *Development* **132**: 2215-2223.

Chaumeil J, Micsinai M, Ntziachristos P, Deriano L, Wang JM, Ji Y, Nora EP, Rodesch MJ, Jeddeloh JA, Aifantis I et al. 2013. Higher-order looping and nuclear organization of Tcra facilitate targeted rag cleavage and regulated rearrangement in recombination centers. *Cell reports* **3**: 359-370.

Cheloufi S, Dos Santos CO, Chong MM, Hannon GJ. 2010. A dicer-independent miRNA biogenesis pathway that requires Ago catalysis. *Nature* **465**: 584-589.

Chen CZ, Li L, Lodish HF, Bartel DP. 2004. MicroRNAs modulate hematopoietic lineage differentiation. *Science* **303**: 83-86.

Chen CZ, Schaffert S, Fragoso R, Loh C. 2013. Regulation of immune responses and tolerance: the microRNA perspective. *Immunological reviews* **253**: 112-128.

Chen JL, Huisinga KL, Viering MM, Ou SA, Wu CT, Geyer PK. 2002. Enhancer action in trans is permitted throughout the Drosophila genome. *Proceedings of the National Academy of Sciences of the United States of America* **99**: 3723-3728.

Chen X, Xu H, Yuan P, Fang F, Huss M, Vega VB, Wong E, Orlov YL, Zhang W, Jiang J et al. 2008. Integration of external signaling pathways with the core transcriptional network in embryonic stem cells. *Cell* **133**: 1106-1117.

Chepelev I, Wei G, Wangsa D, Tang Q, Zhao K. 2012. Characterization of genome-wide enhancer-promoter interactions reveals co-expression of interacting genes and modes of higher order chromatin organization. *Cell research* **22**: 490-503.

Chernukhin I, Shamsuddin S, Kang SY, Bergstrom R, Kwon YW, Yu W, Whitehead J, Mukhopadhyay R, Docquier F, Farrar D et al. 2007. CTCF interacts with and recruits the largest subunit of RNA polymerase II to CTCF target sites genome-wide. *Molecular and cellular biology* **27**: 1631-1648.

Chi AW, Bell JJ, Zlotoff DA, Bhandoola A. 2009. Untangling the T branch of the hematopoiesis tree. *Current opinion in immunology* **21**: 121-126.

Chiang HR, Schoenfeld LW, Ruby JG, Auyeung VC, Spies N, Baek D, Johnston WK, Russ C, Luo S, Babiarz JE et al. 2010. Mammalian microRNAs: experimental evaluation of novel and previously annotated genes. *Genes & development* **24**: 992-1009.

Chien R, Zeng W, Kawauchi S, Bender MA, Santos R, Gregson HC, Schmiesing JA, Newkirk DA, Kong X, Ball AR, Jr. et al. 2011. Cohesin mediates chromatin interactions that regulate mammalian beta-globin expression. *The Journal of biological chemistry* **286**: 17870-17878.

Cho WK, Spille JH, Hecht M, Lee C, Li C, Grube V, Cisse, II. 2018. Mediator and RNA polymerase II clusters associate in transcription-dependent condensates. *Science* **361**: 412-415.

Chong MM, Rasmussen JP, Rudensky AY, Littman DR. 2008. The RNAseIII enzyme Drosha is critical in T cells for preventing lethal inflammatory disease. *The Journal of experimental medicine* **205**: 2005-2017.

Chong MM, Zhang G, Cheloufi S, Neubert TA, Hannon GJ, Littman DR. 2010. Canonical and alternate functions of the microRNA biogenesis machinery. *Genes & development* **24**: 1951-1960.

Chong S, Dugast-Darzacq C, Liu Z, Dong P, Dailey GM, Cattoglio C, Heckert A, Banala S, Lavis L, Darzacq X et al. 2018. Imaging dynamic and selective low-complexity domain interactions that control gene transcription. *Science* **361**.

Chuang CH, Carpenter AE, Fuchsova B, Johnson T, de Lanerolle P, Belmont AS. 2006. Long-range directional movement of an interphase chromosome site. *Current biology : CB* **16**: 825-831.

Cichocki F, Felices M, McCullar V, Presnell SR, Al-Attar A, Lutz CT, Miller JS. 2011. Cutting edge: microRNA-181 promotes human NK cell development by regulating Notch signaling. *Journal of immunology* **187**: 6171-6175.

Cifuentes D, Xue H, Taylor DW, Patnode H, Mishima Y, Cheloufi S, Ma E, Mane S, Hannon GJ, Lawson ND et al. 2010. A novel miRNA processing pathway independent of Dicer requires Argonaute2 catalytic activity. *Science* **328**: 1694-1698.

Cirera-Salinas D, Yu J, Bodak M, Ngondo RP, Herbert KM, Ciaudo C. 2017. Noncanonical function of DGCR8 controls mESC exit from pluripotency. *The Journal of cell biology* **216**: 355-366.

Clark SJ, Argelaguet R, Kapourani CA, Stubbs TM, Lee HJ, Alda-Catalinas C, Krueger F, Sanguinetti G, Kelsey G, Marioni JC et al. 2018. scNMT-seq enables joint profiling of chromatin accessibility DNA methylation and transcription in single cells. *Nature communications* **9**: 781.

Clowney EJ, LeGros MA, Mosley CP, Clowney FG, Markenskoff-Papadimitriou EC, Myllys M, Barnea G, Larabell CA, Lomvardas S. 2012. Nuclear aggregation of olfactory receptor genes governs their monogenic expression. *Cell* **151**: 724-737.

Comet I, Schuettengruber B, Sexton T, Cavalli G. 2011. A chromatin insulator driving three-dimensional Polycomb response element (PRE) contacts and Polycomb association with

the chromatin fiber. *Proceedings of the National Academy of Sciences of the United States of America* **108**: 2294-2299.

Consortium EP. 2012. An integrated encyclopedia of DNA elements in the human genome. *Nature* **489**: 57-74.

Cordes KR, Srivastava D. 2009. MicroRNA regulation of cardiovascular development. *Circulation research* **104**: 724-732.

Cremer C, Rappold G, Gray JW, Muller CR, Ropers HH. 1984. Preparative dual-beam sorting of the human Y chromosome and in situ hybridization of cloned DNA probes. *Cytometry* **5**: 572-579.

Cremer M, Kupper K, Wagler B, Wizelman L, von Hase J, Weiland Y, Kreja L, Diebold J, Speicher MR, Cremer T. 2003. Inheritance of gene density-related higher order chromatin arrangements in normal and tumor cell nuclei. *The Journal of cell biology* **162**: 809-820.

Cremer M, von Hase J, Volm T, Brero A, Kreth G, Walter J, Fischer C, Solovei I, Cremer C, Cremer T. 2001. Non-random radial higher-order chromatin arrangements in nuclei of diploid human cells. *Chromosome research : an international journal on the molecular, supramolecular and evolutionary aspects of chromosome biology* **9**: 541-567.

Cremer T, Cremer M. 2010. Chromosome territories. *Cold Spring Harbor perspectives in biology* **2**: a003889.

Cremer T, Lichter P, Borden J, Ward DC, Manuelidis L. 1988. Detection of chromosome aberrations in metaphase and interphase tumor cells by in situ hybridization using chromosome-specific library probes. *Human genetics* **80**: 235-246.

Croft JA, Bridger JM, Boyle S, Perry P, Teague P, Bickmore WA. 1999. Differences in the localization and morphology of chromosomes in the human nucleus. *The Journal of cell biology* **145**: 1119-1131.

Crotty S. 2011. Follicular helper CD4 T cells (TFH). *Annual review of immunology* **29**: 621-663.

Cusanovich DA, Daza R, Adey A, Pliner HA, Christiansen L, Gunderson KL, Steemers FJ, Trapnell C, Shendure J. 2015. Multiplex single cell profiling of chromatin accessibility by combinatorial cellular indexing. *Science* **348**: 910-914.

Cusanovich DA, Hill AJ, Aghamirzaie D, Daza RM, Pliner HA, Berletch JB, Filippova GN, Huang X, Christiansen L, DeWitt WS et al. 2018. A Single-Cell Atlas of In Vivo Mammalian Chromatin Accessibility. *Cell* **174**: 1309-1324 e1318.

d'Adda di Fagagna F. 2014. A direct role for small non-coding RNAs in DNA damage response. *Trends in cell biology* **24**: 171-178.

D'Angelo MA. 2018. Nuclear pore complexes as hubs for gene regulation. *Nucleus* **9**: 142-148.

de Wit E, Bouwman BA, Zhu Y, Klous P, Splinter E, Verstegen MJ, Krijger PH, Festuccia N, Nora EP, Welling M et al. 2013. The pluripotent genome in three dimensions is shaped around pluripotency factors. *Nature* **501**: 227-231.

de Wit E, Vos ES, Holwerda SJ, Valdes-Quezada C, Verstegen MJ, Teunissen H, Splinter E, Wijchers PJ, Krijger PH, de Laat W. 2015. CTCF Binding Polarity Determines Chromatin Looping. *Molecular cell* **60**: 676-684.

Dechat T, Adam SA, Taimen P, Shimi T, Goldman RD. 2010. Nuclear lamins. *Cold Spring Harbor perspectives in biology* **2**: a000547.

Dekker J. 2006. The three 'C' s of chromosome conformation capture: controls, controls, controls. *Nature methods* **3**: 17-21.

Dekker J, Heard E. 2015. Structural and functional diversity of Topologically Associating Domains. *FEBS letters* **589**: 2877-2884.

Dekker J, Misteli T. 2015. Long-Range Chromatin Interactions. *Cold Spring Harbor perspectives in biology* **7**: a019356.

Dekker J, Rippe K, Dekker M, Kleckner N. 2002. Capturing chromosome conformation. *Science* **295**: 1306-1311.

Deligianni C, Spilianakis CG. 2012. Long-range genomic interactions epigenetically regulate the expression of a cytokine receptor. *EMBO reports* **13**: 819-826.

Deng L, Ren R, Liu Z, Song M, Li J, Wu Z, Ren X, Fu L, Li W, Zhang W et al. 2019. Stabilizing heterochromatin by DGCR8 alleviates senescence and osteoarthritis. *Nature communications* **10**: 3329.

Deng Q, Ramskold D, Reinius B, Sandberg R. 2014a. Single-cell RNA-seq reveals dynamic, random monoallelic gene expression in mammalian cells. *Science* **343**: 193-196.

Deng W, Lee J, Wang H, Miller J, Reik A, Gregory PD, Dean A, Blobel GA. 2012. Controlling long-range genomic interactions at a native locus by targeted tethering of a looping factor. *Cell* **149**: 1233-1244.

Deng W, Rupon JW, Krivega I, Breda L, Motta I, Jahn KS, Reik A, Gregory PD, Rivella S, Dean A et al. 2014b. Reactivation of developmentally silenced globin genes by forced chromatin looping. *Cell* **158**: 849-860.

Denholtz M, Bonora G, Chronis C, Splinter E, de Laat W, Ernst J, Pellegrini M, Plath K. 2013. Long-range chromatin contacts in embryonic stem cells reveal a role for pluripotency factors and polycomb proteins in genome organization. *Cell stem cell* **13**: 602-616.

Dillon N. 2008. The impact of gene location in the nucleus on transcriptional regulation. *Developmental cell* **15**: 182-186.

Dittmer TA, Misteli T. 2011. The lamin protein family. *Genome biology* **12**: 222.

Dixon JR, Jung I, Selvaraj S, Shen Y, Antosiewicz-Bourget JE, Lee AY, Ye Z, Kim A, Rajagopal N, Xie W et al. 2015. Chromatin architecture reorganization during stem cell differentiation. *Nature* **518**: 331-336.

Dixon JR, Selvaraj S, Yue F, Kim A, Li Y, Shen Y, Hu M, Liu JS, Ren B. 2012. Topological domains in mammalian genomes identified by analysis of chromatin interactions. *Nature* **485**: 376-380.

Dooley J, Linterman MA, Liston A. 2013. MicroRNA regulation of T-cell development. *Immunological reviews* **253**: 53-64.

Dostie J, Richmond TA, Arnaout RA, Selzer RR, Lee WL, Honan TA, Rubio ED, Krumm A, Lamb J, Nusbaum C et al. 2006. Chromosome Conformation Capture Carbon Copy (5C): a massively parallel solution for mapping interactions between genomic elements. *Genome research* **16**: 1299-1309.

Drissen R, Palstra RJ, Gillemans N, Splinter E, Grosveld F, Philipsen S, de Laat W. 2004. The active spatial organization of the beta-globin locus requires the transcription factor EKLF. *Genes & development* **18**: 2485-2490.

Duan Z, Andronescu M, Schutz K, McIlwain S, Kim YJ, Lee C, Shendure J, Fields S, Blau CA, Noble WS. 2010. A three-dimensional model of the yeast genome. *Nature* **465**: 363-367.

Ea V, Baudement MO, Lesne A, Forne T. 2015. Contribution of Topological Domains and Loop Formation to 3D Chromatin Organization. *Genes* **6**: 734-750.

Ebert PJ, Jiang S, Xie J, Li QJ, Davis MM. 2009. An endogenous positively selecting peptide enhances mature T cell responses and becomes an autoantigen in the absence of microRNA miR-181a. *Nature immunology* **10**: 1162-1169.

Elbashir SM, Harborth J, Lendeckel W, Yalcin A, Weber K, Tuschl T. 2001. Duplexes of 21-nucleotide RNAs mediate RNA interference in cultured mammalian cells. *Nature* **411**: 494-498.

Elkord E. 2014. Thymus-Derived, Peripherally Derived, and in vitro-Induced T Regulatory Cells. *Frontiers in immunology* **5**: 17.

Ender C, Krek A, Friedlander MR, Beitzinger M, Weinmann L, Chen W, Pfeffer S, Rajewsky N, Meister G. 2008. A human snoRNA with microRNA-like functions. *Molecular cell* **32**: 519-528.

Fabian MR, Sonenberg N. 2012. The mechanics of miRNA-mediated gene silencing: a look under the hood of miRISC. *Nature structural & molecular biology* **19**: 586-593.

Fabian MR, Sonenberg N, Filipowicz W. 2010. Regulation of mRNA translation and stability by microRNAs. *Annual review of biochemistry* **79**: 351-379.

Fan W, Liang D, Tang Y, Qu B, Cui H, Luo X, Huang X, Chen S, Higgs BW, Jallal B et al. 2012. Identification of microRNA-31 as a novel regulator contributing to impaired interleukin-2 production in T cells from patients with systemic lupus erythematosus. *Arthritis and rheumatism* **64**: 3715-3725.

Feng S, Cokus SJ, Schubert V, Zhai J, Pellegrini M, Jacobsen SE. 2014. Genome-wide Hi-C analyses in wild-type and mutants reveal high-resolution chromatin interactions in Arabidopsis. *Molecular cell* **55**: 694-707.

Ferraiuolo MA, Sanyal A, Naumova N, Dekker J, Dostie J. 2012. From cells to chromatin: capturing snapshots of genome organization with 5C technology. *Methods* **58**: 255-267.

Filippova GN, Fagerlie S, Klenova EM, Myers C, Dehner Y, Goodwin G, Neiman PE, Collins SJ, Lobanenkov VV. 1996. An exceptionally conserved transcriptional repressor, CTCF, employs different combinations of zinc fingers to bind diverged promoter sequences of avian and mammalian c-myc oncogenes. *Molecular and cellular biology* **16**: 2802-2813.

Finlan LE, Sproul D, Thomson I, Boyle S, Kerr E, Perry P, Ylstra B, Chubb JR, Bickmore WA. 2008. Recruitment to the nuclear periphery can alter expression of genes in human cells. *PLoS genetics* **4**: e1000039.

Fire A, Xu S, Montgomery MK, Kostas SA, Driver SE, Mello CC. 1998. Potent and specific genetic interference by double-stranded RNA in Caenorhabditis elegans. *Nature* **391**: 806-811.

Fiserova J, Efenberkova M, Sieger T, Maninova M, Uhlirova J, Hozak P. 2017. Chromatin organization at the nuclear periphery as revealed by image analysis of structured illumination microscopy data. *Journal of cell science* **130**: 2066-2077.

Fitzgerald KA, Caffrey DR. 2014. Long noncoding RNAs in innate and adaptive immunity. *Current opinion in immunology* **26**: 140-146.

Flynt AS, Greimann JC, Chung WJ, Lima CD, Lai EC. 2010. MicroRNA biogenesis via splicing and exosome-mediated trimming in Drosophila. *Molecular cell* **38**: 900-907.

Ford E, Nikopoulou C, Kokkalis A, Thanos D. 2014. A method for generating highly multiplexed ChIP-seq libraries. *BMC research notes* **7**: 312.

Forstemann K, Horwich MD, Wee L, Tomari Y, Zamore PD. 2007. Drosophila microRNAs are sorted into functionally distinct argonaute complexes after production by dicer-1. *Cell* **130**: 287-297.

Fragoso R, Mao T, Wang S, Schaffert S, Gong X, Yue S, Luong R, Min H, Yashiro-Ohtani Y, Davis M et al. 2012. Modulating the strength and threshold of NOTCH oncogenic signals by mir-181a-1/b-1. *PLoS genetics* **8**: e1002855.

Frangini A, Sjoberg M, Roman-Trufero M, Dharmalingam G, Haberle V, Bartke T, Lenhard B, Malumbres M, Vidal M, Dillon N. 2013. The aurora B kinase and the polycomb protein ring1B combine to regulate active promoters in quiescent lymphocytes. *Molecular cell* **51**: 647-661.

Franks TM, McCloskey A, Shokirev MN, Benner C, Rathore A, Hetzer MW. 2017. Nup98 recruits the Wdr82-Set1A/COMPASS complex to promoters to regulate H3K4 trimethylation in hematopoietic progenitor cells. *Genes & development* **31**: 2222-2234.

Fraser J, Rousseau M, Shenker S, Ferraiuolo MA, Hayashizaki Y, Blanchette M, Dostie J. 2009. Chromatin conformation signatures of cellular differentiation. *Genome biology* **10**: R37.

Fraser P, Bickmore W. 2007. Nuclear organization of the genome and the potential for gene regulation. *Nature* **447**: 413-417.

Friedman RC, Farh KK, Burge CB, Bartel DP. 2009. Most mammalian mRNAs are conserved targets of microRNAs. *Genome research* **19**: 92-105.

Furlong EEM, Levine M. 2018. Developmental enhancers and chromosome topology. *Science* **361**: 1341-1345.

Galande S, Purbey PK, Notani D, Kumar PP. 2007. The third dimension of gene regulation: organization of dynamic chromatin loopscape by SATB1. *Current opinion in genetics & development* **17**: 408-414.

Gallo E, Katzman S, Villarino AV. 2012. IL-13-producing Th1 and Th17 cells characterize adaptive responses to both self and foreign antigens. *European journal of immunology* **42**: 2322-2328.

Gangaraju VK, Lin H. 2009. MicroRNAs: key regulators of stem cells. *Nature reviews Molecular cell biology* **10**: 116-125.

Ganji M, Shaltiel IA, Bisht S, Kim E, Kalichava A, Haering CH, Dekker C. 2018. Real-time imaging of DNA loop extrusion by condensin. *Science* **360**: 102-105.

Gavrilov AA, Gushchanskaya ES, Strelkova O, Zhironkina O, Kireev, II, Iarovaia OV, Razin SV. 2013. Disclosure of a structural milieu for the proximity ligation reveals the elusive nature of an active chromatin hub. *Nucleic acids research* **41**: 3563-3575.

Georgakilas G, Vlachos IS, Paraskevopoulou MD, Yang P, Zhang Y, Economides AN, Hatzigeorgiou AG. 2014. microTSS: accurate microRNA transcription start site identification reveals a significant number of divergent pri-miRNAs. *Nature communications* **5**: 5700.

Georgi N, Taipaleenmaki H, Raiss CC, Groen N, Portalska KJ, van Blitterswijk C, de Boer J, Post JN, van Wijnen AJ, Karperien M. 2015. MicroRNA Levels as Prognostic Markers for the Differentiation Potential of Human Mesenchymal Stromal Cell Donors. *Stem cells and development* **24**: 1946-1955.

Germain RN. 2002. T-cell development and the CD4-CD8 lineage decision. *Nature reviews Immunology* **2**: 309-322.

Gilbert DM, Takebayashi SI, Ryba T, Lu J, Pope BD, Wilson KA, Hiratani I. 2010. Space and time in the nucleus: developmental control of replication timing and chromosome architecture. *Cold Spring Harbor symposia on quantitative biology* **75**: 143-153.

Giles KE, Gowher H, Ghirlando R, Jin C, Felsenfeld G. 2010. Chromatin boundaries, insulators, and long-range interactions in the nucleus. *Cold Spring Harbor symposia on quantitative biology* **75**: 79-85.

Griffith OL, Montgomery SB, Bernier B, Chu B, Kasaian K, Aerts S, Mahony S, Sleumer MC, Bilenky M, Haeussler M et al. 2008. ORegAnno: an open-access community-driven resource for regulatory annotation. *Nucleic acids research* **36**: D107-113.

Griffiths-Jones S, Saini HK, van Dongen S, Enright AJ. 2008. miRBase: tools for microRNA genomics. *Nucleic acids research* **36**: D154-158.

Grigoryev YA, Kurian SM, Hart T, Nakorchevsky AA, Chen C, Campbell D, Head SR, Yates JR, 3rd, Salomon DR. 2011. MicroRNA regulation of molecular networks mapped by global microRNA, mRNA, and protein expression in activated T lymphocytes. *Journal of immunology* **187**: 2233-2243.

Grimson A, Srivastava M, Fahey B, Woodcroft BJ, Chiang HR, King N, Degnan BM, Rokhsar DS, Bartel DP. 2008. Early origins and evolution of microRNAs and Piwi-interacting RNAs in animals. *Nature* **455**: 1193-1197.

Gromak N, Dienstbier M, Macias S, Plass M, Eyras E, Caceres JF, Proudfoot NJ. 2013. Drosha regulates gene expression independently of RNA cleavage function. *Cell reports* **5**: 1499-1510.

Grossniklaus U, Paro R. 2014. Transcriptional silencing by polycomb-group proteins. *Cold Spring Harbor perspectives in biology* **6**: a019331.

Gruenbaum Y, Foisner R. 2015. Lamins: nuclear intermediate filament proteins with fundamental functions in nuclear mechanics and genome regulation. *Annual review of biochemistry* **84**: 131-164.

Guelen L, Pagie L, Brasset E, Meuleman W, Faza MB, Talhout W, Eussen BH, de Klein A, Wessels L, de Laat W et al. 2008. Domain organization of human chromosomes revealed by mapping of nuclear lamina interactions. *Nature* **453**: 948-951.

Guenther MG, Levine SS, Boyer LA, Jaenisch R, Young RA. 2007. A chromatin landmark and transcription initiation at most promoters in human cells. *Cell* **130**: 77-88.

Guillou E, Ibarra A, Coulon V, Casado-Vela J, Rico D, Casal I, Schwob E, Losada A, Mendez J. 2010. Cohesin organizes chromatin loops at DNA replication factories. *Genes & development* **24**: 2812-2822.

Gupta RS, Golding GB. 1996. The origin of the eukaryotic cell. *Trends in biochemical sciences* **21**: 166-171.

Ha M, Kim VN. 2014. Regulation of microRNA biogenesis. *Nature reviews Molecular cell biology* **15**: 509-524.

Haarhuis JHI, van der Weide RH, Blomen VA, Yanez-Cuna JO, Amendola M, van Ruiten MS, Krijger PHL, Teunissen H, Medema RH, van Steensel B et al. 2017. The Cohesin Release Factor WAPL Restricts Chromatin Loop Extension. *Cell* **169**: 693-707 e614.

Hadjimichael C, Nikolaou C, Papamatheakis J, Kretsovali A. 2016. MicroRNAs for Fine-Tuning of Mouse Embryonic Stem Cell Fate Decision through Regulation of TGF-beta Signaling. *Stem cell reports* **6**: 292-301.

Hadjur S, Williams LM, Ryan NK, Cobb BS, Sexton T, Fraser P, Fisher AG, Merkenschlager M. 2009. Cohesins form chromosomal cis-interactions at the developmentally regulated IFNG locus. *Nature* **460**: 410-413.

Hagege H, Klous P, Braem C, Splinter E, Dekker J, Cathala G, de Laat W, Forne T. 2007. Quantitative analysis of chromosome conformation capture assays (3C-qPCR). *Nature protocols* **2**: 1722-1733.

Hamilton AJ, Baulcombe DC. 1999. A species of small antisense RNA in posttranscriptional gene silencing in plants. *Science* **286**: 950-952.

Hammond SM, Boettcher S, Caudy AA, Kobayashi R, Hannon GJ. 2001. Argonaute2, a link between genetic and biochemical analyses of RNAi. *Science* **293**: 1146-1150.

Han J, Lee Y, Yeom KH, Nam JW, Heo I, Rhee JK, Sohn SY, Cho Y, Zhang BT, Kim VN. 2006. Molecular basis for the recognition of primary microRNAs by the Drosha-DGCR8 complex. *Cell* **125**: 887-901.

Han J, Pedersen JS, Kwon SC, Belair CD, Kim YK, Yeom KH, Yang WY, Haussler D, Blelloch R, Kim VN. 2009. Posttranscriptional crossregulation between Drosha and DGCR8. *Cell* **136**: 75-84.

Han YC, Vidigal JA, Mu P, Yao E, Singh I, Gonzalez AJ, Concepcion CP, Bonetti C, Ogrodowski P, Carver B et al. 2015. An allelic series of miR-17 approximately 92-mutant mice uncovers functional specialization and cooperation among members of a microRNA polycistron. *Nature genetics* **47**: 766-775.

Hansen AS, Pustova I, Cattoglio C, Tjian R, Darzacq X. 2017. CTCF and cohesin regulate chromatin loop stability with distinct dynamics. *eLife* **6**.

Hao B, Naik AK, Watanabe A, Tanaka H, Chen L, Richards HW, Kondo M, Taniuchi I, Kohwi Y, Kohwi-Shigematsu T et al. 2015. An anti-silencer- and SATB1-dependent chromatin hub regulates Rag1 and Rag2 gene expression during thymocyte development. *The Journal of experimental medicine* **212**: 809-824.

Hark AT, Schoenherr CJ, Katz DJ, Ingram RS, Levorse JM, Tilghman SM. 2000. CTCF mediates methylation-sensitive enhancer-blocking activity at the H19/Igf2 locus. *Nature* **405**: 486-489.

Harr JC, Luperchio TR, Wong X, Cohen E, Wheelan SJ, Reddy KL. 2015. Directed targeting of chromatin to the nuclear lamina is mediated by chromatin state and A-type lamins. *The Journal of cell biology* **208**: 33-52.

Harwig A, Jongejan A, van Kampen AH, Berkhout B, Das AT. 2016. Tat-dependent production of an HIV-1 TAR-encoded miRNA-like small RNA. *Nucleic acids research* **44**: 4340-4353.

Havens MA, Reich AA, Duelli DM, Hastings ML. 2012. Biogenesis of mammalian microRNAs by a non-canonical processing pathway. *Nucleic acids research* **40**: 4626-4640.

He C, Li Z, Chen P, Huang H, Hurst LD, Chen J. 2012. Young intragenic miRNAs are less coexpressed with host genes than old ones: implications of miRNA-host gene coevolution. *Nucleic acids research* **40**: 4002-4012.

He X, Park K, Wang H, He X, Zhang Y, Hua X, Li Y, Kappes DJ. 2008. CD4-CD8 lineage commitment is regulated by a silencer element at the ThPOK transcription-factor locus. *Immunity* **28**: 346-358.

Hegazy AN, Peine M, Helmstetter C, Panse I, Frohlich A, Bergthaler A, Flatz L, Pinschewer DD, Radbruch A, Lohning M. 2010. Interferons direct Th2 cell reprogramming to generate a

stable GATA-3(+)T-bet(+) cell subset with combined Th2 and Th1 cell functions. *Immunity* **32**: 116-128.

Henao-Mejia J, Williams A, Goff LA, Staron M, Licona-Limon P, Kaech SM, Nakayama M, Rinn JL, Flavell RA. 2013. The microRNA miR-181 is a critical cellular metabolic rheostat essential for NKT cell ontogenesis and lymphocyte development and homeostasis. *Immunity* **38**: 984-997.

Hertel J, Bartschat S, Wintsche A, Otto C, Students of the Bioinformatics Computer L, Stadler PF. 2012. Evolution of the let-7 microRNA family. *RNA biology* **9**: 231-241.

Hirano Y, Hizume K, Kimura H, Takeyasu K, Haraguchi T, Hiraoka Y. 2012. Lamin B receptor recognizes specific modifications of histone H4 in heterochromatin formation. *The Journal of biological chemistry* **287**: 42654-42663.

Hiratani I, Ryba T, Itoh M, Yokochi T, Schwaiger M, Chang CW, Lyou Y, Townes TM, Schubeler D, Gilbert DM. 2008. Global reorganization of replication domains during embryonic stem cell differentiation. *PLoS biology* **6**: e245.

Hogquist KA, Jameson SC. 2014. The self-obsession of T cells: how TCR signaling thresholds affect fate 'decisions' and effector function. *Nature immunology* **15**: 815-823.

Horike S, Cai S, Miyano M, Cheng JF, Kohwi-Shigematsu T. 2005. Loss of silent-chromatin looping and impaired imprinting of DLX5 in Rett syndrome. *Nature genetics* **37**: 31-40.

Hosoya T, Kuroha T, Moriguchi T, Cummings D, Maillard I, Lim KC, Engel JD. 2009. GATA-3 is required for early T lineage progenitor development. *The Journal of experimental medicine* **206**: 2987-3000.

Hu G, Cui K, Fang D, Hirose S, Wang X, Wangsa D, Jin W, Ried T, Liu P, Zhu J et al. 2018. Transformation of Accessible Chromatin and 3D Nucleome Underlies Lineage Commitment of Early T Cells. *Immunity* **48**: 227-242 e228.

Huang C, Liu XJ, QunZhou, Xie J, Ma TT, Meng XM, Li J. 2016. MiR-146a modulates macrophage polarization by inhibiting Notch1 pathway in RAW264.7 macrophages. *International immunopharmacology* **32**: 46-54.

Huang P, Keller CA, Giardine B, Grevet JD, Davies JOJ, Hughes JR, Kurita R, Nakamura Y, Hardison RC, Blobel GA. 2017. Comparative analysis of three-dimensional chromosomal architecture identifies a novel fetal hemoglobin regulatory element. *Genes & development* **31**: 1704-1713.

Humphreys DT, Westman BJ, Martin DI, Preiss T. 2005. MicroRNAs control translation initiation by inhibiting eukaryotic initiation factor 4E/cap and poly(A) tail function. *Proceedings of the National Academy of Sciences of the United States of America* **102**: 16961-16966.

Hutchison N, Weintraub H. 1985. Localization of DNAase I-sensitive sequences to specific regions of interphase nuclei. *Cell* **43**: 471-482.

Hutvagner G, McLachlan J, Pasquinelli AE, Balint E, Tuschl T, Zamore PD. 2001. A cellular function for the RNA-interference enzyme Dicer in the maturation of the let-7 small temporal RNA. *Science* **293**: 834-838.

Ibarra A, Benner C, Tyagi S, Cool J, Hetzer MW. 2016a. Nucleoporin-mediated regulation of cell identity genes. *Genes & development* **30**: 2253-2258.

-. 2016b. Nucleoporin-mediated regulation of cell identity genes. *Genes & development*.

Igarashi K, Hoshino H, Muto A, Suwabe N, Nishikawa S, Nakauchi H, Yamamoto M. 1998. Multivalent DNA binding complex generated by small Maf and Bach1 as a possible

biochemical basis for beta-globin locus control region complex. *The Journal of biological chemistry* **273**: 11783-11790.

Ikegami K, Egelhofer TA, Strome S, Lieb JD. 2010. Caenorhabditis elegans chromosome arms are anchored to the nuclear membrane via discontinuous association with LEM-2. *Genome biology* **11**: R120.

Imakaev M, Fudenberg G, McCord RP, Naumova N, Goloborodko A, Lajoie BR, Dekker J, Mirny LA. 2012. Iterative correction of Hi-C data reveals hallmarks of chromosome organization. *Nature methods* **9**: 999-1003.

Isik M, Korswagen HC, Berezikov E. 2010. Expression patterns of intronic microRNAs in Caenorhabditis elegans. *Silence* **1**: 5.

Issuree PD, Day K, Au C, Raviram R, Zappile P, Skok JA, Xue HH, Myers RM, Littman DR. 2018. Stage-specific epigenetic regulation of CD4 expression by coordinated enhancer elements during T cell development. *Nature communications* **9**: 3594.

Jacinto FV, Benner C, Hetzer MW. 2015. The nucleoporin Nup153 regulates embryonic stem cell pluripotency through gene silencing. *Genes & development* **29**: 1224-1238.

Jeker LT, Bluestone JA. 2010. Small RNA regulators of T cell-mediated autoimmunity. *Journal of clinical immunology* **30**: 347-357.

-. 2013. MicroRNA regulation of T-cell differentiation and function. *Immunological reviews* **253**: 65-81.

Jeong G, Lim YH, Kim YK. 2016. Precise mapping of the transcription start sites of human microRNAs using DROSHA knockout cells. *BMC genomics* **17**: 908.

Ji X, Dadon DB, Powell BE, Fan ZP, Borges-Rivera D, Shachar S, Weintraub AS, Hnisz D, Pegoraro G, Lee TI et al. 2016. 3D Chromosome Regulatory Landscape of Human Pluripotent Cells. *Cell stem cell* **18**: 262-275.

Jin W, Tang Q, Wan M, Cui K, Zhang Y, Ren G, Ni B, Sklar J, Przytycka TM, Childs R et al. 2015. Genome-wide detection of DNase I hypersensitive sites in single cells and FFPE tissue samples. *Nature* **528**: 142-146.

Johanson TM, Keown AA, Cmero M, Yeo JH, Kumar A, Lew AM, Zhan Y, Chong MM. 2015. Drosha controls dendritic cell development by cleaving messenger RNAs encoding inhibitors of myelopoiesis. *Nature immunology* **16**: 1134-1141.

Jost KL, Haase S, Smeets D, Schrode N, Schmiedel JM, Bertulat B, Herzel H, Cremer M, Cardoso MC. 2011. 3D-Image analysis platform monitoring relocation of pluripotency genes during reprogramming. *Nucleic acids research* **39**: e113.

Kalverda B, Pickersgill H, Shloma VV, Fornerod M. 2010. Nucleoporins directly stimulate expression of developmental and cell-cycle genes inside the nucleoplasm. *Cell* **140**: 360-371.

Kaneko H, Dridi S, Tarallo V, Gelfand BD, Fowler BJ, Cho WG, Kleinman ME, Ponicsan SL, Hauswirth WW, Chiodo VA et al. 2011. DICER1 deficit induces Alu RNA toxicity in age-related macular degeneration. *Nature* **471**: 325-330.

Katainen R, Dave K, Pitkanen E, Palin K, Kivioja T, Valimaki N, Gylfe AE, Ristolainen H, Hanninen UA, Cajuso T et al. 2015. CTCF/cohesin-binding sites are frequently mutated in cancer. *Nature genetics* **47**: 818-821.

Kawamata T, Seitz H, Tomari Y. 2009. Structural determinants of miRNAs for RISC loading and slicer-independent unwinding. *Nature structural & molecular biology* **16**: 953-960.

Kawamata T, Tomari Y. 2010. Making RISC. *Trends in biochemical sciences* **35**: 368-376.

Ketting RF, Fischer SE, Bernstein E, Sijen T, Hannon GJ, Plasterk RH. 2001. Dicer functions in RNA interference and in synthesis of small RNA involved in developmental timing in C. elegans. *Genes & development* **15**: 2654-2659.

Khvorova A, Reynolds A, Jayasena SD. 2003. Functional siRNAs and miRNAs exhibit strand bias. *Cell* **115**: 209-216.

Kim B, Jeong K, Kim VN. 2017. Genome-wide Mapping of DROSHA Cleavage Sites on Primary MicroRNAs and Noncanonical Substrates. *Molecular cell* **66**: 258-269 e255.

Kim DH, Saetrom P, Snove O, Jr., Rossi JJ. 2008. MicroRNA-directed transcriptional gene silencing in mammalian cells. *Proceedings of the National Academy of Sciences of the United States of America* **105**: 16230-16235.

Kim S, Shendure J. 2019. Mechanisms of Interplay between Transcription Factors and the 3D Genome. *Molecular cell* **76**: 306-319.

Kim SH, McQueen PG, Lichtman MK, Shevach EM, Parada LA, Misteli T. 2004. Spatial genome organization during T-cell differentiation. *Cytogenetic and genome research* **105**: 292-301.

Kim VN, Han J, Siomi MC. 2009. Biogenesis of small RNAs in animals. *Nature reviews Molecular cell biology* **10**: 126-139.

Kim YK, Kim B, Kim VN. 2016. Re-evaluation of the roles of DROSHA, Export in 5, and DICER in microRNA biogenesis. *Proceedings of the National Academy of Sciences of the United States of America* **113**: E1881-1889.

Kim YK, Kim VN. 2007. Processing of intronic microRNAs. *The EMBO journal* **26**: 775-783.

Kind J, Pagie L, de Vries SS, Nahidiazar L, Dey SS, Bienko M, Zhan Y, Lajoie B, de Graaf CA, Amendola M et al. 2015. Genome-wide maps of nuclear lamina interactions in single human cells. *Cell* **163**: 134-147.

Kluiver J, Kroesen BJ, Poppema S, van den Berg A. 2006. The role of microRNAs in normal hematopoiesis and hematopoietic malignancies. *Leukemia* **20**: 1931-1936.

Knight SW, Bass BL. 2001. A role for the RNase III enzyme DCR-1 in RNA interference and germ line development in Caenorhabditis elegans. *Science* **293**: 2269-2271.

Knuckles P, Vogt MA, Lugert S, Milo M, Chong MM, Hautbergue GM, Wilson SA, Littman DR, Taylor V. 2012. Drosha regulates neurogenesis by controlling neurogenin 2 expression independent of microRNAs. *Nature neuroscience* **15**: 962-969.

Koch U, Radtke F. 2011. Mechanisms of T cell development and transformation. *Annual review of cell and developmental biology* **27**: 539-562.

Koeman JM, Russell RC, Tan MH, Petillo D, Westphal M, Koelzer K, Metcalf JL, Zhang Z, Matsuda D, Dykema KJ et al. 2008. Somatic pairing of chromosome 19 in renal oncocytoma is associated with deregulated EGLN2-mediated [corrected] oxygen-sensing response. *PLoS genetics* **4**: e1000176.

Komatsu N, Mariotti-Ferrandiz ME, Wang Y, Malissen B, Waldmann H, Hori S. 2009. Heterogeneity of natural Foxp3+ T cells: a committed regulatory T-cell lineage and an uncommitted minor population retaining plasticity. *Proceedings of the National Academy of Sciences of the United States of America* **106**: 1903-1908.

Kondo M, Tanaka Y, Kuwabara T, Naito T, Kohwi-Shigematsu T, Watanabe A. 2016. SATB1 Plays a Critical Role in Establishment of Immune Tolerance. *Journal of immunology* **196**: 563-572.

Korfali N, Wilkie GS, Swanson SK, Srsen V, de Las Heras J, Batrakou DG, Malik P, Zuleger N, Kerr AR, Florens L et al. 2012. The nuclear envelope proteome differs notably between tissues. *Nucleus* **3**: 552-564.

Korn T, Bettelli E, Oukka M, Kuchroo VK. 2009. IL-17 and Th17 Cells. *Annual review of immunology* **27**: 485-517.

Kozomara A, Griffiths-Jones S. 2014. miRBase: annotating high confidence microRNAs using deep sequencing data. *Nucleic acids research* **42**: D68-73.

Ktistaki E, Garefalaki A, Williams A, Andrews SR, Bell DM, Foster KE, Spilianakis CG, Flavell RA, Kosyakova N, Trifonov V et al. 2010. CD8 locus nuclear dynamics during thymocyte development. *Journal of immunology* **184**: 5686-5695.

Kumar PP, Bischof O, Purbey PK, Notani D, Urlaub H, Dejean A, Galande S. 2007. Functional interaction between PML and SATB1 regulates chromatin-loop architecture and transcription of the MHC class I locus. *Nature cell biology* **9**: 45-56.

Kumar PP, Purbey PK, Ravi DS, Mitra D, Galande S. 2005. Displacement of SATB1-bound histone deacetylase 1 corepressor by the human immunodeficiency virus type 1 transactivator induces expression of interleukin-2 and its receptor in T cells. *Molecular and cellular biology* **25**: 1620-1633.

Kumaran RI, Spector DL. 2008. A genetic locus targeted to the nuclear periphery in living cells maintains its transcriptional competence. *The Journal of cell biology* **180**: 51-65.

Kung JT, Kesner B, An JY, Ahn JY, Cifuentes-Rojas C, Colognori D, Jeon Y, Szanto A, del Rosario BC, Pinter SF et al. 2015. Locus-specific targeting to the X chromosome revealed by the RNA interactome of CTCF. *Molecular cell* **57**: 361-375.

Kupper K, Kolbl A, Biener D, Dittrich S, von Hase J, Thormeyer T, Fiegler H, Carter NP, Speicher MR, Cremer T et al. 2007. Radial chromatin positioning is shaped by local gene density, not by gene expression. *Chromosoma* **116**: 285-306.

Kwon SC, Nguyen TA, Choi YG, Jo MH, Hohng S, Kim VN, Woo JS. 2016. Structure of Human DROSHA. *Cell* **164**: 81-90.

Labbaye C, Testa U. 2012. The emerging role of MIR-146A in the control of hematopoiesis, immune function and cancer. *Journal of hematology & oncology* **5**: 13.

Lai B, Gao W, Cui K, Xie W, Tang Q, Jin W, Hu G, Ni B, Zhao K. 2018. Principles of nucleosome organization revealed by single-cell micrococcal nuclease sequencing. *Nature* **562**: 281-285.

Lai F, Orom UA, Cesaroni M, Beringer M, Taatjes DJ, Blobel GA, Shiekhattar R. 2013. Activating RNAs associate with Mediator to enhance chromatin architecture and transcription. *Nature* **494**: 497-501.

Lajoie BR, van Berkum NL, Sanyal A, Dekker J. 2009. My5C: web tools for chromosome conformation capture studies. *Nature methods* **6**: 690-691.

Lambert SA, Jolma A, Campitelli LF, Das PK, Yin Y, Albu M, Chen X, Taipale J, Hughes TR, Weirauch MT. 2018. The Human Transcription Factors. *Cell* **175**: 598-599.

Lanctot C, Cheutin T, Cremer M, Cavalli G, Cremer T. 2007. Dynamic genome architecture in the nuclear space: regulation of gene expression in three dimensions. *Nature reviews Genetics* **8**: 104-115.

Lang MF, Shi Y. 2012. Dynamic Roles of microRNAs in Neurogenesis. *Frontiers in neuroscience* **6**: 71.

Langmead B, Salzberg SL. 2012. Fast gapped-read alignment with Bowtie 2. *Nature methods* **9**: 357-359.

Lee JT. 2000. Disruption of imprinted X inactivation by parent-of-origin effects at Tsix. *Cell* **103**: 17-27.

Lee RC, Feinbaum RL, Ambros V. 1993. The C. elegans heterochronic gene lin-4 encodes small RNAs with antisense complementarity to lin-14. *Cell* **75**: 843-854.

Lee Y, Kim M, Han J, Yeom KH, Lee S, Baek SH, Kim VN. 2004a. MicroRNA genes are transcribed by RNA polymerase II. *The EMBO journal* **23**: 4051-4060.

Lee Y, Kim VN. 2007. In vitro and in vivo assays for the activity of Drosha complex. *Methods in enzymology* **427**: 89-106.

Lee YK, Turner H, Maynard CL, Oliver JR, Chen D, Elson CO, Weaver CT. 2009. Late developmental plasticity in the T helper 17 lineage. *Immunity* **30**: 92-107.

Lee YS, Dutta A. 2009. MicroRNAs in cancer. *Annual review of pathology* **4**: 199-227.

Lee YS, Nakahara K, Pham JW, Kim K, He Z, Sontheimer EJ, Carthew RW. 2004b. Distinct roles for Drosophila Dicer-1 and Dicer-2 in the siRNA/miRNA silencing pathways. *Cell* **117**: 69-81.

Levantini E, Lee S, Radomska HS, Hetherington CJ, Alberich-Jorda M, Amabile G, Zhang P, Gonzalez DA, Zhang J, Basseres DS et al. 2011. RUNX1 regulates the CD34 gene in haematopoietic stem cells by mediating interactions with a distal regulatory element. *The EMBO journal* **30**: 4059-4070.

Li G, Yu M, Lee WW, Tsang M, Krishnan E, Weyand CM, Goronzy JJ. 2012. Decline in miR-181a expression with age impairs T cell receptor sensitivity by increasing DUSP6 activity. *Nature medicine* **18**: 1518-1524.

Li QJ, Chau J, Ebert PJ, Sylvester G, Min H, Liu G, Braich R, Manoharan M, Soutschek J, Skare P et al. 2007. miR-181a is an intrinsic modulator of T cell sensitivity and selection. *Cell* **129**: 147-161.

Li Z, Rana TM. 2014. Therapeutic targeting of microRNAs: current status and future challenges. *Nature reviews Drug discovery* **13**: 622-638.

Liang T, Guo L, Liu C. 2012. Genome-wide analysis of mir-548 gene family reveals evolutionary and functional implications. *Journal of biomedicine & biotechnology* **2012**: 679563.

Liang Y, Franks TM, Marchetto MC, Gage FH, Hetzer MW. 2013. Dynamic association of NUP98 with the human genome. *PLoS genetics* **9**: e1003308.

Lichter P, Cremer T, Tang CJ, Watkins PC, Manuelidis L, Ward DC. 1988. Rapid detection of human chromosome 21 aberrations by in situ hybridization. *Proceedings of the National Academy of Sciences of the United States of America* **85**: 9664-9668.

Lieberman-Aiden E, van Berkum NL, Williams L, Imakaev M, Ragoczy T, Telling A, Amit I, Lajoie BR, Sabo PJ, Dorschner MO et al. 2009. Comprehensive mapping of long-range interactions reveals folding principles of the human genome. *Science* **326**: 289-293.

Light WH, Brickner DG, Brand VR, Brickner JH. 2010. Interaction of a DNA zip code with the nuclear pore complex promotes H2A.Z incorporation and INO1 transcriptional memory. *Molecular cell* **40**: 112-125.

Liu H, Huang J, Wang J, Jiang S, Bailey AS, Goldman DC, Welcker M, Bedell V, Slovak ML, Clurman B et al. 2008. Transvection mediated by the translocated cyclin D1 locus in mantle cell lymphoma. *The Journal of experimental medicine* **205**: 1843-1858.

Liu Z, Fan H, Jiang S. 2013. CD4(+) T-cell subsets in transplantation. *Immunological reviews* **252**: 183-191.

Llaurado M, Majem B, Altadill T, Lanau L, Castellvi J, Sanchez-Iglesias JL, Cabrera S, De la Torre J, Diaz-Feijoo B, Perez-Benavente A et al. 2014. MicroRNAs as prognostic markers in ovarian cancer. *Molecular and cellular endocrinology* **390**: 73-84.

Lomvardas S, Barnea G, Pisapia DJ, Mendelsohn M, Kirkland J, Axel R. 2006. Interchromosomal interactions and olfactory receptor choice. *Cell* **126**: 403-413.

Love PE, Warzecha C, Li L. 2014. Ldb1 complexes: the new master regulators of erythroid gene transcription. *Trends in genetics : TIG* **30**: 1-9.

Lu J, Getz G, Miska EA, Alvarez-Saavedra E, Lamb J, Peck D, Sweet-Cordero A, Ebert BL, Mak RH, Ferrando AA et al. 2005. MicroRNA expression profiles classify human cancers. *Nature* **435**: 834-838.

Lu LF, Boldin MP, Chaudhry A, Lin LL, Taganov KD, Hanada T, Yoshimura A, Baltimore D, Rudensky AY. 2010. Function of miR-146a in controlling Treg cell-mediated regulation of Th1 responses. *Cell* **142**: 914-929.

Lu LF, Thai TH, Calado DP, Chaudhry A, Kubo M, Tanaka K, Loeb GB, Lee H, Yoshimura A, Rajewsky K et al. 2009. Foxp3-dependent microRNA155 confers competitive fitness to regulatory T cells by targeting SOCS1 protein. *Immunity* **30**: 80-91.

Lu M, Kawamoto H, Katsube Y, Ikawa T, Katsura Y. 2002. The common myelolymphoid progenitor: a key intermediate stage in hemopoiesis generating T and B cells. *Journal of immunology* **169**: 3519-3525.

Lujambio A, Lowe SW. 2012. The microcosmos of cancer. *Nature* **482**: 347-355.

Lund E, Guttinger S, Calado A, Dahlberg JE, Kutay U. 2004. Nuclear export of microRNA precursors. *Science* **303**: 95-98.

Luo L, Gassman KL, Petell LM, Wilson CL, Bewersdorf J, Shopland LS. 2009. The nuclear periphery of embryonic stem cells is a transcriptionally permissive and repressive compartment. *Journal of cell science* **122**: 3729-3737.

Macias S, Cordiner RA, Gautier P, Plass M, Caceres JF. 2015. DGCR8 Acts as an Adaptor for the Exosome Complex to Degrade Double-Stranded Structured RNAs. *Molecular cell* **60**: 873-885.

Macias S, Plass M, Stajuda A, Michlewski G, Eyras E, Caceres JF. 2012. DGCR8 HITS-CLIP reveals novel functions for the Microprocessor. *Nature structural & molecular biology* **19**: 760-766.

Maden BE, Hughes JM. 1997. Eukaryotic ribosomal RNA: the recent excitement in the nucleotide modification problem. *Chromosoma* **105**: 391-400.

Malhas AN, Lee CF, Vaux DJ. 2009. Lamin B1 controls oxidative stress responses via Oct-1. *The Journal of cell biology* **184**: 45-55.

Manley NR, Richie ER, Blackburn CC, Condie BG, Sage J. 2011. Structure and function of the thymic microenvironment. *Frontiers in bioscience* **16**: 2461-2477.

Mansson R, Hultquist A, Luc S, Yang L, Anderson K, Kharazi S, Al-Hashmi S, Liuba K, Thoren L, Adolfsson J et al. 2007. Molecular evidence for hierarchical transcriptional lineage priming in fetal and adult stem cells and multipotent progenitors. *Immunity* **26**: 407-419.

Manuelidis L. 1985. Individual interphase chromosome domains revealed by in situ hybridization. *Human genetics* **71**: 288-293.

Marini B, Kertesz-Farkas A, Ali H, Lucic B, Lisek K, Manganaro L, Pongor S, Luzzati R, Recchia A, Mavilio F et al. 2015. Nuclear architecture dictates HIV-1 integration site selection. *Nature* **521**: 227-231.

Marsico A, Huska MR, Lasserre J, Hu H, Vucicevic D, Musahl A, Orom U, Vingron M. 2013. PROmiRNA: a new miRNA promoter recognition method uncovers the complex regulation of intronic miRNAs. *Genome biology* **14**: R84.

Mattout A, Pike BL, Towbin BD, Bank EM, Gonzalez-Sandoval A, Stadler MB, Meister P, Gruenbaum Y, Gasser SM. 2011. An EDMD mutation in C. elegans lamin blocks muscle-specific gene relocation and compromises muscle integrity. *Current biology : CB* **21**: 1603-1614.

Maurice D, Hooper J, Lang G, Weston K. 2007. c-Myb regulates lineage choice in developing thymocytes via its target gene Gata3. *The EMBO journal* **26**: 3629-3640.

McKee BD. 2004. Homologous pairing and chromosome dynamics in meiosis and mitosis. *Biochimica et biophysica acta* **1677**: 165-180.

Mehta A, Baltimore D. 2016. MicroRNAs as regulatory elements in immune system logic. *Nature reviews Immunology* **16**: 279-294.

Mehta I, Chakraborty S, Rao BJ. 2013. IMACULAT - an open access package for the quantitative analysis of chromosome localization in the nucleus. *PloS one* **8**: e61386.

Mellert DJ, Truman JW. 2012. Transvection is common throughout the Drosophila genome. *Genetics* **191**: 1129-1141.

Merkenschlager M, Nora EP. 2016. CTCF and Cohesin in Genome Folding and Transcriptional Gene Regulation. *Annual review of genomics and human genetics* **17**: 17-43.

Merkenschlager M, Odom DT. 2013. CTCF and cohesin: linking gene regulatory elements with their targets. *Cell* **152**: 1285-1297.

Meshorer E. 2007. Chromatin in embryonic stem cell neuronal differentiation. *Histology and histopathology* **22**: 311-319.

Meshorer E, Misteli T. 2006. Chromatin in pluripotent embryonic stem cells and differentiation. *Nature reviews Molecular cell biology* **7**: 540-546.

Meuleman W, Peric-Hupkes D, Kind J, Beaudry JB, Pagie L, Kellis M, Reinders M, Wessels L, van Steensel B. 2013. Constitutive nuclear lamina-genome interactions are highly conserved and associated with A/T-rich sequence. *Genome research* **23**: 270-280.

Misteli T, Soutoglou E. 2009. The emerging role of nuclear architecture in DNA repair and genome maintenance. *Nature reviews Molecular cell biology* **10**: 243-254.

Mitchell JA, Fraser P. 2008. Transcription factories are nuclear subcompartments that remain in the absence of transcription. *Genes & development* **22**: 20-25.

Miyao T, Floess S, Setoguchi R, Luche H, Fehling HJ, Waldmann H, Huehn J, Hori S. 2012. Plasticity of Foxp3(+) T cells reflects promiscuous Foxp3 expression in conventional T cells but not reprogramming of regulatory T cells. *Immunity* **36**: 262-275.

Miyoshi K, Miyoshi T, Siomi H. 2010. Many ways to generate microRNA-like small RNAs: non-canonical pathways for microRNA production. *Molecular genetics and genomics : MGG* **284**: 95-103.

Monahan K, Horta A, Lomvardas S. 2019. LHX2- and LDB1-mediated trans interactions regulate olfactory receptor choice. *Nature* **565**: 448-453.

Monteys AM, Spengler RM, Wan J, Tecedor L, Lennox KA, Xing Y, Davidson BL. 2010. Structure and activity of putative intronic miRNA promoters. *Rna* **16**: 495-505.

Morlando M, Ballarino M, Gromak N, Pagano F, Bozzoni I, Proudfoot NJ. 2008. Primary microRNA transcripts are processed co-transcriptionally. *Nature structural & molecular biology* **15**: 902-909.

Mosmann TR, Coffman RL. 1989. TH1 and TH2 cells: different patterns of lymphokine secretion lead to different functional properties. *Annual review of immunology* **7**: 145-173.

Muljo SA, Ansel KM, Kanellopoulou C, Livingston DM, Rao A, Rajewsky K. 2005. Aberrant T cell differentiation in the absence of Dicer. *The Journal of experimental medicine* **202**: 261-269.

Nagano T, Lubling Y, Stevens TJ, Schoenfelder S, Yaffe E, Dean W, Laue ED, Tanay A, Fraser P. 2013. Single-cell Hi-C reveals cell-to-cell variability in chromosome structure. *Nature* **502**: 59-64.

Nagano T, Varnai C, Schoenfelder S, Javierre BM, Wingett SW, Fraser P. 2015. Comparison of Hi-C results using in-solution versus in-nucleus ligation. *Genome biology* **16**: 175.

Nagele RG, Freeman T, McMorrow L, Thomson Z, Kitson-Wind K, Lee H. 1999. Chromosomes exhibit preferential positioning in nuclei of quiescent human cells. *Journal of cell science* **112 (Pt 4)**: 525-535.

Nakagawa A, Shi Y, Kage-Nakadai E, Mitani S, Xue D. 2010. Caspase-dependent conversion of Dicer ribonuclease into a death-promoting deoxyribonuclease. *Science* **328**: 327-334.

Nasmyth K, Haering CH. 2009. Cohesin: its roles and mechanisms. *Annual review of genetics* **43**: 525-558.

Nativio R, Wendt KS, Ito Y, Huddleston JE, Uribe-Lewis S, Woodfine K, Krueger C, Reik W, Peters JM, Murrell A. 2009. Cohesin is required for higher-order chromatin conformation at the imprinted IGF2-H19 locus. *PLoS genetics* **5**: e1000739.

Nguyen TA, Jo MH, Choi YG, Park J, Kwon SC, Hohng S, Kim VN, Woo JS. 2015. Functional Anatomy of the Human Microprocessor. *Cell* **161**: 1374-1387.

Niwa R, Slack FJ. 2007. The evolution of animal microRNA function. *Current opinion in genetics & development* **17**: 145-150.

Noguer-Dance M, Abu-Amero S, Al-Khtib M, Lefevre A, Coullin P, Moore GE, Cavaille J. 2010. The primate-specific microRNA gene cluster (C19MC) is imprinted in the placenta. *Human molecular genetics* **19**: 3566-3582.

Nojima T, Gomes T, Grosso ARF, Kimura H, Dye MJ, Dhir S, Carmo-Fonseca M, Proudfoot NJ. 2015. Mammalian NET-Seq Reveals Genome-wide Nascent Transcription Coupled to RNA Processing. *Cell* **161**: 526-540.

Noordermeer D, de Wit E, Klous P, van de Werken H, Simonis M, Lopez-Jones M, Eussen B, de Klein A, Singer RH, de Laat W. 2011. Variegated gene expression caused by cell-specific long-range DNA interactions. *Nature cell biology* **13**: 944-951.

Nora EP, Heard E. 2010. Chromatin structure and nuclear organization dynamics during X-chromosome inactivation. *Cold Spring Harbor symposia on quantitative biology* **75**: 333-344.

Nora EP, Lajoie BR, Schulz EG, Giorgetti L, Okamoto I, Servant N, Piolot T, van Berkum NL, Meisig J, Sedat J et al. 2012. Spatial partitioning of the regulatory landscape of the X-inactivation centre. *Nature* **485**: 381-385.

Notani D, Gottimukkala KP, Jayani RS, Limaye AS, Damle MV, Mehta S, Purbey PK, Joseph J, Galande S. 2010. Global regulator SATB1 recruits beta-catenin and regulates T(H)2 differentiation in Wnt-dependent manner. *PLoS biology* **8**: e1000296.

Nozaki T, Imai R, Tanbo M, Nagashima R, Tamura S, Tani T, Joti Y, Tomita M, Hibino K, Kanemaki MT et al. 2017. Dynamic Organization of Chromatin Domains Revealed by Super-Resolution Live-Cell Imaging. *Molecular cell* **67**: 282-293 e287.

Nozawa M, Miura S, Nei M. 2012. Origins and evolution of microRNA genes in plant species. *Genome biology and evolution* **4**: 230-239.

O'Brien J, Hayder H, Zayed Y, Peng C. 2018. Overview of MicroRNA Biogenesis, Mechanisms of Actions, and Circulation. *Frontiers in endocrinology* **9**: 402.

O'Connell RM, Kahn D, Gibson WS, Round JL, Scholz RL, Chaudhuri AA, Kahn ME, Rao DS, Baltimore D. 2010. MicroRNA-155 promotes autoimmune inflammation by enhancing inflammatory T cell development. *Immunity* **33**: 607-619.

O'Connell RM, Taganov KD, Boldin MP, Cheng G, Baltimore D. 2007. MicroRNA-155 is induced during the macrophage inflammatory response. *Proceedings of the National Academy of Sciences of the United States of America* **104**: 1604-1609.

O'Malley RC, Huang SC, Song L, Lewsey MG, Bartlett A, Nery JR, Galli M, Gallavotti A, Ecker JR. 2016. Cistrome and Epicistrome Features Shape the Regulatory DNA Landscape. *Cell* **165**: 1280-1292.

O'Shea JJ, Paul WE. 2010. Mechanisms underlying lineage commitment and plasticity of helper CD4+ T cells. *Science* **327**: 1098-1102.

Oertli M, Engler DB, Kohler E, Koch M, Meyer TF, Muller A. 2011. MicroRNA-155 is essential for the T cell-mediated control of Helicobacter pylori infection and for the induction of chronic Gastritis and Colitis. *Journal of immunology* **187**: 3578-3586.

Ohlsson R, Lobanenkov V, Klenova E. 2010. Does CTCF mediate between nuclear organization and gene expression? *BioEssays : news and reviews in molecular, cellular and developmental biology* **32**: 37-50.

Ohno S, Itano K, Harada Y, Asada K, Oikawa K, Kashiwazako M, Okuyama H, Kumagai K, Takanashi M, Sudo K et al. 2016. Development of Novel Small Hairpin RNAs That do not Require Processing by Dicer or AGO2. *Molecular therapy : the journal of the American Society of Gene Therapy* **24**: 1278-1289.

Okada C, Yamashita E, Lee SJ, Shibata S, Katahira J, Nakagawa A, Yoneda Y, Tsukihara T. 2009. A high-resolution structure of the pre-microRNA nuclear export machinery. *Science* **326**: 1275-1279.

Okamura K, Hagen JW, Duan H, Tyler DM, Lai EC. 2007. The mirtron pathway generates microRNA-class regulatory RNAs in Drosophila. *Cell* **130**: 89-100.

Okamura K, Lai EC. 2010. A deathly DNase activity for dicer. *Developmental cell* **18**: 692-694.

Okamura K, Liu N, Lai EC. 2009. Distinct mechanisms for microRNA strand selection by Drosophila Argonautes. *Molecular cell* **36**: 431-444.

Otsuka S, Ellenberg J. 2018. Mechanisms of nuclear pore complex assembly - two different ways of building one molecular machine. *FEBS letters* **592**: 475-488.

Ozsolak F, Poling LL, Wang Z, Liu H, Liu XS, Roeder RG, Zhang X, Song JS, Fisher DE. 2008. Chromatin structure analyses identify miRNA promoters. *Genes & development* **22**: 3172-3183.

Palstra RJ, Simonis M, Klous P, Brasset E, Eijkelkamp B, de Laat W. 2008. Maintenance of long-range DNA interactions after inhibition of ongoing RNA polymerase II transcription. *PloS one* **3**: e1661.

Pant V, Kurukuti S, Pugacheva E, Shamsuddin S, Mariano P, Renkawitz R, Klenova E, Lobanenkov V, Ohlsson R. 2004. Mutation of a single CTCF target site within the H19 imprinting control region leads to loss of Igf2 imprinting and complex patterns of de novo methylation upon maternal inheritance. *Molecular and cellular biology* **24**: 3497-3504.

Parelho V, Hadjur S, Spivakov M, Leleu M, Sauer S, Gregson HC, Jarmuz A, Canzonetta C, Webster Z, Nesterova T et al. 2008. Cohesins functionally associate with CTCF on mammalian chromosome arms. *Cell* **132**: 422-433.

Park JH, Choi Y, Song MJ, Park K, Lee JJ, Kim HP. 2016. Dynamic Long-Range Chromatin Interaction Controls Expression of IL-21 in CD4+ T Cells. *Journal of immunology* **196**: 4378-4389.

Pascual-Garcia P, Debo B, Aleman JR, Talamas JA, Lan Y, Nguyen NH, Won KJ, Capelson M. 2017. Metazoan Nuclear Pores Provide a Scaffold for Poised Genes and Mediate Induced Enhancer-Promoter Contacts. *Molecular cell* **66**: 63-76 e66.

Pauli A, van Bemmel JG, Oliveira RA, Itoh T, Shirahige K, van Steensel B, Nasmyth K. 2010. A direct role for cohesin in gene regulation and ecdysone response in Drosophila salivary glands. *Current biology : CB* **20**: 1787-1798.

Pennacchio LA, Bickmore W, Dean A, Nobrega MA, Bejerano G. 2013. Enhancers: five essential questions. *Nature reviews Genetics* **14**: 288-295.

Penso-Dolfin L, Moxon S, Haerty W, Di Palma F. 2018. The evolutionary dynamics of microRNAs in domestic mammals. *Scientific reports* **8**: 17050.

Peric-Hupkes D, Meuleman W, Pagie L, Bruggeman SW, Solovei I, Brugman W, Graf S, Flicek P, Kerkhoven RM, van Lohuizen M et al. 2010. Molecular maps of the reorganization of genome-nuclear lamina interactions during differentiation. *Molecular cell* **38**: 603-613.

Perry MM, Williams AE, Tsitsiou E, Larner-Svensson HM, Lindsay MA. 2009. Divergent intracellular pathways regulate interleukin-1beta-induced miR-146a and miR-146b expression and chemokine release in human alveolar epithelial cells. *FEBS letters* **583**: 3349-3355.

Peters JM, Tedeschi A, Schmitz J. 2008. The cohesin complex and its roles in chromosome biology. *Genes & development* **22**: 3089-3114.

Petersen CP, Bordeleau ME, Pelletier J, Sharp PA. 2006. Short RNAs repress translation after initiation in mammalian cells. *Molecular cell* **21**: 533-542.

Petrie HT, Zuniga-Pflucker JC. 2007. Zoned out: functional mapping of stromal signaling microenvironments in the thymus. *Annual review of immunology* **25**: 649-679.

Petrovic J, Zhou Y, Fasolino M, Goldman N, Schwartz GW, Mumbach MR, Nguyen SC, Rome KS, Sela Y, Zapataro Z et al. 2019. Oncogenic Notch Promotes Long-Range Regulatory Interactions within Hyperconnected 3D Cliques. *Molecular cell* **73**: 1174-1190 e1112.

Pfeffer S, Sewer A, Lagos-Quintana M, Sheridan R, Sander C, Grasser FA, van Dyk LF, Ho CK, Shuman S, Chien M et al. 2005. Identification of microRNAs of the herpesvirus family. *Nature methods* **2**: 269-276.

Phillips-Cremins JE, Corces VG. 2013. Chromatin insulators: linking genome organization to cellular function. *Molecular cell* **50**: 461-474.

Phillips-Cremins JE, Sauria ME, Sanyal A, Gerasimova TI, Lajoie BR, Bell JS, Ong CT, Hookway TA, Guo C, Sun Y et al. 2013. Architectural protein subclasses shape 3D organization of genomes during lineage commitment. *Cell* **153**: 1281-1295.

Phillips JE, Corces VG. 2009. CTCF: master weaver of the genome. *Cell* **137**: 1194-1211.

Pickersgill H, Kalverda B, de Wit E, Talhout W, Fornerod M, van Steensel B. 2006. Characterization of the Drosophila melanogaster genome at the nuclear lamina. *Nature genetics* **38**: 1005-1014.

Pillai RS, Bhattacharyya SN, Artus CG, Zoller T, Cougot N, Basyuk E, Bertrand E, Filipowicz W. 2005. Inhibition of translational initiation by Let-7 MicroRNA in human cells. *Science* **309**: 1573-1576.

Piriyapongsa J, Jordan IK. 2007. A family of human microRNA genes from miniature inverted-repeat transposable elements. *PloS one* **2**: e203.

Pirrotta V, Li HB. 2012. A view of nuclear Polycomb bodies. *Current opinion in genetics & development* **22**: 101-109.

Pong SK, Gullerova M. 2018. Noncanonical functions of microRNA pathway enzymes - Drosha, DGCR8, Dicer and Ago proteins. *FEBS letters* **592**: 2973-2986.

Postberg J, Lipps HJ, Cremer T. 2010. Evolutionary origin of the cell nucleus and its functional architecture. *Essays in biochemistry* **48**: 1-24.

Pott S. 2017. Simultaneous measurement of chromatin accessibility, DNA methylation, and nucleosome phasing in single cells. *eLife* **6**.

Pratt AJ, MacRae IJ. 2009. The RNA-induced silencing complex: a versatile gene-silencing machine. *The Journal of biological chemistry* **284**: 17897-17901.

Purbey PK, Singh S, Notani D, Kumar PP, Limaye AS, Galande S. 2009. Acetylation-dependent interaction of SATB1 and CtBP1 mediates transcriptional repression by SATB1. *Molecular and cellular biology* **29**: 1321-1337.

Quick-Cleveland J, Jacob JP, Weitz SH, Shoffner G, Senturia R, Guo F. 2014. The DGCR8 RNA-binding heme domain recognizes primary microRNAs by clamping the hairpin. *Cell reports* **7**: 1994-2005.

Quinlan AR, Hall IM. 2010. BEDTools: a flexible suite of utilities for comparing genomic features. *Bioinformatics* **26**: 841-842.

Quinodoz S, Guttman M. 2014. Long noncoding RNAs: an emerging link between gene regulation and nuclear organization. *Trends in cell biology* **24**: 651-663.

Ragoczy T, Bender MA, Telling A, Byron R, Groudine M. 2006. The locus control region is required for association of the murine beta-globin locus with engaged transcription factories during erythroid maturation. *Genes & development* **20**: 1447-1457.

Rao SS, Huntley MH, Durand NC, Stamenova EK, Bochkov ID, Robinson JT, Sanborn AL, Machol I, Omer AD, Lander ES et al. 2014. A 3D map of the human genome at kilobase resolution reveals principles of chromatin looping. *Cell* **159**: 1665-1680.

Rao SSP, Huang SC, Glenn St Hilaire B, Engreitz JM, Perez EM, Kieffer-Kwon KR, Sanborn AL, Johnstone SE, Bascom GD, Bochkov ID et al. 2017. Cohesin Loss Eliminates All Loop Domains. *Cell* **171**: 305-320 e324.

Rawlings JS, Gatzka M, Thomas PG, Ihle JN. 2011. Chromatin condensation via the condensin II complex is required for peripheral T-cell quiescence. *The EMBO journal* **30**: 263-276.

Rawlings JS, Rosler KM, Harrison DA. 2004. The JAK/STAT signaling pathway. *Journal of cell science* **117**: 1281-1283.

Raz V, Vermolen BJ, Garini Y, Onderwater JJ, Mommaas-Kienhuis MA, Koster AJ, Young IT, Tanke H, Dirks RW. 2008. The nuclear lamina promotes telomere aggregation and centromere peripheral localization during senescence of human mesenchymal stem cells. *Journal of cell science* **121**: 4018-4028.

Razin SV, Iarovaia OV, Sjakste N, Sjakste T, Bagdoniene L, Rynditch AV, Eivazova ER, Lipinski M, Vassetzky YS. 2007. Chromatin domains and regulation of transcription. *Journal of molecular biology* **369**: 597-607.

Reddy KL, Zullo JM, Bertolino E, Singh H. 2008. Transcriptional repression mediated by repositioning of genes to the nuclear lamina. *Nature* **452**: 243-247.

Reik W, Walter J. 2001. Genomic imprinting: parental influence on the genome. *Nature reviews Genetics* **2**: 21-32.

Reinius B, Sandberg R. 2015. Random monoallelic expression of autosomal genes: stochastic transcription and allele-level regulation. *Nature reviews Genetics* **16**: 653-664.

Reynolds N, O'Shaughnessy A, Hendrich B. 2013. Transcriptional repressors: multifaceted regulators of gene expression. *Development* **140**: 505-512.

Ricci MA, Manzo C, Garcia-Parajo MF, Lakadamyali M, Cosma MP. 2015. Chromatin fibers are formed by heterogeneous groups of nucleosomes in vivo. *Cell* **160**: 1145-1158.

Roberts JT, Cardin SE, Borchert GM. 2014. Burgeoning evidence indicates that microRNAs were initially formed from transposable element sequences. *Mobile genetic elements* **4**: e29255.

Roberts TC. 2014. The MicroRNA Biology of the Mammalian Nucleus. *Molecular therapy Nucleic acids* **3**: e188.

Robson MI, de Las Heras JI, Czapiewski R, Sivakumar A, Kerr ARW, Schirmer EC. 2017. Constrained release of lamina-associated enhancers and genes from the nuclear envelope during T-cell activation facilitates their association in chromosome compartments. *Genome research* **27**: 1126-1138.

Rodewald HR. 2008. Thymus organogenesis. *Annual review of immunology* **26**: 355-388.

Rodriguez A, Griffiths-Jones S, Ashurst JL, Bradley A. 2004. Identification of mammalian microRNA host genes and transcription units. *Genome research* **14**: 1902-1910.

Rodriguez A, Vigorito E, Clare S, Warren MV, Couttet P, Soond DR, van Dongen S, Grocock RJ, Das PP, Miska EA et al. 2007. Requirement of bic/microRNA-155 for normal immune function. *Science* **316**: 608-611.

Roh TY, Cuddapah S, Cui K, Zhao K. 2006. The genomic landscape of histone modifications in human T cells. *Proceedings of the National Academy of Sciences of the United States of America* **103**: 15782-15787.

Roix JJ, McQueen PG, Munson PJ, Parada LA, Misteli T. 2003. Spatial proximity of translocation-prone gene loci in human lymphomas. *Nature genetics* **34**: 287-291.

Rolando C, Taylor V. 2017. Non-canonical post-transcriptional RNA regulation of neural stem cell potential. *Brain plasticity* **3**: 111-116.

Roth BM, Ishimaru D, Hennig M. 2013. The core microprocessor component DiGeorge syndrome critical region 8 (DGCR8) is a nonspecific RNA-binding protein. *The Journal of biological chemistry* **288**: 26785-26799.

Rottiers V, Naar AM. 2012. MicroRNAs in metabolism and metabolic disorders. *Nature reviews Molecular cell biology* **13**: 239-250.

Rousseau M, Ferraiuolo MA, Crutchley JL, Wang XQ, Miura H, Blanchette M, Dostie J. 2014. Classifying leukemia types with chromatin conformation data. *Genome biology* **15**: R60.

Ruby JG, Jan CH, Bartel DP. 2007. Intronic microRNA precursors that bypass Drosha processing. *Nature* **448**: 83-86.

Rupaimoole R, Calin GA, Lopez-Berestein G, Sood AK. 2016. miRNA Deregulation in Cancer Cells and the Tumor Microenvironment. *Cancer discovery* **6**: 235-246.

Sabari BR, Dall'Agnese A, Boija A, Klein IA, Coffey EL, Shrinivas K, Abraham BJ, Hannett NM, Zamudio AV, Manteiga JC et al. 2018. Coactivator condensation at super-enhancers links phase separation and gene control. *Science* **361**.

Saini HK, Enright AJ, Griffiths-Jones S. 2008. Annotation of mammalian primary microRNAs. *BMC genomics* **9**: 564.

Sambandam A, Maillard I, Zediak VP, Xu L, Gerstein RM, Aster JC, Pear WS, Bhandoola A. 2005. Notch signaling controls the generation and differentiation of early T lineage progenitors. *Nature immunology* **6**: 663-670.

Sanchez-Alvarez M, Sanchez-Hernandez N, Sune C. 2011. Spatial Organization and Dynamics of Transcription Elongation and Pre-mRNA Processing in Live Cells. *Genetics research international* **2011**: 626081.

Sanyal A, Lajoie BR, Jain G, Dekker J. 2012. The long-range interaction landscape of gene promoters. *Nature* **489**: 109-113.

Sati S, Cavalli G. 2017. Chromosome conformation capture technologies and their impact in understanding genome function. *Chromosoma* **126**: 33-44.

Sato T, Ohno S, Hayashi T, Sato C, Kohu K, Satake M, Habu S. 2005. Dual functions of Runx proteins for reactivating CD8 and silencing CD4 at the commitment process into CD8 thymocytes. *Immunity* **22**: 317-328.

Savova V, Patsenker J, Vigneau S, Gimelbrant AA. 2016. dbMAE: the database of autosomal monoallelic expression. *Nucleic acids research* **44**: D753-756.

Sayegh CE, Jhunjhunwala S, Riblet R, Murre C. 2005. Visualization of looping involving the immunoglobulin heavy-chain locus in developing B cells. *Genes & development* **19**: 322-327.

Schardin M, Cremer T, Hager HD, Lang M. 1985. Specific staining of human chromosomes in Chinese hamster x man hybrid cell lines demonstrates interphase chromosome territories. *Human genetics* **71**: 281-287.

Schirmer EC, Foisner R. 2007. Proteins that associate with lamins: many faces, many functions. *Experimental cell research* **313**: 2167-2179.

Schmitt AD, Hu M, Ren B. 2016. Genome-wide mapping and analysis of chromosome architecture. *Nature reviews Molecular cell biology* **17**: 743-755.

Schmitt E, Klein M, Bopp T. 2014. Th9 cells, new players in adaptive immunity. *Trends in immunology* **35**: 61-68.

Schneider R, Grosschedl R. 2007. Dynamics and interplay of nuclear architecture, genome organization, and gene expression. *Genes & development* **21**: 3027-3043.

Schoenfelder S, Sexton T, Chakalova L, Cope NF, Horton A, Andrews S, Kurukuti S, Mitchell JA, Umlauf D, Dimitrova DS et al. 2010. Preferential associations between co-regulated genes reveal a transcriptional interactome in erythroid cells. *Nature genetics* **42**: 53-61.

Schreiber KH, Kennedy BK. 2013. When lamins go bad: nuclear structure and disease. *Cell* **152**: 1365-1375.

Schwarz DS, Hutvagner G, Du T, Xu Z, Aronin N, Zamore PD. 2003. Asymmetry in the assembly of the RNAi enzyme complex. *Cell* **115**: 199-208.

Schwarzer W, Abdennur N, Goloborodko A, Pekowska A, Fudenberg G, Loe-Mie Y, Fonseca NA, Huber W, Haering CH, Mirny L et al. 2017. Two independent modes of chromatin organization revealed by cohesin removal. *Nature* **551**: 51-56.

Scott MS, Ono M. 2011. From snoRNA to miRNA: Dual function regulatory non-coding RNAs. *Biochimie* **93**: 1987-1992.

Scruggs BS, Gilchrist DA, Nechaev S, Muse GW, Burkholder A, Fargo DC, Adelman K. 2015. Bidirectional Transcription Arises from Two Distinct Hubs of Transcription Factor Binding and Active Chromatin. *Molecular cell* **58**: 1101-1112.

See YX, Wang BZ, Fullwood MJ. 2019. Chromatin Interactions and Regulatory Elements in Cancer: From Bench to Bedside. *Trends in genetics : TIG* **35**: 145-158.

Seitan VC, Hao B, Tachibana-Konwalski K, Lavagnolli T, Mira-Bontenbal H, Brown KE, Teng G, Carroll T, Terry A, Horan K et al. 2011. A role for cohesin in T-cell-receptor rearrangement and thymocyte differentiation. *Nature* **476**: 467-471.

Seitz H, Royo H, Bortolin ML, Lin SP, Ferguson-Smith AC, Cavaille J. 2004. A large imprinted microRNA gene cluster at the mouse Dlk1-Gtl2 domain. *Genome research* **14**: 1741-1748.

Seto AG, Kingston RE, Lau NC. 2007. The coming of age for Piwi proteins. *Molecular cell* **26**: 603-609.

Setoguchi R, Tachibana M, Naoe Y, Muroi S, Akiyama K, Tezuka C, Okuda T, Taniuchi I. 2008. Repression of the transcription factor Th-POK by Runx complexes in cytotoxic T cell development. *Science* **319**: 822-825.

Severin J, Waterhouse AM, Kawaji H, Lassmann T, van Nimwegen E, Balwierz PJ, de Hoon MJ, Hume DA, Carninci P, Hayashizaki Y et al. 2009. FANTOM4 EdgeExpressDB: an integrated database of promoters, genes, microRNAs, expression dynamics and regulatory interactions. *Genome biology* **10**: R39.

Sexton T, Cavalli G. 2015. The role of chromosome domains in shaping the functional genome. *Cell* **160**: 1049-1059.

Sexton T, Schober H, Fraser P, Gasser SM. 2007. Gene regulation through nuclear organization. *Nature structural & molecular biology* **14**: 1049-1055.

Sexton T, Yaffe E, Kenigsberg E, Bantignies F, Leblanc B, Hoichman M, Parrinello H, Tanay A, Cavalli G. 2012. Three-dimensional folding and functional organization principles of the Drosophila genome. *Cell* **148**: 458-472.

Shachar S, Voss TC, Pegoraro G, Sciascia N, Misteli T. 2015. Identification of Gene Positioning Factors Using High-Throughput Imaging Mapping. *Cell* **162**: 911-923.

Shaklai S, Amariglio N, Rechavi G, Simon AJ. 2007. Gene silencing at the nuclear periphery. *The FEBS journal* **274**: 1383-1392.

Shao P, Liao JY, Guan DG, Yang JH, Zheng LL, Jing Q, Zhou H, Qu LH. 2012. Drastic expression change of transposon-derived piRNA-like RNAs and microRNAs in early stages of chicken embryos implies a role in gastrulation. *RNA biology* **9**: 212-227.

Shapiro JS, Schmid S, Aguado LC, Sabin LR, Yasunaga A, Shim JV, Sachs D, Cherry S, tenOever BR. 2014. Drosha as an interferon-independent antiviral factor. *Proceedings of the National Academy of Sciences of the United States of America* **111**: 7108-7113.

Shen Q, Temple S. 2009. Fine control: microRNA regulation of adult neurogenesis. *Nature neuroscience* **12**: 369-370.

Shevelyov YY, Ulianov SV. 2019. The Nuclear Lamina as an Organizer of Chromosome Architecture. *Cells* **8**.

Shi G, Cox CA, Vistica BP, Tan C, Wawrousek EF, Gery I. 2008. Phenotype switching by inflammation-inducing polarized Th17 cells, but not by Th1 cells. *Journal of immunology* **181**: 7205-7213.

Sigova AA, Abraham BJ, Ji X, Molinie B, Hannett NM, Guo YE, Jangi M, Giallourakis CC, Sharp PA, Young RA. 2015. Transcription factor trapping by RNA in gene regulatory elements. *Science* **350**: 978-981.

Simonis M, Klous P, Splinter E, Moshkin Y, Willemsen R, de Wit E, van Steensel B, de Laat W. 2006. Nuclear organization of active and inactive chromatin domains uncovered by chromosome conformation capture-on-chip (4C). *Nature genetics* **38**: 1348-1354.

Smalheiser NR, Torvik VI. 2005. Mammalian microRNAs derived from genomic repeats. *Trends in genetics : TIG* **21**: 322-326.

So AY, Garcia-Flores Y, Minisandram A, Martin A, Taganov K, Boldin M, Baltimore D. 2012. Regulation of APC development, immune response, and autoimmunity by Bach1/HO-1 pathway in mice. *Blood* **120**: 2428-2437.

Solovei I, Kreysing M, Lanctot C, Kosem S, Peichl L, Cremer T, Guck J, Joffe B. 2009. Nuclear architecture of rod photoreceptor cells adapts to vision in mammalian evolution. *Cell* **137**: 356-368.

Sonkoly E, Stahle M, Pivarcsi A. 2008. MicroRNAs and immunity: novel players in the regulation of normal immune function and inflammation. *Seminars in cancer biology* **18**: 131-140.

Sood V, Brickner JH. 2014. Nuclear pore interactions with the genome. *Current opinion in genetics & development* **25**: 43-49.

Spector DL. 2001. Nuclear domains. *Journal of cell science* **114**: 2891-2893.

Spector DL, Lamond AI. 2011. Nuclear speckles. *Cold Spring Harbor perspectives in biology* **3**.

Spilianakis CG, Flavell RA. 2004. Long-range intrachromosomal interactions in the T helper type 2 cytokine locus. *Nature immunology* **5**: 1017-1027.

Spilianakis CG, Lalioti MD, Town T, Lee GR, Flavell RA. 2005. Interchromosomal associations between alternatively expressed loci. *Nature* **435**: 637-645.

Spitz F, Furlong EE. 2012. Transcription factors: from enhancer binding to developmental control. *Nature reviews Genetics* **13**: 613-626.

Starling S. 2017. Gene regulation: The nuclear pore - a scaffold for inducible genes. *Nature reviews Genetics* **18**: 273.

Stavreva DA, Hager GL. 2015. Chromatin structure and gene regulation: a dynamic view of enhancer function. *Nucleus* **6**: 442-448.

Steiner DF, Thomas MF, Hu JK, Yang Z, Babiarz JE, Allen CD, Matloubian M, Blelloch R, Ansel KM. 2011. MicroRNA-29 regulates T-box transcription factors and interferon-gamma production in helper T cells. *Immunity* **35**: 169-181.

Strom L, Lindroos HB, Shirahige K, Sjogren C. 2004. Postreplicative recruitment of cohesin to double-strand breaks is required for DNA repair. *Molecular cell* **16**: 1003-1015.

Su H, Trombly MI, Chen J, Wang X. 2009. Essential and overlapping functions for mammalian Argonautes in microRNA silencing. *Genes & development* **23**: 304-317.

Sun H, Palaniswamy SK, Pohar TT, Jin VX, Huang TH, Davuluri RV. 2006. MPromDb: an integrated resource for annotation and visualization of mammalian gene promoters and ChIP-chip experimental data. *Nucleic acids research* **34**: D98-103.

Suzuki HI, Young RA, Sharp PA. 2017. Super-Enhancer-Mediated RNA Processing Revealed by Integrative MicroRNA Network Analysis. *Cell* **168**: 1000-1014 e1015.

Taddei A, Van Houwe G, Hediger F, Kalck V, Cubizolles F, Schober H, Gasser SM. 2006. Nuclear pore association confers optimal expression levels for an inducible yeast gene. *Nature* **441**: 774-778.

Takahama Y. 2006. Journey through the thymus: stromal guides for T-cell development and selection. *Nature reviews Immunology* **6**: 127-135.

Tam W. 2001. Identification and characterization of human BIC, a gene on chromosome 21 that encodes a noncoding RNA. *Gene* **274**: 157-167.

Tam W, Dahlberg JE. 2006. miR-155/BIC as an oncogenic microRNA. *Genes, chromosomes & cancer* **45**: 211-212.

Tang KF, Ren H. 2012. The role of dicer in DNA damage repair. *International journal of molecular sciences* **13**: 16769-16778.

Tang Z, Luo OJ, Li X, Zheng M, Zhu JJ, Szalaj P, Trzaskoma P, Magalska A, Wlodarczyk J, Ruszczycki B et al. 2015. CTCF-Mediated Human 3D Genome Architecture Reveals Chromatin Topology for Transcription. *Cell* **163**: 1611-1627.

Taniuchi I, Osato M, Egawa T, Sunshine MJ, Bae SC, Komori T, Ito Y, Littman DR. 2002. Differential requirements for Runx proteins in CD4 repression and epigenetic silencing during T lymphocyte development. *Cell* **111**: 621-633.

Tanizawa H, Iwasaki O, Tanaka A, Capizzi JR, Wickramasinghe P, Lee M, Fu Z, Noma K. 2010. Mapping of long-range associations throughout the fission yeast genome reveals global genome organization linked to transcriptional regulation. *Nucleic acids research* **38**: 8164-8177.

Tempel S, Pollet N, Tahi F. 2012. ncRNAclassifier: a tool for detection and classification of transposable element sequences in RNA hairpins. *BMC bioinformatics* **13**: 246.

Thai TH, Calado DP, Casola S, Ansel KM, Xiao C, Xue Y, Murphy A, Frendewey D, Valenzuela D, Kutok JL et al. 2007. Regulation of the germinal center response by microRNA-155. *Science* **316**: 604-608.

Thatcher KN, Peddada S, Yasui DH, Lasalle JM. 2005. Homologous pairing of 15q11-13 imprinted domains in brain is developmentally regulated but deficient in Rett and autism samples. *Human molecular genetics* **14**: 785-797.

Therizols P, Illingworth RS, Courilleau C, Boyle S, Wood AJ, Bickmore WA. 2014. Chromatin decondensation is sufficient to alter nuclear organization in embryonic stem cells. *Science* **346**: 1238-1242.

Tian D, Sun S, Lee JT. 2010. The long noncoding RNA, Jpx, is a molecular switch for X chromosome inactivation. *Cell* **143**: 390-403.

Toda T, Hsu JY, Linker SB, Hu L, Schafer ST, Mertens J, Jacinto FV, Hetzer MW, Gage FH. 2017. Nup153 Interacts with Sox2 to Enable Bimodal Gene Regulation and Maintenance of Neural Progenitor Cells. *Cell stem cell* **21**: 618-634 e617.

Tolhuis B, Palstra RJ, Splinter E, Grosveld F, de Laat W. 2002. Looping and interaction between hypersensitive sites in the active beta-globin locus. *Molecular cell* **10**: 1453-1465.

Trifari S, Kaplan CD, Tran EH, Crellin NK, Spits H. 2009. Identification of a human helper T cell population that has abundant production of interleukin 22 and is distinct from T(H)-17, T(H)1 and T(H)2 cells. *Nature immunology* **10**: 864-871.

Tsutsumi A, Kawamata T, Izumi N, Seitz H, Tomari Y. 2011. Recognition of the pre-miRNA structure by Drosophila Dicer-1. *Nature structural & molecular biology* **18**: 1153-1158.

Upadhyaya B, Yin Y, Hill BJ, Douek DC, Prussin C. 2011. Hierarchical IL-5 expression defines a subpopulation of highly differentiated human Th2 cells. *Journal of immunology* **187**: 3111-3120.

van Bemmel JG, Pagie L, Braunschweig U, Brugman W, Meuleman W, Kerkhoven RM, van Steensel B. 2010. The insulator protein SU(HW) fine-tunes nuclear lamina interactions of the Drosophila genome. *PloS one* **5**: e15013.

Van Bortle K, Corces VG. 2012. Nuclear organization and genome function. *Annual review of cell and developmental biology* **28**: 163-187.

van de Werken HJ, de Vree PJ, Splinter E, Holwerda SJ, Klous P, de Wit E, de Laat W. 2012. 4C technology: protocols and data analysis. *Methods in enzymology* **513**: 89-112.

van Steensel B, Dekker J. 2010. Genomics tools for unraveling chromosome architecture. *Nature biotechnology* **28**: 1089-1095.

van Steensel B, Henikoff S. 2000. Identification of in vivo DNA targets of chromatin proteins using tethered dam methyltransferase. *Nature biotechnology* **18**: 424-428.

Vaquerizas JM, Suyama R, Kind J, Miura K, Luscombe NM, Akhtar A. 2010. Nuclear pore proteins nup153 and megator define transcriptionally active regions in the Drosophila genome. *PLoS genetics* **6**: e1000846.

Ventura A, Young AG, Winslow MM, Lintault L, Meissner A, Erkeland SJ, Newman J, Bronson RT, Crowley D, Stone JR et al. 2008. Targeted deletion reveals essential and overlapping functions of the miR-17 through 92 family of miRNA clusters. *Cell* **132**: 875-886.

Vidal C, Bermeo S, Fatkin D, Duque G. 2012. Role of the nuclear envelope in the pathogenesis of age-related bone loss and osteoporosis. *BoneKEy reports* **1**: 62.

Vieira KF, Levings PP, Hill MA, Crusselle VJ, Kang SH, Engel JD, Bungert J. 2004. Recruitment of transcription complexes to the beta-globin gene locus in vivo and in vitro. *The Journal of biological chemistry* **279**: 50350-50357.

Vigorito E, Kohlhaas S, Lu D, Leyland R. 2013. miR-155: an ancient regulator of the immune system. *Immunological reviews* **253**: 146-157.

Vigorito E, Perks KL, Abreu-Goodger C, Bunting S, Xiang Z, Kohlhaas S, Das PP, Miska EA, Rodriguez A, Bradley A et al. 2007. microRNA-155 regulates the generation of immunoglobulin class-switched plasma cells. *Immunity* **27**: 847-859.

Volinia S, Calin GA, Liu CG, Ambs S, Cimmino A, Petrocca F, Visone R, Iorio M, Roldo C, Ferracin M et al. 2006. A microRNA expression signature of human solid tumors defines cancer

gene targets. *Proceedings of the National Academy of Sciences of the United States of America* **103**: 2257-2261.

Volpi EV, Chevret E, Jones T, Vatcheva R, Williamson J, Beck S, Campbell RD, Goldsworthy M, Powis SH, Ragoussis J et al. 2000. Large-scale chromatin organization of the major histocompatibility complex and other regions of human chromosome 6 and its response to interferon in interphase nuclei. *Journal of cell science* **113 (Pt 9)**: 1565-1576.

Wagschal A, Rousset E, Basavarajaiah P, Contreras X, Harwig A, Laurent-Chabalier S, Nakamura M, Chen X, Zhang K, Meziane O et al. 2012. Microprocessor, Setx, Xrn2, and Rrp6 co-operate to induce premature termination of transcription by RNAPII. *Cell* **150**: 1147-1157.

Wang H, Xu X, Nguyen CM, Liu Y, Gao Y, Lin X, Daley T, Kipniss NH, La Russa M, Qi LS. 2018. CRISPR-Mediated Programmable 3D Genome Positioning and Nuclear Organization. *Cell* **175**: 1405-1417 e1414.

Wang L, Wildt KF, Zhu J, Zhang X, Feigenbaum L, Tessarollo L, Paul WE, Fowlkes BJ, Bosselut R. 2008. Distinct functions for the transcription factors GATA-3 and ThPOK during intrathymic differentiation of CD4(+) T cells. *Nature immunology* **9**: 1122-1130.

Wang Z, Yang X, Chu X, Zhang J, Zhou H, Shen Y, Long J. 2012. The structural basis for the oligomerization of the N-terminal domain of SATB1. *Nucleic acids research* **40**: 4193-4202.

Wei G, Wei L, Zhu J, Zang C, Hu-Li J, Yao Z, Cui K, Kanno Y, Roh TY, Watford WT et al. 2009. Global mapping of H3K4me3 and H3K27me3 reveals specificity and plasticity in lineage fate determination of differentiating CD4+ T cells. *Immunity* **30**: 155-167.

Wei W, Ba Z, Gao M, Wu Y, Ma Y, Amiard S, White CI, Rendtlew Danielsen JM, Yang YG, Qi Y. 2012. A role for small RNAs in DNA double-strand break repair. *Cell* **149**: 101-112.

Wei W, Pelechano V, Jarvelin AI, Steinmetz LM. 2011. Functional consequences of bidirectional promoters. *Trends in genetics : TIG* **27**: 267-276.

Weiner HL. 2001. Induction and mechanism of action of transforming growth factor-beta-secreting Th3 regulatory cells. *Immunological reviews* **182**: 207-214.

Weintraub AS, Li CH, Zamudio AV, Sigova AA, Hannett NM, Day DS, Abraham BJ, Cohen MA, Nabet B, Buckley DL et al. 2017. YY1 Is a Structural Regulator of Enhancer-Promoter Loops. *Cell* **171**: 1573-1588 e1528.

Weitzel RP, Lesniewski ML, Haviernik P, Kadereit S, Leahy P, Greco NJ, Laughlin MJ. 2009. microRNA 184 regulates expression of NFAT1 in umbilical cord blood CD4+ T cells. *Blood* **113**: 6648-6657.

Wen M, Shen Y, Shi S, Tang T. 2012. miREvo: an integrative microRNA evolutionary analysis platform for next-generation sequencing experiments. *BMC bioinformatics* **13**: 140.

West AG, Gaszner M, Felsenfeld G. 2002. Insulators: many functions, many mechanisms. *Genes & development* **16**: 271-288.

Wiblin AE, Cui W, Clark AJ, Bickmore WA. 2005. Distinctive nuclear organisation of centromeres and regions involved in pluripotency in human embryonic stem cells. *Journal of cell science* **118**: 3861-3868.

Widlak P, Kalinowska M, Parseghian MH, Lu X, Hansen JC, Garrard WT. 2005. The histone H1 C-terminal domain binds to the apoptotic nuclease, DNA fragmentation factor (DFF40/CAD) and stimulates DNA cleavage. *Biochemistry* **44**: 7871-7878.

Williams A, Spilianakis CG, Flavell RA. 2010. Interchromosomal association and gene regulation in trans. *Trends in genetics : TIG* **26**: 188-197.

Williams RR, Azuara V, Perry P, Sauer S, Dvorkina M, Jorgensen H, Roix J, McQueen P, Misteli T, Merkenschlager M et al. 2006. Neural induction promotes large-scale chromatin reorganisation of the Mash1 locus. *Journal of cell science* **119**: 132-140.

Williams RR, Broad S, Sheer D, Ragoussis J. 2002. Subchromosomal positioning of the epidermal differentiation complex (EDC) in keratinocyte and lymphoblast interphase nuclei. *Experimental cell research* **272**: 163-175.

Wilusz JE, Sharp PA. 2013. Molecular biology. A circuitous route to noncoding RNA. *Science* **340**: 440-441.

Winter J, Jung S, Keller S, Gregory RI, Diederichs S. 2009. Many roads to maturity: microRNA biogenesis pathways and their regulation. *Nature cell biology* **11**: 228-234.

Worman HJ. 2012. Nuclear lamins and laminopathies. *The Journal of pathology* **226**: 316-325.

Worman HJ, Fong LG, Muchir A, Young SG. 2009. Laminopathies and the long strange trip from basic cell biology to therapy. *The Journal of clinical investigation* **119**: 1825-1836.

Wu H, Ye C, Ramirez D, Manjunath N. 2009. Alternative processing of primary microRNA transcripts by Drosha generates 5' end variation of mature microRNA. *PloS one* **4**: e7566.

Wu L, Fan J, Belasco JG. 2006. MicroRNAs direct rapid deadenylation of mRNA. *Proceedings of the National Academy of Sciences of the United States of America* **103**: 4034-4039.

Wu S, Huang S, Ding J, Zhao Y, Liang L, Liu T, Zhan R, He X. 2010. Multiple microRNAs modulate p21Cip1/Waf1 expression by directly targeting its 3' untranslated region. *Oncogene* **29**: 2302-2308.

Wurtele H, Chartrand P. 2006. Genome-wide scanning of HoxB1-associated loci in mouse ES cells using an open-ended Chromosome Conformation Capture methodology. *Chromosome research : an international journal on the molecular, supramolecular and evolutionary aspects of chromosome biology* **14**: 477-495.

Xia W, Chen Q, Wang J, Mao Q, Dong G, Shi R, Zheng Y, Xu L, Jiang F. 2015. DNA methylation mediated silencing of microRNA-145 is a potential prognostic marker in patients with lung adenocarcinoma. *Scientific reports* **5**: 16901.

Xiao C, Srinivasan L, Calado DP, Patterson HC, Zhang B, Wang J, Henderson JM, Kutok JL, Rajewsky K. 2008. Lymphoproliferative disease and autoimmunity in mice with increased miR-17-92 expression in lymphocytes. *Nature immunology* **9**: 405-414.

Xiao ZD, Diao LT, Yang JH, Xu H, Huang MB, Deng YJ, Zhou H, Qu LH. 2013. Deciphering the transcriptional regulation of microRNA genes in humans with ACTLocater. *Nucleic acids research* **41**: e5.

Xie M, Steitz JA. 2014. Versatile microRNA biogenesis in animals and their viruses. *RNA biology* **11**: 673-681.

Xu J, Ma H, Jin J, Uttam S, Fu R, Huang Y, Liu Y. 2018. Super-Resolution Imaging of Higher-Order Chromatin Structures at Different Epigenomic States in Single Mammalian Cells. *Cell reports* **24**: 873-882.

Xu N, Tsai CL, Lee JT. 2006. Transient homologous chromosome pairing marks the onset of X inactivation. *Science* **311**: 1149-1152.

Xu W, Li JY. 2007. MicroRNA gene expression in malignant lymphoproliferative disorders. *Chinese medical journal* **120**: 996-999.

Yamauchi T, Moroishi T. 2019. Hippo Pathway in Mammalian Adaptive Immune System. *Cells* **8**.

Yang F, Deng X, Ma W, Berletch JB, Rabaia N, Wei G, Moore JM, Filippova GN, Xu J, Liu Y et al. 2015. The lncRNA Firre anchors the inactive X chromosome to the nucleolus by binding CTCF and maintains H3K27me3 methylation. *Genome biology* **16**: 52.

Yang JS, Maurin T, Robine N, Rasmussen KD, Jeffrey KL, Chandwani R, Papapetrou EP, Sadelain M, O'Carroll D, Lai EC. 2010. Conserved vertebrate mir-451 provides a platform for Dicer-independent, Ago2-mediated microRNA biogenesis. *Proceedings of the National Academy of Sciences of the United States of America* **107**: 15163-15168.

Yang L, Boldin MP, Yu Y, Liu CS, Ea CK, Ramakrishnan P, Taganov KD, Zhao JL, Baltimore D. 2012. miR-146a controls the resolution of T cell responses in mice. *The Journal of experimental medicine* **209**: 1655-1670.

Yao RW, Wang Y, Chen LL. 2019. Cellular functions of long noncoding RNAs. *Nature cell biology* **21**: 542-551.

Yasui D, Miyano M, Cai S, Varga-Weisz P, Kohwi-Shigematsu T. 2002. SATB1 targets chromatin remodelling to regulate genes over long distances. *Nature* **419**: 641-645.

Ye T, Krebs AR, Choukrallah MA, Keime C, Plewniak F, Davidson I, Tora L. 2011. seqMINER: an integrated ChIP-seq data interpretation platform. *Nucleic acids research* **39**: e35.

Yeom KH, Lee Y, Han J, Suh MR, Kim VN. 2006. Characterization of DGCR8/Pasha, the essential cofactor for Drosha in primary miRNA processing. *Nucleic acids research* **34**: 4622-4629.

Yi R, Qin Y, Macara IG, Cullen BR. 2003. Exportin-5 mediates the nuclear export of pre-microRNAs and short hairpin RNAs. *Genes & development* **17**: 3011-3016.

Yin Y, Morgunova E, Jolma A, Kaasinen E, Sahu B, Khund-Sayeed S, Das PK, Kivioja T, Dave K, Zhong F et al. 2017. Impact of cytosine methylation on DNA binding specificities of human transcription factors. *Science* **356**.

Yoda M, Cifuentes D, Izumi N, Sakaguchi Y, Suzuki T, Giraldez AJ, Tomari Y. 2013. Poly(A)-specific ribonuclease mediates 3'-end trimming of Argonaute2-cleaved precursor microRNAs. *Cell reports* **5**: 715-726.

Zeng H, Zhang R, Jin B, Chen L. 2015. Type 1 regulatory T cells: a new mechanism of peripheral immune tolerance. *Cellular & molecular immunology* **12**: 566-571.

Zeng Y, Yi R, Cullen BR. 2005. Recognition and cleavage of primary microRNA precursors by the nuclear processing enzyme Drosha. *The EMBO journal* **24**: 138-148.

Zhang H, Kolb FA, Jaskiewicz L, Westhof E, Filipowicz W. 2004. Single processing center models for human Dicer and bacterial RNase III. *Cell* **118**: 57-68.

Zhang JA, Mortazavi A, Williams BA, Wold BJ, Rothenberg EV. 2012a. Dynamic transformations of genome-wide epigenetic marking and transcriptional control establish T cell identity. *Cell* **149**: 467-482.

Zhang SB, Qian RL. 2002. The interaction between the human beta-globin locus control region and nuclear matrix. *Cell research* **12**: 411-416.

Zhang Y, Liu T, Meyer CA, Eeckhoute J, Johnson DS, Bernstein BE, Nusbaum C, Myers RM, Brown M, Li W et al. 2008. Model-based analysis of ChIP-Seq (MACS). *Genome biology* **9**: R137.

Zhang Y, McCord RP, Ho YJ, Lajoie BR, Hildebrand DG, Simon AC, Becker MS, Alt FW, Dekker J. 2012b. Spatial organization of the mouse genome and its role in recurrent chromosomal translocations. *Cell* **148**: 908-921.

Zhao H, Sifakis EG, Sumida N, Millan-Arino L, Scholz BA, Svensson JP, Chen X, Ronnegren AL, Mallet de Lima CD, Varnoosfaderani FS et al. 2015. PARP1- and CTCF-Mediated

Interactions between Active and Repressed Chromatin at the Lamina Promote Oscillating Transcription. *Molecular cell* **59**: 984-997.

Zhao JL, Rao DS, Boldin MP, Taganov KD, O'Connell RM, Baltimore D. 2011. NF-kappaB dysregulation in microRNA-146a-deficient mice drives the development of myeloid malignancies. *Proceedings of the National Academy of Sciences of the United States of America* **108**: 9184-9189.

Zhao Z, Tavoosidana G, Sjolinder M, Gondor A, Mariano P, Wang S, Kanduri C, Lezcano M, Sandhu KS, Singh U et al. 2006. Circular chromosome conformation capture (4C) uncovers extensive networks of epigenetically regulated intra- and interchromosomal interactions. *Nature genetics* **38**: 1341-1347.

Zheng X, Hu J, Yue S, Kristiani L, Kim M, Sauria M, Taylor J, Kim Y, Zheng Y. 2018. Lamins Organize the Global Three-Dimensional Genome from the Nuclear Periphery. *Molecular cell* **71**: 802-815 e807.

Zhou X, Jeker LT, Fife BT, Zhu S, Anderson MS, McManus MT, Bluestone JA. 2008. Selective miRNA disruption in T reg cells leads to uncontrolled autoimmunity. *The Journal of experimental medicine* **205**: 1983-1991.

Zhu F, Farnung L, Kaasinen E, Sahu B, Yin Y, Wei B, Dodonova SO, Nitta KR, Morgunova E, Taipale M et al. 2018. The interaction landscape between transcription factors and the nucleosome. *Nature* **562**: 76-81.

Zhu J, Paul WE. 2010. Heterogeneity and plasticity of T helper cells. *Cell research* **20**: 4-12.

Zink D, Amaral MD, Englmann A, Lang S, Clarke LA, Rudolph C, Alt F, Luther K, Braz C, Sadoni N et al. 2004. Transcription-dependent spatial arrangements of CFTR and adjacent genes in human cell nuclei. *The Journal of cell biology* **166**: 815-825.

Zuin J, Dixon JR, van der Reijden MI, Ye Z, Kolovos P, Brouwer RW, van de Corput MP, van de Werken HJ, Knoch TA, van IWF et al. 2014. Cohesin and CTCF differentially affect chromatin architecture and gene expression in human cells. *Proceedings of the National Academy of Sciences of the United States of America* **111**: 996-1001.

Zuleger N, Boyle S, Kelly DA, de las Heras JI, Lazou V, Korfali N, Batrakou DG, Randles KN, Morris GE, Harrison DJ et al. 2013. Specific nuclear envelope transmembrane proteins can promote the location of chromosomes to and from the nuclear periphery. *Genome biology* **14**: R14.

Zuleger N, Robson MI, Schirmer EC. 2011. The nuclear envelope as a chromatin organizer. *Nucleus* **2**: 339-349.

Zullo JM, Demarco IA, Pique-Regi R, Gaffney DJ, Epstein CB, Spooner CJ, Luperchio TR, Bernstein BE, Pritchard JK, Reddy KL et al. 2012. DNA sequence-dependent compartmentalization and silencing of chromatin at the nuclear lamina. *Cell* **149**: 1474-1487.

SCIENTIFIC PUBLICATIONS

PLOS ONE

RESEARCH ARTICLE

Developmental conservation of microRNA gene localization at the nuclear periphery

Eralda Salataj[1,2☯], Chrysoula Stathopoulou[1,3☯], Róbert A. Hafþórsson[4], Christoforos Nikolaou[1,2], Charalampos G. Spilianakis[1,2]*

1 Institute of Molecular Biology and Biotechnology—Foundation for Research and Technology Hellas, Heraklion, Crete, Greece, **2** Department of Biology, University of Crete, Heraklion, Crete, Greece, **3** Department of Molecular Biology and Genetics, Democritus University of Thrace, Alexandroupolis, Greece, **4** Department of Biology, Lund University, Lund, Sweden

☯ These authors contributed equally to this work.
* spiliana@imbb.forth.gr

Citation: Salataj E, Stathopoulou C, Hafþórsson RA, Nikolaou C, Spilianakis CG (2019) Developmental conservation of microRNA gene localization at the nuclear periphery. PLoS ONE 14 (11): e0223759. https://doi.org/10.1371/journal.pone.0223759

Editor: Hodaka Fujii, Hirosaki University Graduate School of Medicine, JAPAN

Received: July 13, 2019

Accepted: September 27, 2019

Published: November 4, 2019

Data Availability Statement: All relevant data are within the manuscript and its Supporting Information files.

Funding: This research is funded by CGS, European Union (European Social Fund ESF) and Greek national funds through the Operational Program "Education and Lifelong Learning" of the National Strategic Reference Framework (NSRF) Research Funding Programs THALES (miREG, Mis: 380247) and ARISTEIA (MIRACLE 42). The funders had no role in study design, data collection

Abstract

microRNAs are of vital importance for the regulation of the adaptive and innate immune responses, modulating gene expression at the post transcriptional level. Although there is cumulative information regarding the steady state mature microRNA levels and their respective targets, little is known about the effect of the three-dimensional chromatin architecture on the transcriptional regulation of microRNA gene loci. Here, we sought to investigate the effect of subnuclear localization on the transcriptional activation of eight murine microRNA loci in the immune system. Our results show that microRNA genes display a preferential monoallelic gene expression profile accompanied with perinuclear localization irrespectively of their transcription status or differentiation state. The expression profile and perinuclear localization are developmentally conserved while microRNA gene loci localization outside constitutive lamin associated domains is cross-species conserved. Our findings provide support for an active nuclear periphery and its role in chromatin organization of the non-coding genome.

Introduction

The last few years it has become increasingly clear that higher order chromatin organization controls the regulation of genome activity and serves as an additional epigenetic mechanism that modulates cellular functions and gene expression programs in diverse biological processes. Spatial positioning of different gene loci can be directly linked to gene expression [1–3] while other findings confirm that deregulation of the nuclear architecture can be linked to severe diseases [4–6]. Apart from the organization of chromatin *per se*, the metazoan interphase nuclei are also functionally compartmentalized, with different repressive and active nuclear sub-compartments governing gene expression. Compartments such as the nuclear lamina and the nucleolus gather repressed genes, while RNA Pol II factories attract expressing genes [7, 8]. Allelic interactions and gene repositioning with functional importance are common during the regulation of immune responses [9–11]. Chromatin loops, constituting

and analysis, decision to publish, or preparation of the manuscript.

Competing interests: The authors have declared that no competing interests exist.

Lamina Associated Domains (LADs), modify their proximity to the nuclear lamina offering a plausible explanation to past reports documenting the relocalization of gene loci, upon their transcriptional activation, away from the nuclear periphery, further supporting the implication of nuclear lamina in gene silencing [12].

In contrast to the nuclear lamina, association of chromatin with the Nuclear Pore Complex (NPC) has been reported to favor gene expression. Nuclear pore is a multiprotein complex of nucleoporins, that mediates molecule transport between the cytoplasm and the nucleus. Additional to molecule transportation, the NPC exerts multiple roles that are associated with regulation of gene expression, chromatin organization and virus infection [13–17].

Prior studies have introduced the role of non-coding RNAs as prominent factors that control gene expression and chromatin organization [18]. Non-coding RNAs can be subdivided into two discrete classes based on their physical properties (long and small non-coding RNAs). They are implicated in the regulation of several developmental and physiological processes in plants, fungi, worms and animals where they regulate gene expression, either through transcriptional modulation or via post-transcriptional regulatory mechanisms [19]. Although a plethora of reports have highlighted the significance of the long non-coding genome in nuclear organization [20], there are also few well characterized groups of small non coding RNAs with functional roles that can control genome stability and chromatin organization [21].

microRNAs constitute another abundant class of endogenous and highly conserved small non coding RNA molecules that show tremendous flexibility in controlling gene expression at the transcriptional and post-transcriptional level [22]. Several reports have described the functional role of microRNAs in controlling the myeloid and lymphoid cell development and function of the innate and adaptive immune system [23].

Mammalian microRNA gene transcription is initiated in the cell nucleus by either RNA Polymerase II (Pol II) or RNA Polymerase III (Pol III) and it may yield a several kb (pri-miRNA) transcript that is co-transcriptionally processed to an ~70 bp premature RNA (pre-miRNA) by the Microprocessor complex [comprised by DROSHA and DiGeorge syndrome critical region gene 8 (DGCR8) proteins] [24–28]. DICER further processes the pre-microRNA and releases a 20–24 nt RNA duplex ready to obtain its functional targeting role in the cytoplasm [29–31]. Despite the fact that microRNA biogenesis and the microRNA-mediated gene regulation mechanisms are well documented, little is known about the transcription regulation of the microRNA genes themselves. So far, only a few studies have referred to the subnuclear positioning of microRNA genes as an epigenetic mechanism regulating immune responses [32, 33].

Therefore, in this study we sought to investigate the impact of nuclear architecture as an epigenetic mechanism regulating the expression of eight microRNA genes in the murine innate and adaptive immune system. We investigated the role of subnuclear localization of microRNA gene loci as a potential mechanism affecting non-coding genome expression. Apart from highlighting the impact of the nuclear periphery in microRNA gene expression, we also introduce other factors that may modulate the subnuclear positioning or the expression of the microRNA genes studied. Our results pinpoint the impact of nuclear periphery in microRNA gene expression, shed light on chromatin organization at the nuclear periphery and allow for a better understanding of the mammalian genome organization.

Results

microRNA genes are preferentially expressed in a monoallelic manner

To study the impact of nuclear architecture in the transcriptional regulation of microRNA gene loci, eight microRNA genes (*miR-181a1b1*, *miR-181a2b2*, *miR-181c*, *miR-142*, *miR-146a*,

miR-17-92, *miR-155* and *miR-let7e*) were selected which are expressed during the murine myeloid and lymphoid cell development. Initially, our study focused on unraveling the allelic expression profile of these microRNA genes. RNA-DNA fluorescence *in situ* hybridization (FISH) experiments were performed in T cells [murine thymocytes, $CD4^+$, T helper type 1 (TH1) and type 2 (TH2) cells] and in macrophages (thioglycollate elicited peritoneal macrophages–TEPMs, and bone marrow derived macrophages–BMDMs) before and after lipopolysaccharide (LPS) stimulation.

Our results revealed a profound tendency for monoallelic microRNA gene expression both in T cells (Fig 1A and 1B) and macrophages (Fig 1C and 1D). RNA-DNA FISH experiments allowed the simultaneous detection of both the newly synthesized pri-miRNA and the gene locus from which it is transcribed (Fig 1E). Upon terminal differentiation of $CD4^+$ T cells into the TH1 and TH2 cell lineages and after LPS stimulation of TEPMs or BMDMs, the expression of microRNA genes remained monoallelic although a low fraction of cells exhibited biallelic expression. The higher frequency of monoallelically expressed microRNA gene alleles is due to the low expression levels of primary microRNA transcripts and not due to imprinting. These results are in line with bioinformatic predictions regarding the allelic expression profile of both microRNA genes and coding genes and does not seem to be affected by neighboring gene transcription status (S1 Fig and S1 Table).

microRNA gene loci are perinuclearly positioned and colocalize with the nuclear lamina

Collectively, the RNA/DNA FISH analysis on three-dimensionally (3D) preserved cell nuclei, provided us with interesting preliminary data indicating that microRNA gene loci localize in the nuclear periphery. Considering that the subnuclear localization of gene loci can directly impact their gene expression [11, 34] we performed 3D-DNA FISH experiments in murine T and macrophage cell lineages (Fig 2A). The *Tnfα* gene locus was used as a control, given that its expression displays well characterized spatiotemporal kinetics [11]. Intranuclear distances (between each gene allele and the nuclear periphery) were measured and normalized to the nuclear radius of each cell in order to correct for differences in the size of the cell nuclei. To quantitate the relative localization of microRNA gene loci in cell nuclei, the normalized distances (NDs) of gene alleles were grouped in ten concentric shells, in which normalized distances ranging from 0 to 1 are denoting the border and the center of the cell nucleus respectively (S2A Fig). Thymocytes and $CD4^+$ T cells demonstrated a peripheral distribution for all eight microRNA gene loci, with the most peripheral cluster ND = 0–0.1 including more than 40% of all the microRNA gene alleles (Figs 2B and S2B and S1 Video). Upon differentiation of CD4 cells into TH1 and TH2 cells the external cluster ND = 0–0.1 included as much as 65% and 60% of the total microRNA gene alleles, respectively. Although microRNA gene loci displayed a perinuclear relocalization during differentiation, *Tnfα* alleles exhibited an expanded distribution up to a more internal cluster ND = 0.6–0.7 with a low percentage of the alleles (15%) located at the nuclear periphery (ND = 0–0.1) in thymocytes. During T cell differentiation, *Tnfα* was relocalized towards the center of the nucleus in TH1 cells (ND = 0.3–0.4 including the highest fraction of alleles) while in TH2 cells the allelic distribution of *Tnfα* was similar to $CD4^+$ cells.

A perinuclear localization of microRNA gene alleles was also observed in TEPMs (Figs 2B and S2B) and BMDMs (S2C Fig). More specifically, in TEPMs irrespectively of LPS stimulation, more than 50% of the microRNA gene alleles localized in the nuclear periphery (0–0.1). As for the *Tnfα* alleles localization, the corresponding *Tnfα* allelic ND values clustering in the ND = 0–0.1 zone were 5.8% and 1.5% before and after LPS stimulation respectively, following

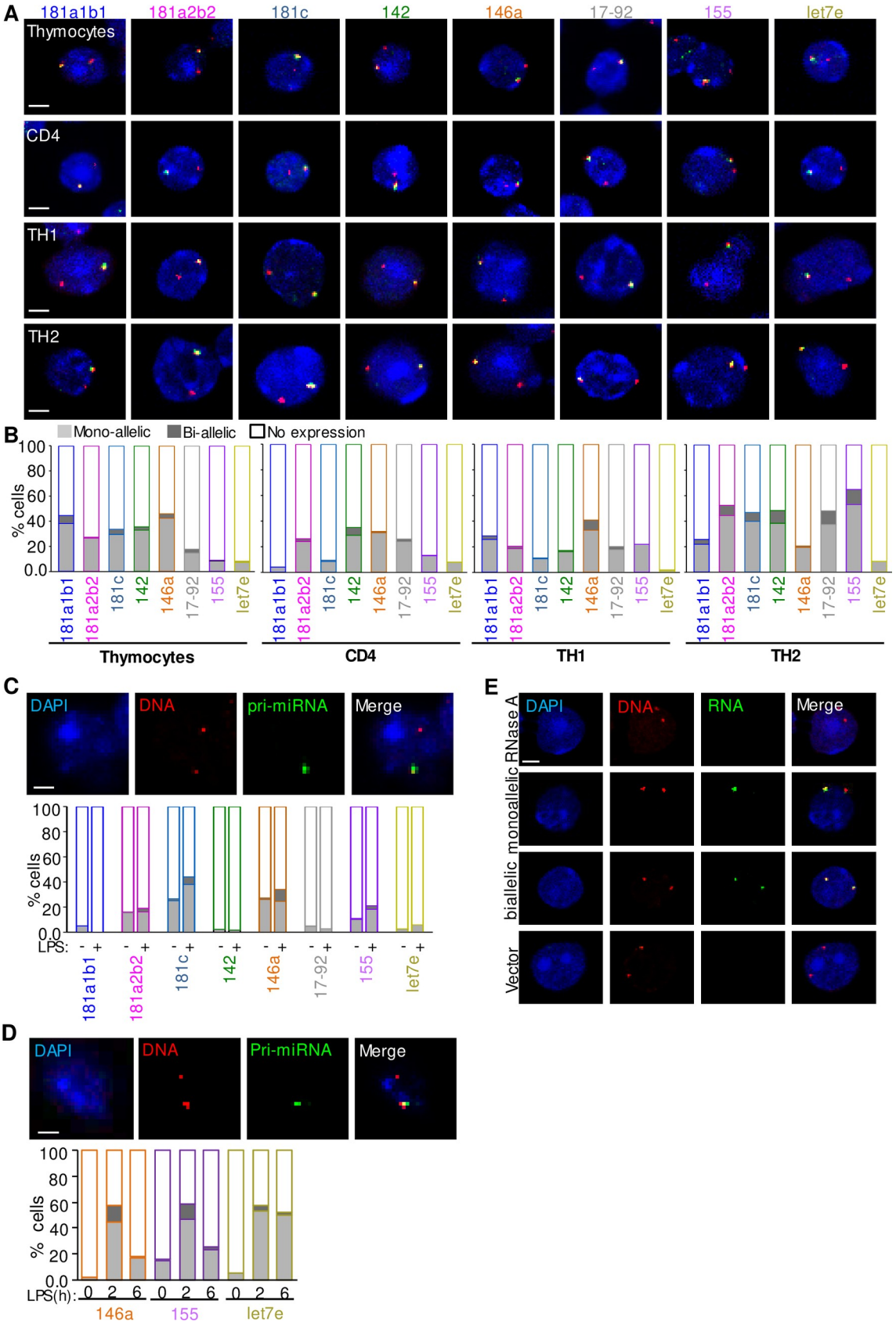
A
181a1b1
181a2b2
181c
142
146a
17-92
155
let7e
Thymocytes
CD4
TH1
TH2
B
Mono-allelic
Bi-allelic
No expression
% cells
Thymocytes
CD4
TH1
TH2
C
DAPI
DNA
pri-miRNA
Merge
% cells
LPS:
D
DAPI
DNA
Pri-miRNA
Merge
% cells
LPS(h):
146a
155
let7e
E
DAPI
DNA
RNA
Merge
RNase A
monoallelic
biallelic
Vector

Fig 1. Allelic expression profile analysis of microRNA gene loci reveals their preferential monoallelic expression in the murine immune system. A) Representative images of RNA-DNA FISH experiments for microRNA genes in thymocytes, $CD4^+$, TH1, TH2 cells. microRNA gene locus DNA (red) and biotinylated cDNA probes (green) were used to detect the nascent microRNA transcript. The number of nuclei measured in the RNA-DNA FISH experiments were: n = 1950 thymocytes, n = 2348 $CD4^+$, n = 3417 TH1, n = 3057 TH2. Scale bar 2μm. B) The mono- and bi-allelic expression profile of the portrayed microRNAs in the graph corresponds to the percentage of cells expressing either one or both alleles, before and after differentiation of the cells into the TH1 and TH2 cell lineages. The number of nuclei measured are the same as in Fig 1A. C) Representative confocal microscopy images of RNA-DNA FISH experiments showing the allelic expression profile of microRNA genes in thioglycollate elicited peritoneal macrophages (TEPMs). Bar graphs indicate the percentage of cells with either mono- or bi-allelic expression of the nascent pri-miRNA transcript before and after LPS stimulation of macrophages. A total number of 3558 and 2606 nuclei were measured in naive (-LPS) and LPS activated (+LPS) TEPMs respectively. Scale bar 2μm. D) Confocal microscopy single z-stack images indicating the colocalization of nascent *pri-miR-155* transcript (green) along with its corresponding gene locus (red), in 2h LPS-stimulated BMDMs (blue-DAPI, for DNA counterstain). Bar graph portraying the mono- and bi-allelic expression pattern of *miR-146a*, *miR-155* and *miR-let7e* in naive and LPS-stimulated BMDMs. The total number of nuclei measured for each microRNA locus were n = 691 for *miR-146a*, n = 931 for *miR-155* and n = 168 for *miR-let7e*. Scale bar 2 μm. E) Representative confocal microscopy images of RNA-DNA FISH experiments for microRNA gene loci (DNA- *miR-155* red) with the respective nascent pri-microRNA transcript (green) in thymocytes (DNA counterstained with DAPI—blue). The upper panel depicts DNA, but not RNA signals in RNase A treated cells. The second and third panel depict mono- and biallelically expressing cells. The fourth panel presents RNA-DNA hybridization with the TOPO-TA cloning vector used for RNA FISH probe synthesis. Scale bar 2 μm.

https://doi.org/10.1371/journal.pone.0223759.g001

a reverse distribution pattern compared to the microRNA genes. The same perinuclear positioning of the microRNA genes was observed in BMDMs (S2C Fig). These results indicate that in cell types of the murine innate (macrophages) and adaptive ($CD4^+$ T cells) immune system, the eight microRNA gene loci under study preferentially localize in the nuclear periphery irrespectively of the differentiation or activation state of the cell.

In order to experimentally test whether the peripheral distribution of the investigated microRNA gene loci was attributed to a dynamic interplay with the nuclear lamina, as already described for coding genes [35], we performed 3D-DNA FISH in concert with immunofluorescence experiments and assessed the fraction of cells with at least one gene allele colocalized with the nuclear lamina (Fig 2C). We found that more than 50% of the thymocytes displayed at least one microRNA gene allele colocalized with Lamin-B1 (Fig 2D and S2 Video). Upon activation and differentiation of $CD4^+$ T cells towards the TH1 and TH2 cell lineages, the fraction of alleles that colocalized with Lamin-B1 was increased with over 50% of the cells displaying at least one microRNA gene allele colocalized with Lamin-B1 (Fig 2D). Our experiments in TEPMs indicated that for *miR-181a1b1*, *miR-181c* (unstimulated cells), *miR-17-92* and *miR-let7e*, more than 50% of the total cell population bore at least one allele colocalized with the nuclear lamina. *miR-181a2b2*, *miR-146a* and *miR-155* colocalized with the nuclear lamina in cell fractions higher than 40% while *miR-142* exhibited a lower tendency to colocalize with Lamin-A/C (20%). In BMDMs we tested the microRNA genes for which the expression was upregulated upon LPS stimulation and found that at least one allele colocalized with Lamin-B1 in more than 50% of the total cell population assessed (S2D Fig). In conclusion, the observed colocalization of microRNA gene loci with the nuclear lamina did not significantly change before and after T cell differentiation or macrophage LPS stimulation with the striking exception of the LPS-induced *miR-181c* gene locus in TEPMs (Fig 2D), which demonstrated the lowest percentage of colocalization with the nuclear lamina in $CD4^+$ cells and LPS stimulated TEPMs.

microRNA genes are actively transcribed in the nuclear lamina

In order to investigate the repercussions of microRNA gene colocalization with the nuclear lamina and its effect on the allelic microRNA gene expression profile, we performed IF-RNA/DNA FISH (for the pri-microRNA and the gene locus) and assessed the frequency of microRNA gene alleles that were actively expressed and were either colocalized or not with the

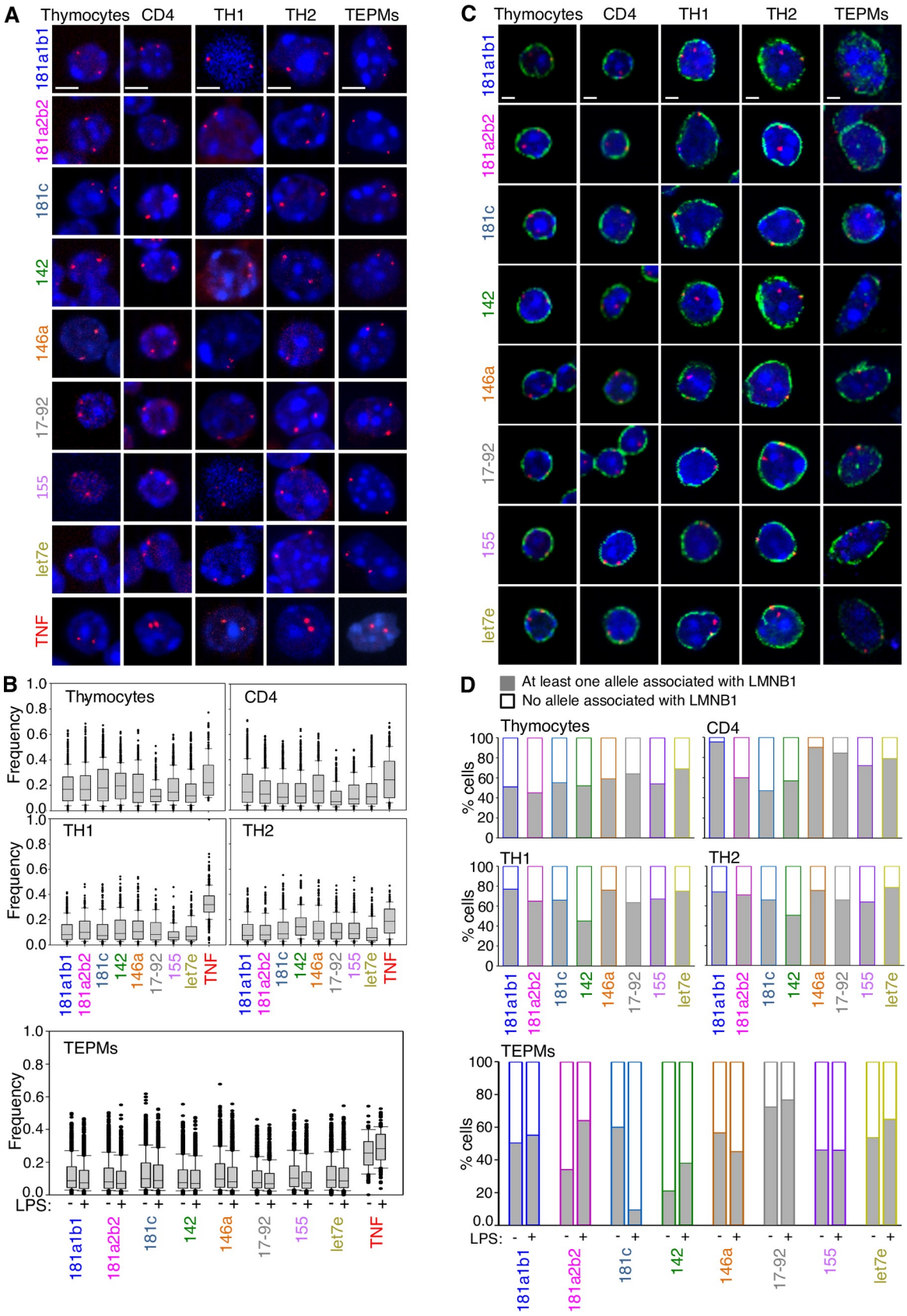
A
Thymocytes
CD4
TH1
TH2
TEPMs
181a1b1
181a2b2
181c
142
146a
17-92
155
let7e
TNF
B
Thymocytes
CD4
TH1
TH2
TEPMs
Frequency
LPS:
C
D
At least one allele associated with LMNB1
No allele associated with LMNB1
% cells

Fig 2. microRNA gene loci are localized in the cell nuclear periphery. (A) DNA FISH single z-stack images displaying the perinuclear localization of microRNA and *Tnfα* gene loci in thymocytes, $CD4^+$, TH1, TH2 and TEPMs. Scale bar 2μm. (B) Bar graphs represent the intranuclear normalized distances (NDs) measured between the microRNA gene signals and the edges of the nuclei as defined by DAPI staining. Allele distances from the nucleus edge were measured in 3D-preserved cell nuclei using the Volocity 3D Image Analysis Software and normalized to the nuclear radius. ND = 1 defines the center of the nucleus, whereas ND = 0 defines the nuclear periphery. The total number of nuclei measured in each dataset were: Thymocytes n = 4021, $CD4^+$ n = 4030, TH1 n = 1337, TH2 n = 1331, TEPMs/-LPS n = 4762, TEPMs/+LPS n = 4882. Scale bar 2μm. (C) Single z-stack images of DNA FISH combined with immunofluorescence analysis indicating the colocalization of microRNA gene alleles (red) with the nuclear lamina (LMNB1 green) in thymocytes, $CD4^+$, TH1, TH2 cells and TEPMs. Scale bar 2μm. (D) Bar graphs represent the percentages of cells bearing at least one allele associated with the nuclear lamina. Number of nuclei assessed: thymocytes n = 2008, $CD4^+$ n = 1984, TH1 n = 1232, TH2 n = 1320, TEPMs/-LPS n = 958, TEPMs/+LPS n = 1151.

https://doi.org/10.1371/journal.pone.0223759.g002

nuclear lamina (either LMNB1 or LMNA/C). Our results indicated expression and collateral colocalization with Lamin-B1 for all microRNA genes tested. More specifically, in thymocytes, almost 45% of the expressing alleles of *mir-181c*, *miR-17-92* and *miR-155* colocalized with Lamin-B1 while in macrophages before and after LPS stimulation more than 40% of all the *miR-146a* and *miR-155* expressing alleles were colocalized with Lamin-B1 (Fig 3A). The latter was also confirmed by the distributions of normalized distances between the expressed and the non-expressed microRNA gene alleles in thymocytes, $CD4^+$, TH1, TH2 (S3A Fig), TEPMs and BMDMs before and after LPS stimulation (S3B Fig). We did not detect any tendency for localization of the expressing microRNA gene alleles to more internal nuclear compartments or *vice versa*.

To obtain a global view on the microRNA perinuclear positioning we tested whether the peripheral localization could be attributed to the localization in lamin associated domains (LADs). LADs are AT-rich, genomic regions known to constitute anchorage domains of gene loci to the nuclear lamina compartment and constitute almost 40% of the mouse genome [12, 36, 37]. Data obtained from DamID experiments on different cell types showed three different groups of LADs: constitutive LADs (cLADs) as regions that are lamin-associated regions, constitutive inter-LADs (ciLADs) that are chromatin regions between LADs and facultative LADs (fLADs) that are cell-type dependent lamin-associated regions [36]. Using published cLAD coordinates in the mouse genome [12], we tracked the position of the eight microRNA gene loci under study along with the TNF*α* locus in four different murine cell types: mouse embryonic stem cells (ESCs), mouse embryonic fibroblasts (MEFs), neuronal progenitor cells (NPCs) and astrocytes (ACs). We observed that all gene loci tested, resided outside cLAD regions in the mouse genome (Fig 3B). Subsequently, we questioned whether the observed perinuclear localization of microRNA gene loci reflected their localization in proximity to the borders of ciLADs. Our analysis revealed that *miR-181a2b2*, *miR-17-92*, *miR-155* and *miR-let7e* were localized closer to the ciLAD boundary, whereas *miR-181c*, *miR-142* and *Tnfα* gene loci were localized towards the center of their corresponding domains (Fig 3C). When the comparative analysis was scaled up to all the murine microRNA genes annotated in the miR-base, we found that microRNA gene loci did not exhibit a distinct tendency of localization towards either the border or the center of ciLAD/cLAD compartments (Fig 3C). microRNA genes located proximal to cLADs were positioned far from the corresponding boundaries, whereas ciLAD-associated microRNA genes were preferentially positioned within the domain, exhibiting a slight preference towards the center of the domain.

It is well established [38–40] that upon transcriptional activation genes may re/localize within the cell nucleus. Furthermore, during development and differentiation of T cells, a dynamic change in chromatin is observed [41–44]. Based on these findings, we next tested whether transcription inhibition could have an impact on the perinuclear localization of a microRNA gene locus or whether it would induce its relocalization. Therefore, we performed

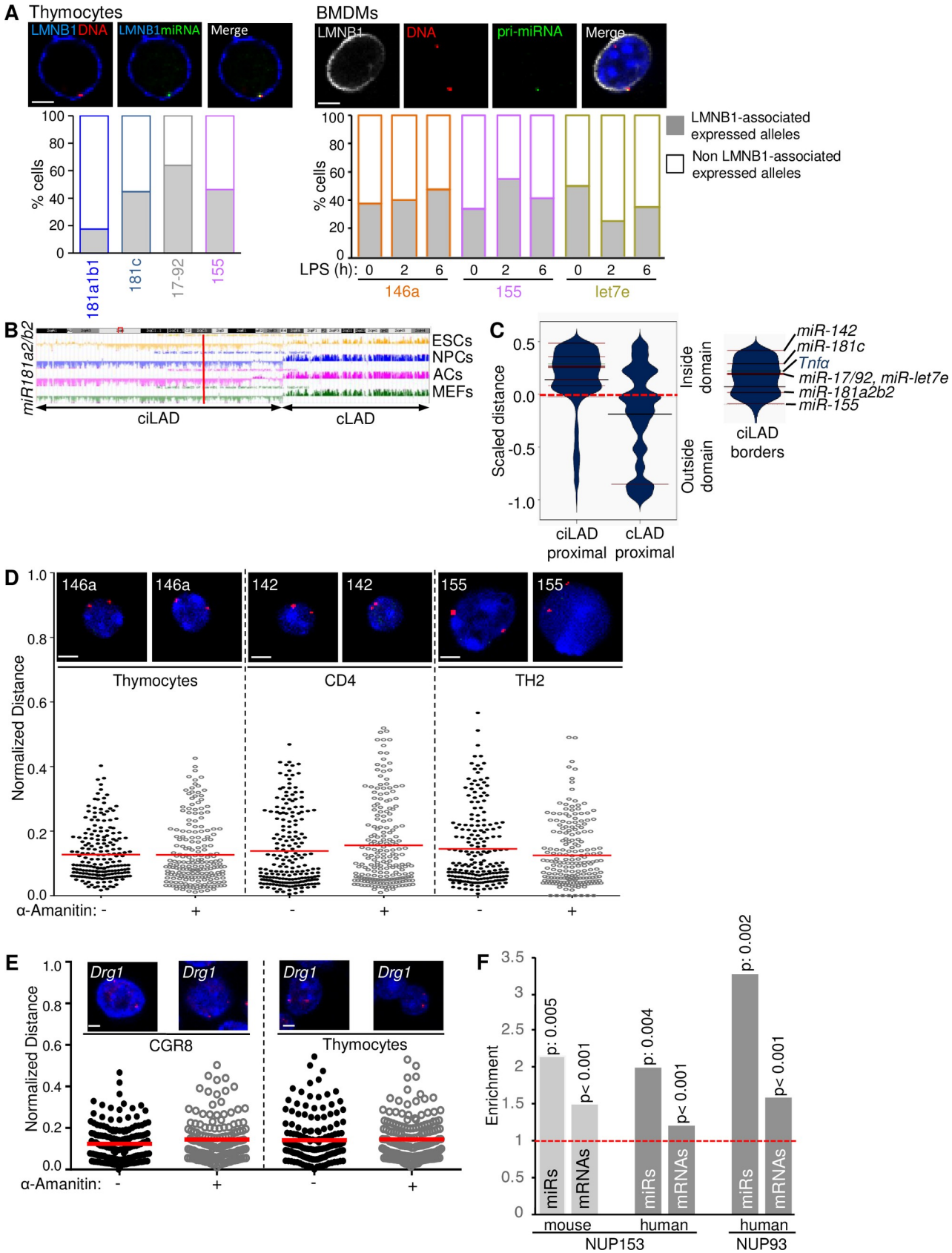
A
Thymocytes
LMNB1 DNA
LMNB1 miRNA
Merge
BMDMs
LMNB1
DNA
pri-miRNA
Merge
% cells
181a1b1
181c
17-92
155
LPS (h): 0 2 6 0 2 6 0 2 6
146a
155
let7e
LMNB1-associated expressed alleles
Non LMNB1-associated expressed alleles
B
miR181a2/b2
ESCs
NPCs
ACs
MEFs
ciLAD
cLAD
C
Scaled distance
ciLAD proximal
cLAD proximal
Inside domain
Outside domain
miR-142
miR-181c
Tnfα
miR-17/92, miR-let7e
miR-181a2b2
miR-155
ciLAD borders
D
146a
142
155
Thymocytes
CD4
TH2
Normalized Distance
α-Amanitin: - + - + - +
E
Drg1
CGR8
Thymocytes
Normalized Distance
α-Amanitin: - + - +
F
Enrichment
p: 0.005
p< 0.001
p: 0.004
p< 0.001
p: 0.002
p< 0.001
miRs
mRNAs
mouse
human
NUP153
NUP93

Fig 3. The perinuclear localization of microRNA gene loci is independent of their transcriptional activity. (A) Single z-stack images displaying the colocalization of expressed (green) microRNA gene alleles (red) with Lamin-B1 in thymocytes and BMDMs (before and upon LPS stimulation for the indicated time points). Bar graphs represent the percentage of expressed alleles colocalized with the nuclear lamina. Number of nuclei assessed: thymocytes n = 705, BMDMs/-LPS n = 492, BMDMs/+2h LPS n = 1128, BMDMs/+6h LPS n = 1028. Scale bar 2μm. B) 2Mbp region of mouse chromosome 2 with *miR-181a2b2* gene. ciLAD/cLAD analysis in four distinct cell types, embryonic stem cells (ESCs), neural progenitors (NPCs), astrocytes (ACs) and mouse embryonic fibroblasts (MEFs). (C) Beanplots portraying the scaled distance distribution of microRNA genomic sequences to their most proximal ciLAD/cLAD regions. Red lines represent the microRNA genes under study, whereas the green line corresponds to TNFα locus. Small but interesting tendencies for the localization of microRNA sequences either towards the centers of ciLADs, or at the cLAD/ciLAD boundaries are observed and recapitulated by the Wilcoxon rank-sum test (p-value < = 10e-90). (D) Single z-stack images of 3D DNA-FISH nuclei and scatter plot indicating the ND distribution of microRNA gene alleles before and upon transcriptional inhibition with α-amanitin treatment in thymocytes, $CD4^+$ and TH2 cells. Number of nuclei assessed: thymocytes n = 400, $CD4^+$ n = 400, TH2 n = 398. Scale bar 2μm. (E) Scatter plot indicating the ND distribution of the cLAD localized *Drg1* gene before and after α-amanitin treatment of CGR8 mouse embryonic stem cells and thymocytes. Number of nuclei assessed: CGR8/(-)α-amanitin n = 170, CGR8/(+)α-amanitin n = 144, thymocytes/(-)α-amanitin n = 158, thymocytes/(+)α-amanitin n = 164. (F) Assessment of overlap tendencies between a) microRNA and b) protein coding mRNA gene loci with peaks corresponding to human and mouse nucleoporins. Enrichment of colocalization was calculated as observed over expected ratios of overlaps between the compared genomic regions. P-values were calculated on the basis of 1000 random permutations of the peaks' regions. Values <0.001 indicate not one out of 1000 permutations had a value as high as the observed.

https://doi.org/10.1371/journal.pone.0223759.g003

DNA FISH experiments in T cells, before and upon treatment with α-amanitin for 6h (Fig 3D). The efficiency of transcription inhibition was confirmed by both qRT-PCR and RNA FISH for all the cell types under investigation (S3C and S3D Fig). Our results demonstrated that in thymocytes, inhibition of transcription did not alter the gene allelic distribution of *miR-146a* locus. 48% of the gene alleles located at the nuclear periphery (ND = 0–0.1) in untreated cells compared to 50% of the gene alleles in α -amanitin treated cells. For *miR-142*, 46% of the alleles in untreated CD4 cells were located at the nuclear periphery (ND = 0–0.1) compared to 51% of the gene alleles being perinuclear in α-amanitin treated cells. In TH2 cells 48% of *miR-155* gene alleles were perinuclear (ND = 0–0.1) in untreated compared to 50% in treated cells (Fig 3D). Furthermore, Kolmogorov Smirnov (KS) analysis of the normalized distances for each population displayed a non-significant difference before and after α-amanitin treatment of cells (S3E Fig). We also performed the same experiments for a cLAD-located gene [Developmentally-regulated GTP-binding protein 1 (*Drg1*)] in both ES cells and thymocytes. Our results indicated that trancription inhibition did not cause any statistically significant relocalization of *DRG1* alleles towards the nuclear interior in either of the two cell types (Figs 3E and S3F). In conclusion, the α-amanitin-dependent inhibition of active transcription did not affect the perinuclear localization of either the ciLAD-located microRNA genes, nor the cLAD-located control coding gene (*Drg1)*.

Based on the previous results, we concluded that the microRNA gene loci under study localize in the nuclear periphery in close proximity to the nuclear lamina, irrespectively of their transcription status. Therefore, we questioned whether microRNA genes colocalize with NPCs. Such an interaction of NPCs with euchromatin could promote transcription and control chromatin organization as previously reported [45–47]. We analyzed publicly available ChIP-seq data for NUP153, NUP93 and NUP98 (GEO numbers are provided in the corresponding Supporting information section). We found that microRNA gene loci were significantly enriched, compared to coding genes, for NUP153 and NUP93 proteins (Fig 3F). While NUP153 and NUP93 displayed similar results, this was not the case for NUP98 where we did not observe any significant enrichment between microRNA gene loci and mRNAs (S3G Fig). Based on these results we conclude that nuclear pore proteins may be implicated in tethering microRNA gene loci to the nuclear periphery.

Ablation of the BACH1 transcriptional regulator does not affect the expression or peripheral localization of microRNA genes

Cell type specific transcription factors may be implicated in gene positioning and spatial chromatin organization [34, 48–50]. BACH1 is a transcription factor highly expressed in the bone

marrow and was characterized as an architectural transcription factor mediating chromatin interactions among Maf recognition elements-MAREs [51]. Additionally, *Bach1* deletion has a significant impact on lymphoid- and myeloid-mediated inflammatory responses [52] and its binding is enriched on microRNA gene promoters [53]. To investigate whether the ablation of BACH1 could affect either the subnuclear localization, or the allelic expression profile of microRNA genes, we performed DNA FISH experiments in both wild type (wt) and *Bach1*$^{-/-}$ thymocytes and BMDMs and analyzed the subnuclear distribution of *miR-155* gene alleles, which we previously found to localize in the nuclear periphery. Our analysis in *Bach1*$^{-/-}$ reconfirmed the peripheral localization of *miR-155* and *miR-146a* gene alleles in thymocytes and BMDMs that was not statistically different between wild type (wt) and *Bach1*$^{-/-}$ cells (Fig 4A–4D).

To test whether *Bach1* ablation impacted microRNA transcriptional activation after LPS stimulation, we analyzed the allelic expression profile of *miR-155* and *miR-146a* in wild type and *Bach1*$^{-/-}$ BMDMs with *in situ* pri-microRNA hybridization (Fig 4E). Our analysis revealed that *Bach1* ablation in BMDMs did not affect the allelic expression profile or subnuclear localization of *miR-155* and *miR-146a* genes.

Developmentally conserved perinuclear localization of microRNA gene loci

Based on the consistency of our findings regarding the perinuclear positioning of microRNA genes tested, we next investigated whether this preferential localization constitutes an immune cell specific phenomenon or has been established in earlier developmental stages in a manner that excludes the tested microRNA genes from internal nuclear positions. We examined the allelic distribution of the aforementioned microRNA gene loci in whole bone marrow derived cells (composed of myeloid precursors, eosinophils, basophils and monocytes, erythroid progenitors and lymphocytes) and in mouse embryonic germline competent cells (JM8.N4 and CGR8 cell lines). The allelic distribution of microRNA gene loci compared to the *Tnfα* gene locus in bone marrow cells displayed a similar pattern with T cells and macrophages. Gene allele frequencies in the 0–0.1 ND cluster ranged between 28% (*miR-146a*) to 57% (*miR-155*), while *Tnfα* alleles were mainly distributed (*56%*) in the 0.2–0.4 ND cluster. In ESCs microRNA gene alleles were mostly located to the nuclear periphery, with more than 80% of the alleles occupying the most perinuclear cluster (ND = 0–0.1) (Figs 5A and S4A–S4C). Interestingly, the *Tnfα* locus also demonstrated a perinuclear localization in ESCs with 80% of its gene alleles ND frequencies included in the most perinuclear cluster (ND = 0–0.1). In conclusion, although the *Tnfα* gene locus gradually relocalized from the nuclear periphery (ESCs) to the nuclear interior during myeloid and lymphoid differentiation (T cells, TEPMs, BMDMs), microRNA gene loci constantly displayed a perinuclear localization in cell lineages ranging from embryonic stem cells to more differentiated cell types of the innate and adaptive immune system.

It was previously suggested that cLAD domains are highly conserved across species, while ciLAD domains show a strong conservation between mouse and human [36]. Based on these reports we next investigated the correlation between microRNA gene localization and cLADs in four different species (*M.musculus*, *H.sapiens*, *D.melanogaster* and *C.elegans)*, details on the LAD coordinates are provided in the corresponding Supporting information section) [12, 54–56]. Our results indicated that in *M.musculus* 14% of the microRNA genes were localized within cLAD regions while the rest were positioned within ciLADs. Interestingly, chromosome 2 which contains a cluster of microRNAs that spans an area of around 50000bp, displayed an unusual high number of microRNAs inside cLADs, with 78 microRNA genes positioned within cLADs from a total of 147 microRNA genes (Fig 5B). *In silico* analysis revealed that,

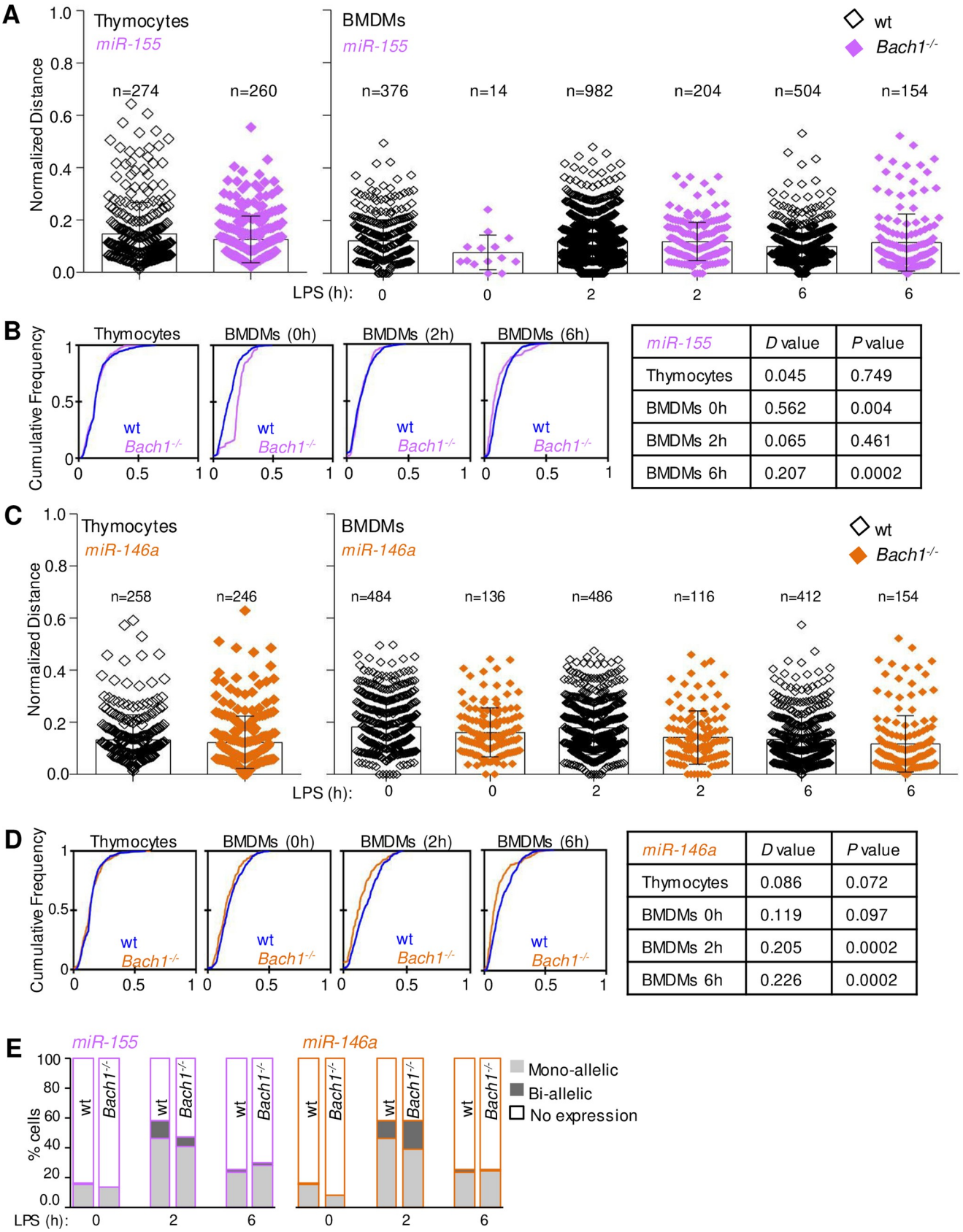

miR-155	D value	P value
Thymocytes	0.045	0.749
BMDMs 0h	0.562	0.004
BMDMs 2h	0.065	0.461
BMDMs 6h	0.207	0.0002

miR-146a	D value	P value
Thymocytes	0.086	0.072
BMDMs 0h	0.119	0.097
BMDMs 2h	0.205	0.0002
BMDMs 6h	0.226	0.0002

Fig 4. Perinuclear localization of microRNA gene loci in *Bach1*$^{-/-}$ thymocytes and BMDMs. (A) *miR-155* gene alleles distribution in wild type (wt) and *Bach1*$^{-/-}$ thymocytes and BMDMs. (B) Cumulative frequency graphs and KS-test for the comparison of *miR-155* gene alleles distribution in wt versus *Bach1*$^{-/-}$ thymocytes and BMDMs before and after LPS stimulation for the indicated time points. (C) *miR-146α* gene alleles distribution in wt and *Bach1*$^{-/-}$ thymocytes and BMDMs. (D) Cumulative frequency graphs of *miR-146α* gene alleles NDs in wt and *Bach1*$^{-/-}$ thymocytes and BMDMs before and after LPS stimulation for the indicated time points. KS-test analysis results are portrayed on the table. (E) Allelic expression profile of *pri-miRNA-155 and pri-miRNA-146α* in naive (0h) and LPS stimulated (2h, 6h) BMDMs, following RNA-DNA FISH.

https://doi.org/10.1371/journal.pone.0223759.g004

similarly to *M.musculus*, *H.sapiens* microRNA genes displayed a tendency to avoid the constitutive LAD domains. We found that 18% of microRNA genes were located within cLADs while the rest were located within ciLADs. Chromosome X displayed the highest number of microRNA genes localized within a cLAD region (54 out of 118 microRNAs). Chromosome 19, displaying the highest gene density, demonstrated the highest number of microRNA genes outside cLADs (Figs 5B and S4D). *D.melanogaster* demonstrated a similar pattern as observed in humans and mice, with only 25% of microRNAs located within cLAD regions. *C. elegans* was the only species with a different distribution of cLAD/ciLAD-containing microRNA genes, where 47% of the microRNA genes were located within cLADs (Fig 5B).

We expanded our comparative analysis and investigated the relative enrichment of all microRNA and protein coding genes in LADs. We next tested whether the observed enrichment of microRNA genes outside cLADs exhibited significant cross-species conservation. Our results in the mouse indicated that both microRNA and protein coding gene loci were significantly enriched in ciLAD regions (Fig 5C). We found significant depletion of microRNA gene loci in LADs except for the *C.elegans* dataset where the observed depletion of microRNA gene loci in LADs was not significant. The same trend was identified for protein-coding genes, albeit to a lesser extent among the four compared species, with enrichment values being below the baseline (value 1), but always higher than the corresponding ones for microRNA genes. This result is indicative of a cross-species conserved increased tendency of microRNA gene loci to avoid LAD regions.

Discussion

Our study provides substantial information on the allelic expression profile of eight microRNA genes implicated in the regulation of the murine innate and adaptive immune responses. We have attributed the monoallelic expression pattern to the moderate expression levels of these genes [57, 58] and excluded the potential of imprinting for the aforementioned loci, since low frequency biallelic expression was detected in cell populations with maximal pri-microRNA expression, following T cell receptor (TCR) activation of CD4^{+} T cells and LPS stimulation of macrophages [59]. Although monoallelic expression has been reported for a wide range of coding genes [58, 60] it has also been documented for the non-coding genome [61, 62] such as for imprinted microRNA gene clusters found both on mouse and human chromosomes [59, 63]. In parallel, the preference for the monoallelic expression of microRNA genes could be attributed to differential methylation of regulatory elements controlling gene expression.

Regarding the subnuclear spatiotemporal localization of the microRNA gene loci we studied, our analysis indicated that in both naïve, non-stimulated cells, but also in TCR-activated CD4^{+} T cells or LPS-induced macrophages, microRNA genes localize in the nuclear periphery, irrespectively of their transcriptional activity or differentiation status. The role of the nuclear periphery in gene expression control still remains unclear. Nowadays, the capacity of high-resolution capacity imaging approaches [64–66] in concert with chromosome conformation capture (3C)-based technologies [67], combined with modeling for interpreting chromatin interactions, or tethering loci to specific nuclear compartments [68] provides strong support in deciphering the exact role of the nuclear periphery during development.

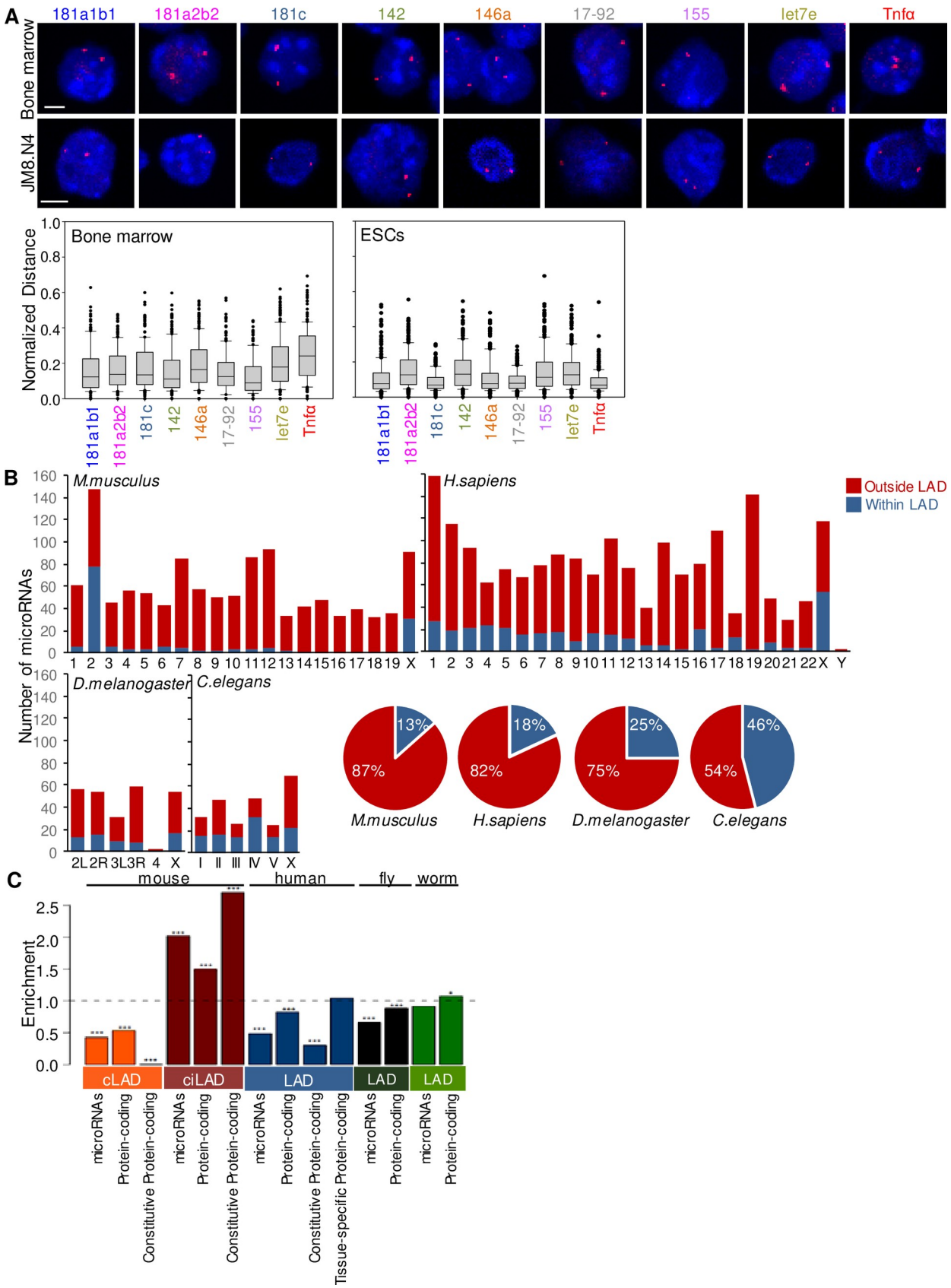
A
181a1b1
181a2b2
181c
142
146a
17-92
155
let7e
Tnfα
Bone marrow
JM8.N4
Normalized Distance
Bone marrow
ESCs
B
M.musculus
H.sapiens
Outside LAD
Within LAD
Number of microRNAs
D.melanogaster
C.elegans
13%
87%
18%
82%
25%
75%
46%
54%
M.musculus
H.sapiens
D.melanogaster
C.elegans
C
mouse
human
fly
worm
Enrichment
cLAD
ciLAD
LAD
LAD
LAD
microRNAs
Protein-coding
Constitutive Protein-coding
Tissue-specific Protein-coding

Fig 5. The perinuclear localization of microRNA gene loci is developmentally conserved. (A) Representative 3D DNA FISH confocal images in bone marrow and JM8.N4 ESCs. Number of nuclei assessed: bone marrow n = 200 alleles, ESCs n = 260 alleles. Scale bar 2μm. (B) Number of microRNA genes located within and outside cLADs per chromosome (Bar graphs) and total percentage of cLAD/ciLAD microRNA gene colocalization (Pie charts) in *M.musculus*, *H. sapiens*, *D.melanogaster* and *C.elegans*. (C) Enrichment values of microRNA and protein-coding genes within and outside LAD regions. Permutation *p*-values are depicted as ***:<0.001, **:<0.01 and *:<0.05 respectively, and calculated on the basis of 1000 permutations.

https://doi.org/10.1371/journal.pone.0223759.g005

Although accumulating evidence supports the notion that gene transcription might be linked with repositioning into the nuclear interior [38–40], several studies have shown that nuclear periphery can also be a transcriptionally "active environment" [35, 42, 69]. Despite the fact that transcription-induced relocalization of protein-coding genes or lamina associated enhancers [41, 69–72] were shown to precede the actual transcription-mediated responses in the murine immune system [41, 43, 44, 73] we have not observed such relocalization of microRNA gene loci before and after activation/differentiation of T cells and macrophages. It still remains unresolved whether transcription actually controls chromatin organization and gene repositioning or *vice versa*. It has been reported that chromatin loops [8] and contacts between regulatory DNA elements and genes in the β-globin locus were unaffected upon transcription inhibition. These reports are in line with our findings in which transcription inhibition did not affect the localization of microRNA genes nor caused a repositioning in T cells.

Perinuclear positioning of microRNA genes was not affected by changes in chromatin conformation during murine development. Our results in bone marrow cells and ESCs support that subnuclear localization of these microRNA gene loci is conserved between embryonic stem cells and terminally differentiated immune cells. In contrary, the protein-coding *Tnfα* gene locus altered its subnuclear localization during development. However, the unique and intriguing chromatin landscape of ESCs has been well documented [74–76], with their nuclear periphery being at the same time a transcriptionally permissive and repressive compartment [77]. Core pluripotency genes expressed in ESCs, such as *Sox2*, *Nanog* and *Oct4* avoid peripheral localization [78], whereas up-regulated genes such as *Ptn*, *Sox6*, and *Nrp1* relocate from the nuclear periphery to the nuclear center during ESC differentiation [12, 79]. These reports are in line with our findings, where *miR-17-92* cluster, which is perinuclearly localized from embryonic stem cells to differentiated myeloid cells, was highly expressed in mESCs [80].

Studies in *S.cerevisiae* and *D.melanogaster* indicated that active transcription occurs in the NPC vicinity, causing chromatin recruitment to the nuclear periphery [14, 16, 81]. In addition to nuclear transport, NUP153 and NUP93 are considered as gene expression regulators since they control cell type specific gene expression transcriptional programs [82, 83]. Depletion of NUP153 does not affect nuclear transport, though it induces changes in gene transcription [15]. DamID experiments reported that these nucleoporins interact with ciLAD domains and bind to SE in U2OS and IMR-90 cells [83]. These findings are in accordance with our observations regarding the transcriptionally active microRNA genes at the nuclear periphery. In addition, NUP98 also regulates gene expression [84]. It has been reported that in *D.melanogaster* NUP98 interacts with transcriptionally active developmental and cell cycle associated genes in the nucleoplasm [13]. This nucleoporin is characterized as a more dynamic molecule that can detach from the nuclear periphery and bind to promoters at a distance from the NPC [85]. This is in accordance with our findings suggesting no significant differences in NUP98 binding between the peripheral microRNA loci and all the protein-coding genes. Therefore, a potential explanation for the perinuclear localization of microRNA gene loci might be their interaction with NPCs.

Our comparative analysis of DamID-derived sequencing data revealed that microRNA genes are preferentially positioned outside constitutively-repressed LAD regions in *M*.

musculus and this localization pattern is conserved among four different species (*H.sapiens*, *M. musculus*, *C.elegans* and *D.melanogaster*). We also documented that both microRNA genes and protein-coding genes display the same preference to avoid cLAD localization. This result is compatible with our immuno-RNA-DNA FISH analysis, showing that microRNA genes are actively transcribed even when colocalized with Lamin-B1. This is in line with previous reports documenting transcriptionally active gene loci in concert with ciLAD-localization [12, 86]. Conclusively, our results are in accordance with reports showing that the frequency of gene colocalization with the nuclear lamina can be locus-specific [87] and that in general microRNA gene colocalization with the nuclear lamina is not associated with attenuated pri-microRNA transcription.

Ultimately, the peripheral positioning of microRNA gene loci might also represent an evolutionary aspect of chromatin organization. cLAD domains are enriched for LINE (Long Interspersed Elements) sequences [36] and the evolution of microRNA genes is speculated to descent from transposable elements integration into the genome [88, 89]. Next-generation sequencing and computational comparative analyses of small RNAs have demonstrated that sequence homology is more frequent for MITEs (Miniature Inverted-repeat Transposable Elements) and DNA transposons and less prevalent for LTR (Long Terminal Repeat) or non-LTR retrotransposons (SINEs, LINEs) or satellite repeats, supporting the notion of microRNA gene derivation from transposable elements [88, 90]. Additionally, it was documented that in human $CD4^+$ cells, HIV-1 integrates preferentially in regions of the eukaryotic genome found at the nuclear periphery, in proximity to nuclear pores, avoiding the heterochromatic LAD regions in order to facilitate the transcriptional regulation of the viral genome [91]. These findings provide additional evidence for the evolutionary denouements of peripheral localization and reconfirm the subnuclear positioning of the microRNA genes observed in our study.

In conclusion, our report elucidates the interplay between subnuclear localization of microRNA gene loci and their transcriptional regulation in the murine innate and adaptive immune system, providing valuable additional knowledge of chromatin organization and gene regulation at the nuclear periphery.

Materials and methods

Ethics

All procedures were conducted according to Greek national legislations and institutional policies upon ethical committee approval. Mice were maintained at the Institute of Molecular Biology and Biotechnology (IMBB) animal facility following the institutional guidelines based on the Greek ethical committee of animal experimentation, approved by the General Directorate of Veterinary Services, Region of Crete (license number: EL91BIO-02). *Bach1*$^{-/-}$ mice were kindly provided by Dr. Kazuhiko Igarashi (Tohoku University). Mice were bedded in sawdust cages with up to three cage mates and exposed to a 12-hour light-dark cycle (dark from 19:00 to 07:00 h). The room temperature where the animals were housed was stable at 23˚C and room humidity was 50%.

Cell culture

Thymocytes were isolated from 4-week old mice, and peripheral $CD4^+$ cells were obtained from axillary, popliteal lymph nodes and spleens of 5-6-week-old mice by positive selection with CD4 MicroBeads and MACS separation columns. Differentiation of naive $CD4^+$ T cells was carried out by stimulation with plate-bound αCD3 and αCD28 antibodies. Cells were cultured in CLICK's medium supplemented with 10% FBS, 100 μg/ml Penicillin/Streptomycin, 0.05 mM β-mercaptoethanol, 2 mM L-Glutamine and 25 mM HEPES for five to six days. For

TH1 cell differentiation, culture media were supplemented with 20 units/ml IL-2, 3.5 μg/ml IL-12 and 10 mg/ml IL-4. For TH2 cell differentiation 20–50 units/ml of IL-2, 10 μg/ml IL-4 and 10 mg/ml IFNγ were used. Re-stimulation of terminally differentiated TH1 and TH2 cells was carried out with αCD3 plate-bound antibodies for one hour. Cell identity upon opposing conditions of differentiation was further assessed by qRT-PCR analysis for the expression of *Il4* and *Ifnγ* genes. Peritoneal macrophages were elicited from 10-week old mice, 4 days after intraperitoneal treatment with thioglycollate medium, and *in vitro* stimulated at various timepoints with 50 ng/mL LPS (Invivogen). Bone marrow cells were isolated from 10-week old mice femurs and tibia and cultured with 30% custom-made L929 conditioned media for 7 days to achieve a complete differentiation towards the macrophage lineage. Macrophages were cultured in Dulbecco's Modified Eagle's Medium supplemented with 10% FBS, 1% L-Glutamine, 1% penicillin and streptomycin and stimulated at various timepoints with 50 ng/mL LPS (Invivogen). Macrophage cell identity was further assessed with both immunofluorescence and flow cytometry analyses for the expression of CD11b and F4/80 macrophage-specific surface markers. The feeder-independent mouse embryonic stem cell lines JM8.N4 and CGR8 were cultured on 0.1% gelatinized tissue culture plates using the Dulbecco's Modified Eagle's Medium supplemented with 15% fetal bovine serum, 1% L-Glutamine, 1% penicillin and streptomycin, 500 U/ml leukemia inhibitory factor and 100 μM β-mercaptoethanol.

cDNA synthesis and RT-PCR

For quantitative pri-miRNA expression analysis following α-amanitin treatment, whole cell RNA was prepared using the TRI-REAGENT (SIGMA, T9424) following the manufacturer's instructions. In order to eliminate DNA contamination, RNA samples were treated with DNase I (New England Biolabs, M0303L) for 3 hours at 37˚C. cDNA synthesis was performed using 500 ng precipitated RNA and 5pmol of oligo-d(T) primer. For each reverse transcription reaction 200 units M-MuLV Reverse Transcriptase (NEB, M0253S) were used. In parallel with reverse transcriptase reactions, control reactions devoid of the enzyme were prepared in order to verify the absence of DNA contamination in the subsequent quantitative PCR (qPCR) reactions. 10% of the cDNA produced was used for qPCR using the SYBR Green PCR Master mix (Applied Biosystems, Cat.No.4309155) according to the manufacturer's instructions. Normalization was performed utilizing *Hprt1* mRNA levels. The primer sets used for pri-miRNA quantitation were the following: *miR-142*.F 5′-GAAGAATCCCCGTGGACAGA-3′, *miR-142*.R 5′-CCCAAGTATCAGGGGTCAGG-3′, *miR-146a*.F 5′-GCCAG CCCTGTAAAAACACA-3′, *miR-146a*.R 5′-TCTTCGCTGGGATTATGGGG-3′, *miR-155*.F 5′-ACCCTGCTGGATGAACGTAG-3′, *miR-155*.R 5′-CATGTGGGCTTGAA GTTGAG-3′, *Hprt1*.F 5′-GTCCCAGCGTCGTGATTAGC-3′, *Hprt1*.R 5′-TTCCA AATCCTCGGCATAATG-3′

3D fluorescence *in situ* hybridization (RNA-DNA FISH)

To remove the cytoplam, cells were treated for either 2.5 minutes (thymocytes and CD4) or 3 minutes (TH1, TH2 and BMDMs) or 4 minutes (TEPMs) with cytoskeletal buffer (CSK) containing 100mM NaCl, 300mM sucrose, 3mM MgCl2, 10mM PIPES, 0.5% Triton X-100, 1mM EGTA, and 2mM vanadyl-ribonucleoside complex. Cells were then fixed with 4% PFA/1X PBS for 10 minutes, washed three times with 70% ethanol. For each hybridization 100ng from each probe (DNA and RNA probes), 1μg mouse COT-1 DNA and 20μg yeast transfer RNA were lyophilized for 15 minutes at 45˚C, resuspended in 5μl de-ionized formamide and incubated at 37˚C for one hour. Probes were further denatured at 95˚C for 10 minutes and then thoroughly mixed with 5μl of 2X hybridization buffer (4X SSC, 20% Dextran sulfate, 2mg/ml

acetylated BSA, 50mM Sodium Phosphate). Cells were then dehydrated through an ethanol series and hybridization was done overnight at 37˚C after either 2.5 minutes (thymocytes, CD4) or 4 minutes (TH1, TH2, TEMPs and BMDMs) denauration at 73˚C. After the post hybridization washes, a tyramide signal ampilificaion (TSA) of primary microRNA transcripts was performed. Tyramide signal amplification reaction was performed using TSA biotin system kit (Perkin Elmer). More specifically, cells were blocked for 30 minutes with TNB blocking buffer (100mM Tris-HCl pH 7.5, 150mM NaCl, 0.5% blocking reagent provided with the kit) and then incubated with streptavidin (SA), conjugated with horseradish peroxidase (HRP) in a dilution of 1/200 in TNB for additional 30 minutes at RT. The hybridized cells were washed twice with TNT buffer (100mM Tris-HCl pH 7.5, 150mM NaCl, 0.05% Tween 20) for 3 minutes at RT. The cells were then incubated for 10 minutes at RT with biotinylated tyramide in a dilution of 1/50 in amplification diluent and rinsed twice with TNT buffer for 3 minutes. For the visualization of the amplified RNA signal, cells were incubated with fluorophore-conjugated SA-488 for 30 minutes at RT, washed twice with TNT buffer and once with 1X PBS for 3 minutes each and mounted with ProLong Gold antifade reagent containing 4′,6-diamidino-2-phenylindole (DAPI).

3D fluorescence *in situ* hybridization (DNA FISH)

Cells were fixed with 4% PFA/1X PBS for 10 minutes, permeabilized with 0.5% Triton X-100 for 5 minutes, rinsed with 1X PBS and incubated in 20% glycerol/1X PBS for 30 minutes. After three freeze-thaw cycles in liquid nitrogen, cells were incubated in 0.1N HCl for 5 minutes, rinsed with 2X SSC and dehydrated through an ethanol series. DNA probe (0.1 μg) was denatured for 5 min at 95˚C and applied to coverslips. Hybridization of fixed cells was performed overnight at 37˚C after 5 minutes denaturation at 73˚C. Cells were rinsed three times with 2X SSC, once with 1X PBS and mounted in ProLong Gold containing DAPI (Invitrogen).

RNA FISH probes

cDNA probes were constructed to detect the pri-microRNA transcript. The procedure entailed the creation of 1kb probes cloned into a TOPO® TA vector. BAC DNA containing each microRNA gene was used as template for the amplification of 1kb PCR fragments encompassing the manure microRNA genomic region. The primer sets used for PCR amplification are listed below. The ~1kb PCR products were subsequently purified and cloned into a TOPO® TA vector. The isolated cloned plasmids were used for the preparation of the cDNA FISH probes. To confirm the cDNA probe specificity, we conducted RNA FISH on RNAse A treatment cells for 45 minutes. Furthermore, the empty TOPO® TA vector was also used for the preparation of biotinylated probes and used as a negative control. Primers used for the amplification of the 1Kb pri-microRNA fragments: *miR-181a1b1*.F: 5′-CATGCGTCCTTGCAGTTCTTT-3′, *miR-181a1b1*.R: 5′-GGATAACGGGGCAGGAAGTA-3′, *miR-181a2b2*.F: 5′-GTGAGAGACCCAACAGCAG-3′, *miR-181a2b2*.R: 5′-CCTGGAGCAGTACTTCCGTA-3′, *miR-181c*.F: 5′-GGTCGATGGTTTGTCTGAGC-3′, *miR181c*.R: 5′-GCAGGAGTTTCACACAAGCA-3′, *miR-142*.F: 5′-GCCATTTCTGCCAACACACT-3′, *miR-142*.R: 5′-CCCCAGGCTGTGTCTTAGTC-3′, *miR-146a*.F: 5′-AGCACTGTCAACCTGACACA-3′, *miR-146a*.R: 5′-GGACCAGCAGTCCTCTTGAT-3′, *miR-17/92*.F: 5′-ACTTCTGGCTATTGGCTCC-3′, *miR-17/92*.R: 5′-AACTTCACCTAAGCCCCCAC-3′, *miR-155*.F: 5′-CGGTTTGTGAGTCCCCAAAG-3′, *miR-155*.R: 5′-ATGTCAGTCGAGAATGGCCG-3′, *miR-let7e*.F: 5′-CACCCTCCCTACTTCTGGTC-3′, *miR-let7e*.R: 5′-AAAGGAACCAGGAGATGCCT-3′.

α-Amanitin treatment

Thymocytes, $CD4^+$ and TH2 cells were treated with Click's culture media supplemented with 10% FBS, 100μg/ml Penicillin/Streptomycin, 0.05mM β-mercaptoethanol, 2mM L-Glutamine, 25mM HEPES, 20–50 U/ml IL-2 and 50μg/ml α-amanitin for 6 hours at 37˚C. Cells treated under the same conditions without α-amanitin were used as a control. CGR8 embryonic stem cells were cultured as previously described and treated with α-amanitin for 6h.

Immuno-DNA-FISH

Combined detection of LMNB1 and microRNA genes was carried out and the procedure followed was a combination of the DNA FISH and Immunofluorescence (IF) analysis. After DNA FISH hybridization, the cells were blocked with IF blocking buffer (1% BSA/1X PBS) for 30 minutes, incubated with the primary antibody (LaminB1 or Lamin A/C 1:200) for 1 hour, with the secondary antibody (Invitrogen 1:500) for 45 minutes, rinsed three times with 1X PBS and mounted as above.

Immuno-RNA-FISH

For the IF/RNA-DNA FISH experiments the steps followed included RNA/DNA FISH (as previously described) prior to IF labeling as described in the IF/DNA FISH section.

Confocal microscopy and quantitative 3D image analysis

Images were acquired using inverted laser scanning confocal microscope with spectral detection (Leica TCS SP8 microscope unit). Maximum projections and deconvolution of the images were performed with Volocity software (Perkin Elmer) by two different investigators. Images of ~25–40 optical sections were captured with a 63x objective (step of 250nm) and acquired at different λs. A 405nm laser was used to excite and detect DAPI staining, whilst 488-nm, 561-nm and 633-nm lasers were used to excite and detect Alexa Fluor 488, Alexa Fluor 561 and Alexa Fluor 647 respectively in separate sequence to avoid bleed-through in different channels. Maximum projections and deconvolution of the images were performed with the Volocity software (Perkin Elmer) by two independent investigators. Intranuclear distances between microRNA gene alleles and the edges of the cell nucleus, were determined from the center of the gene allele to the edge of the cell border, for all DNA- RNA-FISH and IF experiments. The absolute distances were normalized by the nuclear radius for each scored cell. In order to analyze and visualize the normalized distances, we clustered them in 10 concentric circles of equal area (0–0.1, 0.1–0.2, 0.2–0.3, 0.3–0.4, 0.4–0.5, 0.5–0.6, 0.6–0.7, 0.7–0.8, 0.8–0.9, 0.9–1) as presented in S2A Fig where 0 and 1 were determined as the nuclear periphery and the nuclear center respectively. The aforementioned measurements have only been performed for images depicting nuclei with two signals (alleles) and having an intact 3D architecture. For all cell types under investigation, at least 120 nuclei were analyzed per biological replicate. Furthermore, the positions of microRNA gene alleles relative to LMNB1 were also determined through the analysis of 3D-preserved nuclei using the Volocity software. microRNA gene allele (red) and LMNB1 protein (green) colocalization was determined either by juxtaposition and partial overlap of red and green pixels or complete overlap between red and green pixels.

Statistical analysis

Statistical analysis for the randomness of allelic distance distribution was performed using the non-parametric two-tailed Kolmogorov-Smirnov test. The reported p and D values were calculated with the XL-STAT and GraphPad Prism 7 software package. *The* p-value for statistically

significant differences in allele distribution comparisons was set to $p < 0.0001$. Welch's T-test was used to test significant differences between microRNA within and outside of cLADs. Pearson r was used to study the linear correlation between microRNA within or outside cLADs and gene density. For data presentation, graphs were designed using GraphPad Prism 7 and Sigma Plot Software.

Bioinformatic analysis of microRNA cLAD/ciLAD co-localization characterization and distance distribution assessment

Datasets used for the analysis of microRNA cLAD/ciLAD co-localization: mouse pre-miRNA gene coordinates were downloaded from miRBase (Release 21) for four different species (mouse: *Mus musculus*, human: *Homo sapiens*, fly: *Drosophila melanogaster*, worm: *Caenorhabditis elegans*). LAD coordinates for the same species were obtained from published DamID experiments in human [54], mouse [12], fruit fly [55] and worm [56] respectively. For the mouse genome we obtained constitutive LAD domains through comparison of four different tissues [12]. For the same genome and from the same experiments we obtained the constitutive inter-LAD (ciLAD) domains, termed as the regions that constitute domains intervening defined LADs in the aforementioned tissues studied. Coordinates for both microRNA and cLAD/ciLAD were converted to hg19 (human), mm9 (mouse), dm3 (fly) and ce10 (worm). Protein coding gene coordinates were obtained from the UCSC Genome Browser under the RefSeq catalogues of Genes and Gene Prediction Tracks. For human and mouse genomes we made use of EBI's Expression Atlas to define constitutive protein coding genes. Human constitutive genes were called the ones which were designated as highly expressed in at least 80% of the 32 studied tissues, while tissue-specific ones were called on the basis of the corresponding percentage being less than 10%. For the mouse genome as only 6 tissues were available we only called constitutive genes the ones belonging to the top 10% of expressing genes in all 6 tissues. Analysis of microRNA overlap with cLAD and ciLAD: overlap enrichment analysis was conducted as follows. The total overlap percentage between microRNA gene loci and cLAD/ciLAD was calculated through the intersection of the two coordinate files, using BEDTools [92] intersect function. The enrichment of the observed overlap was calculated as the ratio over an expected value obtained through a simple calculation of intersection, based on the genome coverage percentage of each of the two coordinates. Following this analysis, enrichment values greater than 1 correspond to a greater overlap than the one expected by chance, indicative of co-localization preference. Values below 1 are indicative of an avoidance of co-localization preference. The significance of the enrichment values was calculated in all cases on the basis of a permutation test as previously described [93]. The microRNA gene coordinates were shuffled in the genome in random positions, keeping the distribution of sizes and number of elements unchanged and the observed overlap was calculated. This process was repeated for 1000 such permutations and p-values were set as the ratio of times an overlap as big (or as small) as the initial one was found in the total number of trials ($N = 1000$). In cases where not even a single random permutation yielded such a high (or low) overlap value, p-value was set to be $<1/N$, in our case <0.001. Analysis of mouse microRNA distance distribution from cLAD/ciLAD: having observed a clear opposite tendency for co-localization of mouse microRNA genes in cLADs and ciLADs we went on to check whether this tendency was also quantitative in the sense of distance from cLAD/ciLAD boundaries, that is whether microRNAs exhibited preferences towards or away from the regions of transition between the two domain categories. To answer this question for each mouse microRNA gene locus, we calculated the distance to the closest cLAD/ciLAD domain. For microRNA gene loci falling outside the corresponding domains we retained only those that lied within one domain size from the closest

boundary (for instance, if a cLAD was 100 kb and a microRNA gene locus was lying >100 kb upstream or downstream of its closest boundary, the microRNA gene was discarded from the analysis). We then scaled the obtained distances by dividing over the cLAD/ciLAD size in order to accommodate the variability in domain sizes. In this way, a microRNA gene locus could either: a) lie within the domain and thus be no farther than half the domain size from its closest boundary, or b) lie outside of the domain and thus, by definition, not farther than one full domain length. As there is no reason to assume a directional effect that distinguishes between the domain boundaries or upstream/downstream localization, we took all distances within the domains as positive and all distances from outside the domain as negative. In this way the scaled microRNA-cLAD/ciLAD distances were defined in a range of [-1, 0.5], with -1 being the farthest possible element outside the domain, 0 being the boundary and 0.5 being the farthest possible towards the center of the domain.

Analysis of microRNA and mRNA loci overlaps with nucleoporins

An overlap analysis was performed in a way similar to the one described for the cLAD/ciLAD regions. This time the compared coordinates were the ones of protein-coding and microRNA gene loci against the nucleoporin peaks as provided by publicly available datasets.

RNA/GRO-seq analysis

Depending on the dataset used in each analysis, either normalized gene counts (RPKM) or continuous signal values (in the case of GRO-seq) were implemented. In the case of RNA-seq RPKM values were assigned to each gene that was included in the public dataset. For GRO-seq, provided as continuous scores in the form of bigWig files, we calculated a mean aggregate score along the region that corresponded to each locus' coordinates as described above.

GEO accession numbers of datasets used for comparative-analyses

LaminB1 DamID-seq Human: GSE8854, LaminB1 DamID-seq mouse: GSE17051, LaminB1 DamID-seq fruit fly: GSE5089, LEM-2 ChIP-seq worm: GSE25933, RNA-seq mouse ESCs: GSM2095053, RNA-seq mouse Thymocytes: GSM2095060, RNA-seq mouse CD4 cells: GSM1120730, RNA-seq mouse TH1 cells: GSM1120731, https://www.ncbi.nlm.nih.gov/geo/query/acc.cgi?acc=GSM1120731RNA-seq mouse TH2 cells: GSM1120732, RNA-seq mouse BMDMs: GSM940701, GRO-seq mouse ESCs & MEFs: GSE27037, NUP 153 DamID-seq: GSE64008, UP-98 ChIP-seq: GSE48996, NUP-93 DamID-seq: GSE87831.

Supporting information

S1 Fig. Relative expression levels of genes within the BAC clones used for DNA/RNA-DNA FISH experiments of microRNA genes. (A) Bar graphs depicting the relative mRNA levels of both coding and non-coding genes flanking each of the eight microRNA genes under study in each BAC clone. RPKM (Reads Per Kilobase per Million) values calculated from publicly available RNA-seq datasets for the six cell types indicated. (B) Nascent transcription of the genes as in (A) as deduced from aggregate score analysis of publicly available GRO-seq data in $CD4^+$ T-cells and mouse embryonic fibroblasts (MEFs).
(TIF)

S2 Fig. Statistical analysis for the perinuclear distribution of microRNA gene loci. (A) Compartmentalization of measured nuclei based on normalized distances (NDs). Distance between microRNA gene alleles and the edge of the cell nucleus as deduced by DAPI staining were normalized to the nuclear radius yielding 10 concentric shells. ND = 1 defines the center

of the nucleus, whereas ND = 0 is indicative of the nuclear periphery. (B) Cumulative frequency graph of calculated allele ND values, following a reversed distribution pattern compared to the *Tnfα* control in thymocytes, $CD4^+$, TH1, TH2 cells and TEPMs (naive and LPS-stimulated). Kolmogorov Smirnov (KS) non-parametric analysis, showing that the allelic distributions of microRNA gene allele ND values differ from *Tnfα* allele NDs ($p>0.05$). *p*- and D-values characterizing each distribution are depicted in the table. The relative cumulative frequency values of distributions are depicted on the y-axis, whereas their corresponding ND values on the x-axis. KS-test *p*-values are separately depicted for each distribution comparison. (C) Single z-stack confocal images of DNA FISH analysis indicating the perinuclear localization of the microRNA genes tested compared to the internal spatial distribution of the *Tnfα* control locus. Scale bar 2μm. Box plots displaying the quantitative analysis of the intranuclear 3D distance between each allele and the nuclear periphery in naive and LPS-stimulated BMDMs. The reported *p*-values were calculated using the XL-STAT software package. Allele distribution differences were calculated with the Kolmogorov-Smirnov test analysis ($p<0.0001$). (D) Bar graphs representing the frequency of cells bearing at least one allele associated with nuclear lamina in naive (0h) and LPS (2h, 6h) stimulated BMDMs. The total number of nuclei deployed in these measurements were: *miR-146a*: n = 101 (0h), n = 263 (2h), n = 344 (6h), *miR-155*: n = 112 (0h), n = 215 (2h), n = 122 (6h) and *miR-let7e*: n = 33 (0h), n = 86 (2h), n = 48 (6h).
(TIF)

S3 Fig. Perinuclear microRNA gene loci localization irrespective of their transcription activity. Distribution of non-expressing and expressing gene allele ND values. The normalized distances (y-axis) indicated in each box plot for each microRNA gene are characterized by their median. 95% of the ND values are included within the whiskers of each box plot, whereas single allele outliers (remaining 5% of total NDs) are indicated in the vicinity outside the whiskers. (A) T cells: Thymocytes, $CD4^+$, TH1 and TH2 cells. Total number of alleles analyzed for each dataset were n = 623, n = 807, n = 497, n = 472 for thymocytes, $CD4^+$, TH1 and TH2 cells, respectively. (B) TEPMs and BMDMs before and after LPS stimulation. The total allele number contained in each dataset were n = 1154 for TEPMS and n = 2652 for BMDMs. (C) Relative mRNA expression corrected to *Hprt1* mRNA levels of *pri-miRNA-146α*, *-142*, *-155* with/or without *α*-amanitin treatment in thymocytes, $CD4^+$ and TH2 cells. (D) Allelic expression profile of the indicated microRNA genes as deduced by RNA-DNA FISH analysis before and after transcriptional inhibition of cells with *α*-amanitin. (E) KS-test results related to gene alleles ND distribution presented in Fig 3D. (F) KS-test results related to gene alleles ND distribution presented in Fig 3E. (G) Comparison of microRNA and protein coding mRNA gene loci coordinates against peaks from human NUP98. Enrichment was calculated as observed over expected ratios of overlaps between the compared genomic regions. P-value was calculated on the basis of 1000 random permutations of the peaks' regions. A value of <0.001 indicates that not one out of 1000 permutations had a value as high as the one observed.
(TIF)

S4 Fig. Perinuclear distribution of microRNA gene loci in non-differentiated cells. (A) Perinuclear distribution of microRNA genes and *Tnfα*, as a control locus, in CGR8 embryonic stem cells. Single z-stack DNA FISH images portraying the peripheral localization of microRNA gene loci (red). KS non-parametric analysis, showing that the allelic distributions of microRNA gene allele ND values compared to *Tnfα* are alike ($p>0.05$). P- and D-values characterizing the compared distributions are depicted. The relative cumulative frequency values of compared distributions are depicted on the y-axis, whereas their corresponding ND values on the x-axis. KS-test p-values are separately depicted for each distribution comparison. The

analysis was performed in n = 208 total alleles for *miR-181a1b1*, n = 206 for *miR-181a2b2*, n = 240 for *miR-181c*, n = 214 for *miR-142*, n = 188 for *miR-146a*, n = 130 for *miR-17-92*, n = 158 for *miR-155*, n = 214 for *miR-let7e* and n = 160 alleles for *Tnfα* respectively. (B) KS-test indicating the statistically significant ($p<0.001$) differences of microRNA gene allele distributions compared to *Tnfα* in bone marrow cells. A total of 2044 alleles were counted. (C) KS-test results related to gene allele ND distribution presented in Fig 5A for JM8.N4 ESCs. A total of 1968 alleles were measured. (D) Bar graph representing the gene density for each chromosome of *M.musculus*, *H.sapiens*, *D. melanogaster* and *C.elegans*.
(TIF)

S1 Table. Allelic expression profile of genes localized on BAC clones utilized for DNA FISH of microRNA gene loci. Monoallelic expression (blue), biallelic expression (red), undetermined (black), according to "dbMAE: the database of autosomal monoallelic expression". Assembly used for coordinates: GRCm38.p3 (C57BL/6J) [94].
(PDF)

S1 Video. 3D-DNA FISH experiment in $CD4^+$ cells. Visualization of a representative 3D-DNA FISH experiment in $CD4^+$ cells demonstrating *miR-155* gene locus that is preferentially located at the nuclear periphery. *miR-155* gene locus (red) was labeled with Alexa-594 and $CD4^+$ cell DNA counterstained with DAPI (blue). The video was created based on raw confocal microscopy data with the Volocity software (Perkin Elmer).
(MOV)

S2 Video. 3D-IF/DNA FISH in $CD4^+$ cells. Visualization of a representative 3D-IF/DNA FISH in $CD4^+$ cells demonstrating the colocalization of *miR-155* gene locus with the nuclear lamina. As shown here, for most $CD4^+$ cells, *miR-155* alleles are completely embedded in Lamin-B1-stained regions. *miR-155* gene locus (red) was labelled with Alexa-594, Lamin-B1 was labeled with Alexa-488 and $CD4^+$ cell DNA counterstained with DAPI (blue). The video was created based on raw confocal microscopy data with the Volocity software (Perkin Elmer).
(MOV)

Acknowledgments

We thank Dr. Julie Chaumeil for critical reading of the manuscript. We thank Maria Stratigopoulou for lamin staining in TEPMs. CGR8 mESCs were kindly provided by Dr. Androniki Kretsovali. Excellent technical assistance has been provided by Manuela Kapsetaki and Despoina Tsoukatou.

Author Contributions

Conceptualization: Charalampos G. Spilianakis.

Data curation: Eralda Salataj, Chrysoula Stathopoulou, Róbert A. Hafþórsson, Christoforos Nikolaou, Charalampos G. Spilianakis.

Formal analysis: Eralda Salataj, Chrysoula Stathopoulou, Róbert A. Hafþórsson, Christoforos Nikolaou, Charalampos G. Spilianakis.

Funding acquisition: Charalampos G. Spilianakis.

Investigation: Eralda Salataj, Chrysoula Stathopoulou, Róbert A. Hafþórsson, Christoforos Nikolaou, Charalampos G. Spilianakis.

Methodology: Eralda Salataj, Chrysoula Stathopoulou, Róbert A. Hafþórsson, Christoforos Nikolaou, Charalampos G. Spilianakis.

Project administration: Charalampos G. Spilianakis.

Resources: Charalampos G. Spilianakis.

Supervision: Charalampos G. Spilianakis.

Validation: Eralda Salataj, Chrysoula Stathopoulou.

Visualization: Eralda Salataj, Chrysoula Stathopoulou.

Writing – original draft: Eralda Salataj.

Writing – review & editing: Eralda Salataj, Chrysoula Stathopoulou, Christoforos Nikolaou, Charalampos G. Spilianakis.

References

1. Fraser P, Bickmore W. Nuclear organization of the genome and the potential for gene regulation. Nature. 2007; 447(7143):413–7. https://doi.org/10.1038/nature05916 PMID: 17522674.
2. Lanctot C, Cheutin T, Cremer M, Cavalli G, Cremer T. Dynamic genome architecture in the nuclear space: regulation of gene expression in three dimensions. Nature reviews Genetics. 2007; 8(2):104–15. https://doi.org/10.1038/nrg2041 PMID: 17230197.
3. Clowney EJ, LeGros MA, Mosley CP, Clowney FG, Markenskoff-Papadimitriou EC, Myllys M, et al. Nuclear aggregation of olfactory receptor genes governs their monogenic expression. Cell. 2012; 151 (4):724–37. https://doi.org/10.1016/j.cell.2012.09.043 PMID: 23141535; PubMed Central PMCID: PMC3659163.
4. Worman HJ, Fong LG, Muchir A, Young SG. Laminopathies and the long strange trip from basic cell biology to therapy. The Journal of clinical investigation. 2009; 119(7):1825–36. https://doi.org/10.1172/JCI37679 PMID: 19587457; PubMed Central PMCID: PMC2701866.
5. Schreiber KH, Kennedy BK. When lamins go bad: nuclear structure and disease. Cell. 2013; 152 (6):1365–75. https://doi.org/10.1016/j.cell.2013.02.015 PMID: 23498943; PubMed Central PMCID: PMC3706202.
6. Yu M, Ren B. The Three-Dimensional Organization of Mammalian Genomes. Annual review of cell and developmental biology. 2017; 33:265–89. https://doi.org/10.1146/annurev-cellbio-100616-060531 PMID: 28783961; PubMed Central PMCID: PMC5837811.
7. Zullo JM, Demarco IA, Pique-Regi R, Gaffney DJ, Epstein CB, Spooner CJ, et al. DNA sequence-dependent compartmentalization and silencing of chromatin at the nuclear lamina. Cell. 2012; 149 (7):1474–87. https://doi.org/10.1016/j.cell.2012.04.035 PMID: 22726435.
8. Mitchell JA, Fraser P. Transcription factories are nuclear subcompartments that remain in the absence of transcription. Genes & development. 2008; 22(1):20–5. https://doi.org/10.1101/gad.454008 PMID: 18172162; PubMed Central PMCID: PMC2151011.
9. van Steensel B, Belmont AS. Lamina-Associated Domains: Links with Chromosome Architecture, Heterochromatin, and Gene Repression. Cell. 2017; 169(5):780–91. https://doi.org/10.1016/j.cell.2017.04.022 PMID: 28525751; PubMed Central PMCID: PMC5532494.
10. Williams RR, Azuara V, Perry P, Sauer S, Dvorkina M, Jorgensen H, et al. Neural induction promotes large-scale chromatin reorganisation of the Mash1 locus. Journal of cell science. 2006; 119(Pt 1):132–40. https://doi.org/10.1242/jcs.02727 PMID: 16371653.
11. Stratigi K, Kapsetaki M, Aivaliotis M, Town T, Flavell RA, Spilianakis CG. Spatial proximity of homologous alleles and long noncoding RNAs regulate a switch in allelic gene expression. Proc Natl Acad Sci U S A. 2015; 112(13):E1577–86. Epub 2015/03/15. https://doi.org/10.1073/pnas.1502182112 PMID: 25770217; PubMed Central PMCID: PMC4386343.
12. Peric-Hupkes D, Meuleman W, Pagie L, Bruggeman SW, Solovei I, Brugman W, et al. Molecular maps of the reorganization of genome-nuclear lamina interactions during differentiation. Molecular cell. 2010; 38(4):603–13. https://doi.org/10.1016/j.molcel.2010.03.016 PMID: 20513434; PubMed Central PMCID: PMC5975946.
13. Kalverda B, Pickersgill H, Shloma VV, Fornerod M. Nucleoporins directly stimulate expression of developmental and cell-cycle genes inside the nucleoplasm. Cell. 2010; 140(3):360–71. https://doi.org/10.1016/j.cell.2010.01.011 PMID: 20144760.

14. Casolari JM, Brown CR, Komili S, West J, Hieronymus H, Silver PA. Genome-wide localization of the nuclear transport machinery couples transcriptional status and nuclear organization. Cell. 2004; 117 (4):427–39. https://doi.org/10.1016/s0092-8674(04)00448-9 PMID: 15137937.

15. Jacinto FV, Benner C, Hetzer MW. The nucleoporin Nup153 regulates embryonic stem cell pluripotency through gene silencing. Genes & development. 2015; 29(12):1224–38. https://doi.org/10.1101/gad.260919.115 PMID: 26080816; PubMed Central PMCID: PMC4495395.

16. Vaquerizas JM, Suyama R, Kind J, Miura K, Luscombe NM, Akhtar A. Nuclear pore proteins nup153 and megator define transcriptionally active regions in the Drosophila genome. PLoS genetics. 2010; 6 (2):e1000846. https://doi.org/10.1371/journal.pgen.1000846 PMID: 20174442; PubMed Central PMCID: PMC2820533.

17. Van de Vosse DW, Wan Y, Wozniak RW, Aitchison JD. Role of the nuclear envelope in genome organization and gene expression. Wiley interdisciplinary reviews Systems biology and medicine. 2011; 3 (2):147–66. https://doi.org/10.1002/wsbm.101 PMID: 21305702; PubMed Central PMCID: PMC3050641.

18. Bohmdorfer G, Wierzbicki AT. Control of Chromatin Structure by Long Noncoding RNA. Trends in cell biology. 2015; 25(10):623–32. https://doi.org/10.1016/j.tcb.2015.07.002 PMID: 26410408; PubMed Central PMCID: PMC4584417.

19. Guttman M, Amit I, Garber M, French C, Lin MF, Feldser D, et al. Chromatin signature reveals over a thousand highly conserved large non-coding RNAs in mammals. Nature. 2009; 458(7235):223–7. https://doi.org/10.1038/nature07672 PMID: 19182780; PubMed Central PMCID: PMC2754849.

20. Sun Q, Hao Q, Prasanth KV. Nuclear Long Noncoding RNAs: Key Regulators of Gene Expression. Trends in genetics: TIG. 2018; 34(2):142–57. https://doi.org/10.1016/j.tig.2017.11.005 PMID: 29249332; PubMed Central PMCID: PMC6002860.

21. van Wolfswinkel JC, Ketting RF. The role of small non-coding RNAs in genome stability and chromatin organization. Journal of cell science. 2010; 123(Pt 11):1825–39. https://doi.org/10.1242/jcs.061713 PMID: 20484663.

22. Bartel DP. MicroRNAs: genomics, biogenesis, mechanism, and function. Cell. 2004; 116(2):281–97. https://doi.org/10.1016/s0092-8674(04)00045-5 PMID: 14744438.

23. Mehta A, Baltimore D. MicroRNAs as regulatory elements in immune system logic. Nature reviews Immunology. 2016; 16(5):279–94. https://doi.org/10.1038/nri.2016.40 PMID: 27121651.

24. Lee Y, Kim M, Han J, Yeom KH, Lee S, Baek SH, et al. MicroRNA genes are transcribed by RNA polymerase II. The EMBO journal. 2004; 23(20):4051–60. https://doi.org/10.1038/sj.emboj.7600385 PMID: 15372072; PubMed Central PMCID: PMC524334.

25. Cai X, Hagedorn CH, Cullen BR. Human microRNAs are processed from capped, polyadenylated transcripts that can also function as mRNAs. Rna. 2004; 10(12):1957–66. https://doi.org/10.1261/rna.7135204 PMID: 15525708; PubMed Central PMCID: PMC1370684.

26. Morlando M, Ballarino M, Gromak N, Pagano F, Bozzoni I, Proudfoot NJ. Primary microRNA transcripts are processed co-transcriptionally. Nature structural & molecular biology. 2008; 15(9):902–9. PMID: 19172742.

27. Kim YK, Kim VN. Processing of intronic microRNAs. The EMBO journal. 2007; 26(3):775–83. https://doi.org/10.1038/sj.emboj.7601512 PMID: 17255951; PubMed Central PMCID: PMC1794378.

28. Winter J, Jung S, Keller S, Gregory RI, Diederichs S. Many roads to maturity: microRNA biogenesis pathways and their regulation. Nature cell biology. 2009; 11(3):228–34. https://doi.org/10.1038/ncb0309-228 PMID: 19255566.

29. Schwarz DS, Hutvagner G, Du T, Xu Z, Aronin N, Zamore PD. Asymmetry in the assembly of the RNAi enzyme complex. Cell. 2003; 115(2):199–208. https://doi.org/10.1016/s0092-8674(03)00759-1 PMID: 14567917.

30. Ketting RF, Fischer SE, Bernstein E, Sijen T, Hannon GJ, Plasterk RH. Dicer functions in RNA interference and in synthesis of small RNA involved in developmental timing in C. elegans. Genes & development. 2001; 15(20):2654–9. https://doi.org/10.1101/gad.927801 PMID: 11641272; PubMed Central PMCID: PMC312808.

31. Hutvagner G, McLachlan J, Pasquinelli AE, Balint E, Tuschl T, Zamore PD. A cellular function for the RNA-interference enzyme Dicer in the maturation of the let-7 small temporal RNA. Science. 2001; 293 (5531):834–8. https://doi.org/10.1126/science.1062961 PMID: 11452083.

32. Doxaki C, Kampranis SC, Eliopoulos AG, Spilianakis C, Tsatsanis C. Coordinated Regulation of miR-155 and miR-146a Genes during Induction of Endotoxin Tolerance in Macrophages. J Immunol. 2015; 195(12):5750–61. Epub 2015/11/06. https://doi.org/10.4049/jimmunol.1500615 PMID: 26538391.

33. Stathopoulou C, Kapsetaki M, Stratigi K, Spilianakis C. Long non-coding RNA SeT and miR-155 regulate the Tnfalpha gene allelic expression profile. PloS one. 2017; 12(9):e0184788. https://doi.org/10.1371/journal.pone.0184788 PMID: 28910376; PubMed Central PMCID: PMC5599032.

34. Shachar S, Voss TC, Pegoraro G, Sciascia N, Misteli T. Identification of Gene Positioning Factors Using High-Throughput Imaging Mapping. Cell. 2015; 162(4):911–23. https://doi.org/10.1016/j.cell.2015.07.035 PMID: 26276637; PubMed Central PMCID: PMC4538709.

35. Zhao H, Sifakis EG, Sumida N, Millan-Arino L, Scholz BA, Svensson JP, et al. PARP1- and CTCF-Mediated Interactions between Active and Repressed Chromatin at the Lamina Promote Oscillating Transcription. Molecular cell. 2015; 59(6):984–97. https://doi.org/10.1016/j.molcel.2015.07.019 PMID: 26321255.

36. Meuleman W, Peric-Hupkes D, Kind J, Beaudry JB, Pagie L, Kellis M, et al. Constitutive nuclear lamina-genome interactions are highly conserved and associated with A/T-rich sequence. Genome research. 2013; 23(2):270–80. https://doi.org/10.1101/gr.141028.112 PMID: 23124521; PubMed Central PMCID: PMC3561868.

37. Amendola M, van Steensel B. Nuclear lamins are not required for lamina-associated domain organization in mouse embryonic stem cells. EMBO reports. 2015; 16(5):610–7. https://doi.org/10.15252/embr.201439789 PMID: 25784758; PubMed Central PMCID: PMC4428043.

38. Schneider R, Grosschedl R. Dynamics and interplay of nuclear architecture, genome organization, and gene expression. Genes & development. 2007; 21(23):3027–43. https://doi.org/10.1101/gad.1604607 PMID: 18056419.

39. Dillon N. The impact of gene location in the nucleus on transcriptional regulation. Developmental cell. 2008; 15(2):182–6. https://doi.org/10.1016/j.devcel.2008.07.013 PMID: 18694558.

40. Chuang CH, Carpenter AE, Fuchsova B, Johnson T, de Lanerolle P, Belmont AS. Long-range directional movement of an interphase chromosome site. Current biology: CB. 2006; 16(8):825–31. https://doi.org/10.1016/j.cub.2006.03.059 PMID: 16631592.

41. Ktistaki E, Garefalaki A, Williams A, Andrews SR, Bell DM, Foster KE, et al. CD8 locus nuclear dynamics during thymocyte development. J Immunol. 2010; 184(10):5686–95. Epub 2010/04/21. https://doi.org/10.4049/jimmunol.1000170 PMID: 20404270.

42. Kim SH, McQueen PG, Lichtman MK, Shevach EM, Parada LA, Misteli T. Spatial genome organization during T-cell differentiation. Cytogenetic and genome research. 2004; 105(2–4):292–301. https://doi.org/10.1159/000078201 PMID: 15237218.

43. Rawlings JS, Gatzka M, Thomas PG, Ihle JN. Chromatin condensation via the condensin II complex is required for peripheral T-cell quiescence. The EMBO journal. 2011; 30(2):263–76. https://doi.org/10.1038/emboj.2010.314 PMID: 21169989; PubMed Central PMCID: PMC3025460.

44. Spilianakis CG, Lalioti MD, Town T, Lee GR, Flavell RA. Interchromosomal associations between alternatively expressed loci. Nature. 2005; 435(7042):637–45. Epub 2005/05/10. https://doi.org/10.1038/nature03574 PMID: 15880101.

45. Breuer M, Ohkura H. A negative loop within the nuclear pore complex controls global chromatin organization. Genes & development. 2015; 29(17):1789–94. https://doi.org/10.1101/gad.264341.115 PMID: 26341556; PubMed Central PMCID: PMC4573852.

46. D'Angelo MA. Nuclear pore complexes as hubs for gene regulation. Nucleus. 2018; 9(1):142–8. https://doi.org/10.1080/19491034.2017.1395542 PMID: 29095096; PubMed Central PMCID: PMC5973259.

47. Starling S. Gene regulation: The nuclear pore—a scaffold for inducible genes. Nature reviews Genetics. 2017; 18(5):273. https://doi.org/10.1038/nrg.2017.29 PMID: 28400601.

48. Hao B, Naik AK, Watanabe A, Tanaka H, Chen L, Richards HW, et al. An anti-silencer- and SATB1-dependent chromatin hub regulates Rag1 and Rag2 gene expression during thymocyte development. The Journal of experimental medicine. 2015; 212(5):809–24. https://doi.org/10.1084/jem.20142207 PMID: 25847946; PubMed Central PMCID: PMC4419350.

49. Lee HY, Johnson KD, Boyer ME, Bresnick EH. Relocalizing genetic loci into specific subnuclear neighborhoods. The Journal of biological chemistry. 2011; 286(21):18834–44. https://doi.org/10.1074/jbc.M111.221481 PMID: 21398517; PubMed Central PMCID: PMC3099700.

50. Levantini E, Lee S, Radomska HS, Hetherington CJ, Alberich-Jorda M, Amabile G, et al. RUNX1 regulates the CD34 gene in haematopoietic stem cells by mediating interactions with a distal regulatory element. The EMBO journal. 2011; 30(19):4059–70. https://doi.org/10.1038/emboj.2011.285 PMID: 21873977; PubMed Central PMCID: PMC3209778.

51. Igarashi K, Hoshino H, Muto A, Suwabe N, Nishikawa S, Nakauchi H, et al. Multivalent DNA binding complex generated by small Maf and Bach1 as a possible biochemical basis for beta-globin locus control region complex. The Journal of biological chemistry. 1998; 273(19):11783–90. https://doi.org/10.1074/jbc.273.19.11783 PMID: 9565602.

52. So AY, Garcia-Flores Y, Minisandram A, Martin A, Taganov K, Boldin M, et al. Regulation of APC development, immune response, and autoimmunity by Bach1/HO-1 pathway in mice. Blood. 2012; 120 (12):2428–37. https://doi.org/10.1182/blood-2012-04-426247 PMID: 22791292; PubMed Central PMCID: PMC3448256.

53. Jeong G, Lim YH, Kim YK. Precise mapping of the transcription start sites of human microRNAs using DROSHA knockout cells. BMC genomics. 2016; 17(1):908. https://doi.org/10.1186/s12864-016-3252-7 PMID: 27835943; PubMed Central PMCID: PMC5106785.

54. Guelen L, Pagie L, Brasset E, Meuleman W, Faza MB, Talhout W, et al. Domain organization of human chromosomes revealed by mapping of nuclear lamina interactions. Nature. 2008; 453(7197):948–51. https://doi.org/10.1038/nature06947 PMID: 18463634.

55. Pickersgill H, Kalverda B, de Wit E, Talhout W, Fornerod M, van Steensel B. Characterization of the Drosophila melanogaster genome at the nuclear lamina. Nature genetics. 2006; 38(9):1005–14. https://doi.org/10.1038/ng1852 PMID: 16878134.

56. Ikegami K, Egelhofer TA, Strome S, Lieb JD. Caenorhabditis elegans chromosome arms are anchored to the nuclear membrane via discontinuous association with LEM-2. Genome biology. 2010; 11(12): R120. https://doi.org/10.1186/gb-2010-11-12-r120 PMID: 21176223; PubMed Central PMCID: PMC3046480.

57. Deng Q, Ramskold D, Reinius B, Sandberg R. Single-cell RNA-seq reveals dynamic, random monoallelic gene expression in mammalian cells. Science. 2014; 343(6167):193–6. https://doi.org/10.1126/science.1245316 PMID: 24408435.

58. Reinius B, Sandberg R. Random monoallelic expression of autosomal genes: stochastic transcription and allele-level regulation. Nat Rev Genet. 2015; 16(11):653–64. https://doi.org/10.1038/nrg3888 PMID: 26442639.

59. Noguer-Dance M, Abu-Amero S, Al-Khtib M, Lefevre A, Coullin P, Moore GE, et al. The primate-specific microRNA gene cluster (C19MC) is imprinted in the placenta. Hum Mol Genet. 2010; 19(18):3566–82. https://doi.org/10.1093/hmg/ddq272 PMID: 20610438.

60. Reik W, Walter J. Genomic imprinting: parental influence on the genome. Nat Rev Genet. 2001; 2 (1):21–32. https://doi.org/10.1038/35047554 PMID: 11253064.

61. Lee JT. Disruption of imprinted X inactivation by parent-of-origin effects at Tsix. Cell. 2000; 103(1):17–27. https://doi.org/10.1016/s0092-8674(00)00101-x PMID: 11051544.

62. Tian D, Sun S, Lee JT. The long noncoding RNA, Jpx, is a molecular switch for X chromosome inactivation. Cell. 2010; 143(3):390–403. https://doi.org/10.1016/j.cell.2010.09.049 PMID: 21029862; PubMed Central PMCID: PMC2994261.

63. Seitz H, Royo H, Bortolin ML, Lin SP, Ferguson-Smith AC, Cavaille J. A large imprinted microRNA gene cluster at the mouse Dlk1-Gtl2 domain. Genome Res. 2004; 14(9):1741–8. https://doi.org/10.1101/gr.2743304 PMID: 15310658; PubMed Central PMCID: PMC515320.

64. Nozaki T, Imai R, Tanbo M, Nagashima R, Tamura S, Tani T, et al. Dynamic Organization of Chromatin Domains Revealed by Super-Resolution Live-Cell Imaging. Molecular cell. 2017; 67(2):282–93 e7. https://doi.org/10.1016/j.molcel.2017.06.018 PMID: 28712725.

65. Fiserova J, Efenberkova M, Sieger T, Maninova M, Uhlirova J, Hozak P. Chromatin organization at the nuclear periphery as revealed by image analysis of structured illumination microscopy data. Journal of cell science. 2017; 130(12):2066–77. https://doi.org/10.1242/jcs.198424 PMID: 28476938.

66. Xu J, Ma H, Jin J, Uttam S, Fu R, Huang Y, et al. Super-Resolution Imaging of Higher-Order Chromatin Structures at Different Epigenomic States in Single Mammalian Cells. Cell reports. 2018; 24(4):873–82. https://doi.org/10.1016/j.celrep.2018.06.085 PMID: 30044984; PubMed Central PMCID: PMC6154382.

67. Schmitt AD, Hu M, Ren B. Genome-wide mapping and analysis of chromosome architecture. Nature reviews Molecular cell biology. 2016; 17(12):743–55. https://doi.org/10.1038/nrm.2016.104 PMID: 27580841; PubMed Central PMCID: PMC5763923.

68. Wang H, Xu X, Nguyen CM, Liu Y, Gao Y, Lin X, et al. CRISPR-Mediated Programmable 3D Genome Positioning and Nuclear Organization. Cell. 2018. https://doi.org/10.1016/j.cell.2018.09.013 PMID: 30318144.

69. Ragoczy T, Bender MA, Telling A, Byron R, Groudine M. The locus control region is required for association of the murine beta-globin locus with engaged transcription factories during erythroid maturation. Genes Dev. 2006; 20(11):1447–57. https://doi.org/10.1101/gad.1419506 PMID: 16705039; PubMed Central PMCID: PMC1475758.

70. Wiblin AE, Cui W, Clark AJ, Bickmore WA. Distinctive nuclear organisation of centromeres and regions involved in pluripotency in human embryonic stem cells. Journal of cell science. 2005; 118(Pt 17):3861–8. https://doi.org/10.1242/jcs.02500 PMID: 16105879.

71. Zink D, Amaral MD, Englmann A, Lang S, Clarke LA, Rudolph C, et al. Transcription-dependent spatial arrangements of CFTR and adjacent genes in human cell nuclei. J Cell Biol. 2004; 166(6):815–25. https://doi.org/10.1083/jcb.200404107 PMID: 15364959; PubMed Central PMCID: PMC2172106.

72. Robson MI, de Las Heras JI, Czapiewski R, Sivakumar A, Kerr ARW, Schirmer EC. Constrained release of lamina-associated enhancers and genes from the nuclear envelope during T-cell activation facilitates their association in chromosome compartments. Genome Res. 2017; 27(7):1126–38. https://doi.org/10.1101/gr.212308.116 PMID: 28424353; PubMed Central PMCID: PMC5495065.

73. Deligianni C, Spilianakis CG. Long-range genomic interactions epigenetically regulate the expression of a cytokine receptor. EMBO Rep. 2012; 13(9):819–26. Epub 2012/07/28. https://doi.org/10.1038/embor.2012.112 PMID: 22836578; PubMed Central PMCID: PMC3432804.

74. Meshorer E, Misteli T. Chromatin in pluripotent embryonic stem cells and differentiation. Nat Rev Mol Cell Biol. 2006; 7(7):540–6. https://doi.org/10.1038/nrm1938 PMID: 16723974.

75. Gangaraju VK, Lin H. MicroRNAs: key regulators of stem cells. Nat Rev Mol Cell Biol. 2009; 10(2):116–25. https://doi.org/10.1038/nrm2621 PMID: 19165214; PubMed Central PMCID: PMC4118578.

76. Chen CZ, Li L, Lodish HF, Bartel DP. MicroRNAs modulate hematopoietic lineage differentiation. Science. 2004; 303(5654):83–6. https://doi.org/10.1126/science.1091903 PMID: 14657504.

77. Luo L, Gassman KL, Petell LM, Wilson CL, Bewersdorf J, Shopland LS. The nuclear periphery of embryonic stem cells is a transcriptionally permissive and repressive compartment. Journal of cell science. 2009; 122(Pt 20):3729–37. https://doi.org/10.1242/jcs.052555 PMID: 19773359; PubMed Central PMCID: PMC2758804.

78. Jost KL, Haase S, Smeets D, Schrode N, Schmiedel JM, Bertulat B, et al. 3D-Image analysis platform monitoring relocation of pluripotency genes during reprogramming. Nucleic Acids Res. 2011; 39(17): e113. https://doi.org/10.1093/nar/gkr486 PMID: 21700670; PubMed Central PMCID: PMC3177216.

79. Therizols P, Illingworth RS, Courilleau C, Boyle S, Wood AJ, Bickmore WA. Chromatin decondensation is sufficient to alter nuclear organization in embryonic stem cells. Science. 2014; 346(6214):1238–42. https://doi.org/10.1126/science.1259587 PMID: 25477464.

80. Hadjimichael C, Nikolaou C, Papamatheakis J, Kretsovali A. MicroRNAs for Fine-Tuning of Mouse Embryonic Stem Cell Fate Decision through Regulation of TGF-beta Signaling. Stem Cell Reports. 2016; 6(3):292–301. https://doi.org/10.1016/j.stemcr.2016.01.004 PMID: 26876669; PubMed Central PMCID: PMC4788761.

81. Buchwalter A, Kaneshiro JM, Hetzer MW. Coaching from the sidelines: the nuclear periphery in genome regulation. Nature reviews Genetics. 2019; 20(1):39–50. https://doi.org/10.1038/s41576-018-0063-5 PMID: 30356165; PubMed Central PMCID: PMC6355253.

82. Toda T, Hsu JY, Linker SB, Hu L, Schafer ST, Mertens J, et al. Nup153 Interacts with Sox2 to Enable Bimodal Gene Regulation and Maintenance of Neural Progenitor Cells. Cell stem cell. 2017; 21(5):618–34 e7. https://doi.org/10.1016/j.stem.2017.08.012 PMID: 28919367.

83. Ibarra A, Benner C, Tyagi S, Cool J, Hetzer MW. Nucleoporin-mediated regulation of cell identity genes. Genes & development. 2016; 30(20):2253–8. https://doi.org/10.1101/gad.287417.116 PMID: 27807035; PubMed Central PMCID: PMC5110992.

84. Liang Y, Franks TM, Marchetto MC, Gage FH, Hetzer MW. Dynamic association of NUP98 with the human genome. PLoS genetics. 2013; 9(2):e1003308. https://doi.org/10.1371/journal.pgen.1003308 PMID: 23468646; PubMed Central PMCID: PMC3585015.

85. Franks TM, McCloskey A, Shokirev MN, Benner C, Rathore A, Hetzer MW. Nup98 recruits the Wdr82-Set1A/COMPASS complex to promoters to regulate H3K4 trimethylation in hematopoietic progenitor cells. Genes & development. 2017; 31(22):2222–34. https://doi.org/10.1101/gad.306753.117 PMID: 29269482; PubMed Central PMCID: PMC5769767.

86. Akhtar W, de Jong J, Pindyurin AV, Pagie L, Meuleman W, de Ridder J, et al. Chromatin position effects assayed by thousands of reporters integrated in parallel. Cell. 2013; 154(4):914–27. https://doi.org/10.1016/j.cell.2013.07.018 PMID: 23953119.

87. Kind J, Pagie L, de Vries SS, Nahidiazar L, Dey SS, Bienko M, et al. Genome-wide maps of nuclear lamina interactions in single human cells. Cell. 2015; 163(1):134–47. https://doi.org/10.1016/j.cell.2015.08.040 PMID: 26365489; PubMed Central PMCID: PMC4583798.

88. Borchert GM, Holton NW, Williams JD, Hernan WL, Bishop IP, Dembosky JA, et al. Comprehensive analysis of microRNA genomic loci identifies pervasive repetitive-element origins. Mob Genet Elements. 2011; 1(1):8–17. https://doi.org/10.4161/mge.1.1.15766 PMID: 22016841; PubMed Central PMCID: PMC3190270.

89. Roberts TC. The MicroRNA Biology of the Mammalian Nucleus. Mol Ther Nucleic Acids. 2014; 3:e188. https://doi.org/10.1038/mtna.2014.40 PMID: 25137140; PubMed Central PMCID: PMC4221600.

90. Tempel S, Pollet N, Tahi F. ncRNAclassifier: a tool for detection and classification of transposable element sequences in RNA hairpins. BMC Bioinformatics. 2012; 13:246. https://doi.org/10.1186/1471-2105-13-246 PMID: 23009561; PubMed Central PMCID: PMC3495686.

91. Marini B, Kertesz-Farkas A, Ali H, Lucic B, Lisek K, Manganaro L, et al. Nuclear architecture dictates HIV-1 integration site selection. Nature. 2015; 521(7551):227–31. https://doi.org/10.1038/nature14226 PMID: 25731161.

92. Quinlan AR, Hall IM. BEDTools: a flexible suite of utilities for comparing genomic features. Bioinformatics. 2010; 26(6):841–2. https://doi.org/10.1093/bioinformatics/btq033 PMID: 20110278; PubMed Central PMCID: PMC2832824.

93. Andreadis C, Nikolaou C, Fragiadakis GS, Tsiliki G, Alexandraki D. Rad9 interacts with Aft1 to facilitate genome surveillance in fragile genomic sites under non-DNA damage-inducing conditions in S. cerevisiae. Nucleic acids research. 2014; 42(20):12650–67. https://doi.org/10.1093/nar/gku915 PMID: 25300486; PubMed Central PMCID: PMC4227768.

94. Savova V, Patsenker J, Vigneau S, Gimelbrant AA. dbMAE: the database of autosomal monoallelic expression. Nucleic acids research. 2016; 44(D1):D753–6. https://doi.org/10.1093/nar/gkv1106 PMID: 26503248